UNIVERSITEIT VAN PRETORIA
UNIVERSITY OF PRETORIA
YUNIBESITHI YA PRETORIA

MAXIMUM NET POWER OUTPUT FROM AN INTEGRATED DESIGN OF A SMALL-SCALE OPEN AND DIRECT SOLAR THERMAL BRAYTON CYCLE

by

Willem Gabriel le Roux

Submitted in partial fulfilment of the requirements for the degree
MASTER OF ENGINEERING (Mechanical Engineering)

in the

Faculty of Engineering, the Built Environment and Information Technology

UNIVERSITY OF PRETORIA
Pretoria

Supervisors: Dr T Bello-Ochende and Prof JP Meyer

February 2011

Abstract

Title: Maximum net power output from an integrated design of a small-scale open and direct solar thermal Brayton cycle
Author: WG le Roux
Student number: 25105991
Supervisors: Dr T Bello-Ochende and Prof JP Meyer

The geometry of the receiver and recuperator in a small-scale open and direct recuperative solar thermal Brayton cycle can be optimised in such a way that the system produces maximum net power output. The purpose of this work was to apply the second law of thermodynamics and entropy generation minimisation to optimise these geometries using an optimisation method. The dynamic trajectory optimisation method was used and off-the-shelf micro-turbines and a range of parabolic dish concentrator diameters were considered. A modified cavity receiver was used in the analysis with an assumed cavity wall construction method of either a circular tube or a rectangular channel. A maximum temperature constraint of 1 200 K was set for the receiver surface temperature. A counterflow plate-type recuperator was considered and the recuperator length was constrained to the length of the radius of the concentrator. Systems producing a steady-state net power output of 2 – 100 kW were analysed. The effect of various conditions, such as wind, receiver inclination and concentrator rim angle on the maximum net power output, and optimum geometry of the system were investigated. Forty-five different micro-turbines and seven concentrator diameters between 6 and 18 metres were considered. Results show the optimum geometries, optimum operating conditions and minimum entropy generation as a function of the system mass flow rate. The optimum receiver tube diameter was relatively large when compared with the receiver size. The optimum counterflow plate-type recuperator channel aspect ratio is a linear function of the optimum system mass flow rate for a constant recuperator height. The optimum recuperator length and optimum NTU are small at small system mass flow rates but increase as the system mass flow rate increases until the length constraint is reached. For the optimised systems with maximum net power output, the solar receiver is the main contributor to the total rate of minimum entropy generation. The contributions from the recuperator, compressor and turbine are next in line. Results show that the irreversibilities were spread throughout the system in such a way that the minimum internal irreversibility rate was almost three times the minimum external irreversibility rate for all optimum system geometries and for different concentrator diameters. For a specific environment and parameters, there exists

an optimum receiver and recuperator geometry so that the system can produce maximum net power output.

Acknowledgement

My Creator,

who did not come to judge, but to save.

Table of contents

List of figures

List of tables

Nomenclature

Alphabetic Symbols:		Units
a, a	Longer side of rectangle (channel width)	m
A	Area	m^2
b	Shorter side of rectangle (channel height)	m
c	Heat exchanger capacity ratio	-
c	Specific heat (c_p or c_v)	J/kgK
C	Concentration factor	-
CR	Concentration ratio	-
C_W	Optimum ratio of minimum internal to external irreversibility rate	-
d , d	Cavity receiver aperture diameter	m
$\boldsymbol{D}$	Parabolic dish concentrator diameter	m
D , D	Cavity receiver diameter	m
D	Tube / rectangular channel diameter (D_{rec} , $D_{h,rec}$, $D_{h,reg}$)	m
e	Specific exergy	J/kg
$\hat{e}$	Specific energy	J/kg
e_p	Parabolic concentrator error	rad
E	Exergy	J
$\dot{E}$	Exergy rate	W
f	Darcy friction factor	-
F	Heat removal factor	-
F_D	External drag force	N
g	Gravitational constant	m/s^2
GF	Gradient vector of the objective function	-
Gr	Grashof number	-
h	Convection heat transfer coefficient	W/m^2K
h	Planck's constant (solar radiation)	-
h	Small increment	m
h	Specific enthalpy	J/kg

H	Recuperator height	m
I	Irradiance	W/m^2
$\dot{I}$	Irreversibility rate	W
k	Boltzmann's constant (solar radiation)	-
k	Gas constant (c_p / c_v)	-
k	Thermal conductivity	W/mK
K	Constant	-
KE	Kinetic energy	J
L	Length	m
L	Length of channel / tube (L_{rec} , L_{reg})	m
$\dot{m}$	Mass flow rate	kg/s
MT	Micro-turbine model number (Appendix D)	-
n	Number of recuperator flow channels	-
N	Number of fins	-
N_D	Optimum number of tube diameters between receiver edge and aperture edge	-
N_R	Optimum number of rectangular channels between receiver edge and aperture edge	-
NTU	Number of transfer units	-
Nu	Nusselt number	-
P , p, p	Pressure	Pa
PE	Potential energy	J
Pr	Prandtl number	-
q	Specific heat	J/kg
Q, Q	Heat energy	J
$\dot{Q}$	Heat energy rate	W
$\dot{Q}_0$	Rate of solar energy lost due to convection and radiation	W
$\dot{Q}*$	Rate of solar energy intercepted by the cavity receiver aperture	W
$\dot{Q}_{net}$	Net solar energy rate available for receiver fluid	W
r	Pressure ratio (P_2 / P_1)	-
R	Gas constant	J/kgK

Re	Reynolds number	-
$refl$	Mirror surface specular reflectivity	-
R_f	Fouling factor in the calculation of overall heat transfer coefficient	-
s , s	Specific entropy	J/kgK
S	Entropy	J/K
$\dot{S}$	Entropy rate	W/K
t	Thickness of recuperator separator plate	m
t	Time	s
T , T	Temperature	K, ℃
$T*$	The apparent sun's temperature as an exergy source	
u	Specific internal energy	J/kg
U	Heat coefficient (U_L)	W/mK
U	Internal energy	J
U	Overall heat transfer coefficient	W/mK
v	Frequency (solar radiation)	Hz
v	Specific volume	m^3/kg
V	Velocity	m/s
w	Specific work	J/kg
w	Wind factor	-
W	Work	J
$\dot{W}$	Power	W
Wn	Receiver aperture diameter vector	m
x	Discrete least squares approximation constant	-
X	Optimisation vector	-
z	Height	m

Greek symbols:

α	Receiver absorptance	-
β	Inclination of receiver	-
ε	Effectiveness	-
ε	Exergetic efficiency	-
ε	Emissivity	-
ϕ	Horizontal inclination angle	-
φ	Angle	-

η	Efficiency	-
λ	Dimensionless parameter (λ_{BH})	-
λ	Wave length (solar radiation)	m
μ	Dynamic viscosity	kg/ms
ρ	Density	kg/m^3
υ	Volume	m^3
Ω_1	Solid angle subtended by the solar disc seen from earth	rad
Ω_2	Solid angle for the outgoing radiation	rad
ψ	Angle	-

Subscripts:

0, *0*	Surrounding / environment
0	Zero pressure (ideal gas) for c_p
1	State 1
2	State 2
a	Receiver aperture
A	Absorber
atm	Atmospheric
avg	Average
b	Boundary
b	Of blackbody radiation, final
B	Base
BH	Defined by Bahnke and Howard
c	Cold stream
c	Compressor
c	Cross-sectional
$conc$	Concentrator
$conv$	Convection
cv	Control volume
D	Based on receiver diameter
D	Destruction
e	Electric
e	Outlet
ext	External

F	Average of the heat transfer fluid
F	Fuel
$FirstLaw$	According to the first law of thermodynamics
gen	Generation
h	Hot stream
h	Hydraulic
$high$	Highest value on island of maximum compressor efficiency
i	Inlet
i	Inner
in, in	In
int	Internal
L	Loss due to convection and conduction
L	Loss
$loss$	Loss
low	Lowest value on island of maximum compressor efficiency
max	Maximum
min	Minimum
net	Net
o	Out/Outer
opt	Optimum
out, *out*	Out
p	For constant pressure
P	Product
rad	Radiation
rec	Receiver
reg	Recuperator
rim , rim	Concentrator rim
s	Shaft
s	Surface
$sngl$	For a single fin
t	Turbine
th , th	Thermal
v	For constant volume
v	Per unit frequency (solar radiation)

w	Cavity receiver inner surface
∞	Surrounding area / free-stream
ΔP	Due to fluid friction
ΔT	Due to temperature difference

Superscripts:

*	Solar
‘	Per unit length
.	Time rate of change
CH	Chemical

Chapter 1

Introduction

1.1 Historical background

"The optimists say solar power could become as economical and efficient as fossil fuels. The pessimists say they've heard all this before" (Johnson, 2009).

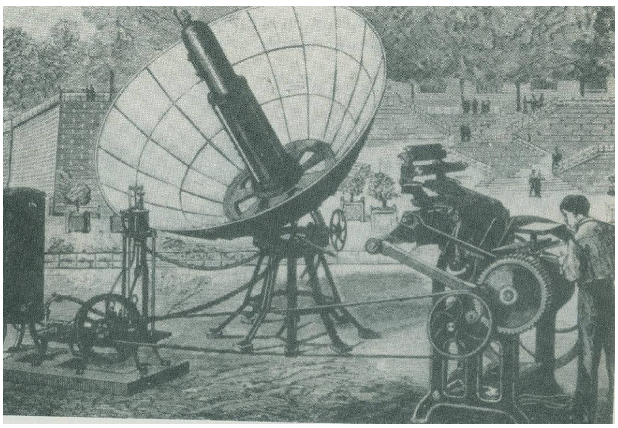

Figure 1.1 A parabolic collector powering a printing press at the 1878 Paris Exposition (Kreith and Kreider, 1978).

The interest and research in solar power have come a long way. Cheremisinoff and Regino (1978) acknowledge the history of solar energy and solar energy availability from the years before Christ up to the 1970s. According to Kreith and Kreider (1978), a diamond was melted for the first time in 1695 in Florence by an early solar practitioner. They also mention that solar combustion experiments were done by the French chemist, Lavoisier, and the English scientist, Joseph Priestley, in 1774. In 1878, a solar steam engine, using a parabolic reflector reflected onto a steam boiler, was exhibited at the World Fair in Paris. This engine, shown in Figure 1.1, was utilised to run a printing press.

In 1901, a 7.5 kW solar steam engine was operated by AG Eneas in Pasadena, California. The focusing collector is shown in Figure 1.2. Between 1907 and 1913, the American engineer F Shuman, developed solar-driven hydraulic pumps. There was very little activity in the field of solar power between 1915 and 1950. The interest was revived in 1949 and in the 1960s, as the objective of NASA's research and development programme was to build a solar electric power

system capable of supplying electricity for the US space programme. Research funds became available and widespread interest grew for the development of earth-bound solar electric power, which increased after the oil crisis in 1973 (Kreith and Kreider, 1978).

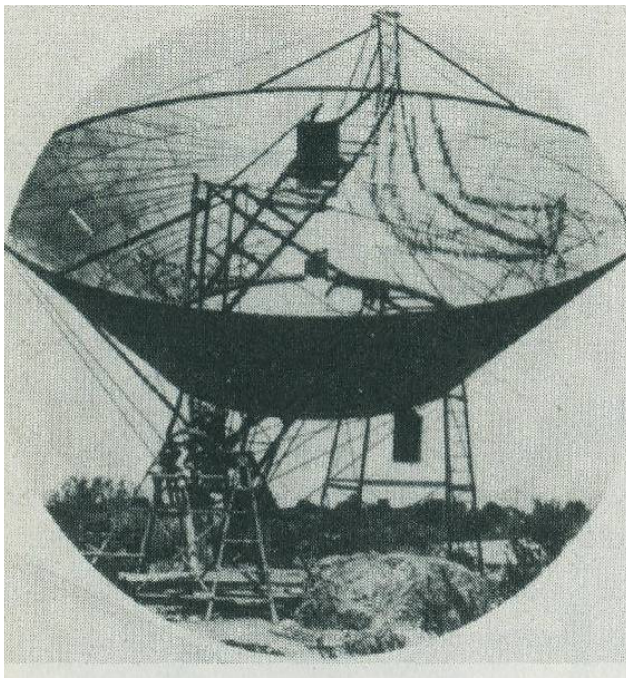

Figure 1.2 A solar-powered steam engine in Arizona in the early 1900s (Kreith and Kreider, 1978).

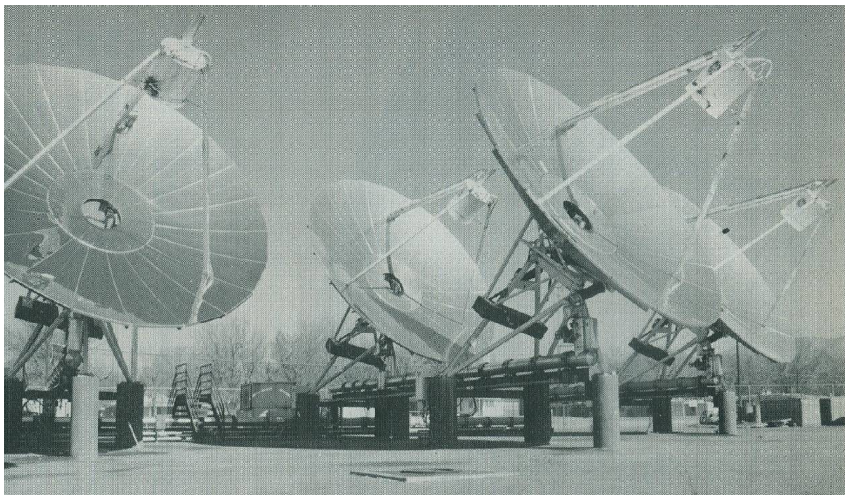

Figure 1.3 Commercially produced point focus concentrators (Howell et al., 1982).

Figure 1.3 shows the Shenandoah solar total energy project at Shenandoah, Georgia, which was installed before 1983. It was designed for application to a solar thermal co-generation project and was commercially procured (Howell et al. 1982; Stine and Harrigan, 1985). The national crisis in 1973 and soaring oil prices in 1979, created a great sense of urgency and called for research into

renewable energy in the US. In 1977, President Jimmy Carter called for a federal push for renewable energy. Nine large solar thermal plants were installed before oil prices plummeted and President Carter left office, leaving solar energy as a minor factor in the energy equation (Johnson, 2009).

Today is a new dawn for solar power. A call for clean and efficient energy can be heard all over the world to ensure a safe and stable environment.

1.2 Problem

South Africa, like southern Africa, has much potential to generate large amounts of its power from solar technologies. Kreith and Kreider (1978) state that there are technological and natural types of solar radiation collections. Natural collection includes phenomena such as wind and ocean temperature differences. There are two main research fields concerning the harnessing of the sun's power: concentrated solar power (or solar thermal power) and photovoltaic panels, which are respectively ±24% and 10-20% efficient in converting the sun's energy into electricity (Johnson, 2009). Concentrated solar power systems use the concentrated power of the sun as a heat source to generate mechanical power.

Fluri (2009) shows that the total potential generation capacity of large-scale concentrated solar power in South Africa is more than 500 GW, when using the best suitable locations for large-scale power plants in the country. These locations, as identified by Fluri (2009), are areas which have sufficient sunshine, are close enough to transmission lines, are flat enough, where the respective vegetation is not under threat and which have suitable land-use profiles. According to Fluri (2009), the solar irradiation in the northern parts of the Northern Cape Province, South Africa, is more than 8 kWh/m^2 in December and 6 kWh/m^2 in June. Most areas in South Africa, however, receive an average of more than 2 500 hours of sunshine per year, with average solar-radiation levels ranging between 4.5 and 6.5 kWh/m^2 per day (DME, 2010), which makes small-scale concentrated solar power applications equally attractive.

Thus far, the world's solar leaders are not necessarily the sunniest countries, but rather the ones that can afford to pay extra for solar power (Johnson, 2009). It is therefore very important to understand the costs involved in solar power and to be able to get the best efficiency from these solar power systems.

Different types of solar thermal power systems exist. According to Chen et al. (2007), the Brayton cycle is definitely worth studying when comparing its efficiency with those of other power cycles. Mills (2004) argues that emphasis may shortly shift to solarised Brayton micro-turbines from Dish-

Stirling technology due to high Stirling engine costs. The highest-efficiency Brayton cycles are regenerative cycles with low pressure ratios (Stine and Harrigan, 1985). The fact that the Brayton cycle can be an open cycle (which means air can be used as working fluid), makes this cycle very attractive for use in the water-scarce southern Africa. The small-scale open and direct solar thermal Brayton cycle with recuperator has several advantages, including lower cost, low operation and maintenance costs and it is highly recommended. The main disadvantages of this cycle are the pressure losses in the recuperator and receiver, turbomachine efficiencies and recuperator effectiveness (Stine and Harrigan, 1985), which limit the net power output of such a system. Maximum net power output is required for a small-scale solar thermal Brayton cycle with recuperator. The net power output can for example be used to drive an electrical generator and the higher the net power output the more electricity can be produced. To obtain this maximum net power output, a combined effort of heat transfer, fluid mechanics and thermodynamic thought is required. Bejan (1982) suggests that the method of entropy generation minimisation combines these thoughts.

The irreversibilities of the recuperative solar thermal Brayton cycle are mainly due to heat transfer across a finite temperature difference and fluid friction. Various studies have emphasised the importance of the optimisation of the global performance of a system, by minimising the sum of the irreversibilities from all the different components or processes of the system (spreading the entropy generation rate through the system by optimally sizing the hardware, in stead of optimising components individually). This emphasis is made by Bejan (1996; 1997), Bejan et al. (1996), Ordóñez and Bejan (2000), Shiba and Bejan (2001) and Zimparov et al. (2006a; 2006c). For the open and direct solar thermal Brayton cycle, an optimisation of this kind is not available from the literature. The geometries of the receiver and recuperator can be optimised in such a way that the total entropy generation rate is minimised to allow maximum net power output.

1.3 Purpose of the study

The objective of this study is to apply the second law of thermodynamics and entropy generation minimisation to optimise the components in a solar thermal power system such that the system produces maximum net power output at steady-state. An analysis is done by looking at the solar thermal power system as a whole and by minimising the total entropy generation rate in the system, instead of optimising components individually. In a solar thermal Brayton cycle with a micro-turbine operating at its highest compressor efficiency, geometric variables of a modified cavity receiver, proposed by Reddy and Sendhil Kumar (2009), and a plate-type counterflow recuperator (Shah, 2005) are optimised. The surface temperature of the receiver should stay below 1 200 K due to material constraints. The dynamic trajectory optimisation method for constrained optimisation (Snyman, 2000) is used. Off-the-shelf micro-turbines (Garrett, 2009)

chosen for low cost, high availability and reliability and a range of parabolic dish concentrator diameters are considered. The technical data of these micro-turbines are also available. A valuable understanding of the optimal distribution of the total entropy generation rate (or irreversibility rate) throughout the open and direct recuperative solar thermal Brayton cycle should be obtained. The effect of various environmental conditions and constraints on the optimum geometries is investigated.

In this study, the open and direct solar thermal Brayton cycle with recuperation is analysed at different steady-state conditions and parameters. The geometries of a modified cavity receiver and counterflow plate-type recuperator are optimised so that the system produces maximum net power output. The net power output of the system is described in terms of the total entropy generation rate within the system. The net power output of the system is maximised, the total entropy generation rate is minimised and the geometries of the receiver and recuperator are optimised.

1.4 Layout of dissertation

At the outset, a literature survey is conducted in Chapter 2. Solar thermal power systems are investigated and compared. Solar collectors and recuperators are explored as well as the second law of thermodynamics and its application to these components. From the literature survey, the problem is formulated in Chapter 3 and the model is described in Chapter 4. An objective function is constructed and the numerical optimisation method is given. In Chapter 5, the results and a validation are presented. Optimum geometries and operating conditions are given for different environmental conditions. The possibilities for future work are examined and in Chapter 6, the concluding remarks are made.

Chapter 2

Literature survey

2.1 Introduction

In this chapter, a literature survey is conducted. Different solar thermal power systems are considered and compared. The solar thermal Brayton cycle is chosen for further investigation. Solar collectors and recuperators are explored as well as the second law of thermodynamics and its application to these components. An overview of concepts such as the second law of thermodynamics, exergy and entropy is given. Entropy generation and its minimisation are introduced and its application to the solar thermal Brayton cycle is identified. Solar radiation and the exergy of solar radiation are explored. Lastly, the concluding remarks are made.

2.2 Solar thermal power systems

2.2.1 Background

Duffie and Beckman (1991) describe solar thermal power systems as the conversion of solar to mechanical and electrical energy. Much of the early solar thermal power systems were for small-scale applications of up to 100 kW (mostly used for water pumping), while after 1975 many large-scale power systems were built in the megawatt range. Three power cycles are mainly considered for solar applications or solar thermal power systems: the Rankine, Stirling and Brayton cycles (Bejan, 1997; Stine and Harrigan, 1985). Brayton and Stirling engines provide high engine efficiencies, but are limited by low gas heat transfer coefficients, which would require large receivers and cavity receivers. The Rankine cycle allows for smaller receivers, which can use fluids with high heat transfer coefficients (Duffie and Beckman, 1991). According to Mills (2004), the Rankine cycle appears to be the best option with trough plants because of temperature limitations in the latter, and Brayton cycle micro-turbines appear to be moving quickly to displace Stirling engines in the two-axis tracking market because of much lower cost. The efficiency of a solar thermal receiver diminishes as its operating temperature rises, while the efficiency of the cycle rises as the operating temperature rises (Duffie and Beckman, 1991; Stine and Harrigan, 1985). It is clear that an optimum operating temperature must exist. For example, Stine and Harrigan (1985) give an operating temperature of 780°C as the optimum for a concentrator when combined with a Carnot-engine.

2.2.2 Power cycles available for solar thermal application

2.2.2.1 The Rankine cycle

According to Stine and Harrigan (1985), the most common cycle used in solar power systems is the Rankine cycle with water, organic liquids or liquid metals as the working fluid. The Rankine cycle is shown in Figure 2.1. Reheating and regeneration can also be used. Stine and Harrigan (1985) also claim that most solar power cycles in operation or under development are Rankine cycles.

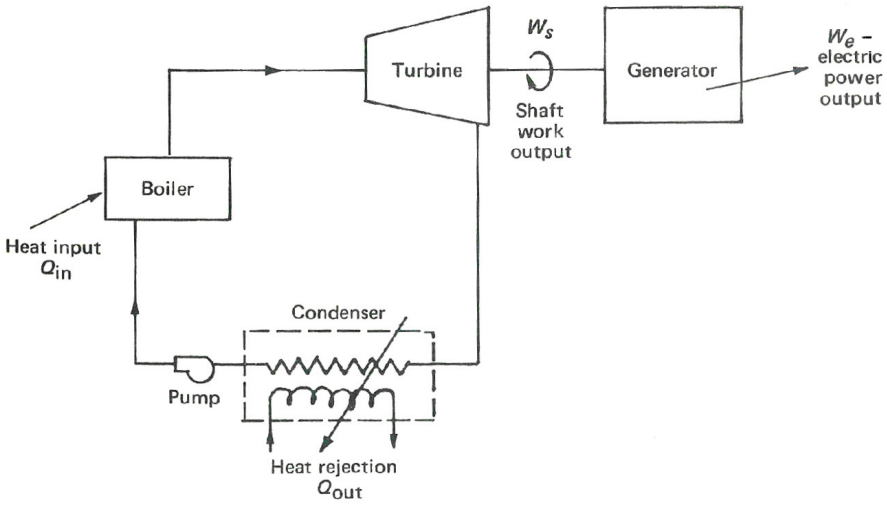

Figure 2.1 The Rankine cycle (Kreith and Kreider, 1978).

The most common condenser for the Rankine cycle is considered to be a shell-and-tube heat exchanger, requiring a supply of cooling water. The radial-flow and axial-flow turbines are considered to be the most common turbines used with the Rankine cycle. The radial-flow turbine is considered to be more efficient for small power output applications (Stine and Harrigan, 1985). An interesting example of a solar Rankine cycle delivering between 10 – 100 kW is a cycle designed for the US Department of Energy's Small Communities Project by Barber-Nichols Engineering (Stine and Harrigan, 1985). It is designed to produce 26 kW of shaft power with a peak operating temperature of 400 ℃, with toluene as working fluid. The turbine rotates at 60 000 rpm and has a mean blade diameter of 12.5 cm. The engine has a thermal efficiency of 24%. STG International (2010) uses an organic Rankine cycle for its solar concentrator module. The module produces 3 kW of electrical power with parabolic trough concentrators.

2.2.2.2 Stirling engines

According to Stine and Harrigan (1985), the Stirling engine placed at the focus of a parabolic dish concentrator is being proposed for many small (10 – 100 kW) solar power applications because

of its high cycle efficiency potential (a Stirling engine can be designed to have the same efficiency as the ideal Carnot cycle). Three major causes of inefficiencies in the Stirling engine exist: sinusoidal motion of the pistons, imperfect regeneration and dead volume (Stine and Harrigan, 1985). Figures 2.2 and 2.3 respectively show an example of a Stirling engine and the T-s diagram of the ideal Stirling cycle.

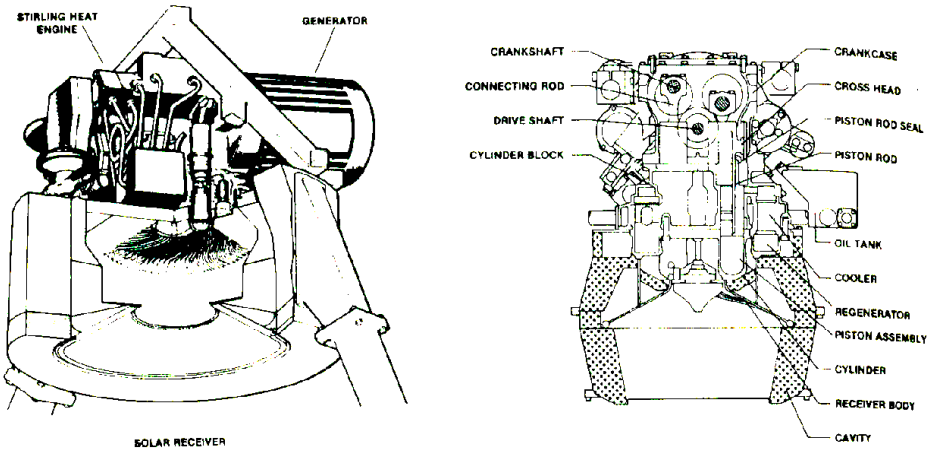

Figure 2.2 The United Stirling Model 4-95 solar Stirling engine (Stine and Harrigan, 1985).

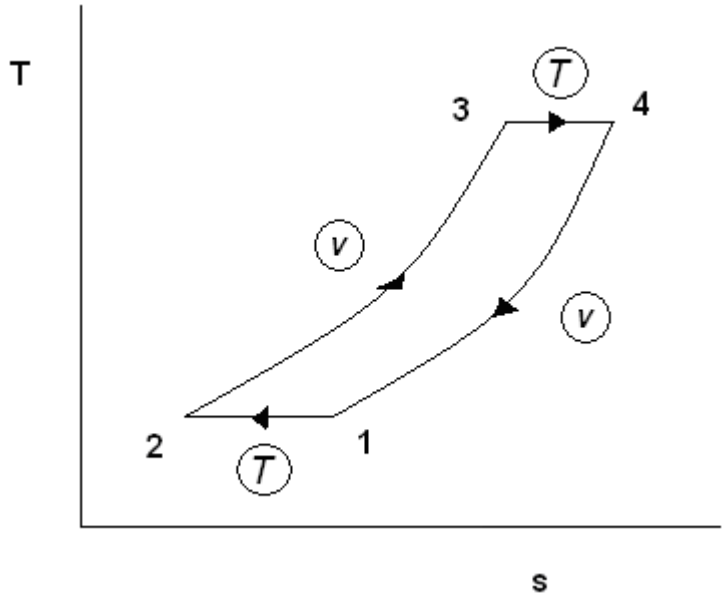

Figure 2.3 The four processes of an ideal Stirling engine cycle.

An example of a Stirling engine is the Solar 4-95 engine, which produces 22 kW of shaft power at a thermal efficiency of 38%. The heater operates at 720℃ (Stine and Harrigan, 1985). One should take note of the free-piston Stirling engine (Stine and Harrigan, 1985). This engine was developed in an attempt to get around the problem of sealing the engines from gas leakage and

to eliminate mechanical friction associated with bearings, crossheads and seals. In this design, a power piston and a displacer bounce back and forth in a harmonic motion with mechanical or gas springs causing reversal of the motion. The engine has a diameter of 3.35 cm and a stroke of 2 cm and produces 100 W of alternating current electrical power with a frequency of 30 Hz when heated to 650℃.

2.2.2.3 The Brayton cycle

Chen et al. (2007) show that the Brayton cycle is definitely worth studying when comparing its efficiency with that of other power cycles. Mills (2004) predicts that emphasis may shortly shift from Dish-Stirling technology to solarised Brayton micro-turbines due to high Stirling engine costs. The lower Brayton costs are due to high production quantities in the current market. Mills (2004) argues that the efficiency of the Brayton cycle is 25 - 33%, while the efficiency of the Stirling engine is 42%. However, according to Mills (2004), it is possible for Brayton cycles to reach peak efficiencies close to 40%.

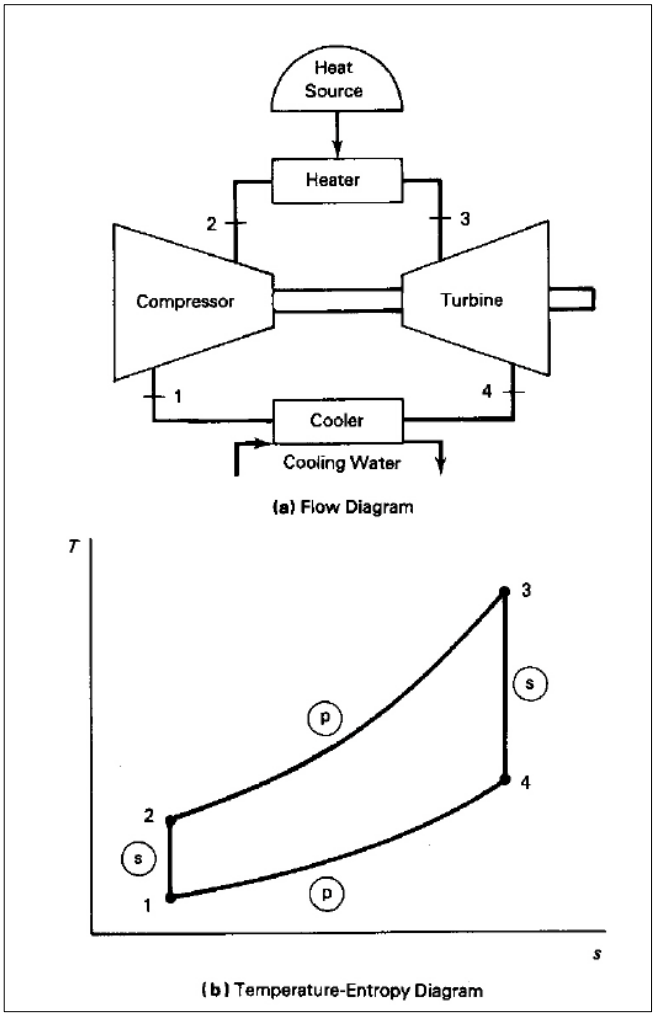

Figure 2.4 The Brayton cycle (Weston, 2000).

A flow diagram of the Brayton cycle, showing the requirement of a heat source, is given in Figure 2.4. This heat source is usually provided by fuel combustion. However, it can also be provided by solar energy. The Brayton cycle is considered for both small-scale and large-scale power applications, with its potential for low operation and maintenance cost as its major advantage. These engines are proposed to be placed at the focus of a parabolic dish concentrator. Operating at relatively low pressure, the Brayton cycle requires large, hot gas receivers. Its major drawback is the high receiver operating temperatures required to get reasonable efficiencies. Most Brayton cycles are not self-sustaining at operating temperatures below 480℃ (Stine and Harrigan, 1985).

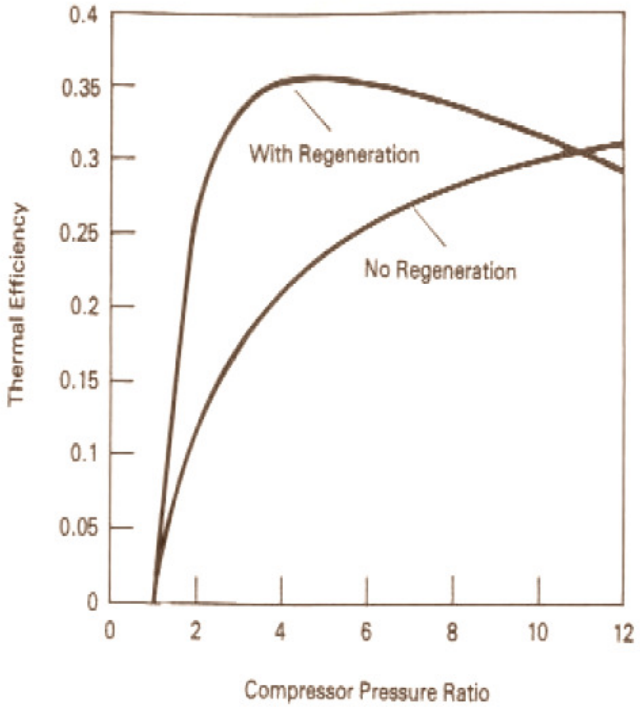

Figure 2.5 The thermal efficiency of a two-shaft gas turbine cycle with and without regeneration, as plotted from an example spreadsheet for different pressure ratios (with recuperator efficiency < 1) (Weston, 2000).

A recuperator (heat exchanger) can be used in the Brayton cycle to extract the heat from the turbine outlet and transfer it to the cold stream before it is heated by the heat source. The effect of regeneration on the thermal efficiency of a Brayton cycle is shown in Figure 2.5. From Figure 2.6, it is concluded that the highest-efficiency Brayton cycles are regenerative cycles with low compressor pressure ratios. If regeneration is not used, high compressor pressure ratios are required to provide high efficiency.

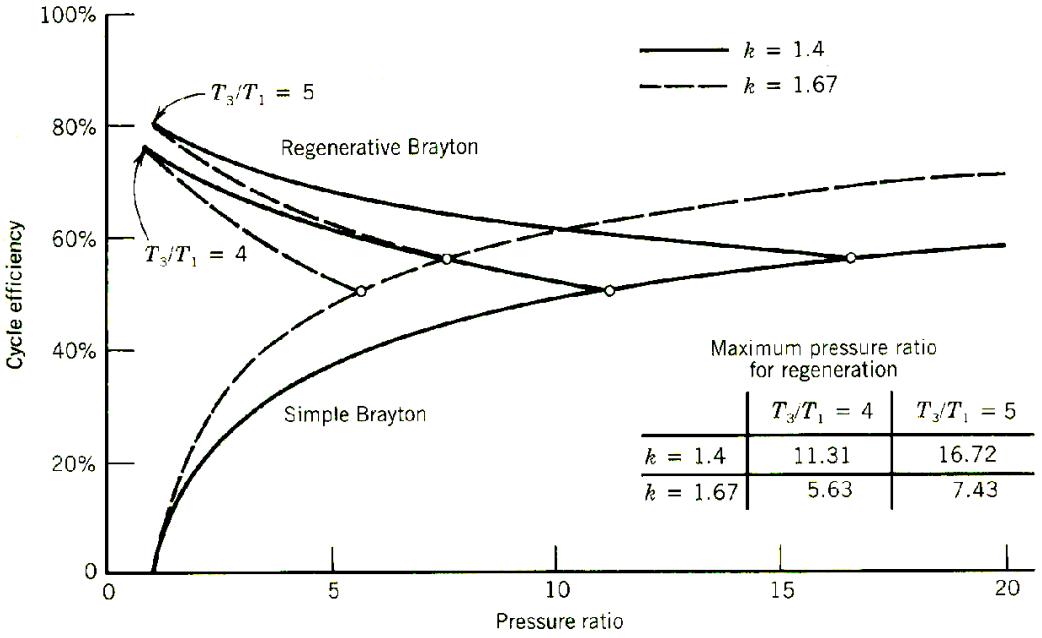

Figure 2.6 The regenerative Brayton cycle efficiency compared with the simple cycle efficiency. These curves are for a recuperator efficiency of 100% (Stine and Harrigan, 1985). Temperature values correspond to the values in Figure 2.4b and $k = c_p / c_v$.

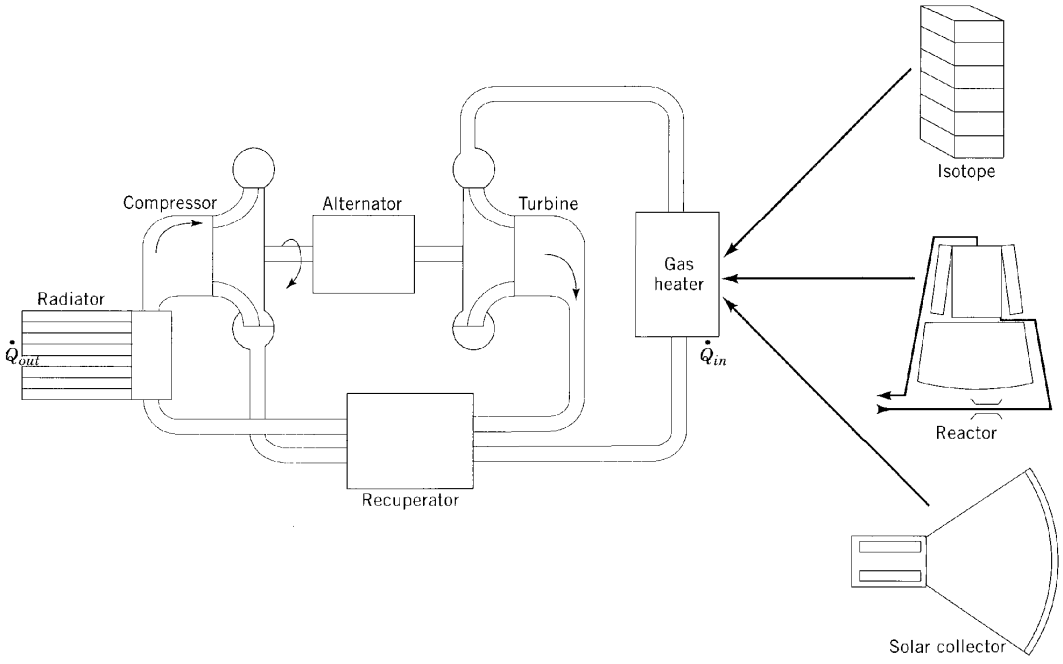

Figure 2.7 A closed Brayton cycle power plant for use in space (Bejan et al., 1996).

An extra heat exchanger can be used to extract heat from the fluid system in direct contact with solar radiation (making the system an indirect system). A radiator might also be used in a closed Brayton cycle. Figure 2.7 gives an example of a closed Brayton cycle for use in space. Bejan et al. (1996) imply that the solar heat source is more suitable than the isotope and nuclear heat

sources when the power plant size is in the range of 2 – 100 kW. Helium has been proposed for closed solar Brayton cycles because of its efficiency advantage plus its high heat transfer capability and because it is inert. For open Brayton cycles, it is essential to have natural air movement past the site to prohibit reinjection of the warm exhaust (Stine and Harrigan, 1985).

Heat exchangers can also be used for intercooling and reheating in a solar thermal Brayton cycle. The major advantage of multistaging (combining a number of compression and expansion stages in series with coolers and heaters respectively) is that the cycle can have the high efficiency associated with low-pressure ratio regenerative cycles, without the extremely large recuperator required for a single-stage cycle of the same power output (Stine and Harrigan, 1985). Maximum efficiency is attained when equal pressure ratios are maintained across each compressor and each turbine stage. The Ericsson cycle has the potential of attaining Carnot efficiency when regeneration is used (Stine and Harrigan, 1985).

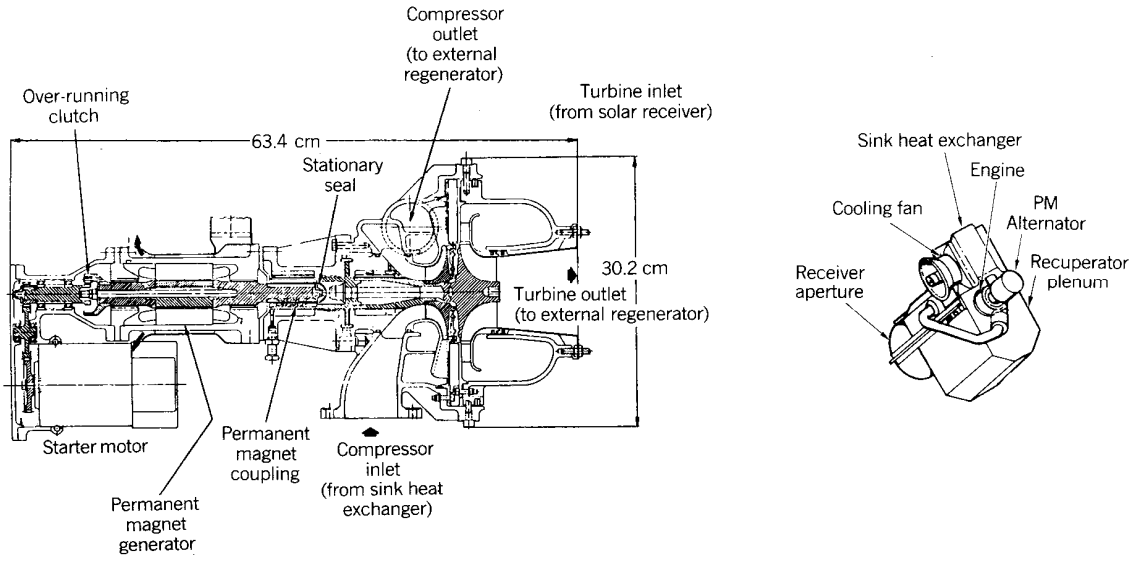

Figure 2.8 A solar sub-atmospheric gas turbine engine for parabolic dish application (Stine and Harrigan, 1985).

According to Stine and Harrigan (1985), there are three major losses in actual Brayton cycle engines: duct pressure losses, turbomachine efficiencies and recuperator effectiveness. Figure 2.8 shows the sub-atmospheric Brayton cycle, an example of the closed Brayton cycle where heat is added to the receiver at atmospheric pressure and rejected at a lower pressure. The receiver design is greatly simplified, which allows for large blade heights in the turbine and compressor. This results in higher efficiencies. According to Stine and Harrigan (1985), such a system's shaft would operate at 71 000 rpm, while air is heated to 871°C and 11 kW of electric power is produced at a cycle efficiency of 27%. The SAGT (a solar version of the Garrett Turbine Engine Company's automotive gas turbine engine), shown in Figure 2.9, is another example. It is

an open cycle with regeneration provided by a rotary porous ceramic wheel regenerator. It operates at 87 000 rpm, a peak pressure and temperature of 0.5 MPa and 1371℃ and at a cycle efficiency of 47% while it produces 75 kW of power (Stine and Harrigan, 1985).

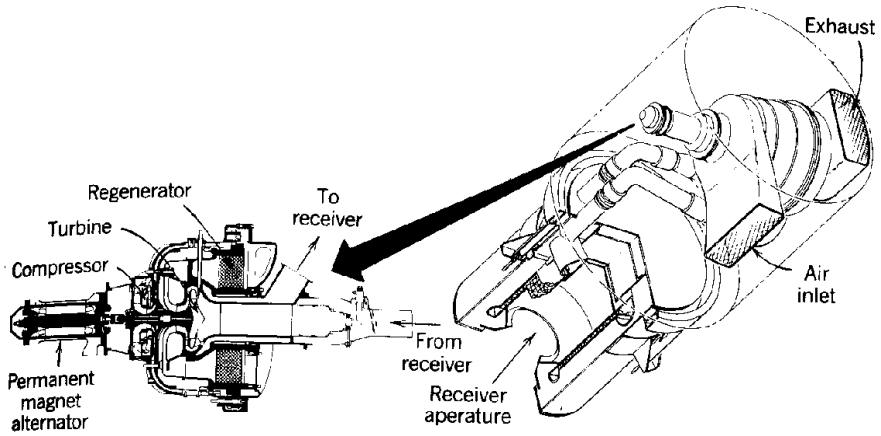

Figure 2.9 A solar version of the Garrett Turbine Company's Brayton cycle automotive gas turbine engine (Stine and Harrigan, 1985).

2.2.2.3.1 Compressors, turbines and the Brayton cycle: micro-turbines

Tsai (2004) explains the design and performance of a gas turbine engine using an automobile turbocharger. The net power output available from this specific system is close to 22 kW. Honeywell Garrett micro-turbines are widely available in South Africa, thanks to the motor industry. Shah (2005) regards the Honeywell turbomachinery as worth mentioning when it comes to the company's development expertise in micro-turbines in recent history. The Garrett range is very attractive from a cost, availability and reliability perspective. Very useful data are also made available at no cost. For each of its micro-turbines, data are available, including compressor and turbine maps. This could not be found as convincingly from other leading micro-turbine manufacturers. These compressor maps show that for each pressure ratio of the compressor, a specific mass flow rate exists for a specific compressor efficiency. Figure 2.10 shows a micro-turbine from the Garrett range.

It is important to know what the maximum operating temperatures of the turbines in the Garrett range are. According to Tsai (2004) and Shah (2005), a maximum operating temperature exists for micro-turbines. According to Garrett (2009) and Shah (2005), it seems that this maximum is more or less 950℃ for the inlet temperature of the turbine and 1050℃ intermittently. The air leaving the solar receiver is thus restricted to this maximum temperature. Thus, the solar receiver's surface temperature would have to be higher than 950℃ to produce these air temperatures at the turbine.

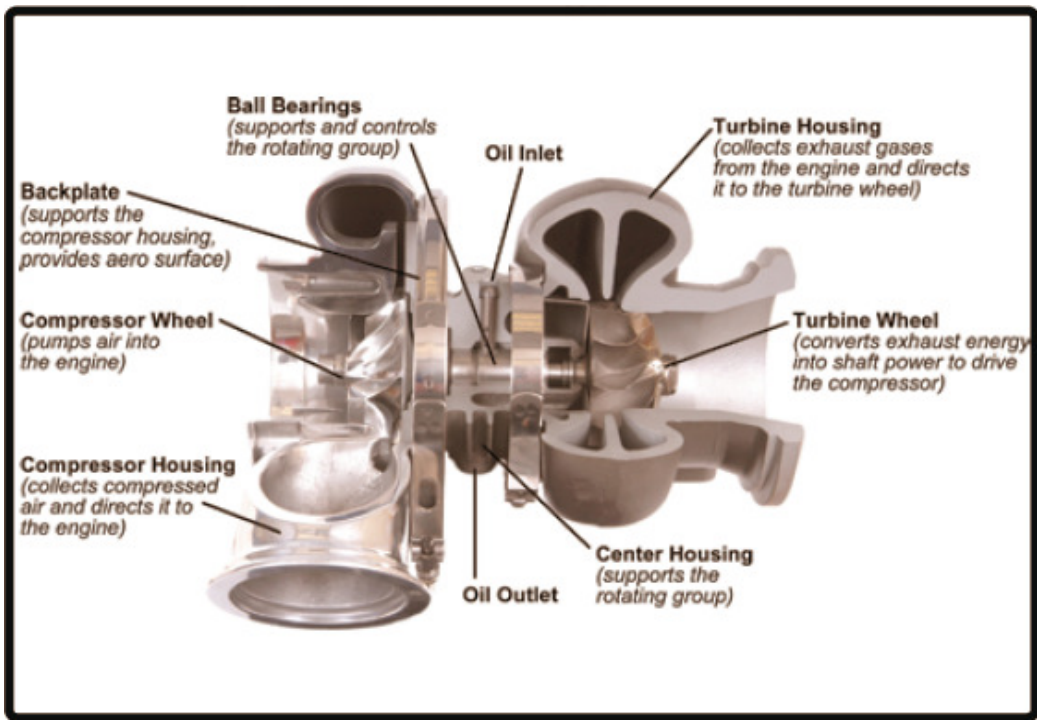

Figure 2.10 A section view of a micro-turbine from the Garrett range (Garrett, 2009).

2.2.2.3.2 Storage for the Brayton cycle

Some disadvantages of the solar thermal Brayton cycle using air as working fluid are that it has few storage options and the receiver and recuperator have to be large. This section shows possibilities for storage in the Brayton cycle, for interest's sake. Bejan (1997) suggests the use of two different working fluids and a melting element for storage. The one fluid transports the heat from the collector to the melting element while the other would be the working fluid in the Brayton cycle, which uses the temperature of the melting element as its heat source. This is called an indirect Brayton cycle and is useful when storage is necessary. An air-rock thermal energy storage system, presented by Stine and Harrigan (1985), is another heat storage option that would be compatible with a Brayton cycle. Magnesium oxide bricks are used together with a hot gas (air or helium) to store heat when extra energy is available, and to extract heat when the solar energy input is low.

2.2.3 Comparison of solar thermal power cycles

In this section, the different solar thermal power cycles are compared. It is important to keep in mind that these cycles are compared for use in South Africa in the range of 2 – 100 kW. Table 2.1 shows the advantages and disadvantages, summarised from the aforementioned text, for the Rankine, Stirling and Brayton solar thermal power cycles.

Table 2.1 Solar thermal power cycles compared (Stine and Harrigan, 1985).

	Advantages	Disadvantages
Rankine	• High heat transfer coefficients - smaller receivers • Most common and most systems in operation or under development • Low operating temperature	• Condenser required (shell-and-tube most common)
Stirling	• High efficiency (can approach ideal Carnot) • Proposed for small applications • Free-piston Stirling engine	• Low gas heat transfer coefficients - large receivers • Inefficiencies: Sinusoidal motion of the pistons, imperfect regeneration, dead volume and not all the gas in the engine participates in the cycle • Seal the engines from gas leakage and eliminate mechanical friction associated with bearings, crossheads and seals
Brayton	• High efficiency, Ericsson cycle – multistaging • Use of recuperator allows highest thermal efficiency at low pressure ratios • Both large- and small-scale application • Low operation cost, low maintenance cost • Open cycle, air – cheap • Solar heat source is more suitable than the isotope and nuclear heat sources when the power plant size is in the range of 2 – 100 kW	• Low gas heat transfer coefficients - large hot gas receivers required • Most Brayton engines are not self-sustaining at operating temperatures below 480°C • Large recuperators required • Major losses in actual Brayton cycle engines: duct pressure losses, turbomachine efficiencies and recuperator effectiveness

The Brayton cycle (Figure 2.4) looks very attractive since its low operation and maintenance costs are valuable. It can also be noted that recuperation in the Brayton cycle not only increases the thermal efficiency, but also allows for lower pressure ratios, which is very beneficial from a design perspective. The fact that the Brayton cycle can be an open cycle and that it uses air, which can be modelled as an ideal gas, makes this cycle very attractive for use in the water-

scarce southern Africa. The Brayton cycle definitely has its disadvantages as well. One of the most important disadvantages is that it is not sustainable at temperatures below 480℃ (Stine and Harrigan, 1985). According to Duffie and Beckman (1991), the energy lost from ducts and pipes leading to and returning from the solar receiver can be significant. Other important disadvantages are the pressure losses in the ducts, recuperator and receiver, turbomachine efficiencies and recuperator effectiveness. The method of entropy generation minimisation can be used to tackle these disadvantages to optimise the receiver and recuperator and to maximise the net power output of the system.

2.2.4 Comparison of working fluids and intermediate fluids

Heat transfer fluids used in central receivers, which are used on centrally located towers, are compared with the information given by Stine and Harrigan (1985) in Table 2.2.

Table 2.2 Comparison of fluids used in solar thermal power cycles (Stine and Harrigan, 1985).

	Max. temp. (℃)	Cost	Freeze (℃)	Positive	Negative
Heat transfer oils	425	High	-10	Low vapour pressure – thermal storage	Flammable
Steam	540	Low	0		De-ionised water
Nitrate-salt mixtures	565	Medium low	140 - 220	Good for storage	
Liquid sodium	600	Very high	98	Storage, low vapour pressure	
Air or helium	850	Free or very low	N.A.	Free	Few and difficult storage methods, large diameter piping required

A question might come to mind: would the efficiency of the overall system be more when the heat-extracting fluid in the receiver is also the working fluid (a direct system)? Would this efficiency be higher than when a specifically chosen optimal fluid extracts heat from the receiver, separately from an optimally chosen working fluid in the power cycle (where heat is exchanged from one to another in the heat exchanger)? It might be better to have the same fluid to perform both functions at once, while at the same time less irreversibilities are generated. According to Duffie and Beckman (1991), there is a penalty involved when such a heat exchanger is included in the system (indirect system). The system would require a larger collector concentrator to

operate at the same temperature as it would have done without the heat exchanger. Stine and Harrigan (1985) and Duffie and Beckman (1991) compared the abovementioned sides of the argument. The advantages and disadvantages of having a direct or indirect cycle/working fluid are given in Table 2.3.

Table 2.3 Advantages and disadvantages of having a direct or indirect cycle/working fluid (Stine and Harrigan, 1985).

	Direct working fluid	Intermediate fluid
Advantages	➢ Concept is simple ➢ Engine can operate at higher temperature ➢ Fewer components and no extra heat loss	➢ Reduces size and weight of receiver ➢ Reduction of heat loss from the otherwise large ducting
Disadvantages	➢ High-pressure field piping ➢ Large ducting required ➢ System is difficult to control during insolation transients (especially Rankine) ➢ Extreme care must be taken in the design to prevent tube burnout	➢ Adds complexity and another fluid ➢ Extra heat exchanger

A direct or indirect system can be used in a solar thermal power cycle. For the Brayton cycle, a direct system seems attractive, especially when considering costs. Air can be used as the working fluid in the power cycle and as the fluid which extracts heat from the heat source (solar receiver).

2.2.5 Conclusion

The solar thermal Brayton cycle is recommended over the other solar thermal power cycles by Mills (2004) and Chen et al. (2007). The power cycle uses air as working fluid and has low operation and maintenance costs. When a recuperator is used, the cycle operates at low compressor pressure ratios. Therefore, the solar thermal Brayton cycle is the foundation for the remainder of the literature study.

2.3 Solar collectors (concentrators and receivers)

2.3.1 Background

It is noted from the literature that there is some confusion regarding the definitions of collectors, concentrators and receivers. Duffie and Beckman (1991) take away the confusion regarding these definitions: the *collector* includes the receiver and concentrator, while the *receiver* is the element of the system where the radiation is absorbed and converted into some other energy form. The receiver consists of the absorber, covers and insulation. The *concentrator* is the part of the collector that directs radiation onto the receiver. The concentrator area reflects or concentrates the sun's rays onto the receiver (with the use of reflective material).

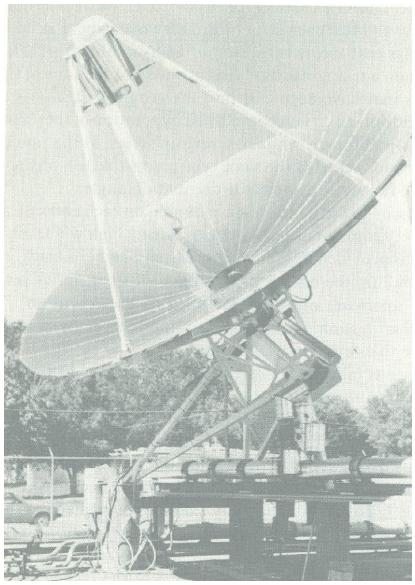

Figure 2.11 Photograph of parabolic dish installed at Shenandoah (Stine and Harrigan, 1985).

The purpose of a solar thermal receiver is to absorb the sun's energy and to transfer the resultant thermal energy to a fluid which, in turn, delivers useful energy (Howell et al., 1982). The method of concentration can be described as the way in which a receiver receives the sun's energy from the concentrator – there are quite a number of different ways in which the sun can be concentrated onto a receiver. The receiver geometry depends on the method of radiation collection. Figure 2.11 shows an example of a small-scale parabolic dish collector, including the concentrator and receiver. According to Duffie and Beckman (1991), many solar power studies showed that the solar collector represents the largest cost in the system.

Literature concerning the basics of solar energy is well established. Kreith and Kreider (1978), Wilson (1979), Howell et al. (1982), Stine and Harrigan (1985) and Duffie and Beckman (1991)

paid much attention to different solar topics. This includes: the sun, history, solar concentrators, flat-plate collectors, energy storage, radiation, sizing, case studies and economics, to name a few. Many of these sources are more focused on solar thermal heating systems than on solar thermal power systems. Stine and Harrigan (1985) paid specific attention to collector performance, basic concentrator optics, parabolic concentrating collectors, central receivers, different types of concentrators and power cycles for solar applications.

2.3.2 Concentration ratio and different types of concentrations

"The higher the temperature at which energy is to be delivered, the higher must be the concentration ratio and the more precise must be the optics of both the concentrator and the orientation system" according to Duffie and Beckman (1991).

Solar collectors can be divided into different classes. Flat plates, which operate without concentration, are regarded as thermal-conversion devices operating over a range of temperatures of up to 380 K (107°C). These collectors are used mainly for service water and space heating (Kreith and Kreider, 1978). Duffie and Beckman (1991) claim that it might be possible to use flat plate collectors to supply energy to heat engines.

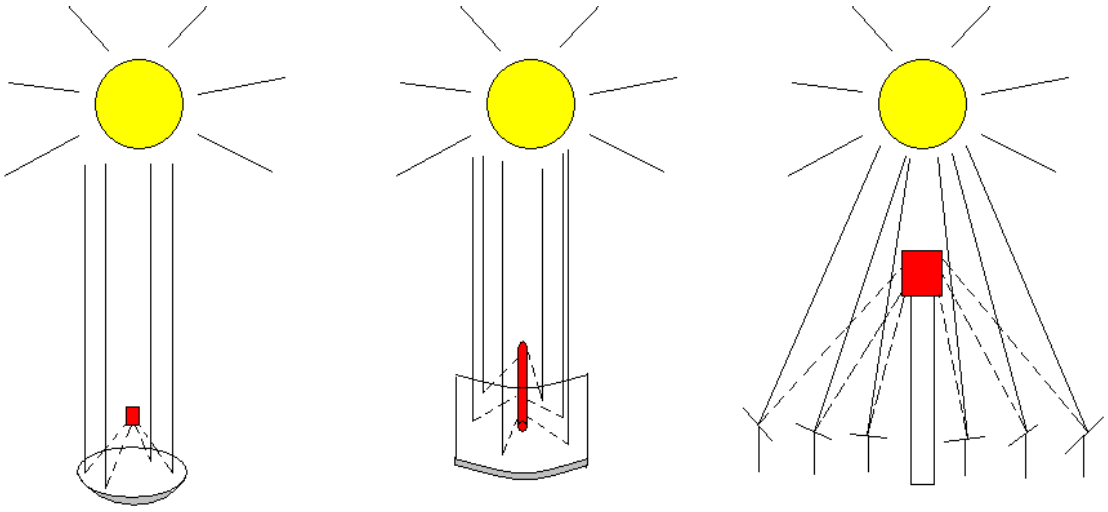

Figure 2.12 Different methods of concentration (dish, trough and tower).

Another group of solar collectors produces very high energy fluxes by accurately tracking the sun (but not always) and by using focusing devices. This is done by using focusing devices connected to a basic absorber-receiver. According to Kreith and Kreider (1978), the highest operating temperatures for concentrated solar power can be as high as 4 000 K. Kreith and Kreider (1978) estimate that the cost of concentrated solar power in the right locations will not be more than that of nuclear power. Figure 2.12 shows the different methods of concentration as dish, trough and

tower. Some other interesting collectors also exist. The hot-line collector uses a wedge-shaped absorber channel and has efficiencies of around 90%. A curved Fresnel lens collector was developed by the Northrup plant in Texas. The compound parabolic concentrator is similar to the natural structure of the eye of the horseshoe crab – one of the most efficient light-gathering structures known (Cheremisinoff and Regino, 1978). Duffie and Beckman (1991) regard honeycombs, compound parabolic concentrators, concentrating collectors and evacuated tubular collectors as recent developments in collector heat loss control or collector efficiency.

Thermodynamic limits to concentration exist. Kreith and Kreider (1978) and Duffie and Beckman (1991) give the theoretical upper limit of concentration for 2D (linear concentration) and 3D concentrators: the maximum linear concentration ratio is in the order of 200, while the maximum 3D concentration ratio is in the order of 40 000. According to Kreith and Kreider (1978), the concentration ratio of single-curvature concentrators (troughs), is usually less than 50, with delivery temperatures of 300°C, while the concentration ratio is higher than 30 and up to several hundreds for double-curvature units. Kreith and Kreider (1978), Stine and Harrigan (1985) and Duffie and Beckman (1991) refer to a *concentration ratio* as the ratio of the net collecting aperture area to the area of the receiver or absorber. Data obtained for solar tower plants by Schwarzbözl et al. (2006) show that the total reflective area divided by the total receiver aperture (or concentration ratio, CR) is on average more or less 700. According to Figure 2.13, a parabolic dish collector should be used when receiver temperatures of between 500 and 1 000°C are required. The shaded area shows the probable range of operation. Figure 2.14 also shows the typical temperatures achievable by concentrating solar collectors.

The high temperatures required for the Brayton cycle would not allow it to be used with troughs. Trough technology cannot reach the high temperatures required. Double-curvature units should be used with a point cavity receiver (Stine and Harrigan, 1985). Figure 2.15 roughly indicates the optimum operating ranges of the different power cycles. A similar figure (Figure 2.16) is given by Wilson (1979) for different concentration optics without a specification of the working fluid used or its mass flow rate.

Figure 2.17 provides another representation of the relationship between fluid temperature and concentration ratio. This figure gives a general guideline of the concentration ratio to be used for a given temperature. The thermal efficiency of the receiver shown in the figure is defined by the ratio of the useful heat to the incoming solar radiation in the receiver aperture. Pitz-Paal (2007) concludes the following from this figure: higher fluid temperatures lead to lower receiver efficiencies, higher concentration factors lead to higher efficiencies and convection and conduction losses are of minor importance at high concentration factors.

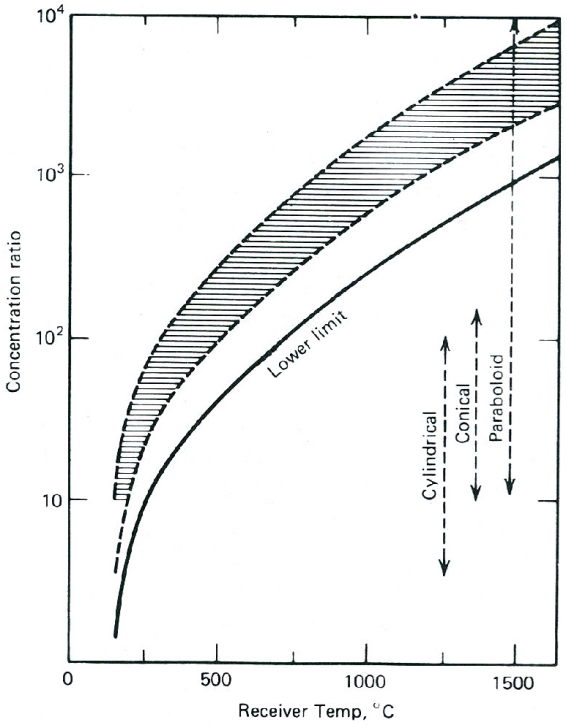

Figure 2.13 Relationship between concentration ratio (area of concentrator divided by the area of receiver) and temperature of receiver operation. The shaded range represents a probable range of operation (Duffie and Beckman, 1991).

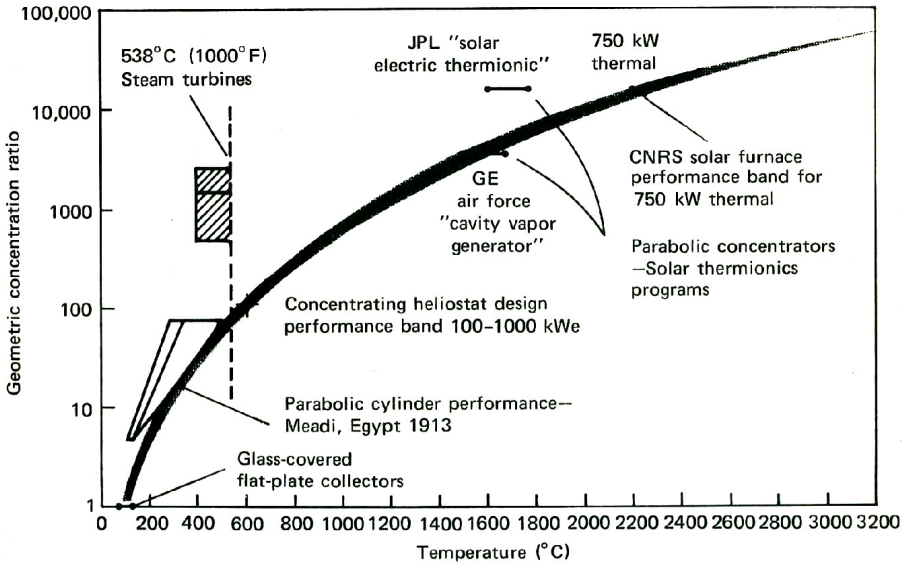

Figure 2.14 Typical temperatures achievable by concentrating solar collectors (Kreith and Kreider, 1978).

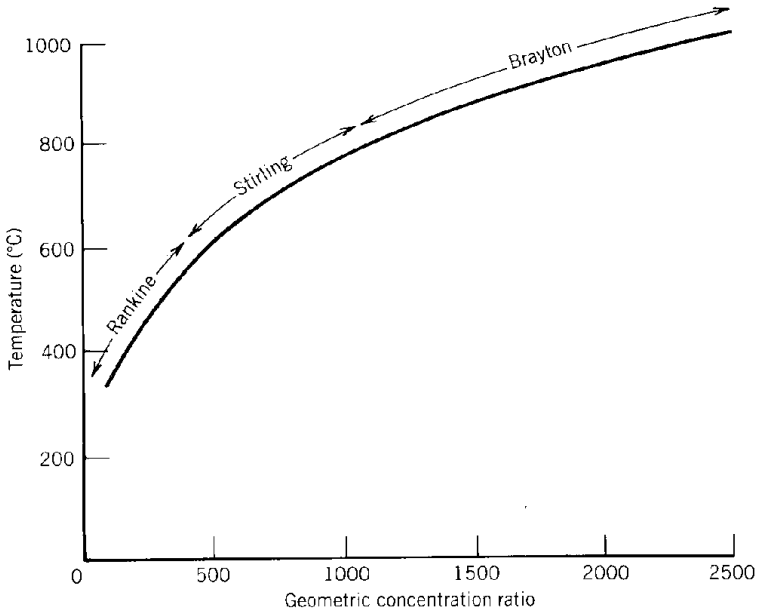

Figure 2.15 Optimum operating temperature change with geometric concentration ratio (Stine and Harrigan 1985).

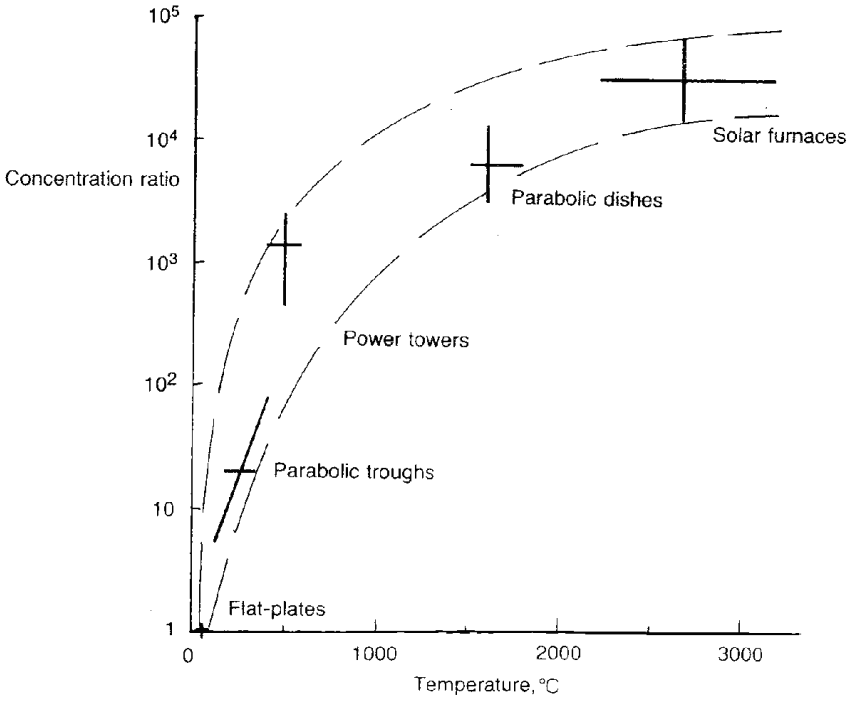

Figure 2.16 Temperature reached by solar absorbers using concentration optics (Wilson, 1979).

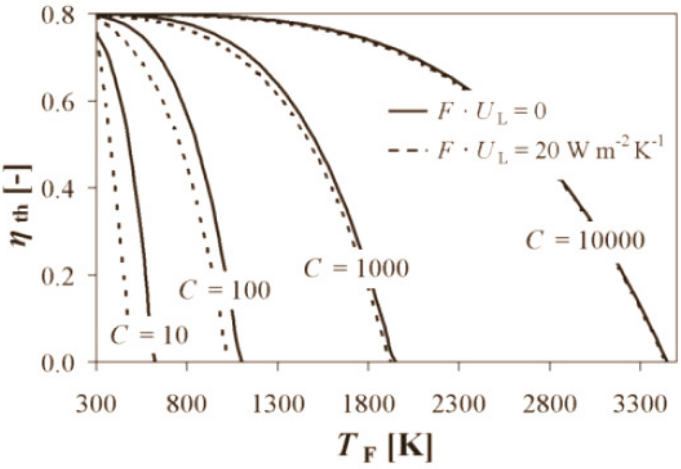

Figure 2.17 The thermal efficiency of a receiver as a function of the fluid temperature and the concentration factor (Pitz-Paal, 2007).

Figures 2.18 and 2.19 conclude that selective absorber properties significantly increase a receiver's performance, specifically in the case of low concentrating systems and high temperatures. In practice, however, selective coatings are only available up to a temperature of about 800 K, so that selective coatings are irrelevant for high-temperature solar concentrators. Pitz-Paal (2007) suggests that a possible solution is the use of a cavity receiver. The concentrated radiation enters through a small aperture in a thermally insulated cavity. The actual absorbers are distributed on the inner-cavity walls (Pitz-Paal, 2007).

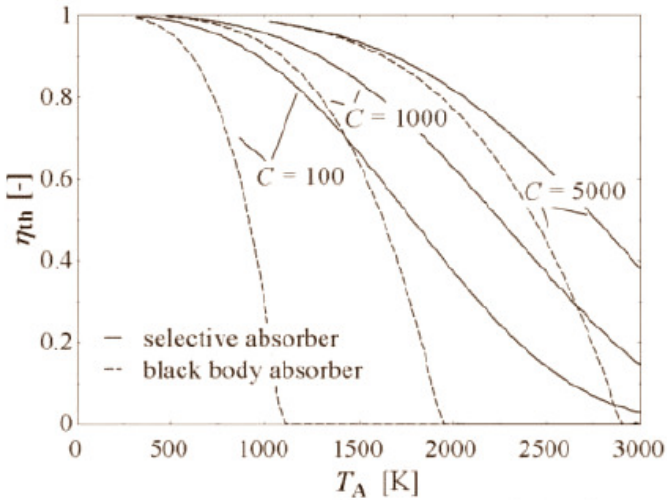

Figure 2.18 The thermal efficiency of a receiver as a function of the absorber temperature and the concentration factor. The use of a selective absorber and a blackbody absorber is considered. Convection heat losses are neglected (Pitz-Paal, 2007).

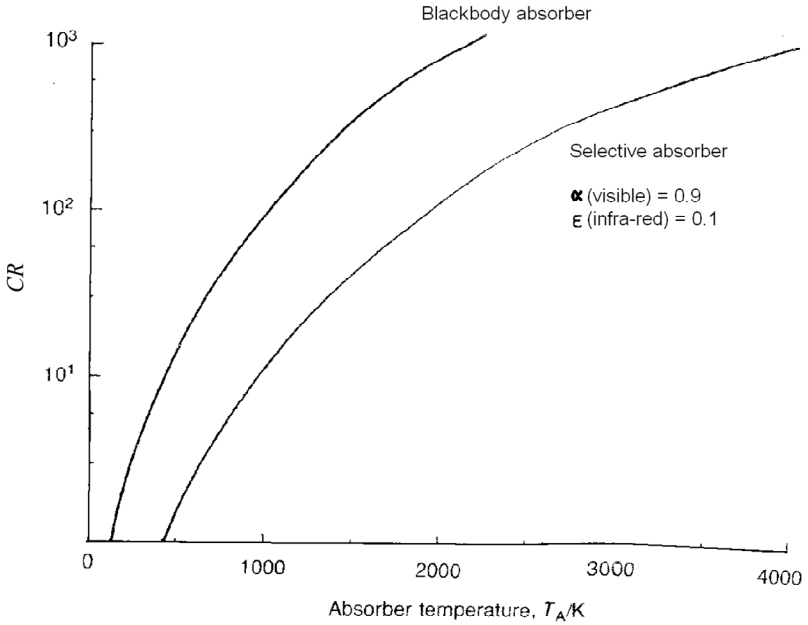

Figure 2.19 Expected stagnation temperatures of evacuated solar collectors with concentrators, where α and ε describe the properties of the selective absorber (Wilson, 1979).

Bejan (1997) found that the optimisation of a collector and engine arrangement can consist of selecting not only the collector temperature but also the cut-off frequency. Omnicolour series of ideal concentrators were evaluated and it was found that it improved only slightly on the maximum work per area ratio (Bejan, 1997).

2.3.3 Rim angle, tracking and solar irradiation

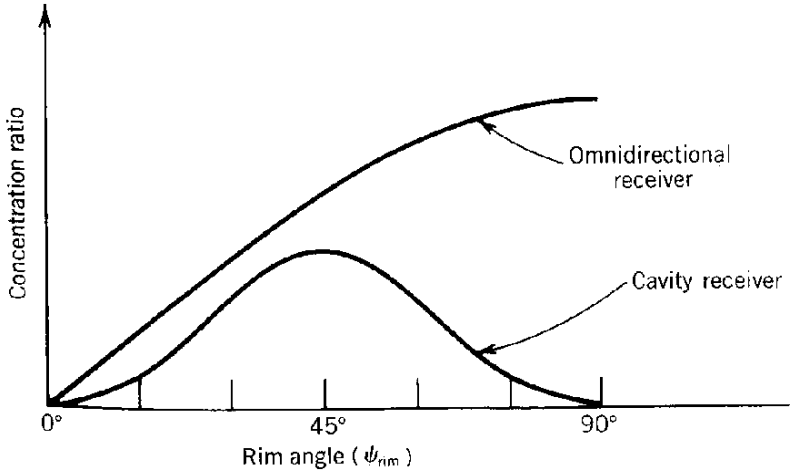

Figure 2.20 Variation of geometric concentration ratio with rim angle (Stine and Harrigan, 1985).

According to Stine and Harrigan (1985), a rim angle of 45° (Figure A.2 in Appendix A, schematically shows the definition of the parabolic dish concentrator rim angle) gives the

maximum concentration ratio for a parabolic dish collector. This is shown in Figure 2.20. This figure also includes the curve for the omnidirectional receiver. Only the trends of these curves are shown and their magnitude relative to each other is not correct.

Concentrated solar thermal power systems usually require tracking of the sun. Two different tracking levels exist: intermittent tilt change or completely fixed and continuously tracking, which is used for high concentration ratios (Duffie and Beckman, 1991). The acceptance angle of focusing collectors decreases with increasing concentration ratio. Stine and Harrigan's (1985) research shows that two-axis tracking can be regarded as the best available tracking method, as shown in Figures 2.21 and 2.22. Focusing collectors must track the sun with a degree of precision that increases with the concentration ratio. If a solar collector moves with two degrees of freedom, it can track the sun at zero incidence angle throughout the day to intercept the maximum amount of beam radiation (Kreith and Kreider, 1978). For the solar thermal Brayton cycle, two-axis tracking will be required.

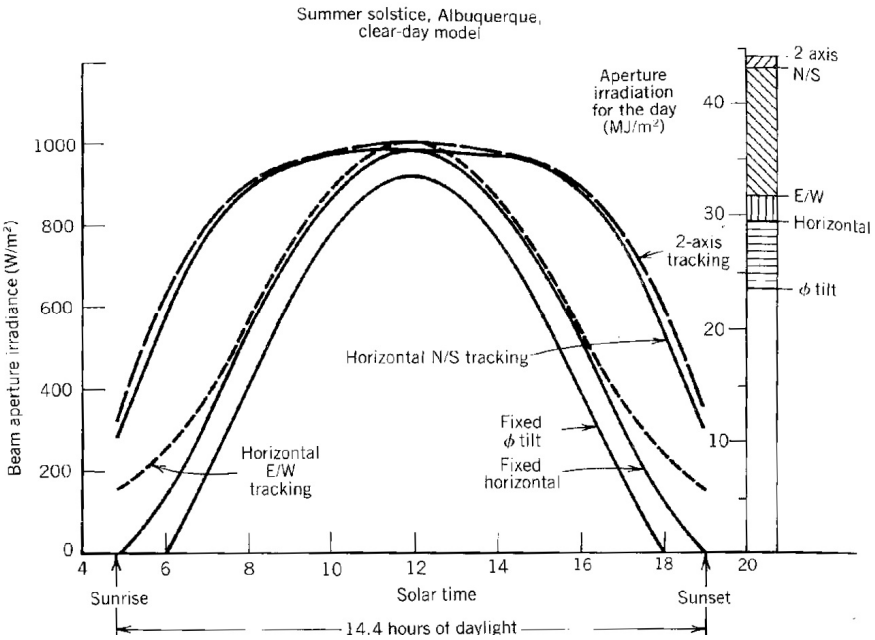

Figure 2.21 Aperture irradiance for different fixed and tracking aperture configurations for Albuquerque, on June 22 (Stine and Harrigan, 1985).

Direct, diffuse and reflected radiations are mentioned as the three different components of solar radiation (Cheremisinoff and Regino, 1978). According to Stine and Harrigan (1985), the radiation falling directly on the earth is 451 – 1 135 W/m^2. The irradiance of Albuquerque (New Mexico, US) can be as high as 1 000 W/m^2 and as low as 500 W/m^2 at noon through summer and winter for different types of tracking methods. Kreith and Kreider (1978) give a value of 300 W/m^2 (in the Red Sea area) as the highest annual mean irradiance (amount of solar radiant energy falling on a

surface per unit area and per unit time). According to Fluri (2009), the solar irradiation in the northern parts of the Northern Cape Province, South Africa, is more than 8 kWh/m^2 in December and 6 kWh/m^2 in June. Most areas in South Africa, however, receive an average of more than 2 500 hours of sunshine per year, with average solar-radiation levels ranging between 4.5 and 6.5 kWh/m^2 per day (DME, 2010). For a steady-state analysis, 1 000 W/m^2 would be an acceptable value for a high irradiance location in South Africa, at noon.

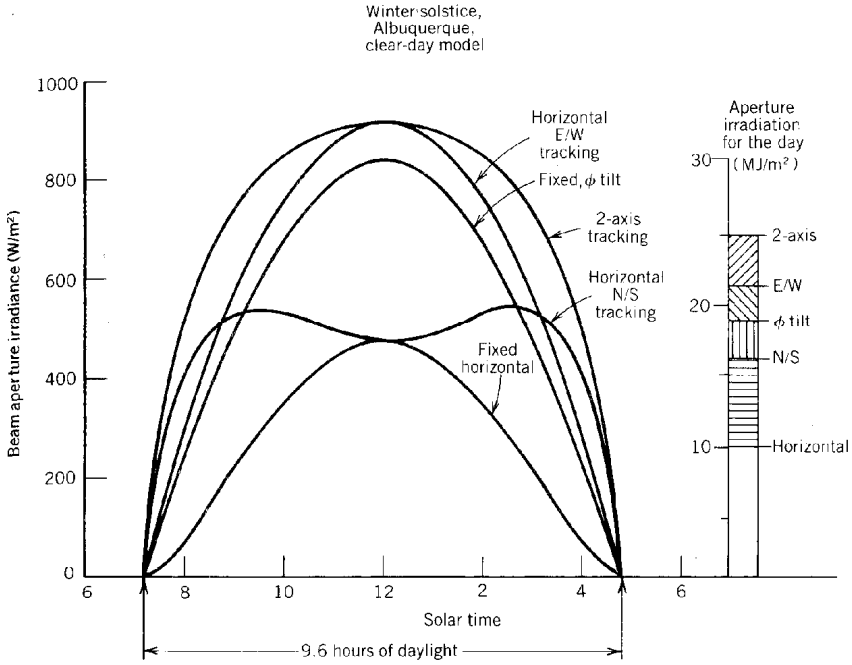

Figure 2.22 Aperture irradiance for different fixed and tracking aperture configurations for Albuquerque, on December 22 (Stine and Harrigan, 1985).

2.3.4 Losses and efficiency

From the literature, it is clear that there are many different collector efficiencies available, each defined differently. According to Howell et al. (1982), there exists a solar collector efficiency (due to inefficiencies in the reflective process). According to Stine and Harrigan (1985), losses associated with reflection typically range from about 5 to 25% and other optical losses that occur in a concentrating collector are transmittance and receiver absorptance. They also mention that a glass cover, which can be used to reduce the convective losses from the receiver, can absorb about 5% of the light energy passing through it. Figure 2.23 shows the specular reflectance of aluminium, silver and gold. Stine and Harrigan (1985) emphasise the importance of good thermal contact between receiver and working fluid, evacuated annulus between glass cover and receiver, a receiver mounted in a cavity (to reduce convection losses) and selective coating for reducing the thermal losses due to radiation. High-absorptance paint has an absorptance of 0.95.

If the absorbing surface is inside a cavity, the effective absorptance increases to about 0.98 (Stine and Harrigan, 1985).

It is clear that collector efficiencies are defined differently. There has yet been no mention of entropy generation in collectors and solar thermal power systems, or the second law of thermodynamics, which would be the focus of this study. A comprehensive section on the second law and the solar thermal Brayton cycle is given in Section 2.6.

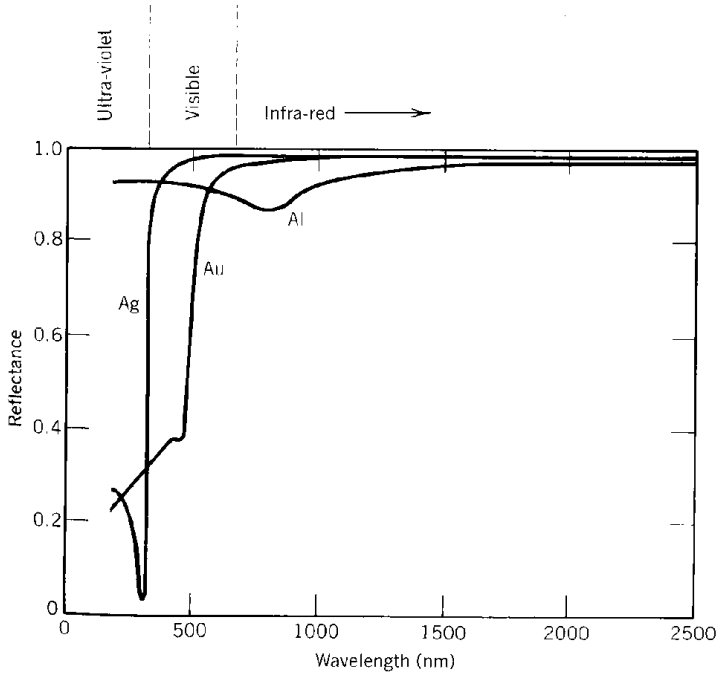

Figure 2.23 Specular reflectance of selected materials: silver, aluminium and gold (Stine and Harrigan, 1985).

2.3.5 Solar receivers

According to Stine and Harrigan (1985), if a black receiver is mounted at the focus of a parabolic dish reflector, the reflected light will be absorbed and converted into heat. According to Bejan (1997), the solar receiver can be viewed as a blackbody that is exposed to blackbody radiation of a higher temperature (as a first-cut model). For the Brayton cycle, large receivers are required due to the low gas heat transfer coefficients (Duffie and Beckman, 1991). Parabolic concentrators reflect light either to a point or a line. The solar receiver intercepts the energy available at this point or line. There are only two widely used receivers: the linear omnidirectional receiver and the point cavity receiver or focal plane receiver. The point cavity receiver can also be used with a parabolic trough when the cavity is linear, but it is commonly used with parabolic dishes (Stine and Harrigan, 1985). The convection and radiation losses are drastically reduced when a receiver is mounted in a cavity with a selective coating. Other types of solar receivers are also found.

Bertocchi et al. (2004) describe the heating of air temperatures to far more than 1 000℃, using a high-temperature solar particle receiver. Heller et al. (2006) demonstrate that volumetric pressurised receivers are able to produce air of 1 000℃ to drive a gas turbine. These receivers are more complex and expensive.

The performance of different cavity receivers was investigated by Shuai et al. (2008), Prakash et al. (2009) and Sendhil Kumar and Reddy (2008). Figure 2.24 shows a typical cavity receiver. According to Pitz-Paal (2007) the inherent characteristic of a cavity receiver aperture is that a blackbody is approximated.

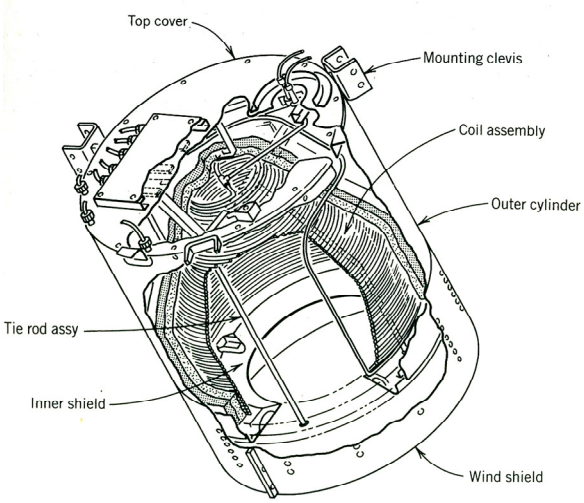

Figure 2.24 A typical cavity receiver (Stine and Harrigan, 1985).

The thermal losses of a cavity receiver include convective and radiative losses to the air in the cavity, as well as conductive heat loss through the insulation used behind the helical tube surface. Shuai et al. (2008) investigated different classical cavity geometries and found that cavity geometry has a significant effect on overall distribution of radiation flux in the cavity receiver. According to Shuai et al. (2008), an upside-down pear cavity might be a desirable shape. Prakash et al. (2009) investigated heat losses from a solar cavity receiver at different inclination angles, with head-on and side-on winds. According to Prakash et al. (2009), the thermal and optical losses occurring from an open-cavity solar receiver are less when compared with other types of receivers and, hence, such receivers are preferred.

Reddy and Sendhil Kumar (2008) compared different types of cavity receivers numerically and found that their modified cavity receiver experienced lower convection heat losses than those of the other receivers and suggested that it may be preferred in a solar dish collector system. A numerical investigation of natural convection heat loss (Sendhil Kumar and Reddy, 2007), an

investigation of the contribution of radiation losses (Reddy and Sendhil Kumar, 2008) and an improved model for natural convection heat loss were presented for the modified cavity (Reddy and Sendhil Kumar, 2009). Figure 2.25 shows the modified cavity receiver.

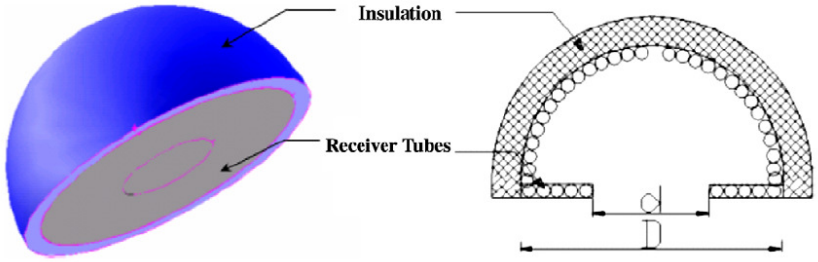

Figure 2.25 Modified cavity receiver (Reddy and Sendhil Kumar, 2009).

Sendhil Kumar and Reddy (2008) suggest the use of their modified cavity receiver with an area ratio of

$$A_w / A_a = 8 \tag{2.1}$$

where A_w is the inner-surface area of the cavity and A_a the aperture area. This area ratio gives the minimum heat loss. Figure 2.26 shows this cavity receiver.

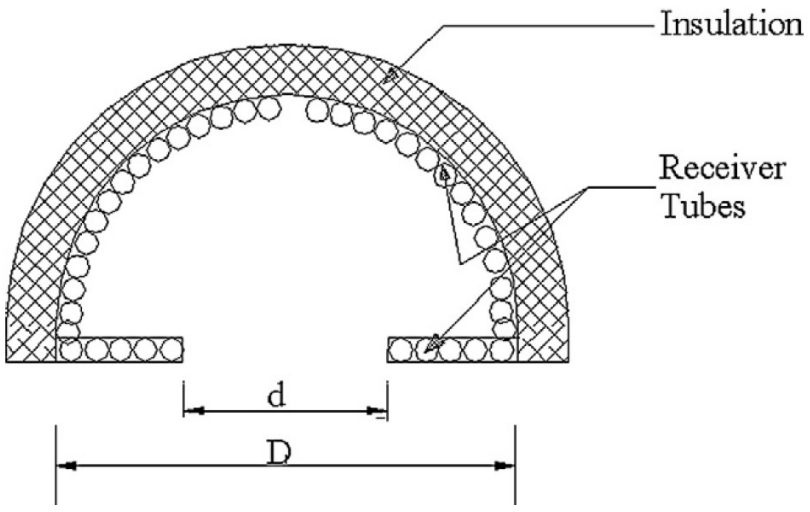

Figure 2.26 Modified cavity receiver (Reddy and Sendhil Kumar, 2008).

The areas of the aperture and the inner wall can be calculated with the following equations respectively:

$$A_a = \frac{\pi d^2}{4} \tag{2.2}$$

and

$$A_w = \frac{3\pi D^2}{4} - A_a \tag{2.3}$$

For a specific concentrator diameter (with constant focal length and rim angle), the net rate of heat absorbed by the working fluid in the receiver depends on the receiver aperture diameter. The sun's rays are not truly parallel and concentrator errors exist, which means that the reflected rays form an image of finite size centred around the focus, instead of a focal point.

Thus, the geometry of a cavity receiver can determine the amount of heat available to be transferred to the working fluid. A receiver can be optimally sized, since the aperture area of the solar receiver will determine the amount of heat intercepted, but also the amount of heat lost due to convection and radiation. The larger the cavity aperture, the more heat can be intercepted, but also the more heat can be lost due to convection and radiation (Stine and Harrigan, 1985). For a fixed dish concentrator area, the amount of heat available for the working fluid, which is the intercepted heat absorbed minus the heat lost due to radiation and convection, is a function of the cavity aperture diameter.

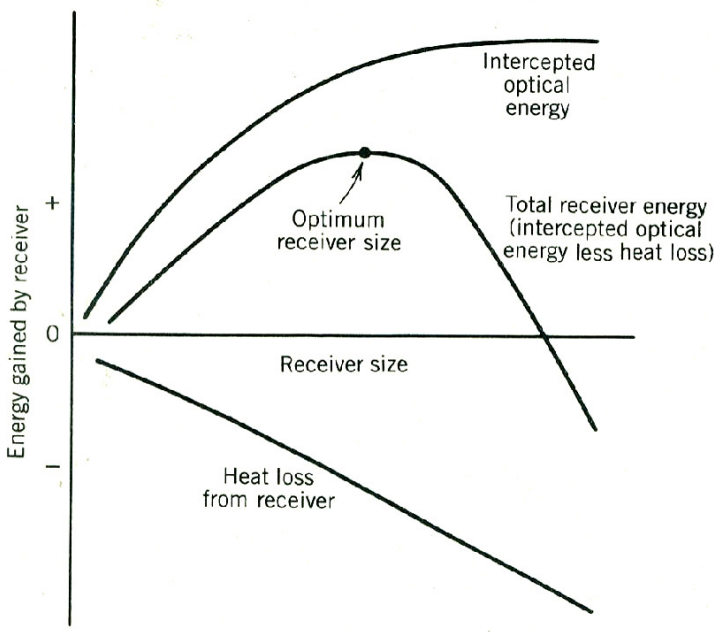

Figure 2.27 Sizing of a collector receiver (Stine and Harrigan, 1985).

Figure 2.27 shows the sizing of receivers in general. There exists a cavity aperture area which allows the maximum net absorbed heat. Steinfeld and Schubnell (1993) present a semi-empirical method to determine the optimum aperture size and optimum operating temperature of a solar cavity receiver, which has a maximum energy conversion efficiency. Figure A.1 in Appendix A, shows the logical flow for a receiver sizing algorithm of Stine and Harrigan (1985) which can be used with a fixed dish concentrator area to get the amount of energy available (intercepted) for a specific cavity aperture area. Appendix A explains the method in which the algorithm is used.

Narendra et al. (2000) believe it is important that extensive work is carried out in the field of material constraints to make solar thermal power a real success because the material constraints of the solar receiver play an important role in exergy loss. This is because the high quality solar energy is used to heat the fluid at a much lower temperature due to the temperature constraint. It is thus important to know what the maximum or melting surface temperature of the receiver could be. This depends on the material used. The melting temperature of copper is 1 084 °C / 1 357 K. According to the Copper Tube Handbook (Copper Development Association, 2006), standard brazing fluxes can protect up to temperatures of 871 °C / 1 144 K and special brazing fluxes up to 1038 °C / 1 311 K.

Thus, a cavity receiver (which can withstand high temperatures) should be used for the solar thermal Brayton cycle. A receiver aperture sizing algorithm should be used to determine the available heat for the power cycle. A heat loss model for the modified cavity receiver is available (Reddy and Sendhil Kumar, 2009).

2.4 Heat exchangers in general and the recuperator

Heat exchangers are required to be efficient, economical, safe, simple and convenient (Yilmaz et al., 2001). Heat transfer and pressure losses as well as the optimisation of size, weight and price should be taken into consideration while the heat exchanger is being designed (Oğulata et al., 2000). According to Bejan (1982), heat exchanger irreversibilities can be reduced by slowing down the movement of fluid through the heat exchanger which is synonymous with employing larger heat exchangers. The irreversibility of a fixed-area heat exchanger can be reduced by properly distributing or arranging the area (Bejan, 1982).

A recuperator (heat exchanger) can be used in the Brayton cycle (Figure 2.4) to extract the heat from the turbine outlet and transfer it to the cold stream before it is heated by the heat source. Kreith and Kreider (1978) suggest that counterflow heat exchangers should be used in solar thermal power systems and parallel-flow heat exchangers should be avoided. They suggest the

use of a heat exchanger penalty, which decreases as heat exchanger effectiveness increases. According to data given by Çengel (2006), it is concluded that the most effective heat exchanger is a counterflow heat exchanger. Bejan (1982) mentions that counterflow heat exchangers find numerous applications in recuperative heating associated with the Brayton cycle. The definitions used for the terms *recuperator efficiency*, according to Çengel (2006), and *effectiveness*, according to Stine and Harrigan (1985), are the same.

Shah (2005) suggests that counterflow plate-type heat exchangers can be used as compact recuperators with micro-turbines. Shah (2005) gives design criteria for micro-turbine recuperators. Some of these criteria are high performance with minimum cost, high exchanger effectiveness, compactness, 40 000 hour operation life without maintenance, low pressure loss (< 5%). According to Shah (2005), the abovementioned criteria translate into a thin foil primary surface recuperator (same surface on both fluid sides) with stamping, folding and welding side edges by an automated operation to form flow passages.

2.5 Summary of literature in Sections 2.2 to 2.4

With the aid of the preceding literature, a few observations were made regarding the solar thermal Brayton cycle, its collector and its recuperator. The open and direct solar thermal Brayton cycle with recuperator, cavity receiver and micro-turbines from Garrett will be used in the analysis. A counterflow plate-type recuperator will be beneficial. A maximum receiver temperature should be specified due to material constraints. The following collector scheme was identified for the power cycle: a parabolic dish concentrator with 45° rim angle, modified cavity receiver, two-axis tracking, concentrator reflectance > 90% and an average irradiance of 1 000 W/m^2.

2.6 The second law of thermodynamics

2.6.1 Background

The second law of thermodynamics is the set of rules which governs all changes occurring in nature. It is an unfortunate case that it is not used enough in design (Sama, 1995). “The first law of thermodynamics states that a certain energy balance will hold when a system undergoes a change of state or a thermodynamic process, but it does not give any information on whether that change of state or the process is at all feasible or not” according to Oğulata et al. (2000). An analysis based on the second law of thermodynamics is necessary for determining the maximum net power output of a solar thermal Brayton cycle.

Shiba and Bejan (2001) regard exergy analysis, irreversibility minimisation, entropy generation minimisation or thermodynamic optimisation and thermoeconomics as the most established

changes in methodology experienced in engineering thermodynamics during the 1980s to 2000. Bejan et al. (1996) present the current status of exergy analysis, EGM (entropy generation minimisation) and thermoeconomics. According to Shiba and Bejan (2001), at the beginning of the 21st century, the focus of engineering thermodynamics was on identifying the mechanisms and system components responsible for thermodynamic losses, as well as the minimisation of these losses subject to global constraints on the system. This includes the minimisation of costs associated with building and operating the energy system.

Bejan (1982) states that the long-term answers to energy questions must rest on a solid thermodynamic foundation and the second law, in particular, should occupy a central place in heat transfer thought. Entropy generation minimisation, according to Bejan (1982), should bridge the gap between three cornerstone subjects: heat transfer, thermodynamics and fluid mechanics. The topic of irreversibility and availability is well covered by Sonntag et al. (2003). In an ideal system, there would be no entropy generation (no irreversibilities). Optimisation studies were carried out for such solar thermal power plants (reversible systems) where the irreversibilities are neglegted. Bejan (1997), for example, optimised a reversible extraterrestrial solar power plant, which was purely focused on radiation heat transfer only. It was found that the receiver area should be about half the size of the radiator area.

Effects which cause irreversibilities, according to Bejan et al. (1996) and Sonntag et al. (2003), are heat transfer through a finite temperature difference, unrestrained expansion of a gas or liquid to a lower pressure, spontaneous chemical reaction, mixing of matter at different compositions or states, friction such as sliding friction as well as friction in the flow of fluids, electric current flow through a resistance, magnetisation or polarisation with hysteresis, and inelastic deformation.

These irreversibilities can be divided into two classes: internal (occurring within a system) and external (occurring within the surroundings). Irreversibilities related to friction, unrestrained expansion and mixing can be regarded as secondary in importance to those of combustion and heat transfer. The irreversibilities of convective heat transfer are due to heat transfer across a non-zero temperature difference and fluid friction (Bejan, 1982; Bejan et al., 1996).

Zimparov et al. (2006a) state that to improve the global thermodynamic performance of a system, “the irreversibilities (entropy generation or exergy destruction) that characterises all the components and processes of the system, must be decreased”. This is done “by spreading the entropy generation rate through the system in an optimal way, by properly sizing, shaping and positioning components” according to Zimparov et al. (2006c).

2.6.2 Exergy

Exergy, or availability, has become an increasingly important tool for the design and analysis of thermal systems since it correctly reveals the principle sites of thermodynamic inefficiencies, owing to irreversibilities. *Exergy* is defined as the maximum theoretical useful work obtainable, as two systems at different states interact to equilibrium (when one of the systems is the environment), with heat transfer occurring with the environment only. Natural resources can be seen as availability reserves (oil, coal, uranium, etc.). The more irreversibilities one has when using these reserves, the greater will be the decrease in availability and the greater the decease in natural reserves (Sonntag et al., 2003). Exergy can thus be destroyed and it can never be negative (Bejan et al., 1996).

2.6.2.1 Closed-system exergy balance

Equation 2.4 shows a closed-system exergy balance (Bejan et al., 1996). From this equation, the following can be concluded: the total number of exergy transfers (into a system) is split up into two parts - the making of an actual exergy change in the closed system between two states and the destruction of exergy (which is a direct function of entropy generation, as shown in the Gouy-Stodola theorem, equation 2.5). Exergy destruction is also known as availability destruction, the irreversibility and the lost work:

$$(E_2 - E_1) = \int_1^2 \left(1 - \frac{T_0}{T_b}\right)\delta Q - [W - p_0(v_2 - v_1)] - T_0 S_{gen} \tag{2.4}$$

$$E_D = T_0 S_{gen} \tag{2.5}$$

It can be concluded that:
Exergy Change = Exergy Transfers - Exergy Destruction.

The exergy transfers in the closed-system exergy balance are split into the exergy transfers associated with the transfer of energies by heat transfer and by work. From equation 2.4 it follows that the work into a system will be regarded as a positive exergy transfer into the system, since the work into a system is regarded as negative. This makes sense since exergy, or available work, should increase when work is put into the system, as opposed to work input, which is regarded as negative, from an energy perspective.

Exergy can also be divided into four components (equation 2.6): physical (function of pressure and temperature), kinetic (function of velocity), potential (function of height) and chemical exergy (not shown in equation 2.6):

$$E_2 - E_1 = (U_2 - U_1) + p_0(V_2 - V_1) - T_0(S_2 - S_1) + (KE_2 - KE_1) + (PE_2 - PE_1) \quad (2.6)$$

The equation for internal energy change (equation 2.7), can be compared with the equation for exergy change (equation 2.6) to show the difference between energy and exergy:

$$(U_2 - U_1) = Q - W - (KE_2 - KE_1) - (PE_2 - PE_1) \quad (2.7)$$

2.6.2.2 Exergy balance for control volumes

Equation 2.8 shows the exergy balance concept extended to a control volume (Bejan et al., 1996; Sonntag et al., 2003), which is more practical. The definitions for specific exergy transfers at inlets and outlets are given in equation 2.9 (Bejan et al., 1996):

$$\frac{dE_{cv}}{dt} = \sum_j \left(1 - \frac{T_0}{T_j}\right)\dot{Q}_j - \left(\dot{W}_{cv} - p_0 \frac{dv_{cv}}{dt}\right) + \sum_i \dot{m}_i e_i - \sum_e \dot{m} e_e - \dot{E}_D \quad (2.8)$$

where

$$e = (h - h_0) - T_0(s - s_0) + \tfrac{1}{2}V^2 + gz + e^{CH} \quad (2.9)$$

against

$$\hat{e} = u + \tfrac{1}{2}V^2 + gz \quad (2.10)$$

The difference between the specific exergy and specific energy can be identified by comparing equations 2.9 and 2.10 respectively (Bejan et al., 1996). Exergy is concerned with giving values from differences between a certain point and the environment while energy is not concerned with its magnitude relative to the environment. The other two terms (concerning velocity and height) stay the same, since velocity's reference point is already zero and height can simply be seen as a distance, regardless of the reference point (although a practical reference point for height in the exergy equation could be sea level). This seems to be the intrinsic difference between energy and exergy: the fact that exergy, unlike energy, uses the environment as its reference point for all

of its components. The exergetic approach seems to be more practical since humans are situated in this environment and one would like to know what the optimal possibilities are for inhabitants of this environment instead of inhabitants of infinite space.

2.6.2.3 Exergetic efficiency

According to Bejan et al. (1996), exergetic efficiency (second law efficiency, effectiveness or rational efficiency) is a parameter for evaluating thermodynamic performance. It provides a true measure of the performance of an energy system from a thermodynamic viewpoint. It is necessary to identify both a product and a fuel for the thermodynamic system being analysed (equation 2.11). Bejan et al. (1996) identify these exergy rates associated with a fuel and product for the compressor, turbine, heat exchanger, mixing unit, combustion chamber and boiler at steady-state. Sonntag et al. (2003) have a similar approach to the efficiency of a heat exchanger, as will be shown later in equation 2.15.

$$\varepsilon = \frac{\dot{E}_P}{\dot{E}_F} = 1 - \frac{\dot{E}_D + \dot{E}_L}{\dot{E}_F} \tag{2.11}$$

According to Bejan et al. (1996), the exergetic efficiency is generally more meaningful and useful than any other efficiency based on the first or second laws of thermodynamics, including the thermal efficiency of a power plant, isentropic efficiency of a compressor or turbine and effectiveness of a heat exchanger. Yilmaz et al. (2001) summarise the interrelations of performance criteria for both exergy and entropy analysis. The exergetic efficiency or second law efficiency, which gives an indication of the degree of thermodynamic perfection, is regarded as of little use for individual plants and units such as heat exchangers and it is stated that it may even lead to false conclusions.

2.6.3 Entropy

Equation 2.12 (second law of thermodynamics) expresses the change of entropy for an irreversible process. According to Sonntag et al. (2003), entropy increase is the change from a less probable to a more probable state and the entropy of a system can be increased in two ways: by transferring heat to it and by having an irreversible process. For the entropy change of an ideal gas, equation 2.13 (Sonntag et al., 2003) can be used with constant specific heat. Consider the design of lifting a weight with a rope. Entropy generation is proportional to additional work wasted for a bad lifting design (Bejan, 1982). Entropy generation can be minimised:

$$S_2 - S_1 = \int_1^2 \frac{\partial Q}{T} + S_{gen} \tag{2.12}$$

$$s_2 - s_1 = c_{p0} \ln \frac{T_2}{T_1} - R \ln \frac{P_2}{P_1} \tag{2.13}$$

From the second law (equation 2.12) follows that only the heat transfer, not work transfer interactions, is accompanied by entropy transfer (Bejan, 1982). Entropy generation is path-dependent and not a thermodynamic property and should not be confused with the thermodynamic property entropy change ($S_2 - S_1$). According to Bejan et al. (1996), the direction of the entropy transfer is the same as that of the heat transfer. Equation 2.14 (Sonntag et al., 2003) gives the expression for the balance of entropy for a control volume:

$$\frac{dS_{cv}}{dt} = \sum \dot{m}_i s_i - \sum \dot{m}_e s_e + \sum \frac{\dot{Q}_{cv}}{T} + \dot{S}_{gen} \tag{2.14}$$

The Gouy-Stodola theorem (equation 2.5) states that the lost available work is directly proportional to the entropy generation in a system (Bejan, 1982; Bejan, 1997; Bejan et al., 1996). Lost available work is a relative quantity that depends on the choice of reference heat reservoir (Bejan, 1982).

Bejan (1982) provides a number of features most guilty of entropy generation (similar to the features guilty of irreversibilities): heat transfer across a non-zero temperature difference, flow with friction, mixing, filling and discharge, compression, expansion and combustion. The overall irreversibility of compression and expansion (in compressors and turbines), is described by the compressor and turbine efficiencies (Bejan, 1982). The definition of these efficiencies is available from Dixon (2005). Bejan et al. (1996) considered the simultaneous effect of heat transfer and fluid friction on entropy generation and showed that they tend to compete with one another when a thermodynamic optimum is needed.

2.6.4 Second law optimisation and examples of entropy generation minimisation (EGM) for individual components and elemental features

The method of entropy generation minimisation is based on equations used to describe entropy generation mechanisms. Appendix B summarises the relevant entropy generation equations available from the literature. A summary of the following literature and its relevance for the solar thermal Brayton cycle is given in Section 2.6.7.

2.6.4.1 Background

In the field of heat transfer, optimisation is mostly carried out at two levels of complexity: optimisation of complete components like heat exchangers and elemental features like fins and ducts. Heat transfer design objectives can be categorised into two large categories: heat transfer augmentation (conductance) problems and thermal insulation problems. In both cases, EGM is the hidden consequence of good engineering thinking applied to both problems. EGM should close the gap between heat transfer and thermodynamics. EGM has shown that optima exist when the thermodynamic optimisation is subjected to finite-size and finite-time constraints (Bejan, 1982; Bejan, 1996).

The following synonyms can be given for EGM: thermodynamic optimisation, finite-time thermodynamics, second law analysis, thermodynamic design, endoreversible thermodynamics and exoirreversible thermodynamics. The field of EGM experienced astonishing growth during the 1980s and 1990s in both engineering and physics. The EGM method relies on the simultaneous application of heat transfer and engineering thermodynamics principles in the pursuit of realistic models, which account for the inherent thermodynamics irreversibility of the heat, mass and fluid flow processes for heat transfer processes, devices and installations (Bejan, 1996).

The first power generation area to use EGM models regularly was that of solar-driven power plants. It was found that, for a solar receiver with convective heat loss, an optimum coupling between the receiver and the power cycle exists, so that the power output is a maximum. The thermodynamic trade-offs can be of two kinds: when an overall size constraint exists, there is an optimal way of allocating the hardware between the different components, while, for a known daily variation of solar heat input, an optimal time-dependent strategy of plant operation exists (Bejan, 1996; Bejan, 1997).

Yilmaz et al. (2001) imply that engineering thermodynamics includes three important types of approaches based on the second law: EGM, exergy analysis and thermoeconomics. Losses due to process irreversibility can be calculated using a second law analysis. According to Yilmaz et al. (2001), the selection of entropy measure as evaluation parameter, rather than exergy measure, has several advantages. Different entropy evaluation parameters are available from Yilmaz et al. (2001): the entropy generation number, augmentation entropy generation number, heat exchange irreversibility norm, Witte-Shamsundar efficiency and the local entropy generation number. These entropy evaluation parameters are mostly used in the literature to perform optimisation with. It works well for EGM of specific individual components.

In the literature, there are many differently defined entropy generation numbers. Yilmaz et al. (2001) present all the different non-dimensional entropy generation numbers, of which the most frequently used number is the number obtained when the entropy generation rate is divided by the capacity flow rate. Very useful references are available from Yilmaz et al. (2001) for optimisation based on entropy generation numbers, for the following heat exchangers: balanced and unbalanced counterflow heat exchangers, cross-flow heat exchangers, external flow heat exchange (like fins), two-phase flow heat exchangers, regenerative heat exchangers, plate-type heat exchangers and shell-and-tube heat exchangers. The entropy generation numbers, or non-dimensionalised entropy generation equations, are used widely in the literature to minimise entropy generation for individual components or elemental features. These equations are based on entropy generation equations, which are available in Appendix B.

2.6.4.2 Applications

2.6.4.2.1 Internal flow

EGM has been applied for internal flow for constant heat flux or constant wall temperature and different cross-sectional shapes. Bejan (1982) and Bejan et al. (1996) determined the optimum tube diameter or Reynolds number for a tube with internal flow using EGM. Ratts and Raut (2004) also determined the optimal Reynolds number for single-phase, fully developed, laminar and turbulent flow with constant heat flux using EGM. They also compared optimal Reynolds numbers and minimum entropy generation for different cross-sections (circular, square, rectangle and equilateral triangle). Ratts and Raut (2004) found that, for the same deviation from optimal Reynolds number in laminar and turbulent flow, the increase in entropy generation is smaller for heat dissipation than for viscous dissipation. A rectangle with an aspect ratio of eight gives the minimum entropy generation in laminar flow and turbulent flow (Ratts and Raut, 2004). Zimparov et al. (2006a; 2006b; 2006c) did the optimisation of various flow geometries using the entropy generation method and assumptions of constant wall temperature or constant heat flux.

2.6.4.2.2 External flow

The length of a plate is the only design variable capable of inducing changes in the rate of entropy generation in external flow. An optimum plate length exists so that the entropy generation rate reaches a minimum, according to Bejan (1982). This result is important in the local optimisation of plate-finned surfaces in heat exchangers. There is competition between heat transfer and fluid mechanics terms to get an optimal body size with minimum entropy generation (Bejan, 1996; Bejan, 1982; Bejan et al., 1996).

2.6.4.2.3 Augmentation techniques

Various authors investigated heat transfer augmentation techniques using an entropy generation analysis. Roughened surfaces, promoters of swirl flow and fins were considered by Bejan (1982). It was found that the use of twisted tape inserts can lead to savings in exergy and that an optimum fin geometry exists, for which the balance between thermal contact irreversibility and fluid drag irreversibility leads to an overall minimum rate of entropy generation. Zimparov (2001) investigated heat transfer enhancements in tubes using a second law analysis, to display inappropriate enhanced surfaces and assist the engineer in designing better heat transfer equipment. Yilmaz et al. (2001) presented various methods which evaluate heat transfer enhancement techniques.

2.6.4.2.4 Local entropy generation

According to Bejan (1996), several authors recommended that commercial computational fluid dynamics packages should have a built-in capacity of displaying local entropy generation rate in both the laminar and turbulent flow regimes. Bejan (1982) presents the entropy generation rate per unit volume and the entropy generation profile or map for Poiseuille flow through a round smooth tube. According to Bejan (1982), the fluid friction irreversibility term is usually neglected in the first law but it is not necessarily negligible in the entropy generation equation.

There are several advantages to evaluating entropy generation in a local sense. In order to determine the entropy generation rates, the coupled momentum and energy equations should be solved. The corresponding entropy generation, using the volumetric rate of entropy generation, can be computed by using the resulting velocity and temperature fields. This would involve the skills of numerical thermoflow. The volumetric entropy generation rate formula may be used to derive irreversibility profiles or maps for convective heat transfer arrangements in which the temperature and velocity gradients are known at each point in the medium (Yilmaz et al., 2001).

Hesselgreaves (2000) performed optimisation of heat exchanger surfaces using local entropy generation. Lerou et al. (2005) did heat exchanger optimisation based on a model which divided the counterflow heat exchanger into a number of elements, each sub-divided into three sub-elements: high-pressure gas-element, material element and low-pressure gas-element. For each sub-element, a heat balance equation for the different heat flows was formulated.

2.6.4.2.5 Heat exchangers

Thermodynamic optimisation can be used for many different heat exchangers in different applications. The irreversibility in a heat exchanger is the sum of the associated irreversibilities of each of the two surfaces of the heat exchanger (Bejan, 1982; Bejan et al., 1996). Work was done

on second law aspects of heat exchanger performance (Bejan, 1982) and ways of reducing irreversibility production were proposed. Two factors, temperature difference and frictional pressure drop, are to blame for irreversibilities in heat exchangers (Bejan, 1982; Oğulata et al., 2000; Yilmaz et al., 2001). Yilmaz et al. (2001) imply that the greatest source of dissipative action comes from fluid friction in the form of pressure drop and they also group evaluation techniques for heat exchangers into two classes: techniques using entropy and techniques using exergy as evaluation parameter. Yilmaz et al (2001) emphasise a second law analysis. Bejan (1982) suggests that an efficient heat exchanger has to be large, which requires large amounts of exergy for consumption during the manufacturing process, exergy loss or capital invested in the hardware. He suggests that a comprehensive optimisation programme, which includes this capital, should be undertaken in the field, in cases of specific units for specific jobs. The exergetic efficiency for a heat exchanger (Figure 2.28) with hot stream (1 - 2) and cold stream (3 - 4) is given by equation 2.15 (Bejan et al., 1996):

$$\varepsilon = \frac{\dot{E}_3 - \dot{E}_4}{\dot{E}_1 - \dot{E}_2} \tag{2.15}$$

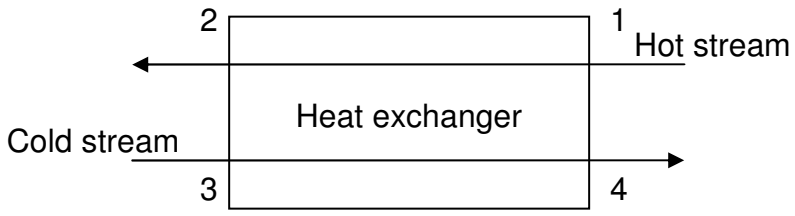

Figure 2.28 Heat exchanger with hot stream (1 – 2) and cold stream (3 – 4).

Sarangi and Chowdhury (1982) expressed the entropy generation in a counterflow heat exchanger and a nearly ideal heat exchanger. The contribution of fluid friction to the entropy generation was neglected. Adiabatic ends were also assumed for the heat exchanger with no heat loss to the surroundings.

Exergetic optimisation was done for tubular heat exchangers. Cornelissen and Hirs (1997) did an exergetic optimisation of a heat exchanger by taking into account the irreversibilities due to frictional pressure drop, the temperature difference between the hot and cold stream and also the irreversibilities due to the production of the materials and the construction of the heat exchanger. Cornelissen and Hirs (1997) mention the LCA method (life cycle analysis), which includes the exergetic effects of all the phases of production, use and recycling, on the environment. A balanced water-to-water counterflow heat exchanger was optimised, neglecting heat loss to the

environment from the heat exchanger and heat resistance of the tube walls. Zimparov (2001) included the effect of fluid temperature variation along the length of a tubular heat exchanger.

Second law analysis and optimisation were done for heat exchangers with ideal gas flow. Hesselgreaves (2000) considered heat exchangers with zero and finite pressure drop. When looking at zero pressure drop, Hesselgreaves (2000) included balanced counterflow, flow imbalance, unbalanced counterflow, parallel flow, condensing on one side and evaporation on one side. The optima for these cases were given. Hesselgreaves (2000) found that, for zero pressure drop, flow imbalance increases entropy generation. Also, it is advantageous to let the highest capacity rate stream be the hot stream. Hesselgreaves (2000) suggests that counterflow should be used, rather than parallel flow, if the heat capacity ratio is small.

Oğulata et al. (2000) did an analysis for a cross-flow plate-type heat exchanger with unmixed fluids and balanced cross-flow. A recuperative plate-type heat exchanger generally used in air or gas applications was examined. Thermodynamic analyses for the balanced cross-flow recuperative plate-type heat exchanger with unmixed fluids were done by Oğulata et al. (2000). Ordóñez and Bejan (2000) did an in-depth numerical optimisation for the parallel-plate heat exchanger with two-fluid ideal gasses, fully developed flow and laminar or turbulent flow. This was done by determining the heat exchanger's architecture using EGM and by constraining the size of the hardware (volume constraint and constraint on the mass of the heat exchanger). All of the lengths which defined the geometry of the heat exchanger were non-dimensionalised.

Ordóñez and Bejan (2000) also included the effect of discharge on entropy generation in a separate analysis of the heat exchanger. Hesselgreaves (2000), Oğulata et al. (2000) and Ordóñez and Bejan (2000) suggest that the $\varepsilon - NTU$ (effectiveness – number of transfer units) method, based on the second law of thermodynamics, can be used to get the outlet temperatures and the total heat transfer from the hot fluid to the cold fluid.

EGM has been utilised in various other applications. Shiba and Bejan (2001) optimised a counterflow heat exchanger that served as a condenser in a vapour-compression-cycle refrigeration system for environmental control of aircrafts with three degrees of freedom and which was subject to two global constraints. It was shown that the minimisation of the total power requirement was completely equivalent to the minimisation of entropy generation rate in the entire installation.

Ishikawa and Hobson (1996) established a thermodynamic optimum surface area for a heat exchanger in an acoustic standing wave (thermoacoustic engine) by minimising entropy

generation due to fluid flow and heat transfer losses. Lerou et al. (2005) optimised a counterflow heat exchanger geometry through minimisation of entropy generation for a cooling cycle in cryogenics. They showed that the width, height and length of the flow channels can be optimised by minimising the entropy. In many counterflow heat exchangers, the heat flow through the material in the longitudinal direction is neglected in determining the temperature profile over the heat exchanger. Equation 2.16 (Bahnke and Howard, 1964, cited in Lerou et al., 2005) is a dimensionless parameter that can be used to see if longitudinal conduction can be neglected or not. k is the thermal conductivity of the heat exchanger material and A_c the cross-sectional area. The longitudinal conduction cannot be neglected if λ_{BH} >10^{-2}.

$$\lambda_{BH} = \frac{kA_c}{L\dot{m}c_{p,\min}} \tag{2.16}$$

For heat exchangers used in cryogenics, this parameter might be in the order of 0.01, while for heat exchangers used in solar thermal applications, the parameter is in the order of 10^{-5}, which means that longitudinal conduction through the material can be neglected in determining the temperature profile over the heat exchanger in these systems.

2.6.5 Solar radiation and the second law of thermodynamics

2.6.5.1 Background

Bejan (1982) presents the topic of exergy waste in solar receivers. He mentions three main features that cause thermodynamic irreversibilities in the operation of any solar receiver: heat exchange between the sun and receiver, receiver-ambient heat loss and the internal irreversibility in the receiver (that is upstream, downstream and inside the receiver). Bejan (1982) applied the concept of irreversibility minimisation to a number of simple solar receiver systems: isothermal receivers, non-isothermal receivers (where a stream of single-phase fluid is circulated through the receiver) and time-varying conditions. These relevant equations for the total rate of entropy generation and entropy generation numbers are given in Appendix B.

Narendra et al. (2000) present an exergetic analysis of a solar thermal power system using the Rankine cycle. The energy analysis showed that losses took place at the condenser of the heat engine part, while the exergetic analysis showed that the collector-receiver assembly was the part where the maximum losses occurred.

2.6.5.2 The exergy of sunlight

When deriving the entropy generation rate at the solar receiver, one firstly needs to better understand the exergy of sunlight. Çengel (2006) presents the topics of thermal radiation and radiation heat transfer from a heat transfer view. According to Çengel (2006), the electromagnetic radiation emitted by the sun is known as solar radiation and nearly all of it falls in the wavelength band of 0.3 – 3 μm. Almost half of the solar radiation is light (visible) and the remaining part is ultraviolet and infrared.

The exact exergy of solar radiation depends on direct and diluted radiation components, the time of day, season of the year, geographic location, and local weather and landscape. It could be determined with spectral measurement and calculation according to Petela (2010). The concept of solar exergy maps was also developed (Joshi et al., 2009).

The solar exergy field was covered extensively by Bejan (1982), who regarded the mission of harvesting solar energy as the placing of exergy at the disposal of humanity for consumption. The sun is regarded as an exergy-rich source and qualifies as a high-temperature fuel. Bejan (1997) presents the thermodynamic properties of thermal radiation in detail. A shift from the heat transfer view of thermal radiation to the thermodynamic view is presented. Bejan (1982; 1997) presents the entropy and exergy (emitted per unit area and per unit time) of blackbody radiation respectively. The entropy of blackbody radiation was found to be a function of temperature only. A collection and interrelation of the fundamental concepts about the second law analysis of thermal radiation are available (Agudelo et al., 2010).

Bejan (1997) gave the entropy generation involved with the transformation of solar radiation into mechanical power (see Appendix B). These include adiabatic free expansion, the transformation of monochromatic radiation into blackbody radiation, scattering and net radiative heat transfer. In the Brayton cycle, adiabatic free expansion and net radiative heat transfer can be excluded. When considering the Gouy-Stodola theorem extended to solar collectors, as described in the literature, Bejan (1982), states that "*the task of maximising the exergy delivered by a collector of fixed cross-section* A_c*, is equivalent to minimising the rate of entropy generation in the 'column' of cross-section* A_c*, extending from the environment temperature* T_0*, to the apparent sun temperature as an exergy source* T^**."* Thus, when the maximum exergy that can be delivered by a collector is considered, the minimisation of the entropy generation rate involved with the transformation of monochromatic radiation into blackbody radiation and the minimisation of the entropy generation rate involved with scattering should be included.

The entropy generation rate due to the transformation of monochromatic/spectral radiation into blackbody radiation, which typically happens at a receiver that is modelled as a blackbody, will be considered first.

2.6.5.2.1 The entropy generation rate involved with the transformation of monochromatic radiation into blackbody radiation

Figure 2.29 gives the entropy increase associated with the constant-energy transformation of monochromatic radiation into blackbody radiation as a function of a dimensionless frequency: $h\nu / kT$. It can be shown that

$$h\nu / kT = 1.439 / \lambda T , \tag{2.17}$$

since it is given that $h\nu / kT$ = 3.921 (the minimum) can be written in terms of the wavelength as: $\lambda T = 0.367$ cmK. This minimum is close to the maximum of the spectral energy distribution located at λT = 0.29 cmK (Çengel, 2006). Thus, for solar radiation falling in the wavelength band of 0.3 – 3 μm, this is equivalent to $0.168 < \lambda T < 1.68$ cmK, where the lowest entropy generation rate is located at λT = 0.367 cmK. This range is also equivalent to: $0.8565 < h\nu / kT < 8.565$. From Figure 2.29, follows that, for this solar radiation range, the entropy increase associated with the transformation of monochromatic radiation into blackbody radiation is close to the minimum.

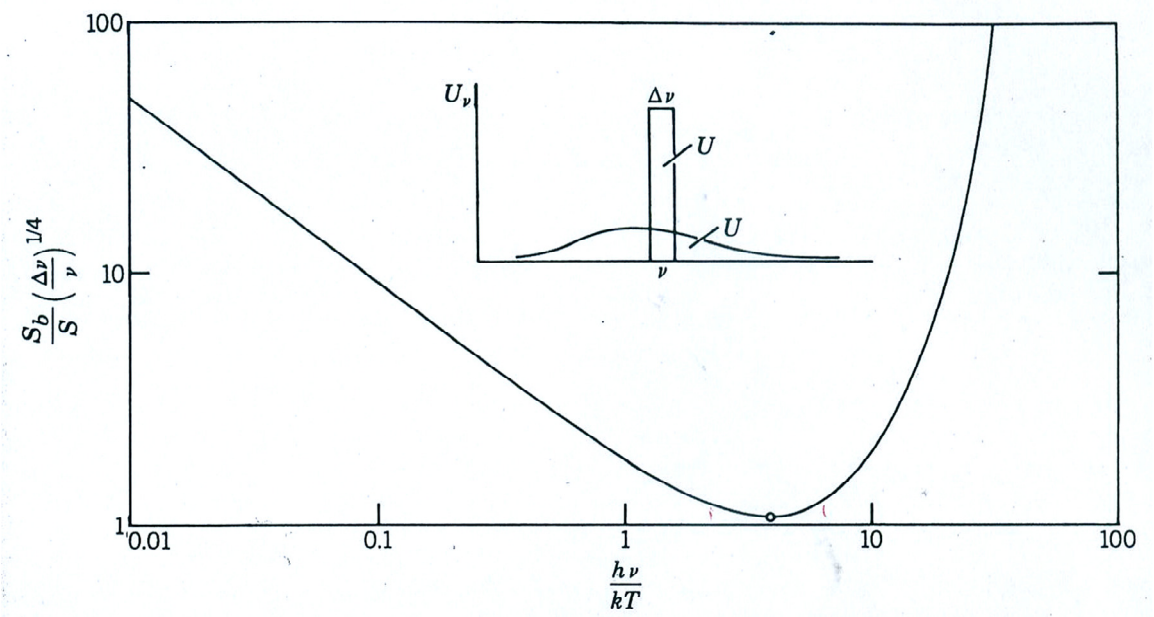

Figure 2.29 The entropy increase associated with the constant-energy transformation of monochromatic radiation into blackbody radiation (Bejan, 1997).

2.6.5.2.2 The entropy generation rate involved with scattering

"In a concentrating device, the maximum theoretical temperature that might be realized at the focal point of a parabolic mirror is that of the radiation beam itself" according to Bejan (1997). When a mirror is assumed to be a specular reflector, this maximum temperature would be the temperature of the sun. One would like to understand the effect of a diffusely reflecting surface on the beam temperature and the entropy generation involved. According to Bejan (1997), scattering from a concentrator decreases the temperature of the original radiation. The decrease in temperature is shown in Figure 2.30 as a function of the dimensionless frequency, hv/kT. From Section 2.6.5.2.1, it is clear that solar radiation falls in the range of $0.8565 < hv/kT < 8.565$. Hence, the temperature ratio from Figure 2.30 will be in the range of 0.07 < T_2 / T_1 < 0.7 due to scattering. With reference to the detail in the top left of Figure 2.30, a solar radiation beam is scattered over a solid angle, $\Omega_2 = 2\pi$ (diffuse reflection by an opaque non-absorbing surface), which is greater than the original angle, Ω_1. T_1 and T_2 represent the monochromatic radiation temperatures before and after scattering.

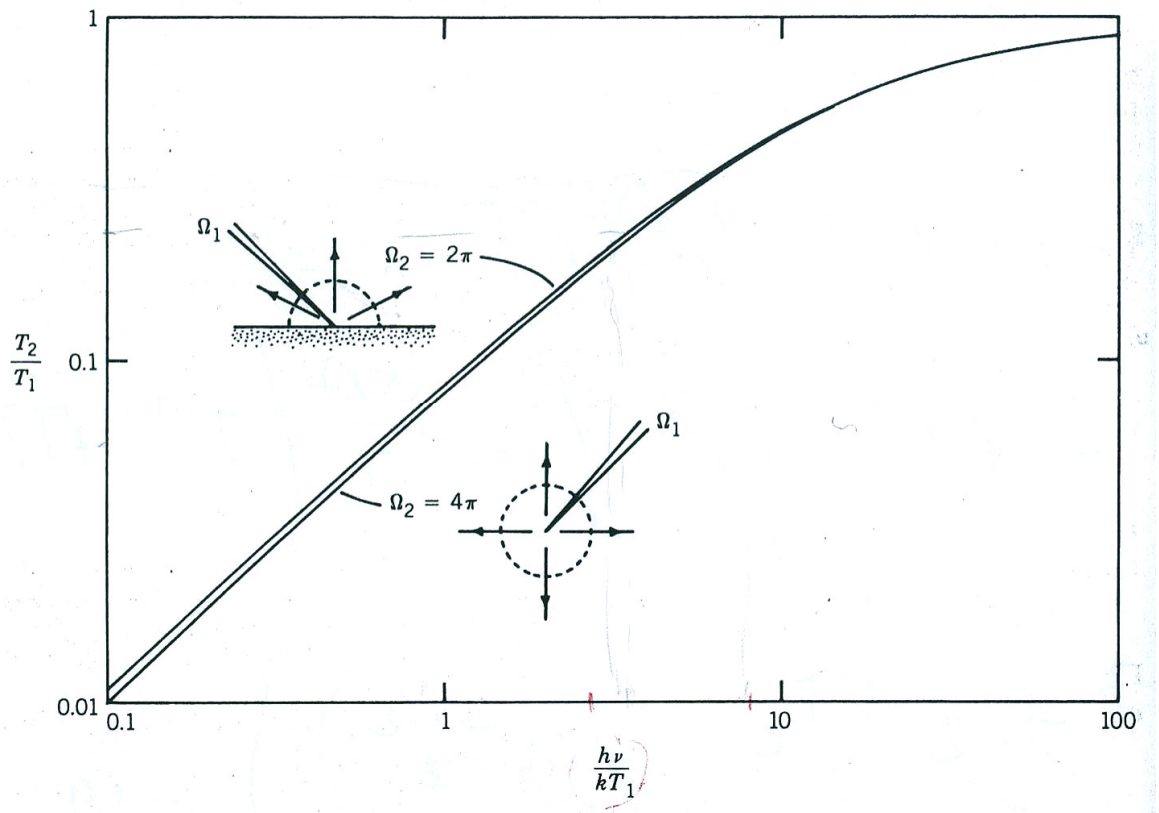

Figure 2.30 The temperature decrease induced by scattering as a function of the dimensionless frequency (Bejan, 1997).

This means that if the sun's temperature is 5 600 K, the monochromatic radiation temperature after scattering would be 393 K – 3 930 K. This temperature decrease causes entropy generation as depicted from the equation given in the entropy generation table (Appendix B, equation 26).

Bejan (1982) gave the exergy of sunlight as:

$$E^* = Q^* \left(1 - \frac{T_0}{T^*} \right) \tag{2.18}$$

where T^* is the equivalent temperature of the sun as an exergy source.

The selection of the control volume around the solar thermal Brayton cycle is very important. If the concentrator is included in the control volume, it has to be kept in mind that entropy is generated at the concentrator due to scattering. The selection of Q^* for this control volume is also very important. Q^* can be chosen to be the heat available at the cavity receiver after the irreversibilities due to scattering and the transformation of monochromatic into blackbody radiation has been deducted.

In this work, the aim is not to determine the precise amount of power available for utilisation at the receiver - methods for determining the exact exergy of solar radiation are available (Petela, 2010; Joshi et al., 2009; Agudelo et al., 2010). The aim is to determine the optimum utilisation of the typical available power at the receiver, with an optimum design.

The available power from the sun varies throughout days, months and environmental conditions. For a steady-state analysis, the power available from the sun is a constant. When assuming a concentrator efficiency, and using a receiver-sizing algorithm (Appendix A) to determine the total intercepted power and heat loss rate at the cavity aperture, the amount of power available for the working fluid in the receiver can be calculated. The aim would then be to determine the optimum utilisation of this available power at the receiver, with an optimum design.

For a control volume around the solar thermal Brayton cycle, the concentrator can be excluded and it can be assumed that T^* = 2 470 K (which is in the range of 393 K – 3 930 K), half of the sun's temperature, since the equivalent temperature of the sun as an exergy source is only 7 - 70% of the sun's temperature after scattering. Bejan (1982) also mentions that Bosjnakovic showed in 1979 that the absolute temperature achievable in a collector is about half of the sun's temperature due to optic limitations.

For the analysis in this work, T^* will be assumed to be 2 470 K at a point between the concentrator and receiver. By doing this, the solar concentrator is not regarded as an entropy-generating mechanism in the analysis. Also, Q^* crossing the boundary of the control volume is the intercepted heat flux at the cavity receiver after the irreversibilities due to scattering and the transformation of monochromatic into blackbody radiation have been deducted.

2.6.6 Exergy analysis for a system as a whole

Narendra et al. (2000) did an exergetic analysis of a solar thermal Rankine heat engine. This analysis was done for the whole system to show the irreversibilities at each part in the system. The collector-receiver assembly was found to be the part where the losses were a maximum. Jubeh (2005) did an exergy analysis for a regenerative Brayton cycle with isothermal heat addition and an isentropic compressor and turbine.

2.6.7 Entropy generation rate equations useful in solar thermal power cycles

Table 2.4 gives a summary of the different entropy generation research fields discussed up to now. This might be a useful starting point for solar thermal power research, where a system with many individual components should be optimised as a whole. This table is useful for identifying entropy generation mechanisms in the solar thermal Brayton cycle. The entropy generation equations from each of these research fields are summarised in the entropy generation table (Appendix B).

The entropy generation rate per unit tube length of circular tube (equation 3, Appendix B) with single-phase fluid and constant heat flux is shown as an example in equation 2.19 (Bejan, 1996). In this equation, D is the tube diameter. This equation shows how thermodynamics is combined with heat transfer and fluid mechanics. An optimum tube diameter, for fixed mass flow rate and heat transfer rate, can be obtained with this equation. When this optimum is available, the entropy generation number can be derived, showing the performance of any design relative to the optimal design. In the literature there are many different ways of non-dimensionalising the entropy generation equations and, therefore, the entropy generation equations are given in Appendix B and not the entropy generation numbers. Appendix B shows all the entropy generation rate equations mentioned in the preceding sections.

$$\dot{S}'_{gen} = \frac{\dot{Q}'^2}{\pi k T^2 Nu} + \frac{32\dot{m}^3 f}{\pi^2 \rho^2 T D^5} \tag{2.19}$$

Table 2.4 A summary of entropy generation literature.

	Entropy generation research field		References
1	**Internal flow**	Internal duct flow (for constant heat flux)	Bejan (1982); Bejan et al. (1996); Hesselgraeves (2000); Yilmaz et al. (2001); Zimparov (2001); Ratts and Raut (2004); Zimparov et al. (2006c)
		Internal duct flow (for constant wall temperature)	Zimparov et al. (2006a)
		Internal duct flow for circular tube (for constant heat flux)	Bejan (1982; 1996); Bejan et al. (1996); Hesselgreaves (2000); Zimparov (2001)
		Internal duct flow for circular tube (for constant wall temperature)	Yilmaz et al. (2001)
		Internal duct flow channel in heat exchanger	Bejan (1982); Bejan et al. (1996); Lerou et al. (2005)
2	**External flow**	External flow	Bejan (1982; 1996); Bejan et al. (1996)
3	**Fins**	For a single fin	Bejan (1982); Bejan et al. (1996)
4	**Local entropy generation**	Local rate of entropy generation (volumetric / 2D)	Bejan (1982); Bejan et al. (1996); Yilmaz et al. (2001); Hesselgreaves (2000)
5	**Heat exchangers**	Counterflow heat exchanger with zero pressure drop	Bejan (1982); Hesselgreaves (2000)
		Counterflow heat exchanger (balanced / unbalanced flow / constant heat flux / ideal gas, etc.)	Bejan (1982; 1997); Sarangi and Chowdhury (1982); Bejan et al. (1996); Cornelissen and Hirs (1997); Ordóñez and Bejan (2000); Yilmaz et al. (2001); Hesselgreaves (2000); Lerou et al. (2005); Zimparov (2001); Ordóñez and Bejan (2000)
		Cross-flow plate-type heat exchanger	Oğulata et al. (2000)
6	**Solar receiver**	Solar receiver (exergy of sunlight, transformation of monochromatic radiation into blackbody radiation, scattering)	Bejan (1982; 1997); Narendra et al. (2000)
7	**Whole system**	Exergy analysis for a solar thermal Rankine heat engine	Narendra et al. (2000)
		Exergy analysis of a regenerative Brayton cycle	Jubeh (2005)

2.7 Useful information, guidelines and points to ponder

- Useful design guidelines, according to Bejan et al. (1996):
  - Keep it simple
  - Consider standard equipment
  - Avoid processes requiring excessively large or small thermodynamic driving forces (differences in temperature, pressure)
  - Maximise the use of co-generation of power
  - Use efficient compressors and turbines
  - Avoid heat transfer at high temperatures directly to the ambient

- Bejan et al. (1996) gave guidelines for evaluating and improving thermodynamic effectiveness:
  - Maximise the use of cogeneration when feasible
  - Minimise the use of combustion
  - Centre efforts on exergy destruction that can actually be avoided
  - Pay more attention to the design of the lower temperature stages of turbines and compressors
  - The lower the temperature level, the greater the need to minimise friction

- Sama (1995) gave very useful guidelines for optimisation using second law insight. Summarised and of most relevance are:
  - Do not use excessively large or small thermodynamic driving forces
  - Do not discard heat at high temperatures to the ambient or to cooling water
  - Try to match heat exchange streams so that final temperature of one is close to initial temperature of the other
  - Choose similar flow heat capacities for the heat-exchanging streams
  - Minimise the use of intermediate heat transfer fluids when exchanging heat between two streams
  - Do not concentrate on the second law inefficiencies which cannot be avoided

- In thermal design and optimisation, two types of independent variables are identified: decision variables (varied in optimisation studies) and parameters (remain fixed). All other variables are dependent variables (Bejan et al., 1996).

- Three problems are encountered in the engineering of solar energy utilisation: low flux density (large surfaces necessary), most solar energy falling on remote areas (transport would be required) and intermittency (little or no power available during bad weather and at night creates a storage need) (Kreith and Kreider, 1978).

- The importance of complying with governmental and environmental regulations throughout the design process as well as the importance of safety, reliability, maintainability and availability (Occupational Safety and Health Acts, published codes and standards, and the Thomas Register) is emphasised by Bejan et al. (1996).

- Shiba and Bejan (2001) argue that the thermodynamic optimisation of the entire system can be pursued on two routes: by either minimising the total power requirement (in the refrigeration case) or by minimising the total rate of entropy generation.

- The internal geometric configuration of a component can be derived by optimising the global performance of the installation that uses the component (Shiba and Bejan, 2001). It is suggested that thermodynamic optimisation by itself (without cost minimisation) may be used in the preliminary stages of design to identify trends and the existence of optimisation opportunities. In the end, the most realistic model is optimised from the start based on cost optimisation. This is also suggested by Ordóñez and Bejan (2000), who furthermore suggest that an entire system can be conceived from the beginning as a system designed to perform certain global objectives optimally, not as an ensemble of already existing parts. According to Bejan et al. (1996), "when a system consists of several components, the overall system should be optimised, since the optimisation of components individually, usually does not guarantee an optimum for the overall system."

2.8 Comments and literature review

The open and direct solar thermal Brayton cycle with counterflow plate-type recuperator, modified cavity receiver and micro-turbines from Garrett will be used in the analysis. A maximum receiver temperature will be specified due to material constraints. A parabolic dish concentrator with 45° rim angle, two-axis tracking and concentrator reflectance larger than 90% will be used.

The second law of thermodynamics and its application in various research fields were shown. EGM was applied in various applications. From the literature, the following general observations and statements can be made:

- Many EGM studies have been done for individual components, but little work has been done on total EGM of overall systems,
- Bejan et al. (1996), Shiba and Bejan (2001) and Ordóñez and Bejan (2000) emphasise that when a system consists of several components, the overall system should be optimised, instead of the optimisation of components individually.

Throughout the literature it is suggested that the overall system should be optimised, since the optimisation of components individually usually does not guarantee an optimum for the overall system. Therefore, the analysis will be done by looking at the solar thermal power system as a whole. Entropy-generating mechanisms can now be identified in the solar thermal Brayton cycle and the total entropy generation can be minimised by optimising the geometry of the components. The apparent temperature of the sun as an exergy source will be assumed to be 2 470 K and at a position between the concentrator and the receiver. An average irradiance of 1 000 W/m^2 will be assumed.

Chapter 3
Problem formulation

3.1 Introduction

This chapter shows how the objective function is formulated and the physical model to be analysed is described. The open and direct solar thermal Brayton cycle will be used in the analysis.

Firstly, the different possibilities of arrangements of components in the solar thermal Brayton cycle are identified to show the uniqueness of the open and direct solar thermal Brayton cycle. The entropy generation rate in each of the heat exchangers and components in the system is identified. The total entropy generation rate for the whole system can be found when adding the entropy generation rates of each component in the system. The net power output of the system can be linked with the total entropy generation rate by doing an exergy analysis for the whole system.

In this chapter, the geometries of the components to be optimised are shown. The objective function is written in terms of the geometry variables. For the objective function, the constraints and assumptions are also listed. The assumption of steady-state is used as was mentioned in Chapter 1.

3.2 Different cases

When a heat source, $\dot{Q}_{net}$, is available (with the use of solar concentration), mechanical power can be generated by means of the solar thermal Brayton cycle. In the following figures, $\dot{Q}_{net}$ represents the net absorbed heat rate by the working fluid in the receiver, or the intercepted power minus the heat loss rate.

For the solar thermal Brayton cycle, there are a few different arrangements of the components to establish a working system. Four cases are shown here, so that the uniqueness of the open and direct solar thermal Brayton cycle can be clear. From the literature, it is concluded that the Brayton cycle has high thermal efficiencies and low compressor pressure ratios when a recuperator is used. A recuperator is used in each of the considered cases. Multistaging is

disregarded, but can be considered for further studies. The benefits and disadvantages of using a direct or indirect system are available in the literature (Stine and Harrigan, 1985).

Case 2 will be used for the analysis. It is the simplest case and has the least components, which means it might also be the cheapest. Minimisation of the entropy generation rate for maximum net power output in the other three cases is recommended for further study to be compared with this work.

3.2.1 Case 1

Figure 3.1 shows a direct system with a closed cycle. The power cycle is closed, meaning that the working fluid cycles through the system and does not exit the system. The radiator cools down the working fluid before it is compressed. The system is also direct – there is no secondary loop which captures the sun's heat and also no heat exchanger to transfer heat between two different working fluids. The solar collector uses the concentrated power of the sun to heat up the working fluid directly.

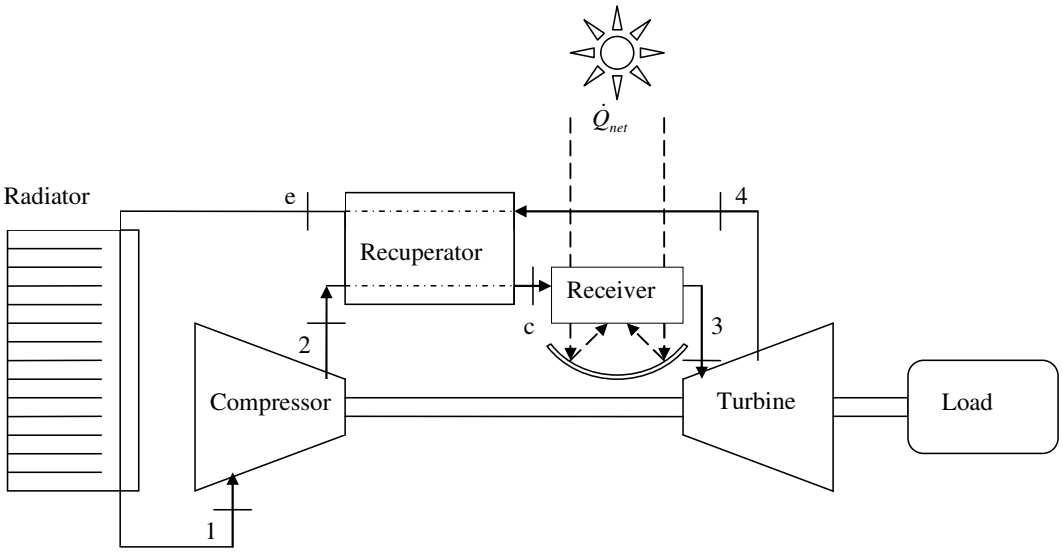

Figure 3.1 Case 1: Direct system, closed cycle.

3.2.2 Case 2

Figure 3.2 shows a direct system with an open cycle (the cycle to be used for this study). The system is open, which means that the working fluid (air) can enter and exit the cycle from and to the surroundings. There is no radiator required, since the air coming in from the surroundings is at the surrounding temperature. It is important that there is a natural flow of air through the system, so that the warm air from the exhaust does not go into the inlet. The system is also direct – there is no secondary loop which captures the sun's heat and also no heat exchanger to

transfer heat between two different working fluids. The solar collector heats up the air directly, using the sun's concentrated power.

3.2.3 Case 3

Figure 3.3 shows an indirect system with a closed cycle. The system is closed, meaning that the working fluid cycles through the system and does not exit the system. The radiator cools down the working fluid before it is compressed. The system is indirect – a secondary loop captures the sun's heat and a heat exchanger transfers heat between the two different fluids.

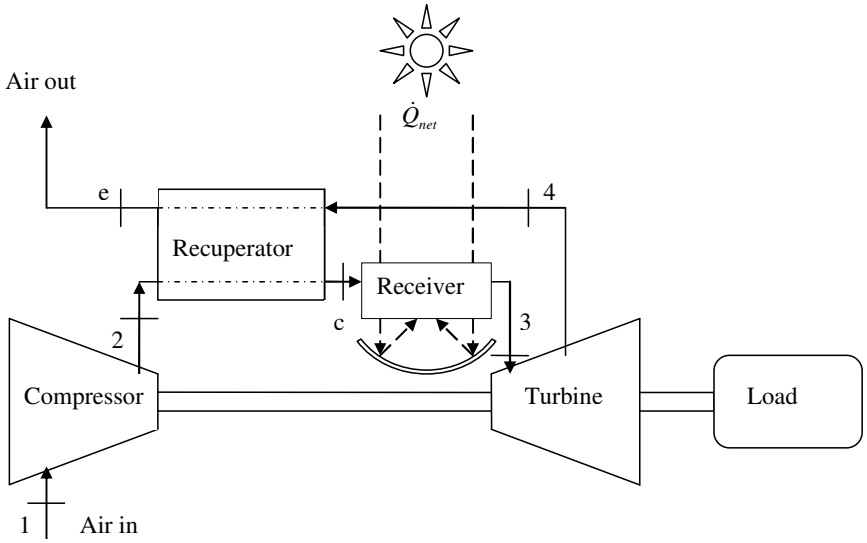

Figure 3.2 Case 2: Direct system, open cycle.

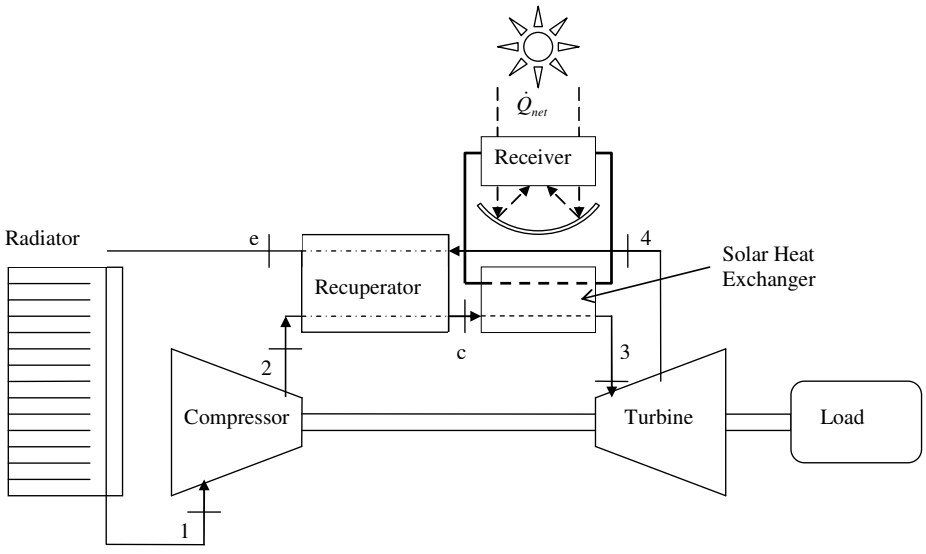

Figure 3.3 Case 3: Indirect system, closed cycle.

3.2.4 Case 4

Figure 3.4 shows an indirect system with an open cycle. The system is open, which means that the air can enter and exit the cycle from and to the surroundings. There is no radiator required, since the air coming in from the surroundings is at the surrounding temperature. It is important that there is a natural flow of air through the system, so that the warm air from the exhaust does not go into the inlet. The system is indirect – there is a secondary loop which captures the sun's heat, and a heat exchanger which transfers heat between the two different fluids.

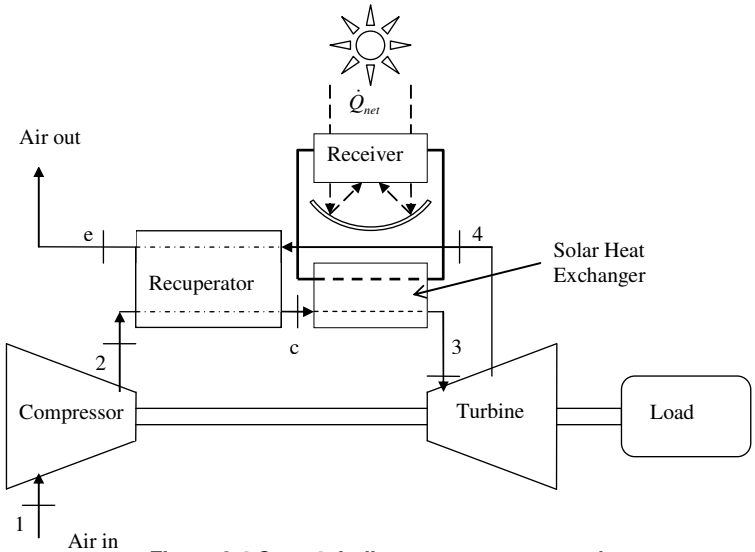

Figure 3.4 Case 4: Indirect system, open cycle.

3.3 Entropy generation in the solar thermal Brayton cycle components

Six different components were identified in the previous section. Not all of them are present in the open and direct solar thermal Brayton cycle. However, it is useful to show the entropy generation rate equations which can be used for each of these six components:

- Solar collector (receiver)
- Recuperator
- Solar heat exchanger (only in indirect systems)
- Radiator (only for closed cycles)
- Compressor
- Turbine

For each of these components, the entropy generation rate is derived using equations 2.12 – 2.14. These equations are then compared with the equations found from the literature in Appendix B.

3.3.1 Solar collector (receiver)

The entropy generation rate in the receiver is given in equation 3.1 for an ideal gas working fluid. Equations 2.13 and 2.14 are employed in the derivation of this equation. $\dot{Q}*$ is the rate of heat transfer from the apparent sun's temperature as an exergy source, $T*$. The rate of heat loss due to convection and radiation is shown in equation 3.2. Equation 3.1 is similar to equations 16, 17, 19 and 24 in the entropy generation table (Appendix B):

$$\dot{S}_{gen} = -\frac{\dot{Q}*}{T*} + \frac{\dot{Q}_0}{T_0} + \dot{m}c_{p0}\ln\left(\frac{T_e}{T_i}\right) - \dot{m}R\ln\left(\frac{P_e}{P_i}\right) \tag{3.1}$$

$$\dot{Q}_0 = \dot{Q}_{loss} = \dot{Q}_{rad} + \dot{Q}_{conv} \tag{3.2}$$

3.3.2 Recuperator

The entropy generation rate in the recuperator is shown in equation 3.3. Again, equations 2.13 and 2.14 are required for its derivation.

$$\dot{S}_{gen} = \dot{m}c_{p0}\ln\left[\frac{T_2T_4}{T_1T_3}\left(\frac{P_2P_4}{P_1P_3}\right)^{(1-k)/k}\right] + \frac{\dot{Q}_{loss,reg}}{T_0} \tag{3.3}$$

The fluid going from T_1 to T_2 is the hot stream and the fluid going from T_3 to T_4 is the cold stream in the heat exchanger as shown in Figure 2.28. This equation is similar to equations 16, 17, 19 and 28 found in the entropy generation table (Appendix B). According to Ordóñez and Bejan (2000) (equation 29 in Appendix B), entropy is also generated due to the discharge at the recuperator in an open cycle - hence equation 3.4. The equation to be used in an analysis depends on the definition of the boundaries of the control volumes of the recuperator and the system.

$$\dot{S}_{gen} = \dot{m}c_{p0}\left[\ln\left[\frac{T_2T_4}{T_1T_3}\left(\frac{P_2P_4}{P_1P_3}\right)^{(1-k)/k}\right] + \frac{T_2 - T_0}{T_0}\right] + \frac{\dot{Q}_{loss,reg}}{T_0} \tag{3.4}$$

3.3.3 Compressor and turbine

Equations 3.5 and 3.6 show the equations for the entropy generation rates for the compressor and turbine. Equations 2.13 and 2.14 were employed to derive these equations. These equations are formulated in terms of the pressures and temperatures, which could be described by the isentropic efficiencies. These equations compare with equation 27 in the entropy generation table (Appendix B).

$$\dot{S}_{gen,c} = \dot{m}c_{p0i-e}\ln\left(T_e/T_i\right) - \dot{m}R\ln\left(P_e/P_i\right) \tag{3.5}$$

$$\dot{S}_{gen,t} = \dot{m}c_{p0i-e}\ln\left(T_e/T_i\right) - \dot{m}R\ln\left(P_e/P_i\right) \tag{3.6}$$

3.3.4 Solar heat exchanger (for indirect systems)

The solar heat exchanger will not be used in this study but its entropy generation rate is shown in equation 3.7. This equation is identical to the equation for entropy generation rate in the recuperator (equation 3.3) with reference to Figure 2.28.

$$\dot{S}_{gen} = \dot{m}c_{p0}\ln\left[\frac{T_2T_4}{T_1T_3}\left(\frac{P_2P_4}{P_1P_3}\right)^{(1-k)/k}\right] + \frac{\dot{Q}_{loss}}{T_0} \tag{3.7}$$

3.3.5 Radiator (used in a closed system)

The radiator is not used in this study but its entropy generation is given for interest's sake. The entropy generation rate depends on the type of heat exchanger used for the radiator. Equation 3.8 is derived for the radiator if fins are used to cool down the working fluid (being an ideal gas) with a natural external flow (being air):

$$\dot{S}_{gen} = \frac{\dot{Q}_B}{T_B} + \dot{m}c_{p0}\ln\left(\frac{T_e}{T_i}\right) - \dot{m}R\ln\left(\frac{P_e}{P_i}\right) \tag{3.8}$$

where the subscript, B, refers to the base where the fins are attached (see Appendix B, equations 10 - 12). According to Bejan (1982), equation 3.8 can also be written as:

$$\dot{S}_{gen} = N\left[\frac{\dot{Q}_{B,sngl}(T_B - T_\infty)}{T_\infty^2} + \frac{F_D V_\infty}{T_\infty}\right] + \dot{m}c_{p0}\ln\left(\frac{T_e}{T_i}\right) - \dot{m}R\ln\left(\frac{P_e}{P_i}\right) \tag{3.9}$$

where it is assumed that $\dot{Q}_B = N\dot{Q}_{B,sngl}$ and N = number of fins.

3.4 Exergy analysis for the system

Consider Case 2 (Section 3.2.2). Taking a control volume around the system and assuming steady-state, it can be determined where exergy is crossing the boundary. This is shown in Figure 3.5.

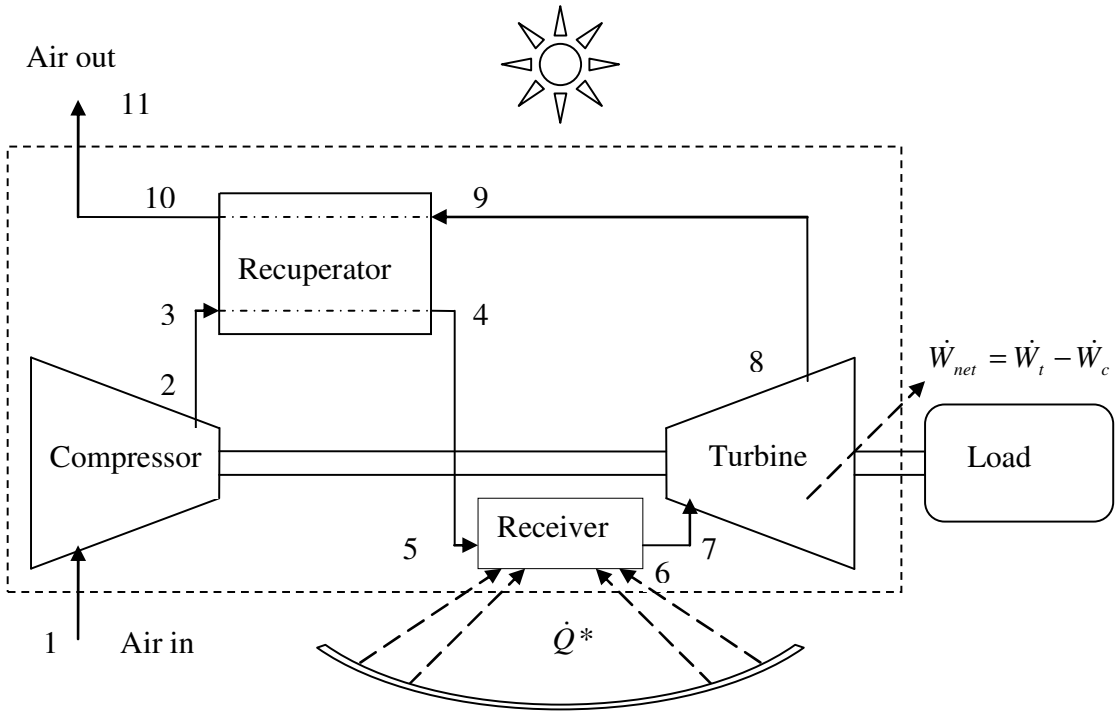

Figure 3.5 Control volume around the open and direct solar thermal Brayton cycle to perform an exergy analysis.

An exergy analysis is performed for the system and it is assumed that $V_1 = V_{11}$ and $z_1 = z_{11}$. Take note that the inlet and outlet temperatures of the system are not the same, but the pressures are. Also note that $T_{10} = T_{11}$ as it is assumed that the control volume boundary is very close to the hot stream exit of the recuperator. The following equation arises:

$$T_0\dot{S}_{gen} = \dot{m}e_i - \dot{m}e_e + \left(1 - \frac{T_0}{T*}\right)\dot{Q}* - \dot{W}_t + \dot{W}_c$$
$$\therefore T_0\dot{S}_{gen} = \dot{m}\left[h_i - h_e - T_0(s_i - s_e) + \frac{1}{2}\left(V_i^2 - V_e^2\right) + g(z_i - z_e)\right] + \left(1 - \frac{T_0}{T*}\right)\dot{Q}* - \dot{W}_{net} \quad (3.10)$$

or

$$\dot{W}_{net} = \dot{W}_t - \dot{W}_c = -T_0 \dot{S}_{gen} + \left(1 - \frac{T_0}{T^*}\right)\dot{Q}^* + \dot{m}c_{p0}\left(T_1 - T_{11}\right) - \dot{m}T_0 c_{p0} \ln\left(\frac{T_1}{T_{11}}\right) \tag{3.11}$$

Furthermore, the total internal entropy generation rate of the system can be written in terms of the sum of the entropy generation rate of each component and duct in the system. Thus, we have the total internal entropy generation rate from Section 3.3 as:

$$\begin{aligned}
\dot{S}_{gen} = \\
&\left[-\dot{m}c_{p0}\ln\left(\frac{T_1}{T_2}\right) + \dot{m}R\ln\left(\frac{P_1}{P_2}\right)\right]_{compressor} + \\
&\left[\frac{\dot{Q}_{loss}}{T_0} + \dot{m}c_{p0}\ln\left(\frac{T_3}{T_2}\right) - \dot{m}R\ln\left(\frac{P_3}{P_2}\right)\right]_{duct23} + \\
&\left[\dot{m}c_{p0}\ln\left[\frac{T_{10}T_4}{T_9T_3}\left(\frac{P_{10}P_4}{P_9P_3}\right)^{(1-k)/k}\right] + \frac{\dot{Q}_{loss}}{T_0}\right]_{recuperator} + \\
&\left[\frac{\dot{Q}_{loss}}{T_0} + \dot{m}c_{p0}\ln\left(\frac{T_5}{T_4}\right) - \dot{m}R\ln\left(\frac{P_5}{P_4}\right)\right]_{duct45} + \\
&\left[-\frac{\dot{Q}^*}{T^*} + \frac{\dot{Q}_0}{T_0} + \dot{m}c_{p0}\ln\left(\frac{T_6}{T_5}\right) - \dot{m}R\ln\left(\frac{P_6}{P_5}\right)\right]_{receiver} + \\
&\left[\frac{\dot{Q}_{loss}}{T_0} + \dot{m}c_{p0}\ln\left(\frac{T_7}{T_6}\right) - \dot{m}R\ln\left(\frac{P_7}{P_6}\right)\right]_{duct67} + \\
&\left[-\dot{m}c_{p0}\ln\left(\frac{T_7}{T_8}\right) + \dot{m}R\ln\left(\frac{P_7}{P_8}\right)\right]_{turbine} + \\
&\left[\frac{\dot{Q}_{loss}}{T_0} + \dot{m}c_{p0}\ln\left(\frac{T_9}{T_8}\right) - \dot{m}R\ln\left(\frac{P_9}{P_8}\right)\right]_{duct89}
\end{aligned} \tag{3.12}$$

Equation 3.12 can then be substituted into equation 3.11 to get the net power output for the open and direct solar thermal Brayton cycle. The net power output is then written in terms of the total entropy generation rate of each of the components and ducts in the system. This equation for the

net power output is the objective function, which should be maximised by optimising the geometry that describes the temperatures and pressures at each point in the system.

3.5 Description of the physical model

An equation is now available describing the net power output of the open and direct solar thermal Brayton cycle in terms of temperatures, pressures, mass flow rate and other constants. The physical models used to describe the geometry of the solar receiver and recuperator will now be shown. Variables also exist, which can be treated as parameters. The objective function can then be formulated in terms of geometry variables and system parameters.

3.5.1 Geometry variables

3.5.1.1 Geometry of the receiver

From the literature, it is concluded that a cavity receiver should be used when an efficient solar thermal Brayton cycle is required. Shuai et al. (2008), Prakash et al. (2009) and Sendhil Kumar and Reddy (2008) investigated the optimisation and performance of different cavity receivers. Sendhil Kumar and Reddy (2007) compared different types of cavity receivers numerically and found that the modified cavity receiver, as shown in Figures 2.25 and 2.26, experiences lower convection heat losses than those of the other receivers and suggested that it may be preferred in a solar dish collector system. In the numerical modelling, A_w is the inner-heat transfer area, which includes the inner-curved and bottom plane areas. Its size depends on the bottom aperture opening area, A_a. The size of the aperture opening is determined by the flux distribution (focal image characteristics of the fuzzy focal solar dish). The receiver inner surface is made up of closely wound copper tubing – these tubes are placed very closely to touch each other to form a continuous hemispherical surface. The convection heat loss takes place through the receiver aperture. It is suggested that an area ratio of A_w / A_a = 8 is used when minimum heat loss is required (Reddy and Sendhil Kumar, 2009).

Reddy and Sendhil Kumar (2008) investigated the modified cavity further by including the contribution of radiation losses and found that, for A_w / A_a = 8 and a 0° tilt angle (vertical aperture plane), the ratio of the contribution of radiation to convection loss is 47:52. This ratio shifts to 57:43 when the tilt angle is 90°. This means that the ratio of radiation heat loss to convection heat loss is a function of receiver inclination and varies between approximately 0.9 and 1.33. From this data, it is assumed that $\dot{Q}_{loss-rad} \approx \dot{Q}_{loss-conv}$ or $\dot{Q}_0 \approx 2\dot{Q}_{loss-conv}$ for this modified cavity receiver. From Reddy and Sendhil Kumar (2009), for A_w / A_a = 8 at a vertical

position (cavity aperture in vertical plane), Nu = 27. This number becomes almost half the value when the cavity receiver is in the horizontal plane. The most heat loss would thus take place when the cavity receiver is placed vertically (when the sun is on the horizon and the collector faces the sun). This would seldom be the case. An average of Nu = 20 would be more accurate since the cavity receiver would be between 0° and 90° most of the time. The most accurate Nusselt number would be the one given by Reddy and Sendhil Kumar (2009), for their three-dimensional model in terms of receiver inclination, and will be used for this analysis:

$$Nu_D = 0.698 Gr_D^{0.209} (1+\cos\beta)^{0.968} (T_w / T_\infty)^{-0.317} (d/D)^{0.425} \tag{3.13}$$

The convection heat transfer coefficient can be calculated with

$$h_{conv} = \frac{Nu_D k}{D} \tag{3.14}$$

The rate of heat loss from the modified cavity receiver due to convection and radiation can be approximated with

$$\dot{Q}_0 = 1.396 Gr_D^{0.209} (1+\cos\beta)^{0.968} (T_w / T_\infty)^{-0.317} (d/D)^{0.425} (kA_a/D)(T_w - T_\infty) \tag{3.15}$$

According to Reddy and Sendhil Kumar (2009), the minimum heat loss occurs when A_w / A_a = 8. From equation 2.3, the modified cavity receiver diameter for minimum heat loss can be calculated with:

$$D = 2\sqrt{\left(\frac{A_w + A_a}{3\pi}\right)} \tag{3.16}$$

Equation 3.17 gives the modified cavity receiver diameter as a function of the receiver aperture, d, for minimum heat loss:

$$D = 2\sqrt{\left(\frac{9A_a}{3\pi}\right)} = 2\sqrt{\left(\frac{3d^2}{4}\right)} = \sqrt{3}d \tag{3.17}$$

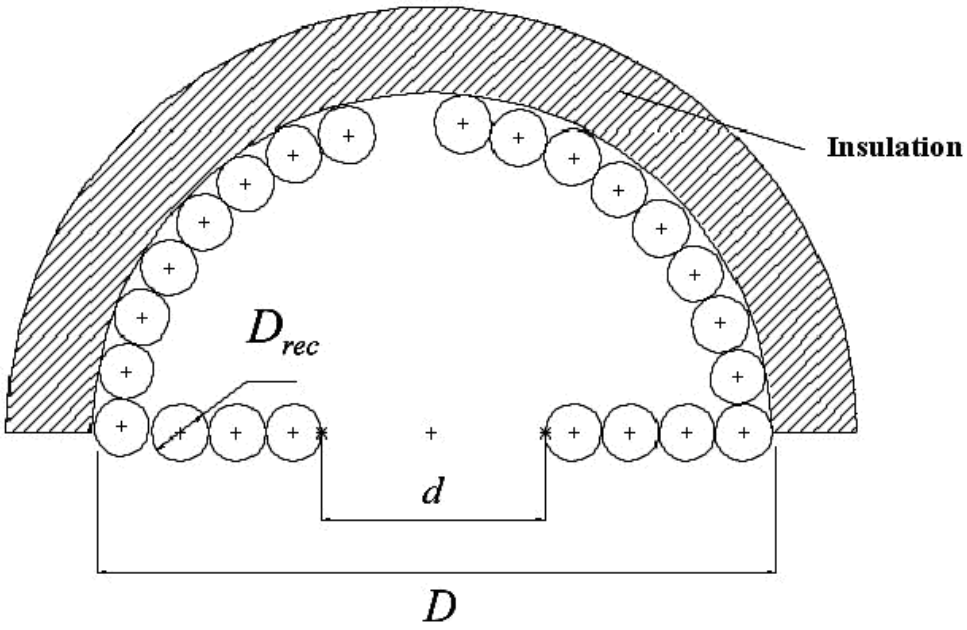

Figure 3.6 Geometry of the cavity receiver constructed with a circular tube.

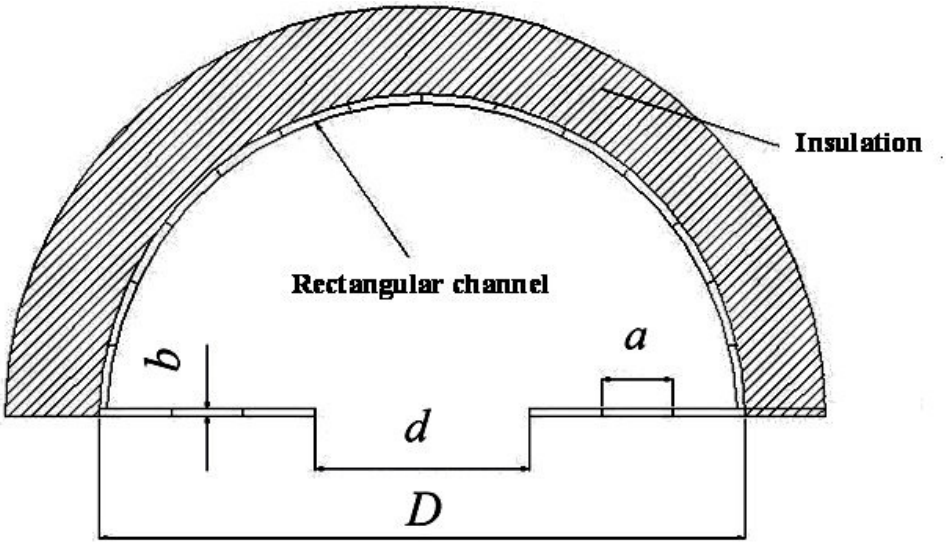

Figure 3.7 Cavity constructed with the use of a rectangular channel (plate) and its dimensions.

The receiver inner surface is made up of closely wound copper tubing with diameter, D_{rec} – these tubes are placed very closely to touch each other to form a continuous hemispherical surface. The working fluid is pumped concentrically through the tube, as is shown in Figure 3.6. The tube with diameter, D_{rec}, and length, L_{rec}, constructs the cavity receiver and its aperture. Another method would be to use flat plate to construct a rectangular channel (Figure 3.7). The receiver channel with hydraulic diameter, $D_{h,rec}$, length, L_{rec}, and aspect ratio, a/b_{rec}, constructs

the cavity receiver and its aperture. Both of these models will be used in the analysis and the results will be compared.

Using the definition of hydraulic diameter for a rectangular channel (the hydraulic diameter is four times the cross-sectional area divided by the wetted perimeter), the longer side, a, can be described with

$$a = \frac{D_{h,rec}\left(\left(\frac{a}{b}\right)_{rec}+1\right)}{2} \tag{3.18}$$

since

$$D_{h,rec} = \frac{4a}{2\left(\left(\frac{a}{b}\right)_{rec}+1\right)} \tag{3.19}$$

Also, the aperture diameter is derived as:

$$d = \sqrt{\frac{D_{h,rec}L_{rec}\left(\left(\frac{a}{b}\right)_{rec}+1\right)}{4\pi}} \tag{3.20}$$

since

$$A_w = aL_{rec} \tag{3.21}$$

When the receiver walls are constructed by winding a circular tube, the aperture diameter, d, can be calculated using a/b_{rec} = 1, in equation 3.20.

3.5.1.2 Geometry of the recuperator

On recommendation of Shah (2005), the counterflow plate-type heat exchanger is considered for the recuperator. In this work, only one recuperator is considered for the system, even though it might seem that the splitting up of the mass flow rate into separate heat exchangers is more

attractive. It was decided to rather keep it simple and also avoid the extra cost and piping due to an extra heat exchanger(s).

The design and assembly will be as illustrated in Figure 3.8. This means that the mass flow rate is divided. Also $A_s = A_i = A_o$ and $A_s = 2aL_{reg}$ (where a is the long side of the rectangle forming the channel). The recuperator is formed by stacking plates and creating counterflow channels. Also note that in Figure 3.8, only a few plates are stacked to show the effect. The number of flow channels, n, in the recuperator depends on the recuperator height, H, channel height, b, and thickness of the channel-separating surface, t. This is shown in equation 3.22.

$$n = H/(t+b) = \frac{H}{t + D_{h,reg}\left((a/b)_{reg}+1\right)/\left(2(a/b)_{reg}\right)} \tag{3.22}$$

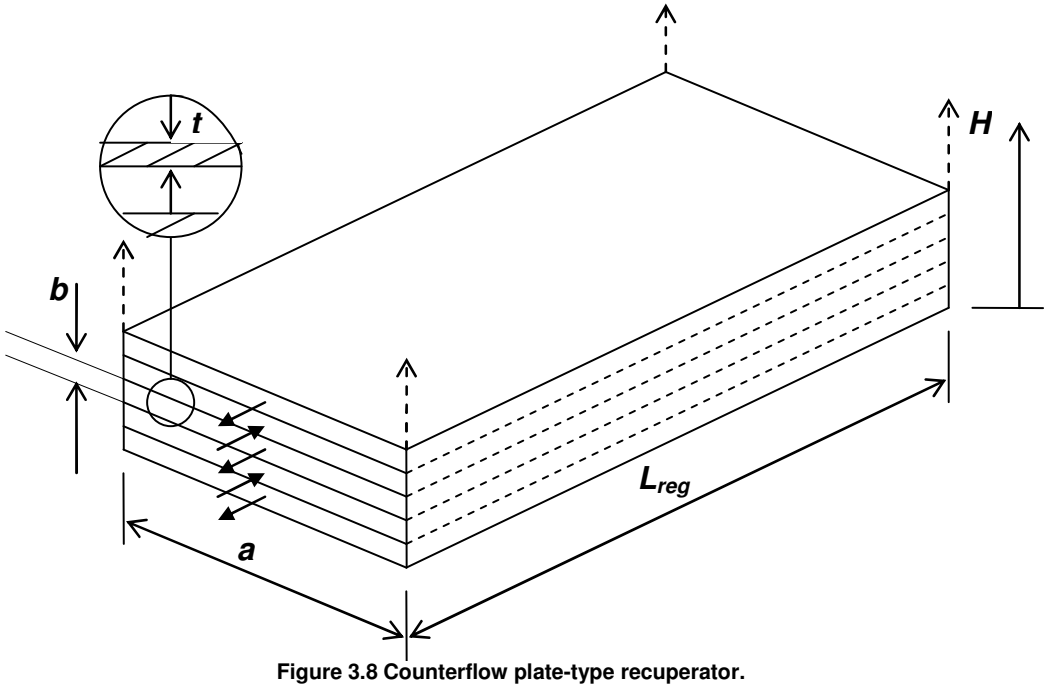

Figure 3.8 Counterflow plate-type recuperator.

The mass flow rate per channel is calculated with:

$$\dot{m}_{reg} = \frac{2\dot{m}}{n} \tag{3.23}$$

The surface area, A_s, for a channel is given by:

$$A_s = 2(a+b)L_{reg} = D_{h,reg}L_{reg}\left(\frac{a}{b}_{reg}+1\right)\left(1+\left(\frac{a}{b}\right)_{reg}^{-1}\right) \tag{3.24}$$

and the Reynolds number for a rectangular channel is:

$$\mathrm{Re} = \frac{4\dot{m}_{reg}\left(\frac{a}{b}\right)_{reg}}{\mu D_{h,reg}\left(\frac{a}{b}_{reg}+1\right)^2} \tag{3.25}$$

The average velocity is calculated as:

$$V_{avg} = \frac{4\dot{m}_{reg}\left(\frac{a}{b}\right)_{reg}}{\rho D_{h,reg}^{\ 2}\left(\frac{a}{b}_{reg}+1\right)^2} \tag{3.26}$$

The recuperator efficiency can be calculated using the $\varepsilon - NTU$ (effectiveness – number of transfer units) method, as suggested from the literature. The Gnielinski equation (Gnielinski, 1976) can be used to calculate the Nusselt number since small Reynolds numbers are most likely to be present in a single channel of the recuperator. The first Petukhov equation (Petukhov, 1970) is used to calculate the friction factor:

$$f = 0.79\ln(\mathrm{Re}) - 1.64)^{-2} \tag{3.27}$$

Using the Gnielinski and Petukhov equations with the Reynolds number above gives:

$$Nu_D = \frac{\mathrm{Pr}(\mathrm{Re}-1000)f/8}{1+12.7(f/8)\left(\mathrm{Pr}^{2/3}-1\right)} \tag{3.28}$$

with

$$h = \frac{kNu_D}{D_{h,rec}} \tag{3.29}$$

With equation 3.29, the convection heat transfer coefficients for the hot and cold stream (h_c and h_h) can be calculated. When these are available, the overall heat transfer coefficient is calculated:

$$U = \left(\frac{1}{h_c} + 2R_f + \frac{L_{reg}}{k_{solid}} + \frac{1}{h_h} \right)^{-1} \tag{3.30}$$

where the fouling factor R_f = 0.004 for air, according to Çengel (2006). The number of transfer units (NTU) is calculated:

$$NTU = \frac{UA_s}{\dot{m}_{reg} c_p} \tag{3.31}$$

and

$$c = \frac{c_{p,c}}{c_{p,h}} \tag{3.32}$$

The recuperator effectiveness can be calculated with equation 3.33.

$$\varepsilon = \frac{1 - \exp[-NTU(1-c)]}{1 - c\exp[-NTU(1-c)]} \tag{3.33}$$

According to Stine and Harrigan (1985), Weston (2000) and Çengel (2006), the heat exchanger efficiency and heat exchanger effectiveness are defined the same way for the recuperator in this analysis (with reference to Figure 3.5):

$$\eta_{reg} = \varepsilon = \frac{\dot{Q}}{\dot{Q}_{\max}} = \frac{\dot{m}c_p(T_4 - T_3)}{\dot{m}c_p(T_9 - T_3)} = \frac{T_4 - T_3}{T_9 - T_3} \tag{3.34}$$

This efficiency will help to produce the temperatures and pressures necessary to describe the objective function. The importance of the recuperator efficiency is shown in Chapter 2.

With the use of the definitions of the Reynolds number (equation 3.25) and the friction factor (equation 3.27) and the definition of the pressure drop (Çengel, 2006), the pressure drop through the recuperator is derived in terms of the geometry variables as:

$$\Delta P = \left(0.79 \ln \frac{4\dot{m}_{reg} \left(a/b\right)_{reg}}{\mu D_{h,reg} \left(a/b_{reg} + 1\right)^2} - 1.64 \right)^{-2} \left(\frac{8\dot{m}_{reg}{}^2 \left(a/b\right)_{reg}{}^2}{\rho \left(a/b_{reg} + 1\right)^4} \right) \left(\frac{L_{reg}}{D_{h,reg}{}^5} \right) \tag{3.35}$$

3.5.2 Parameters

According to Snyman (2009), the pressure ratio, r, of the compressor should be chosen to be a parameter. The objective function can be maximised and the optimum geometry can be found for each pressure ratio in the compressor's range. When considering the mass flow rate through the system, it depends on the compressor, which, in turn, depends on the turbine. There are, unfortunately, many different compressor and turbine designs available. The task and cost of designing one's own turbine and compressor configuration for a specific system, by shaping its geometry using the method of entropy generation minimisation, is in itself a mammoth task and can be considered or recommended for further study. In this work, however, the compressor and turbine configuration comes from an existing source chosen for its low cost, availability and reliability.

From the literature, the advantages of using the micro-turbines from the Garrett range are evident and they will be used in the analysis. The Garrett micro-turbines (Appendix D) as well as their turbine and compressor maps (Garrett, 2009) are freely available in South Africa. For the compressor of a specific micro-turbine, the compressor efficiency, mass flow rate and pressure ratio are intrinsically coupled to each other. Garrett (2009) also gives the turbine efficiencies for each of its micro-turbines. Thanks to these existing micro-turbines from Garrett, the compressor pressure ratio as a parameter would fix the mass flow rate and compressor efficiency as parameters as well. Figure 3.9 shows the compressor map of a micro-turbine (GT2259) with micro-turbine model number 9 (*MT* = 9 in Appendix D). In the compressor map, the coupling of compressor efficiency, mass flow rate and pressure ratio are shown. The rotational speed in revolutions per minute is also shown. Note that the highest compressor efficiency is on the island in the middle of the compressor map (between two mass flow rate values: $\dot{m}_{low}$ and $\dot{m}_{high}$ and between two pressure ratio values: r_{low} and r_{high}). These pressure ratio and mass flow rate ranges are shown for each micro-turbine in Appendix D. When only considering the highest compressor efficiency for the analysis, the pressure ratio (r) – mass flow rate ($\dot{m}$) relation can

be described with a straight line. Hence the equation to find the mass flow rate when the pressure ratio is fixed:

$$\dot{m} = \frac{\left(\dot{m}_{high} - \dot{m}_{low}\right)}{\left(r_{high} - r_{low}\right)}\left(r - r_{low}\right) + \dot{m}_{low} \tag{3.36}$$

An optimum pressure ratio (or operating condition) should exist for a specific micro-turbine, which would (with its optimised geometry) give the maximum net power output.

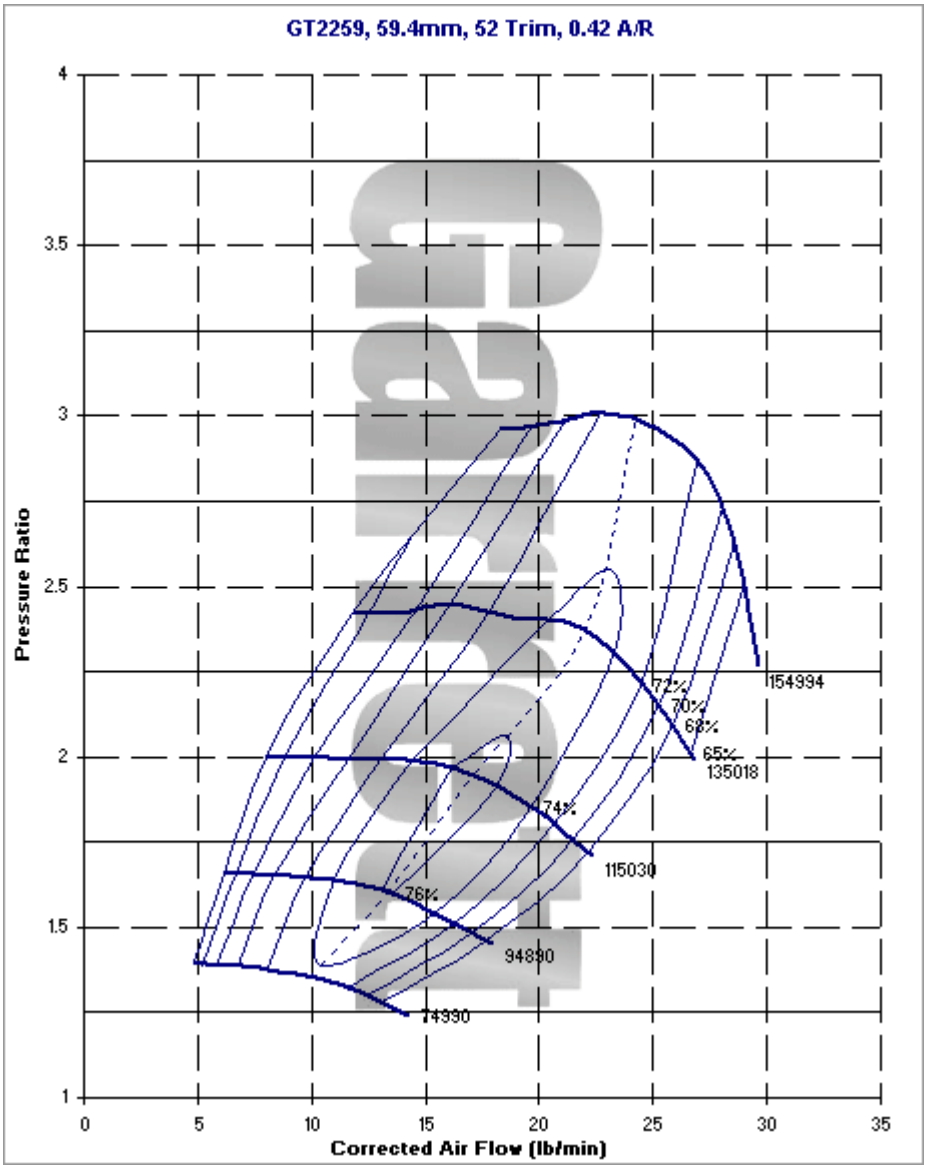

Figure 3.9 Compressor map for a micro-turbine from Garrett (Garrett, 2009).

3.6 Temperatures and pressures in terms of geometry variables

For the objective function, the temperatures and pressures at each point in the system (Figure 3.5) can be determined in terms of the geometry variables. The six geometry variables are:

$D_{h,rec}$ - Hydraulic diameter of the cavity receiver channel (or tube diameter, D_{rec})

L_{rec} - Tube or channel length of the cavity receiver

a/b_{rec} - Aspect ratio of the receiver channel (negligible when the receiver walls are made from circular tube)

$D_{h,reg}$ - Hydraulic diameter of the recuperator channels

L_{reg} - Length of the recuperator channels

a/b_{reg} - Aspect ratio of the recuperator channels

The temperatures and pressures at each point in the system (Figure 3.5) can be determined as is explained below. The process of finding the pressures and temperatures can be divided into five phases. Each phase has a number of steps.

Phase 1 (Pre-receiver):

The inlet temperature of the system is:

$$T_1 = 300 \text{ K} \tag{3.37}$$

T_2 is calculated using the compressor isentropic efficiency, η_c, and the compressor pressure ratio, r, as parameters. T_3 can then be calculated:

$$T_2 = T_1\left[1+\left(K-1\right)/\eta_c\right] \tag{3.38}$$

where

$$K = r^{k-1/k} \tag{3.39}$$

$$T_3 = T_2 - \Delta T_{23} \tag{3.40}$$

A constant is assumed for ΔT_{23} and also for all the other temperature drops in the ducting between components. It is important to note that the temperature in the ducting between components actually depends on the size of the duct and that the size of the ducting might also play a role in the shadow effect of the collector.

Phase 2 (Receiver):

Guess T_5 = 800 K, and then calculate T_6 with:

$$T_6 = \frac{\dot{Q}_{net}}{\dot{m}c_p} + T_5 \tag{3.41}$$

The net rate of absorbed heat in the cavity receiver, $\dot{Q}_{net}$, is a function of the receiver aperture diameter, d. This function can be determined with the use of a sizing algorithm. In this analysis, the sizing algorithm by Stine and Harrigan (1985) is used, as explained in Appendix A. The function determined by the sizing algorithm can be approximated with the discrete least-squares approximation method (Burden and Faires, 2005) ($\dot{Q}_{net} = \sum_{i=0}^{10} x_i d^i$). $\dot{Q}_{net}$ can be written in terms of $D_{h,rec}$, L_{rec} and a/b_{rec} (the geometric variables for the cavity receiver) since $A_w = 8A_a = 8\pi d^2/4 = a_{rec}L_{rec}$. In equation 3.20, d is written in terms of the receiver geometry variables. The net absorbed heat rate can be written in terms of the receiver geometry variables:

$$\dot{Q}_{net} = \sum_{i=0}^{10} x_i \left(\sqrt{\frac{D_{h,rec} L_{rec} \left((a/b)_{rec} + 1 \right)}{4\pi}} \right)^i \tag{3.42}$$

Note that when a circular tube constructs the cavity receiver, a/b_{rec} = 1. With the use of equation 3.42, T_6 can be written in terms of the geometry variables (equation 3.43). For a receiver constructed with circular tube, equation 3.43 can be used with a/b_{rec} = 1. T_7 is calculated with an assumed value for ΔT_{67}.

$$T_6 = \frac{\sum_{i=0}^{10} x_i \left(\sqrt{\frac{D_{h,rec} L_{rec} \left((a/b)_{rec} + 1 \right)}{4\pi}} \right)^i}{\dot{m} c_p} + T_5 \tag{3.43}$$

$$T_7 = T_6 - \Delta T_{67} \tag{3.44}$$

Phase 3 (Pressure field):

The inlet pressure of the system, P_1 and the exit pressure of the compressor, P_2 can be calculated using the following equations:

$$P_1 = P_{atm} \tag{3.45}$$

$$P_2 = rP_1 \tag{3.46}$$

$$P_3 = P_2 \left(1 - \Delta P_{23}\right) \tag{3.47}$$

P_3, P_5, P_7 and P_8 are calculated with an assumed pressure drop in the ducts. P_4 and P_9 can be calculated with equations 3.48 and 3.53 respectively. These equations are written in terms of the geometry variables of the recuperator and are derived using equation 3.35.

$$P_4 = P_3 - \left(0.79 \ln \frac{4\dot{m}_{reg} (a/b)_{reg}}{\mu D_{h,reg} \left(a/b_{reg} + 1 \right)^2} - 1.64 \right)^{-2} \left(\frac{8\dot{m}_{reg}{}^2 (a/b)_{reg}{}^2}{\rho \left(a/b_{reg} + 1 \right)^4} \right) \left(\frac{L_{reg}}{D_{h,reg}{}^5} \right) \tag{3.48}$$

$$P_5 = P_4 \left(1 - \Delta P_{45}\right) \tag{3.49}$$

P_6 is calculated with equation 3.50, which is written in terms of the receiver geometry variables and derived using equation 3.35. Equation 3.50a is for a receiver constructed with a rectangular channel (plate) and equation 3.50b is for a receiver constructed with a circular tube.

Plate:

$$P_6 = P_5 - \left(0.79\ln\frac{4\dot{m}(a/b)_{rec}}{\mu D_{h,rec}((a/b)_{rec}+1)^2} - 1.64\right)^{-2}\left(\frac{8\dot{m}^2(a/b)_{rec}^{\ 2}}{\rho((a/b)_{rec}+1)^4}\right)\left(\frac{L_{rec}}{D_{h,rec}^{\ 5}}\right) \tag{3.50a}$$

Tube:

$$P_6 = P_5 - \left(0.79\ln\frac{4\dot{m}}{\mu\pi D_{h,rec}} - 1.64\right)^{-2}\left(\frac{8\dot{m}^2}{\rho\pi^2}\right)\left(\frac{L_{rec}}{D_{h,rec}^{\ 5}}\right) \tag{3.50b}$$

$$P_7 = P_6(1-\Delta P_{67}) \tag{3.51}$$

The system exit pressure, P_{11}, is the same as the system inlet pressure, P_1, as shown in equation 3.52. Also note that $P_{10} = P_{11}$. P_9 can be calculated using the system exit pressure:

$$P_{11} = P_1 \tag{3.52}$$

$$P_9 = P_{10} + \left(0.79\ln\frac{4\dot{m}_{reg}(a/b)_{reg}}{\mu D_{h,reg}(a/b_{reg}+1)^2} - 1.64\right)^{-2}\left(\frac{8\dot{m}_{reg}^{\ 2}(a/b)_{reg}^{\ 2}}{\rho(a/b_{reg}+1)^4}\right)\left(\frac{L_{reg}}{D_{h,reg}^{\ 5}}\right) \tag{3.53}$$

$$P_8 = P_9(1+\Delta P_{89}) \tag{3.54}$$

Phase 4 (Post-turbine):

T_8 is calculated with equation 3.55 with the use of the turbine isentropic efficiency, η_t, and the turbine pressure ratio. T_{10} is calculated with the recuperator efficiency, η_{reg} (equation 3.33). Also note that $T_{11} = T_{10}$.

$$T_8 = T_7\left[1-\eta_t\left[1-\frac{1}{(P_7/P_8)^{((k-1)/k)}}\right]\right] \tag{3.55}$$

$$T_9 = T_8 - \Delta T_{89} \tag{3.56}$$

$$T_{10} = T_9 - \eta_{reg}\left(T_9 - T_2\right) \tag{3.57}$$

Phase 5 (Iteration):

T_4 is calculated with the recuperator efficiency. T_5 can then be calculated and is used as the new approximation for T_5 in Phase 1. The iteration continues until the error is smaller than 1×10^{-3}. When the iteration is done, the temperatures and pressures are established and can be used in the objective function.

$$T_4 = T_3 + \eta_{reg}\left(T_9 - T_3\right) \tag{3.58}$$

$$T_5 = T_4 - \Delta T_{45} \tag{3.59}$$

3.7 The objective function

The objective function (equations 3.11 and 3.12) can be written in terms of geometry variables, parameters and constants. When looking at the previous section, it should be clear that the objective function, in terms of all the variables, parameters and constants, is very complex and is not shown. Note, however, the cancelling out of the following terms (from equation 3.12 in equation 3.11) so that:

$$\frac{\dot{Q}*T_0}{T*} - \dot{Q}_0 + \dot{Q}* - \frac{\dot{Q}*T_0}{T*} = \dot{Q}_{net} \tag{3.60}$$

The final objective function can be written as:

$$\dot{W}_{net} = \dot{Q}_{net} + \dot{m}c_{p0}(T_1 - T_{11}) - \dot{m}T_0 c_{p0} \ln\left(\frac{T_1}{T_{11}}\right)$$

$$-T_0\left[-\dot{m}c_{p0}\ln\left(\frac{T_1}{T_2}\right)+\dot{m}R\ln\left(\frac{P_1}{P_2}\right)\right]_{compressor}$$

$$-T_0\left[\frac{\dot{Q}_{loss}}{T_0}+\dot{m}c_{p0}\ln\left(\frac{T_3}{T_2}\right)-\dot{m}R\ln\left(\frac{P_3}{P_2}\right)\right]_{duct\,23}$$

$$-T_0\left[\dot{m}c_{p0}\ln\left[\frac{T_{10}T_4}{T_9T_3}\left(\frac{P_{10}P_4}{P_9P_3}\right)^{(1-k)/k}\right]+\frac{\dot{Q}_{loss}}{T_0}\right]_{recuperator}$$

$$-T_0\left[\frac{\dot{Q}_{loss}}{T_0}+\dot{m}c_{p0}\ln\left(\frac{T_5}{T_4}\right)-\dot{m}R\ln\left(\frac{P_5}{P_4}\right)\right]_{duct\,45}$$

$$-T_0\left[\dot{m}c_{p0}\ln\left(\frac{T_6}{T_5}\right)-\dot{m}R\ln\left(\frac{P_6}{P_5}\right)\right]_{receiver}$$

$$-T_0\left[\frac{\dot{Q}_{loss}}{T_0}+\dot{m}c_{p0}\ln\left(\frac{T_7}{T_6}\right)-\dot{m}R\ln\left(\frac{P_7}{P_6}\right)\right]_{duct\,67}$$

$$-T_0\left[-\dot{m}c_{p0}\ln\left(\frac{T_7}{T_8}\right)+\dot{m}R\ln\left(\frac{P_7}{P_8}\right)\right]_{turbine}$$

$$-T_0\left[\frac{\dot{Q}_{loss}}{T_0}+\dot{m}c_{p0}\ln\left(\frac{T_9}{T_8}\right)-\dot{m}R\ln\left(\frac{P_9}{P_8}\right)\right]_{duct\,89} \quad (3.61)$$

Keep in mind that each temperature and pressure in equation 3.61 is defined in terms of parameters and geometry variables, as shown in Section 3.6.

3.8 Constraints

Constraint 1:

The maximum cavity receiver aperture diameter is constrained. The minimum concentration ratio, $CR_{\min}$, will determine the maximum size of the cavity aperture relative to the concentrator area.

From the literature, the concentration ratio seems to be more than 100 for receiver temperatures of more than 1 000 K (see Section 2.3.2). For this work, $CR \geq 100$, hence we have:

$$\begin{aligned} &\frac{\pi}{4}d^2 < A_{s,conc}/100 \\ &\frac{\pi}{4}\left(\frac{D_{h,rec}L_{rec}\left((a/b)_{rec}+1\right)}{4\pi}\right) < A_{s,conc}/100 \\ &\frac{D_{h,rec}L_{rec}\left((a/b)_{rec}+1\right)}{16} - \frac{A_{s,conc}}{100} < 0 \end{aligned} \tag{3.62}$$

The constraint above is for a receiver constructed with a rectangular channel. For a receiver constructed with a circular tube, the same constraint can be used, but with $(a/b)_{rec} = 1$

Constraint 2:

The receiver aperture diameter, d, has a minimum constraint to keep the aperture size from going too small or negative. $Wn(2)$ is the second term in the vector Wn (used in the function 'collector' – see Appendix C).

$$\begin{aligned} &Wn(2) < \sqrt{\frac{D_{h,rec}L_{rec}\left((a/b)_{rec}+1\right)}{4\pi}} \\ &Wn(2) - \sqrt{\frac{D_{h,rec}L_{rec}\left((a/b)_{rec}+1\right)}{4\pi}} < 0 \end{aligned} \tag{3.63}$$

Similarly, for a receiver constructed with circular tube, $(a/b)_{rec} = 1$

Constraint 3:

The width of the rectangular channel, a, in the receiver cannot be larger than the distance between the aperture and the edge of the receiver. With the use of equation 3.17 from Section 3.5.1.1, this distance can be described with equation 3.64.

$$D = \sqrt{3}d \tag{3.17}$$

$$\left(\frac{\sqrt{3}-1}{2}\right)d \geq a \tag{3.64}$$

With equation 3.18 from Section 3.5.1.1, this constraint is written in terms of the geometry variables using equation 3.65.

$$a = \frac{D_{h,rec}\left(\left(a/b\right)_{rec}+1\right)}{2} \tag{3.18}$$

$$\frac{D_{h,rec}\left(\left(a/b\right)_{rec}+1\right)}{2} - \left(\frac{\sqrt{3}-1}{2}\right)\sqrt{\frac{D_{h,rec}L_{rec}\left(\left(a/b\right)_{rec}+1\right)}{4\pi}} \leq 0 \tag{3.65}$$

When a receiver constructed with a circular tube is used, at least two tube diameters should fit in the distance between the aperture edge and the edge of the receiver. Otherwise, the receiver would lose its cavity shape. This is shown in equation 3.66.

$$2D_{h,rec} - \left(\frac{\sqrt{3}-1}{2}\right)\sqrt{\frac{D_{h,rec}L_{rec}}{2\pi}} \leq 0 \tag{3.66}$$

Constraint 4:

The surface temperature of the receiver (of copper) should stay well below its melting temperature and below the maximum inlet temperature of the micro-turbines (more or less 1 220 K or 1 320 K intermittently according to Garrett (2009) and Shah (2005) - see Section 2.3.5 and Section 2.2.2.3.1). A maximum temperature of 1 200 K is chosen. The surface area of the rectangular receiver channel can be defined as:

$$A_s = D_{h,rec}L_{rec}\left(\left(a/b\right)_{rec}+1\right)\left(1+\left(a/b\right)_{rec}{}^{-1}\right) \tag{3.67}$$

Since turbulent flow is expected in the receiver tube or channel, the Nusselt number is defined as (Dittus and Boelter, 1930):

$$Nu = 0.023\,\mathrm{Re}_D{}^{0.8}\,\mathrm{Pr}^{0.4} \tag{3.68}$$

For a receiver constructed with a rectangular channel (plate), the maximum surface temperature can be defined as:

$Plate$:

$$T_{s,\max} = T_6 + \frac{\sum_{i=0}^{10} x_i \left(\sqrt{\frac{D_{h,rec} L_{rec} \left((a/b)_{rec} + 1 \right)}{4\pi}} \right)^i}{0.023 L_{rec} \left((a/b)_{rec} + 1 \right) \left(1 + (a/b)_{rec}^{-1} \right) k \, \mathrm{Pr}^{0.4} \left(\frac{4\dot{m} (a/b)_{rec}}{\mu D_{h,rec} \left((a/b)_{rec} + 1 \right)^2} \right)^{0.8}} \tag{3.69}$$

Note that equation 3.42 is used in the construction of equation 3.69, since $\dot{Q}_{net}$ is required to calculate the maximum surface temperature. When the receiver is constructed with the use of a circular tube, the maximum surface temperature can be defined as:

$Tube$:

$$T_{s,\max} = T_6 + \frac{\sum_{i=0}^{10} x_i \left(\sqrt{\frac{D_{rec} L_{rec}}{2\pi}} \right)^i}{0.023 \pi L_{rec} k \, \mathrm{Pr}^{0.4} \left(4\dot{m} / (\mu \pi D_{rec}) \right)^{0.8}} \tag{3.70}$$

Constraints 5 and 6:

The hydraulic diameter and length of the receiver is always positive:

$$-D_{h,rec} \leq 0 \tag{3.71}$$

$$-L_{rec} \leq 0 \tag{3.72}$$

Constraint 7:

The longer the recuperator, the more beneficial it is to the system from a heat transfer point. However, there needs to be a constraint on its length to make sure the system stays compact. The recuperator's length should not exceed the length of the radius of the dish concentrator. Since there is already a large concentrator, there is no sense in keeping the recuperator many times smaller than the dish to save space. A recuperator can perhaps fit underneath the space occupied by the dish concentrator with relative ease. Therefore:

$$L_{reg} \leq \sqrt{\frac{A_{s,conc}}{\pi}} = \boldsymbol{D} / 2 \tag{3.73}$$

Constraint 8:

This constraint is only necessary when the receiver walls are constructed using a rectangular channel. The channel should have an aspect ratio equal to or larger than 2.5 to ensure that the shape of the cavity receiver is maintained. Hence:

$$2.5 - \left(\frac{a}{b}\right)_{rec} \leq 0 \tag{3.74}$$

3.9 Constants / assumptions

The objective function relies on a number of constants. These constants would depend on the location and available space for the solar thermal power system and are therefore very location- and situation-specific. The most important constants are shown below. For each specific location and situation, a different optimum receiver and recuperator geometry would exist.

Environmental conditions:

- T_0 Surrounding average temperature (K)
- I Irradiance (W/m^2)
- w Non-dimensionalised wind factor (1 – 10) multiplied with convection heat transfer coefficient
- P_{atm} Atmospheric pressure (Pa)

Available space at location:

- $A_{s,conc}$ Parabolic dish concentrator area (m^2)
- H Available space for height of recuperator (m)
- L Available space for length of recuperator (m)

Concentrator and receiver:

- e_p Concentrator error
- φ_{rim} Rim angle of parabolic dish concentrator
- $refl$ Specular reflectivity of the concentrator
- $T_{s,\max}$ Maximum allowable surface temperature of receiver
- β Inclination of receiver (90° for receiver aperture facing down)
- $CR_{\min}$ Minimum concentration ratio

Recuperator:

- t Heat exchanger wall thickness between hot and cold streams
- k Recuperator material conductivity

3.10 Summary

In this chapter, the objective function to be optimised was formulated and the physical model to be analysed was described. The different possibilities of arrangements of components in the solar thermal Brayton cycle were identified and the uniqueness of the open and direct solar thermal Brayton cycle was shown. The rate of entropy generation in each of the system's components was identified. The total rate of entropy generation was obtained for the system by adding the entropy generation rates of each system component. The net power output of the system was linked with the total entropy generation rate by doing an exergy analysis for the whole system. The construction of the objective function in terms of the geometry variables of the receiver and recuperator was shown. The recuperator and receiver models were described in terms of the geometry variables to be optimised. For the objective function, the parameters were described and the constraints and assumptions were listed.

Chapter 4

Numerical Method

4.1 Introduction

In this chapter, the numerical optimisation method is discussed. The settings used in the algorithm are shown. The method of calculating the derivatives of the objective function in each of its geometry variables is given. Different parameters are considered in the optimisation algorithm. The way in which these parameters are incorporated in the analysis is shown.

4.2 Optimisation algorithm

The maximum net power output for the open and direct solar thermal Brayton cycle can be found by maximising the objective function. The optimisation algorithm finds the optimum geometry for the solar receiver and recuperator at a specific operating condition in the pressure ratio range of a specific micro-turbine so that the net power output of the system can be a maximum. The six geometric variables to be optimised are listed in Table 4.1.

Table 4.1 Geometric variables used in numerical optimisation with description.

Variable	Description	Numerical variable
$D_{h,rec}$	Hydraulic diameter of the cavity receiver channel / tube (m)	$X(1)/100$
L_{rec}	Channel / tube length of the cavity receiver (m)	$X(2)$
a/b_{reg}	Aspect ratio of the recuperator channels	$X(3)$
$D_{h,reg}$	Hydraulic diameter of the recuperator channels (m)	$X(4)/1000$
L_{reg}	Length of the recuperator (m)	$X(5)$
a/b_{rec}	Aspect ratio of the cavity receiver channel / tube	$X(6)$

The vector X will be optimised by the optimisation algorithm. Also take note that some of these variables are scaled to ensure that the variables in the variable vector are more or less of the same order. The objective function (net power output of the system), in terms of the geometry

variables, parameters and constants, is maximised using the dynamic trajectory optimisation method by Snyman (2009). Take note that the optimisation algorithm used (LFOPC by Snyman (2000) or the leapfrog method) requires a function input to be minimised. The objective function (equation 3.61) is multiplied with -1, since the objective function should be maximised (see the function '*fun*' in Appendix C). The minimum of the negative function would then be negative, but when multiplied again with -1, it would give the positive maximum of the objective function (Snyman, 2009). Note that, in Appendix C, the leapfrog method is called using the MATLAB function *lfopc([starting vector])* by Snyman (2000). The following settings in Table 4.2 (mostly the default settings) were used for the dynamic trajectory optimisation algorithm by Snyman (2000).

Table 4.2 Settings used for the optimisation algorithm (LFOPC).

Setting	Definition	Chosen Value
x0	Starting point: this depends on the specific micro-turbine	The starting point for small micro-turbines is [5 5 5 5 5 5], while the starting point for large micro-turbines is [10 10 10 10 10 10]
delt	Maximum step size	1 (default)
xtol	Convergence tolerance *ex* on the step movement	1e-7 (the default is 1e-8)
eg	Convergence tolerance *eg* on the norm of the gradient	1e-5 (default)
xmu	Initial penalty value	100 (default)
xmumax	Maximum penalty value	10 000 (default)
kmax	Maximum number of steps per phase	1 000 (default)

The results from two other optimisation algorithms from Snyman (2009) were compared with the dynamic trajectory optimisation method: the spherical quadratic steepest descent (SQSD) method for unconstrained minimisation with no explicit line searches and the gradient-only conjugate gradient method for constrained minimisation with no explicit line searches. These optimisation algorithms were not able to find a solution as sound as the dynamic trajectory optimisation method for constrained optimisation.

4.3 Gradients

The optimisation algorithm by Snyman (2000) requires the gradient of the objective function in each variable. As can be understood, to get the gradient of the objective function for each

variable (in this work) is difficult. As a first attempt, the variables of the objective function were written in symbol form so that the '*grad*' function in MATLAB could be used to give the equations for these gradients. Such an equation was, unfortunately, pages long and made its handling and copying very difficult. Keep in mind that there is an iteration involved in the objective function (see Section 3.6), which makes the calculation of its slope in a certain variable a very difficult process.

The solution was to go back to the definition of the gradient of a function (Stewart, 2003). The gradient of the function for each of the variables in vector X can be obtained by taking a small increment h positive and negative of the variable value, to get two function values (derivative functions). The slope can then be calculated at the specific point in space. Note that in the following equations, X is the vector containing the variables that should be optimised in the optimisation algorithm. In the function '*gradf*' (Appendix C), the following was done to obtain the gradient of the function in a certain variable at a specific point of the vector X :

Let h be very small: $h = 1\times10^{-8}$. The gradient $\frac{dfun}{dX(1)}$ can then be calculated as:

$$GF(1) = \frac{fun(X+) - fun(X-)}{2h} \tag{4.1}$$

where '*fun*' is the objective function (see Appendix C) and

$$X+ = X + [h \;\; 0\;0\;0\;0\;0] \tag{4.2}$$

$$X- = X - [h \;\; 0\;0\;0\;0\;0] \tag{4.3}$$

The gradient of the function in the other five variables is calculated similarly. The same method is used for calculating the slopes of inequality constraints as required from the optimisation algorithm. The functions used in the optimisation algorithm are added in Appendix C. The inequality constraints are shown in the function *'conin'* and their gradients in each variable are given in the function '*gradc'*.

4.4 Structure of the program

Different parameters (***D***, *MT* and r) are used in the objective function and different combinations of parameters are considered. A range of parabolic concentrator diameters (***D*** = 6 – 18 m) is used in increments of two metres. For each concentrator diameter, 45 different standard micro-

turbines are considered and for each micro-turbine, the objective function (equation 3.61) is maximised at each of the micro-turbines' operating conditions (from r_{low} to r_{high} in increments of 0.1). The function '*once*' (see Appendix C) is used to do the abovementioned. It is applied in the following summarised structure.

- Get location-specific constants
- For ***D*** = 6 : 2 : 18
  - Get $\dot{Q}_{net}$ from the function '*collector*' (Appendix C), as a function of the receiver geometry variables (or d) according to the receiver sizing algorithm in Appendix A (see Figure A.4). The function '*collector*' calculates the rate of intercepted heat and rate of heat loss for a range of cavity aperture diameters. The receiver sizing algorithm in Appendix A establishes the link between the concentrator size, cavity aperture size and net absorbed heat rate.
  - For all the compressor and turbine pairs from Garrett in Appendix D (*MT* = 1 : 45)
    - For $r = r_{low}$: 0.1 : r_{high} (along the line of highest compressor efficiency on the compressor map)
      - Get maximum net power output using the optimisation algorithm and objective function (equation 3.61)
      - Get optimum geometry variables: $X(1)$, $X(2)$, $X(3)$, $X(4)$, $X(5)$ and $X(6)$
    - end
  - end
- end

Figure 4.1 shows how different combinations of concentrator diameters and micro-turbines are considered in the analysis.

Also note that, in the objective function '*fun*', an iteration is performed to establish the temperatures and pressures as discussed in Section 3.6. This iteration continues until the error of the iterations is smaller than 1×10^{-3}. The same method is used in the function '*Tsfunc'* (Appendix C), which calculates the receiver surface temperature. In this function, again, an iteration is performed to determine the temperature, and pressure values to determine the output value of the function.

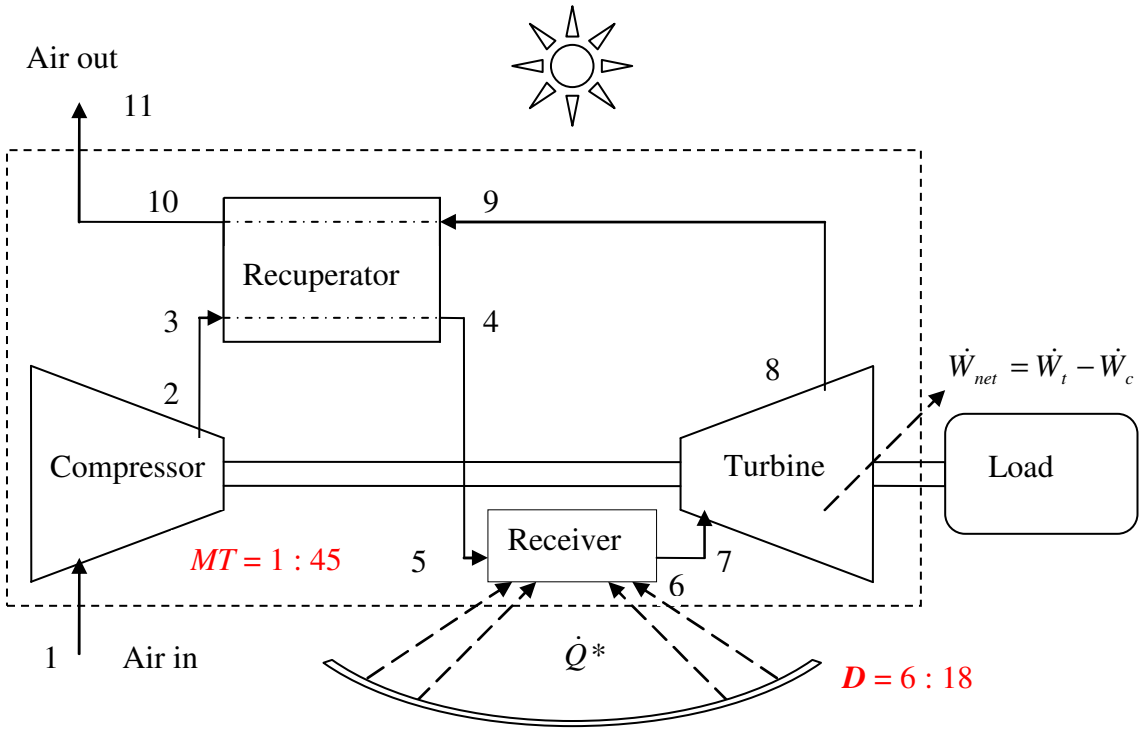

Figure 4.1 The open and direct solar thermal Brayton cycle with a range of concentrator diameters (*D*) and a range of micro-turbines (*MT*).

4.5 Summary

The optimisation algorithm used in the analysis is the leapfrog method (LFOPC) by Snyman (2000). The settings used in the analysis for this algorithm were shown in this chapter. The calculation of the derivatives of the objective function was shown. The structure of the analysis and the incorporation of the parameters were highlighted. The results found with the optimisation algorithm (using different parameters) are shown in Chapter 5.

Chapter 5

Results

5.1 Introduction

The results of the analysis, as described thus far, are shown in this chapter. The optimum geometry and optimum operating conditions for a system with maximum net power output are shown and discussed. Before these results are shown, a validation is done. The validation is done to better understand the effect of the compressor, turbine and recuperator efficiencies on the thermal efficiency of the system. The validation confirms that an optimum operating condition exists for the recuperative open and direct solar thermal Brayton cycle. The first validation shows that the thermal efficiency of the system can be derived in terms of the compressor pressure ratio, compressor efficiency, turbine efficiency, recuperator efficiency and the inlet temperatures of the compressor and turbine as constants. The derivations are compared with equations from the literature.

As a second validation, the net power output is calculated using equation 3.61. In this validation, the temperatures and pressures required to calculate the net power output are calculated using assumptions of pressure and temperature drops across the components. Again, it is evident that an optimum operating condition exists. The pressure and temperature losses should, however, be described in terms of the geometry variables of the system, but in the second validation they are assumed to be constant. The net power output (equation 3.61) as a function of compressor pressure ratio is compared with the net power output as calculated from the first law of thermodynamics.

For the full analysis, the numerical and geometrical model and temperatures and pressures, as discussed in the previous sections, are used. The temperatures and pressures used in the objective function are calculated as shown in Section 3.6. The geometries are thermodynamically optimised and the optimum operating conditions are shown.

5.2 Validation

5.2.1 First validation

One would like to have the thermal efficiency of the system in terms of the efficiency of the recuperator and the isentropic efficiencies of the turbine and compressor. This thermal efficiency curve should give a hint of whether or not a maximum exists in terms of the pressure ratio of the cycle. In this first part of the validation, it is assumed that $r = P_2 / P_1 = P_3 / P_4$ as is shown in Figure 5.1. The thermal efficiency is also written as a function of T_1 and T_3. This section starts off with a derivation of the thermal efficiency of the cycle, without any recuperation and excluding the isentropic efficiencies of the compressor and turbine. The section ends with an equation for the thermal efficiency, which includes the efficiency of the recuperator and the isentropic efficiencies of the compressor and turbine.

5.2.1.1 Thermal efficiency - no recuperator (η_c *and* η_t = 1)

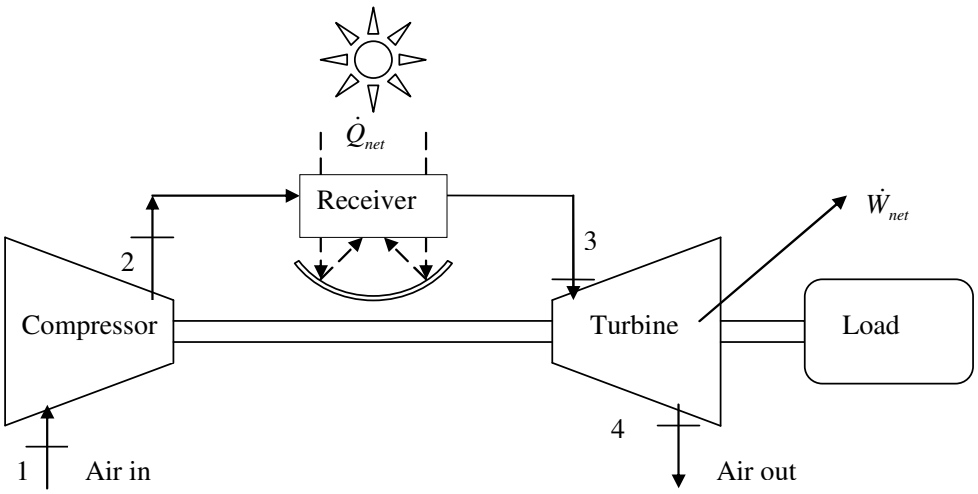

Figure 5.1 The open and direct solar thermal Brayton cycle with no recuperator (Stine and Harrigan, 1985).

Figure 5.1 shows the open solar thermal Brayton cycle without recuperation. The thermal efficiency is defined as:

$$\eta_{th} = \frac{w_{net}}{q_{net}} = \frac{w_t / w_c - 1}{q_{net} / w_c} \tag{5.1}$$

where q_{net} is the net accepted specific heat in the receiver. It can be shown that, for no recuperation and 100% compressor and turbine efficiencies, the thermal efficiency is:

$$\eta_{th} = \frac{w_{net}}{q_{net}} = \frac{K-1}{K} = 1 - 1/K \tag{5.2}$$

since $\frac{w_t}{|w_c|} = \left(\frac{T_3}{T_1}\right)/K$ (Weston, 2000), $K = \left(\frac{P_2}{P_1}\right)^{k-1/k}$ and $w_{net} = w_t - w_c$. Also note that equation 5.2 is derived by writing w_c and q_{net} in terms of the temperatures. Equation 5.2 is confirmed with Weston (2000) and Stine and Harrigan (1985).

5.2.1.2 Thermal efficiency - with recuperator (η_{reg} < 1 and η_c *and* η_t = 1)

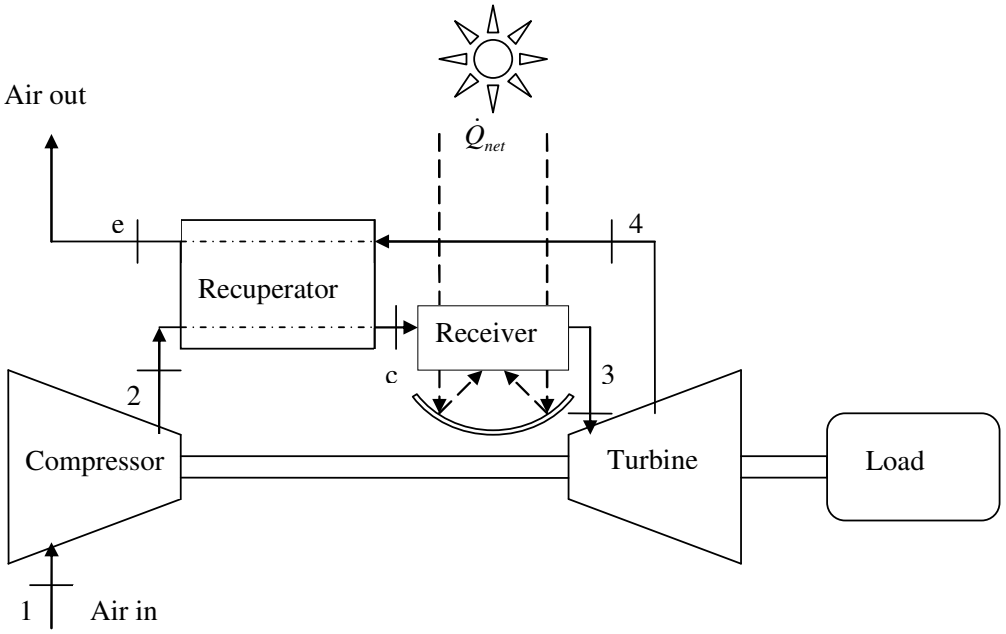

Figure 5.2 The open and direct solar thermal Brayton cycle with recuperator (Weston, 2000).

The inclusion of the recuperator is shown in Figure 5.2. According to Weston (2000), the efficiency of the recuperator can be defined with equation 5.3.

$$\eta_{reg} = \frac{(T_c - T_2)}{(T_4 - T_2)} \tag{5.3}$$

The addition of the recuperator efficiency and 100% compressor and turbine efficiencies results in the following thermal efficiency equation:

$$\eta_{th} = \frac{(K-1)\left(1-\left(\frac{T_1}{T_3}\right)K\right)}{K-\eta_{reg}+(\eta_{reg}-1)\left(\frac{T_1}{T_3}\right)K^2} \tag{5.4}$$

When η_{reg} = 0, equation 5.4 becomes equation 5.2. When η_{reg} = 1, equation 5.4 becomes

$$\eta_{th} = 1-\left(\frac{T_1}{T_3}\right)K \tag{5.5}$$

Equation 5.5 is also given by Stine and Harrigan (1985) and is shown in Figure 2.6. In this figure, the thermal efficiency curves of η_{reg} = 0 and η_{reg} = 1 are compared. Equation 5.4 is plotted in Figure 5.3 for T_3 = 1 200 K, T_1 = 300 K and η_{reg} = 0.77. Also plotted are the curves where η_{reg} = 0 (equation 5.2) and η_{reg} = 1 (equation 5.5). Figure 2.5 from the literature study gives a similarly shaped curve for 0 < η_{reg} < 1.

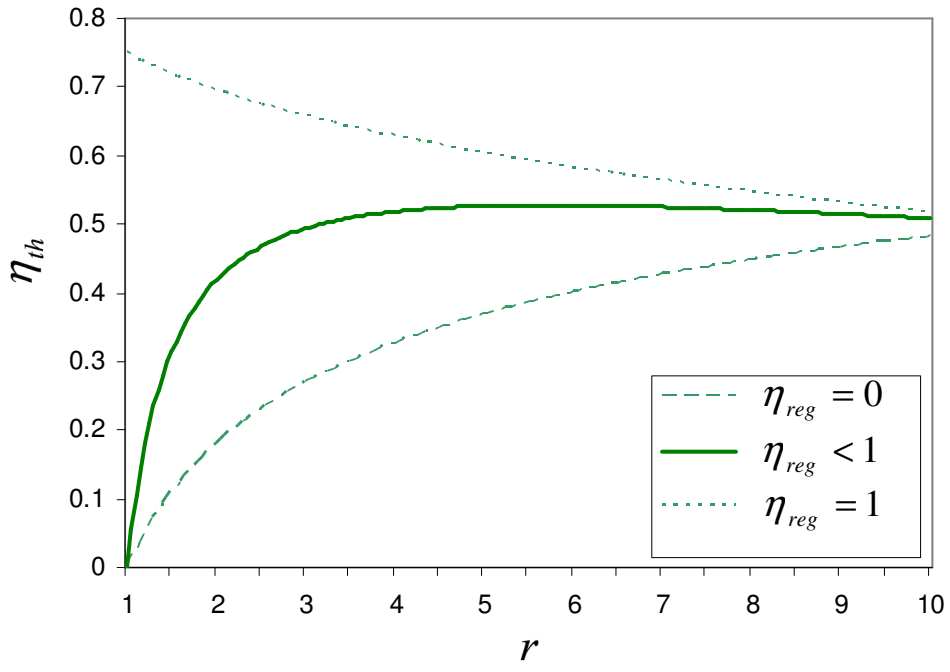

Figure 5.3 Comparison of the thermal efficiency of the Brayton cycle for different cases of recuperation.

Figure 5.3 shows that an optimum thermal efficiency exists when a recuperator is used. Also, this optimum is at a much lower pressure ratio than if the recuperator is not used. The advantages of recuperation are clearly shown. The thermal efficiency curve is bounded by the two curves representing no recuperator and 100% recuperator efficiency respectively.

5.2.1.3 Thermal efficiency - with recuperator and isentropic efficiencies (η_{reg}, η_c, η_t < 1)

The next step would be to include the isentropic efficiency of the turbine and the compressor to see what effect it would have on the thermal efficiency curves. It can be shown that

$$T_2 = T_1\left[1 + (K-1)/\eta_c\right] \tag{5.6}$$

and

$$T_4 = T_3\left[1 - \eta_t\left(1 - \frac{1}{K}\right)\right] \tag{5.7}$$

For this case:

$$\frac{w_t}{|w_c|} = \left(\frac{T_3}{T_1}\right)\frac{\eta_t\eta_c}{K} \tag{5.8}$$

Equation 5.9 shows the thermal efficiency in terms of the recuperator, compressor and turbine efficiencies.

$$\eta_{th} = \left[\frac{\eta_c\eta_t\left(\frac{T_3}{T_1}\right) - K}{K}\right]\left[\frac{K-1}{\eta_c\left(\frac{T_3}{T_1}\right) - \eta_c - (K-1) - \eta_{reg}\eta_c\left(\frac{T_1}{T_3}\right)\left[1 - \eta_t\left(1 - \frac{1}{K}\right)\right] + \eta_{reg}\eta_c + \eta_{reg}(K-1)}\right] \tag{5.9}$$

When η_{reg} = 0, equation 5.9 becomes

$$\eta_{th} = \frac{T_3\eta_c\eta_t - T_1K}{T_3K\left(\frac{\eta_c}{K-1}\right) - T_1K\left(\frac{\eta_c}{K-1}\right) - T_1K} \tag{5.10}$$

When η_{reg} = 1, equation 5.9 becomes

$$\eta_{th} = \left[\frac{\left(\frac{T_3}{T_1}\right)\eta_c\eta_t - K}{K}\right]\left[\frac{K-1}{\eta_t\eta_c\left(\frac{T_3}{T_1}\right)\left(1-\frac{1}{K}\right)}\right] \tag{5.11}$$

Figure 5.4 shows equations 5.9 - 5.11 together with the results of Figure 5.3 (where the isentropic efficiencies were assumed to be 100%).

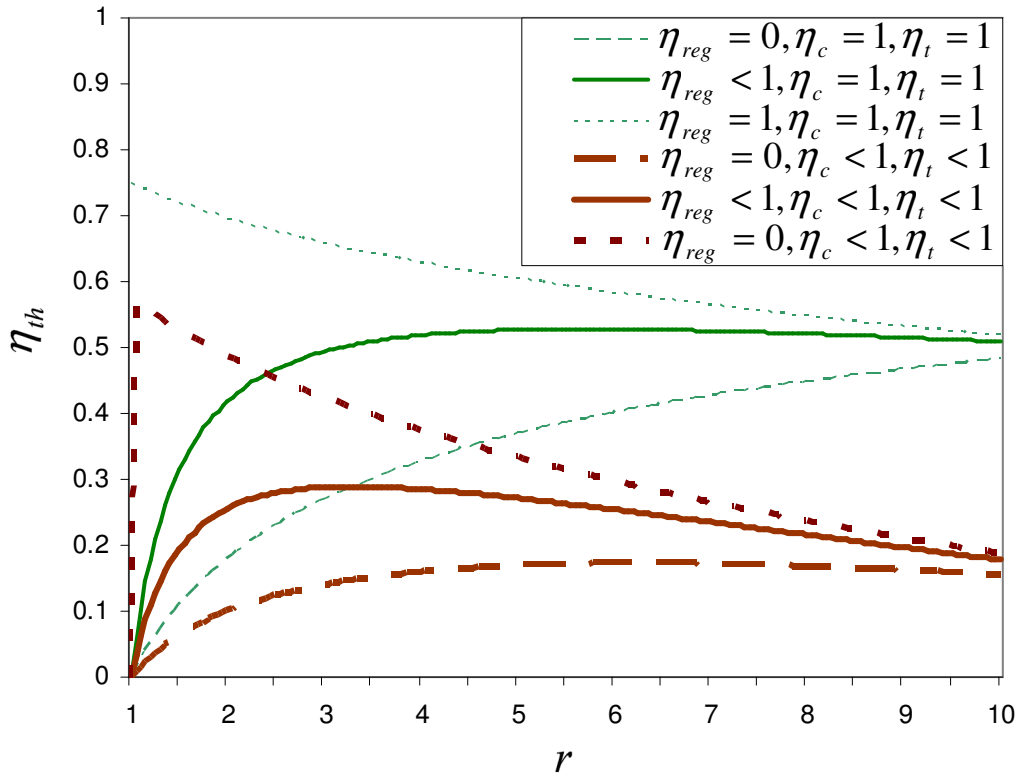

Figure 5.4 The thermal efficiency as a function of pressure ratio for different recuperation situations.

The same shape is generated in Figure 5.4 than in Figure 5.3, except that the curve has shifted lower, due to the isentropic efficiencies of the turbine and compressor being smaller than one. In

this figure, T_3 = 1 200 K, T_1 = 300 K, η_{reg} = 0.77, 0 or 1 and η_c and η_t = 1 or 0.77. It is also shown in Figure 5.4 that a shallow optimum exists. This optimum depends on the temperatures, T_1 and T_3, and the efficiencies of the recuperator, compressor and turbine, as shown in equation 5.9. The thermal efficiency curve is again bounded by two curves from above and below.

5.2.2 Second validation

The net power output is the only reason for interest in the Brayton cycle, or any solar thermal power system for that matter. In equation 3.61, the net power output was defined in terms of the entropy generation rate at each component and duct in the system. By having a similar approach than for the thermal efficiencies in the previous section, equation 3.61 can be plotted as a function of the pressure ratio ($r = P_2 / P_1$) only. For this analysis, all the pressure drops and temperature losses in the system are assumed to be constant. P_3 / P_4 will not be assumed equal to r and T_3 will be a function of r and not a constant. The system mass flow rate is assumed to be a linear function of r. Note that the geometry variables are not yet included. There are also no material constraints for any of the temperatures. All the temperatures and pressures for Figure 3.5 were calculated in a spreadsheet at each pressure ratio, r, by performing an iteration (similar to Section 3.6). The constants used are given in Table 5.1.

The net power output can be plotted in terms of the pressure ratio. Since equation 3.61 was used, the net power output was calculated using the second law of thermodynamics. When plotting the net power output in terms of the first law of thermodynamics with the following equation: $\dot{W}_{net,FirstLaw} = \dot{m} c_p (T_7 - T_8 + T_1 - T_2)$, the first and second law curves can be compared. Equation 3.61 is plotted in Figure 5.5, together with the net power output calculated from the first law of thermodynamics.

Note that these functions were calculated using the temperatures and pressures found with the iteration process and using the constants in Table 5.1. The curves in Figure 5.5 are of the same shape as the thermal efficiencies in Section 5.2.1. For both curves (from the first and second laws of thermodynamics) in Figure 5.5, an optimum exists at a pressure ratio of approximately 1.6. For the second law, the contribution from the ducts to the total entropy generation was assumed negligible and might be the reason for the small difference between these curves. The close comparison of the curves in Figure 5.5 shows that the net power output from equation 3.61 is correctly described in terms of the total entropy generation rate in the system.

Table 5.1 Assumptions for second validation.

Definition	Value	Units
η_{reg}	0.8	-
η_c	0.73	-
η_t	0.73	-
R	287	J/kgK
c_p	1004	J/kgK
T_1	300	K
ΔT_{23}	2	K
ΔT_{45}	2	K
ΔT_{67}	2	K
ΔT_{89}	2	K
P_1	80	kPa
ΔP_{23}	0.1	%
ΔP_{34}	1	%
ΔP_{45}	0.4	%
ΔP_{56}	0.8	%
ΔP_{67}	0.4	%
ΔP_{89}	0.1	%
ΔP_{910}	1	%
$\dot{Q}_{loss,23}$	2	W
$\dot{Q}_{loss,45}$	2	W
$\dot{Q}_{loss,67}$	2	W
$\dot{Q}_{loss,89}$	2	W
$\dot{Q}_{loss,reg}$	2	W
$\dot{Q}_{rec}$*	64 000	W
$\dot{Q}_{loss,rec}$	6 400	W

At higher pressure ratios, the net power output becomes negative, which means that the power output of the turbine is smaller than the power required from the compressor. Such a system would not be possible. However, these data points show the rate of decrease in net power output as the pressure ratio increases, at higher pressure ratios.

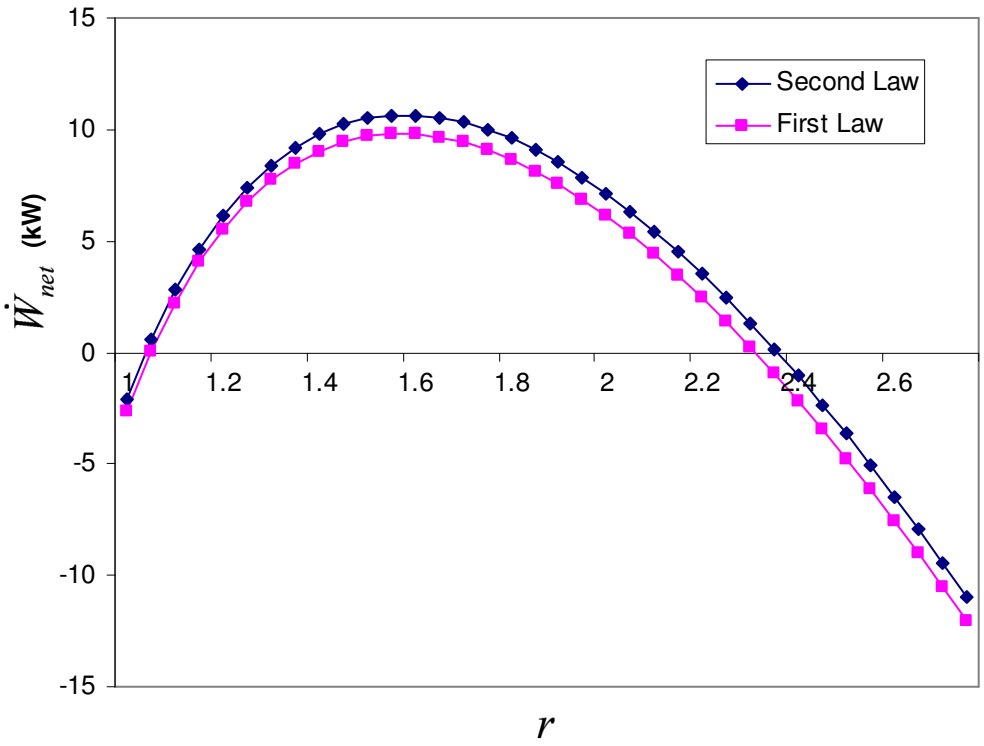

Figure 5.5 Net power output calculated with the first and second laws of thermodynamics as a function of the pressure ratio.

The thermal efficiencies are plotted in Figure 5.6, for different assumptions for the compressor, turbine and recuperator efficiencies (similar to Section 5.2.1.3). The thermal efficiency curve is bounded by two curves. When comparing this figure with Figure 5.4, it seems that the thermal efficiency drops quicker in Figure 5.6. It is as if the curves are 'pulled' downwards. This can be because T_3 is no longer a constant (as in Section 5.2.1), but is now also a function of the compressor pressure ratio. This is a much more realistic curve than the curve shown in Figure 5.3. Also note that the curve, where no recuperator is used and the isentropic efficiencies are included, is not shown. This curve did not appear in the positive region (making a working system with no recuperator and real compressor and turbine efficiencies impossible). The method of entropy generation can be used to get the optimum receiver and recuperator geometries which could 'lift' the thermal efficiency curve to higher values.

Figure 5.7 shows the contribution of the turbine, compressor, recuperator and solar receiver to the total entropy generation rate, based on the assumptions in Table 5.1. The entropy generation rate in the ducts was very small compared with the other components and was neglected. The entropy generation rate in a duct would be very small if the duct is well-insulated and if it has a large hydraulic diameter.

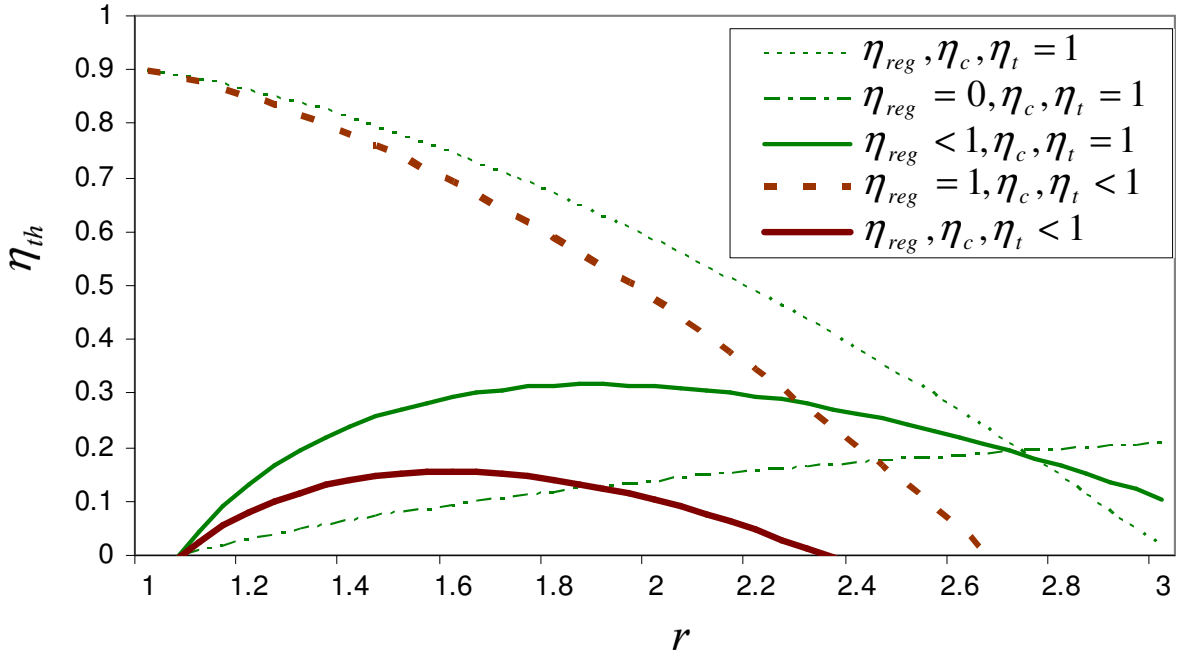

Figure 5.6 Thermal efficiency as a function of the pressure ratio.

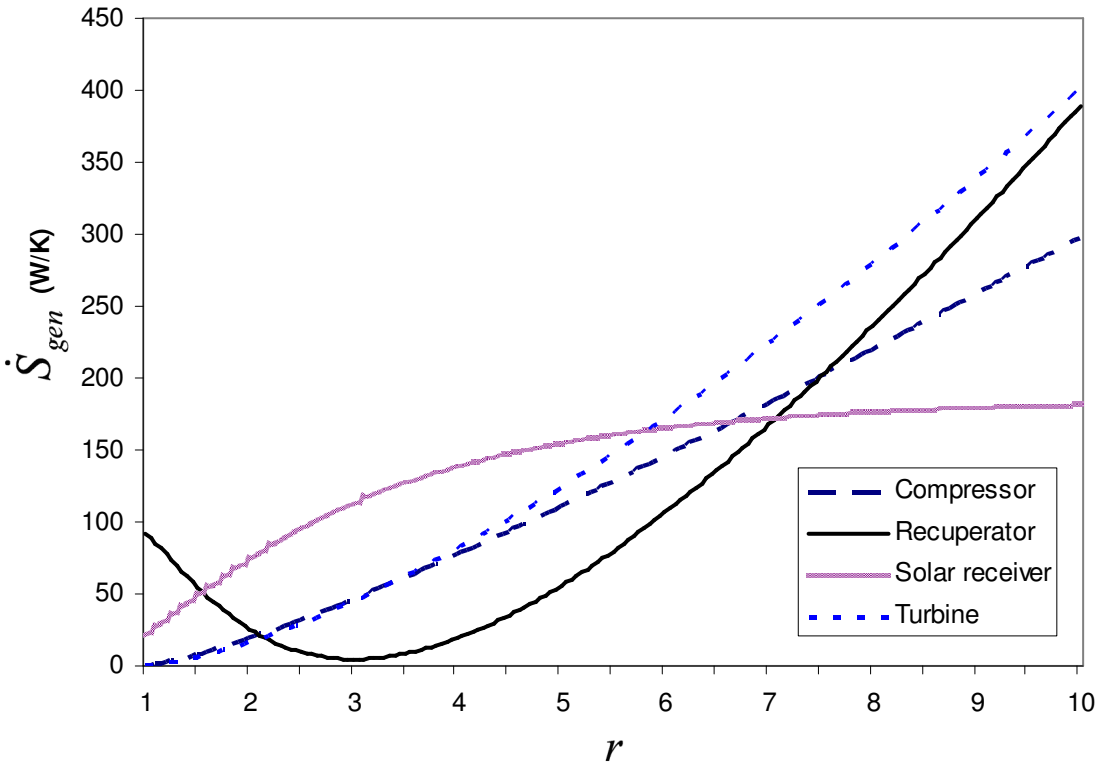

Figure 5.7 Contribution of the compressor, turbine, recuperator and receiver to the total entropy generation rate.

5.2.3 Conclusion of the validation

From the validation, it can be concluded that an optimum pressure ratio exists for a system with a set of constants describing the losses in the system. The net power output of the system is

accurately described in terms of the total entropy generation of the system when comparing the first and second laws of thermodynamics. In the next section, the results are shown from the analysis as described in Chapters 3 and 4. In this full analysis, the pressure ratio was treated as a parameter, the mass flow rate and compressor and turbine efficiencies depended on the micro-turbine used while the pressure losses, temperature losses and recuperator efficiency depended on the geometry of the receiver and recuperator.

5.3 Results of the full analysis

5.3.1 Introduction

Table 5.2 Constants used for the analysis.

Surroundings at location	**Value**	**Unit**
T_0	300	K
I	1 000	W/m^2
w	1 (no wind)	
P_1 or P_{atm}	80	kPa
Concentrator and receiver		
e_p	6.7 (0.38°)	mrad
φ_{rim}	45	degrees
$refl$	0.93	
$T_{s,\max}$	1 200	K
β	90	degrees
$CR_{\min}$	100	-
Recuperator		
t	0.001	m
k	401	W/mK
H	1	m
$L_{\max}$	radius of dish concentrator	m

In this section, the results of the optimum recuperator and solar receiver geometry variables are shown. The results also show the optimum operating conditions of the micro-turbines (or points of highest maximum net power output). The results are shown for different concentrator sizes of

D = 6, 8, 10, 12, 14, 16 and 18 m. For each concentrator diameter, each micro-turbine and each of its operating conditions, the maximum net power output was found. Two cavity receiver models were analysed and results showed no major difference between the maximum net power outputs and optimum recuperator geometry of the two models. However, each receiver construction method had its own optimum geometry. In the remaining sections, the results shown are relevant for the receiver constructed using a circular tube or rectangular channel, except where the cavity construction method is specifically mentioned. The maximum net power output obtained using entropy generation minimisation, is compared with the maximum net power output calculated with the first law of thermodynamics. The results were obtained using the constants in Table 5.2, as explained in Section 3.9.

The constants in Table 5.2 were also changed to see what their effect would be on the maximum net power output and optimum geometry of the system. This means that the effect of surrounding and parameter changes on the maximum net power output and its optimum system geometry required was investigated. These results are also shown. Recommendations for further work are also given.

5.3.2 Optimum geometry for maximum net power output

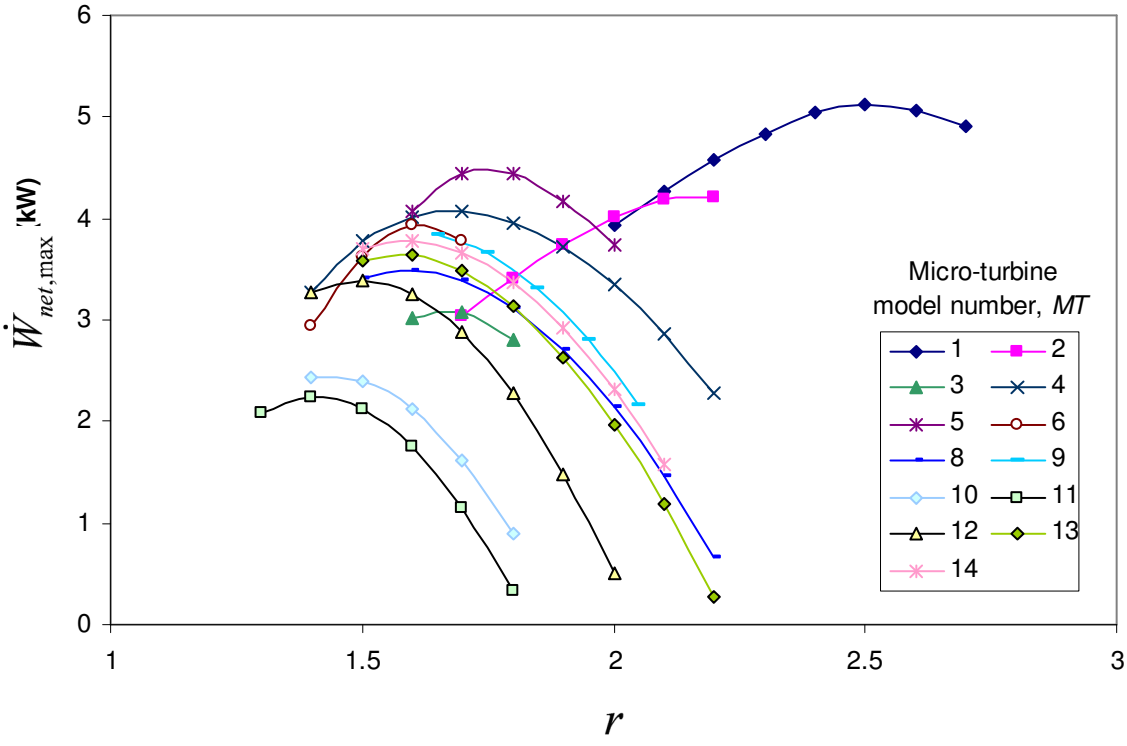

Figure 5.8 Data points for maximum net power output with an optimum geometry for concentrator with *D* = 6 m.

The analysis found the optimum geometry variables, which produce maximum net power output for the system, at the different parameters. These parameters are the concentrator diameter, micro-turbine used and the operating condition (pressure ratio or mass flow rate) in the range of the specific micro-turbine's optimum compressor efficiency (as shown in Section 3.5.2). Figure 5.8 shows the maximum net power output as a function of the pressure ratio for a collector with a concentrator diameter of ***D*** = 6 m as an example. It is very important to note that each data point is a result of the optimisation algorithm and shows a maximum net power output because of its optimised geometry. One should also note that each micro-turbine has an optimum operating point, which produces the highest maximum net power output for the system. The details of the different micro-turbine models are shown in Appendix D. The micro-turbine model number (*MT*) is used to describe a micro-turbine.

Table 5.3 Results showing optimised geometry variables and maximum net power output for *MT* = 4 and *D* = 6 m using a circular tube as receiver construction method, all geometry units in metre, except for the ratios.

r	$\dot{m}$ (kg/s)	$(D_{h,rec})_{opt}$	$(L_{rec})_{opt}$	$(a/b_{rec})_{opt}$	$(D_{h,reg})_{opt}$	$(L_{reg})_{opt}$	$(a/b_{reg})_{opt}$	$(\dot{W}_{net})_{\max}$ (W)
1.4	0.083	0.1098	20.61	-	0.008039	3	5.452	3265
1.5	0.089	0.1098	20.60	-	0.006389	3	6.396	3776
1.6	0.096	0.1098	20.60	-	0.005365	3	7.379	4019
1.7	0.102	0.1008	18.91	-	0.005085	3	8.127	4070
1.8	0.109	0.0995	18.67	-	0.004872	3	8.871	3961
1.9	0.115	0.0981	18.40	-	0.004715	3	9.592	3715
2	0.122	0.0956	17.94	-	0.004600	3	10.30	3343
2.1	0.128	0.0901	16.91	-	0.004525	3	10.99	2858
2.2	0.134	0.0877	16.45	-	0.004487	3	11.64	2269

Table 5.4 Results showing optimised geometry variables and maximum net power output for *MT* = 4 and *D* = 6 m using a rectangular channel as receiver construction method, all geometry units in metre, except for ratios.

r	$\dot{m}$ (kg/s)	$(D_{h,rec})_{opt}$	$(L_{rec})_{opt}$	$(a/b_{rec})_{opt}$	$(D_{h,reg})_{opt}$	$(L_{reg})_{opt}$	$(a/b_{reg})_{opt}$	$(\dot{W}_{net})_{\max}$ (W)
1.4	0.083	0.0741	12.03	4.071	0.008198	3	5.418	3235
1.5	0.089	0.0916	14.11	2.5	0.006581	3	6.331	3770
1.6	0.096	0.0842	9.892	2.5	0.005782	3	7.186	4085
1.7	0.102	0.0825	7.039	2.5	0.005255	3	8.025	4209
1.8	0.109	0.0743	6.100	2.5	0.004851	3	8.883	4120
1.9	0.115	0.0719	5.897	2.5	0.004693	3	9.610	3881
2	0.122	0.0698	5.731	2.5	0.004578	3	10.32	3514
2.1	0.128	0.0683	5.605	2.5	0.004501	3	11.01	3033
2.2	0.134	0.0671	5.506	2.5	0.004462	3	11.67	2447

The data points (as shown in Figure 5.8) of micro-turbine 4 with ***D*** = 6 m and circular tube receiver construction method are shown in Table 5.3. Table 5.4 shows the same data points but a rectangular flow channel (plate) is used as receiver construction method. Take note that the

highest maximum net power output (or optimum operating condition of the micro-turbine) is highlighted for each of these cases.

No significant difference was found between the maximum net power outputs of the different receiver construction methods. However, each receiver construction method had its own optimum geometry. The optimum geometries shown in the tables will be explained in the following section. The remaining results are for both receiver cavity construction methods, except where a specific one is mentioned. Figure 5.9 shows the same results as in Figure 5.8, but as a function of the mass flow rate.

Data points were found for all the concentrator diameters (***D*** = 6 – 18 m) with all the micro-turbines (1 – 45), which gave a reasonable net power output. Figure 5.10 shows the results for ***D*** = 10 m and Figure 5.11 shows the results for ***D*** = 14 m as a function of the system mass flow rate. When comparing Figures 5.9, 5.10 and 5.11, it can be concluded that the larger micro-turbines performed better at larger concentrator diameters and vice versa. Figure 5.12 shows all the data points found in the analysis for each of the different concentrator diameters, micro-turbines and micro-turbine operating conditions.

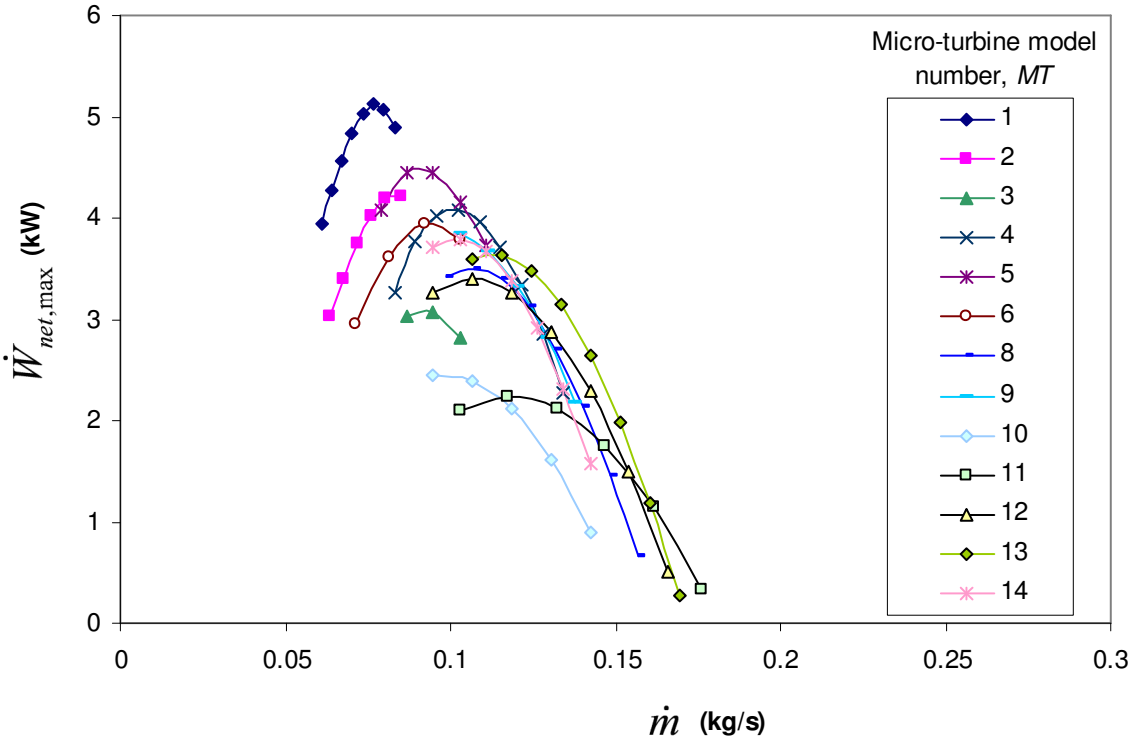

Figure 5.9 Maximum net power output at an optimum geometry for a concentrator with *D* = 6 m.

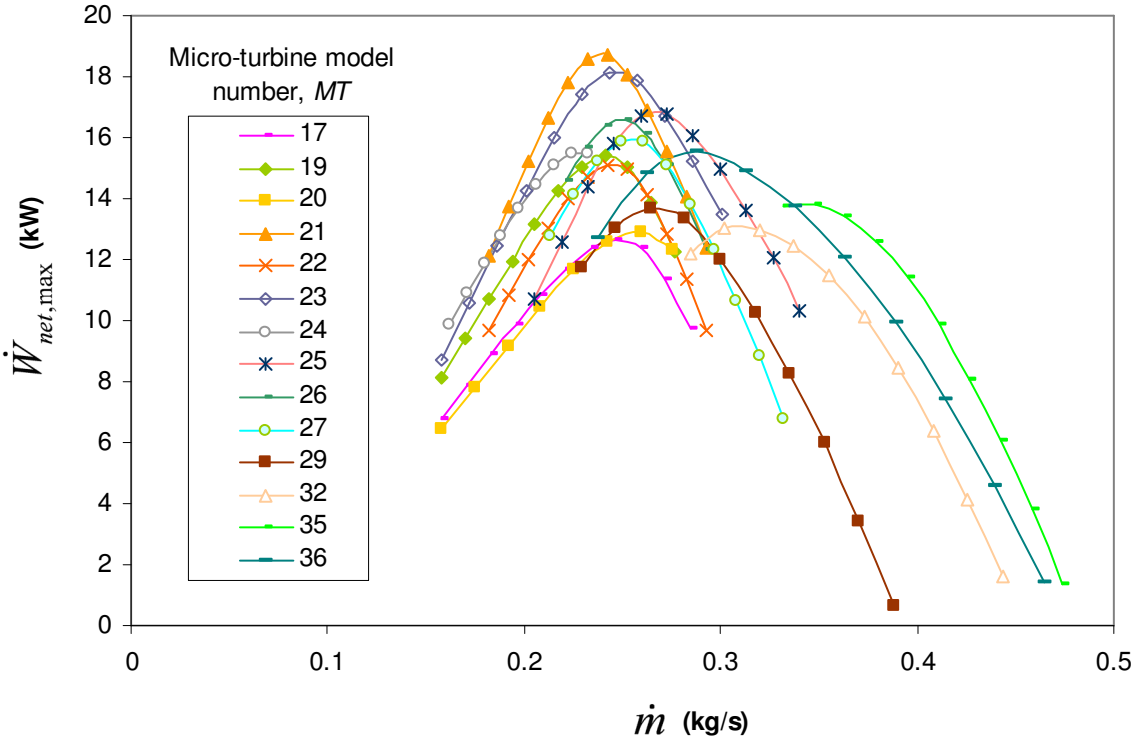

Figure 5.10 Maximum net power output at an optimum geometry for a concentrator with *D* = 10 m.

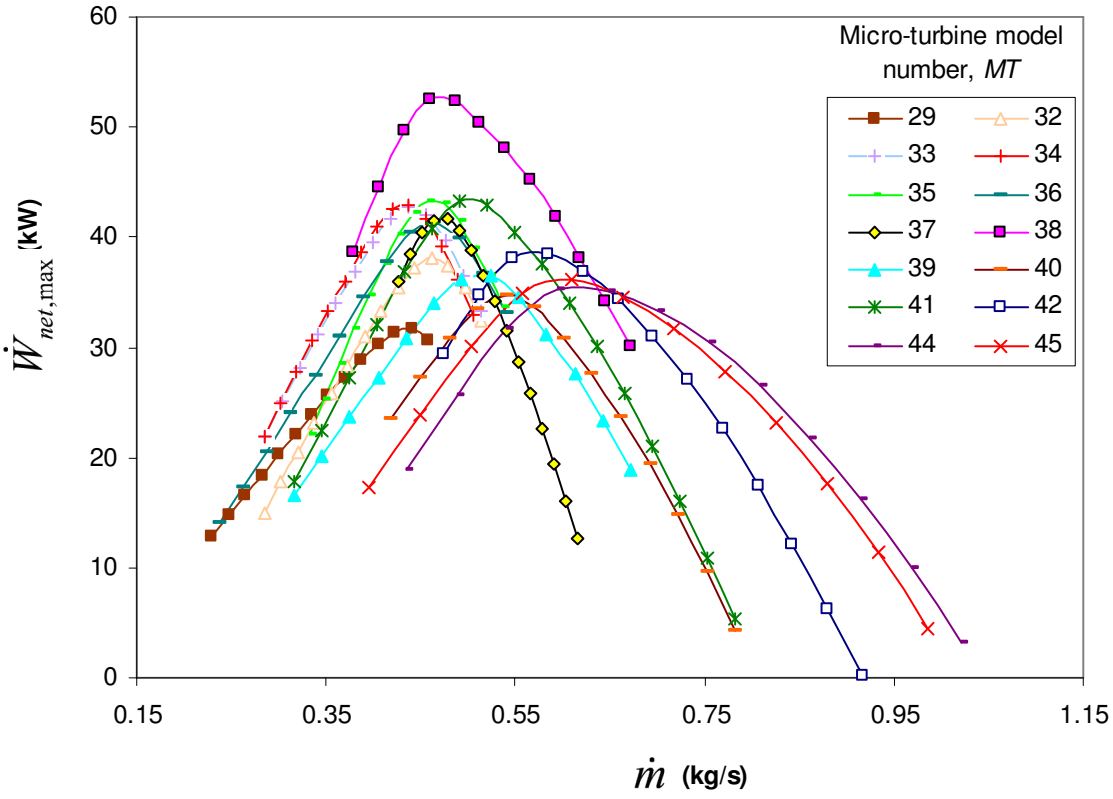

Figure 5.11 Maximum net power output for different micro-turbines and their operating ranges for *D* = 14 m.

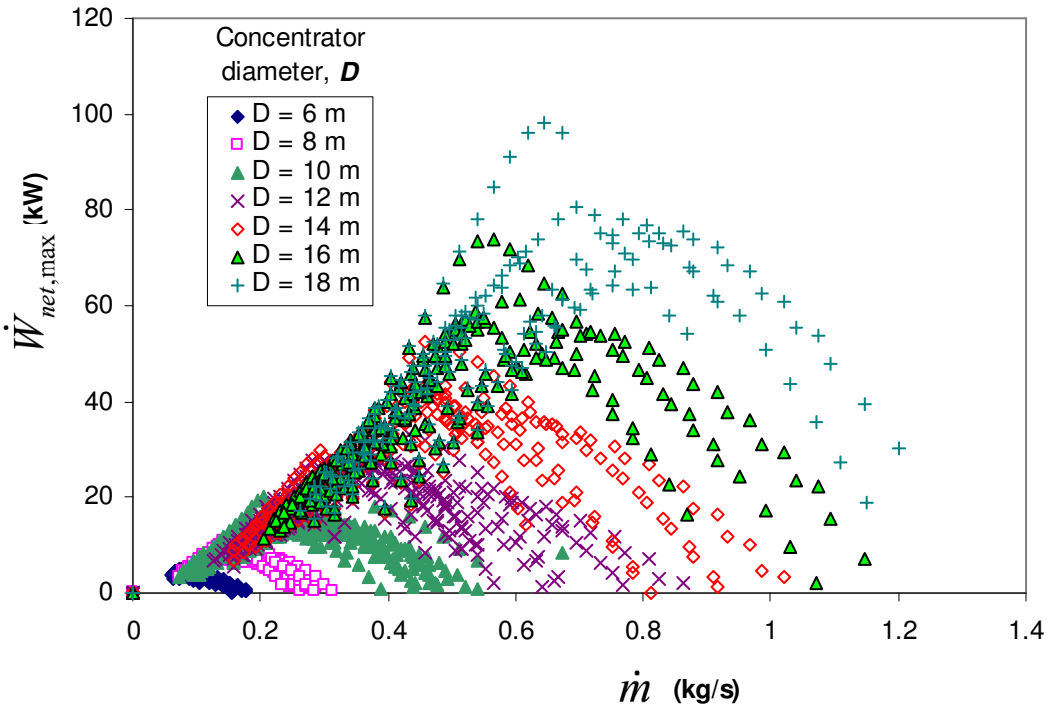

Figure 5.12 All the data points for the range of concentrator diameters and micro-turbines.

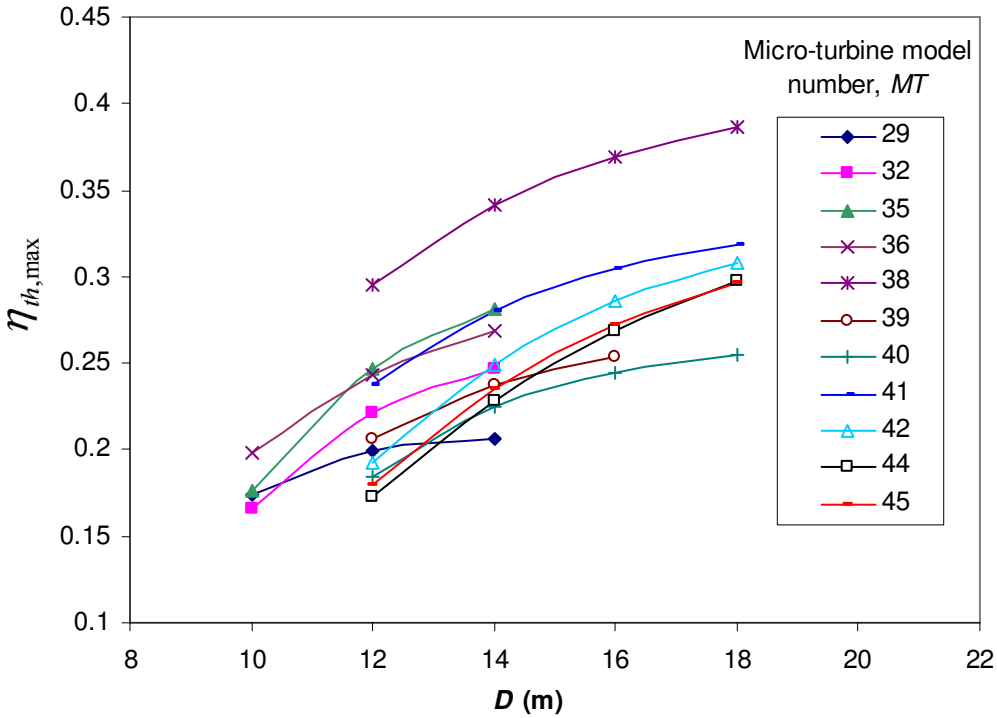

Figure 5.13 Thermal efficiencies of the optimised systems as a function of concentrator diameter and micro-turbine choice.

In some cases, a single micro-turbine had an optimum operating condition (or highest maximum net power output) at a number of different concentrator diameters. This is shown in Figure 5.13, where the maximum thermal efficiencies for each of these optimum points are compared. The thermal efficiency is a function of the concentrator diameter and micro-turbine used. A higher thermal efficiency can be expected when using a larger concentrator, although an even higher thermal efficiency can result when using the correct micro-turbine.

Consider again the data points which give the highest maximum net power output. The optimum recuperator channel aspect ratio of these data points, $(a/b)_{reg,opt}$, as a function of the mass flow rate, is shown in Figure 5.14. The relationship between the optimum aspect ratio as a function of the mass flow rate is a linear relationship. This line can be approximated with equation 5.12. Furthermore, when plotting the optimum recuperator channel width as a function of the mass flow rate, a linear relationship is found again.

$$(a/b)_{reg,opt} \approx 83.3\dot{m}_{opt} \tag{5.12}$$

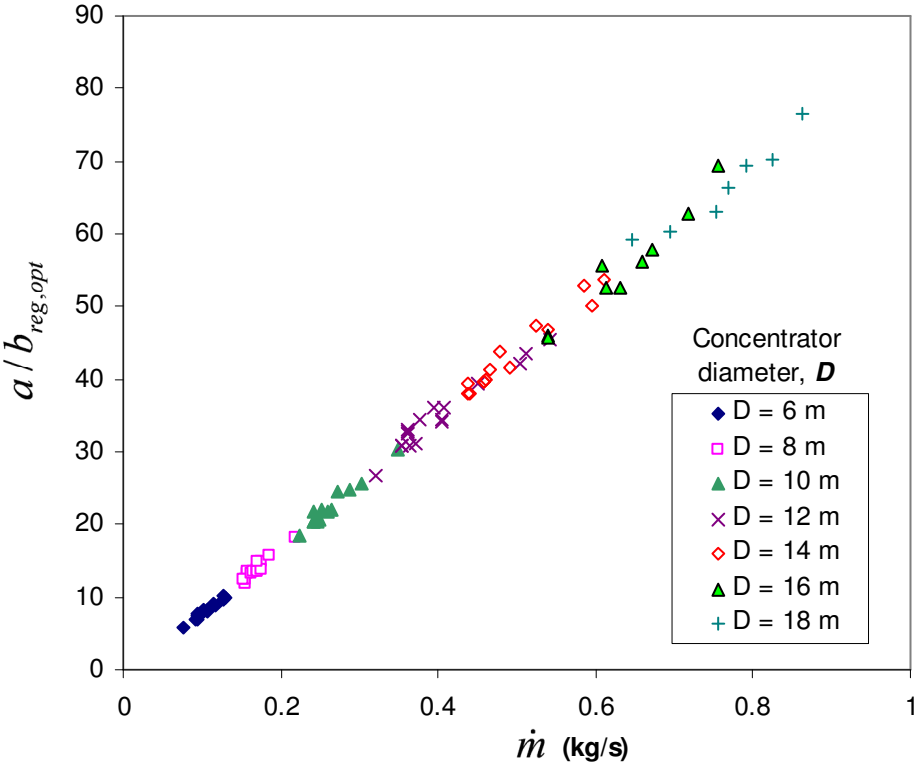

Figure 5.14 Optimum aspect ratio of the recuperator channels at optimum operating conditions of various micro-turbines.

Take note that these data points are the points of the optimum operating conditions for different micro-turbines and different concentrator diameters. When including all of the data points from the analysis, this linear relationship disappears underneath a scattering of data. The linear relationship is thus only valid for an optimised geometry at the optimum operating conditions (with highest maximum net power output) of different micro-turbines. Other studies have found that, for a rectangular channel, an aspect ratio of eight should be used for minimum entropy generation in the channel (Ratts and Raut, 2004). In this work, however, results show that an aspect ratio of eight is not necessarily the optimum aspect ratio for the receiver and recuperator channels in a system which should produce maximum net power output. This is because EGM was done for the whole system, instead of for the components individually.

Figure 5.15 shows that, for a specific micro-turbine (number 27 in this example), there exists a line of maximum net power output as a function of mass flow rate. This is shown more clearly in Figure 5.16 for micro-turbine 41. The larger the concentrator, the more the net power output tends towards this line. The smaller the concentrator diameter and the higher the mass flow rate, the lower maximum net power output can be expected.

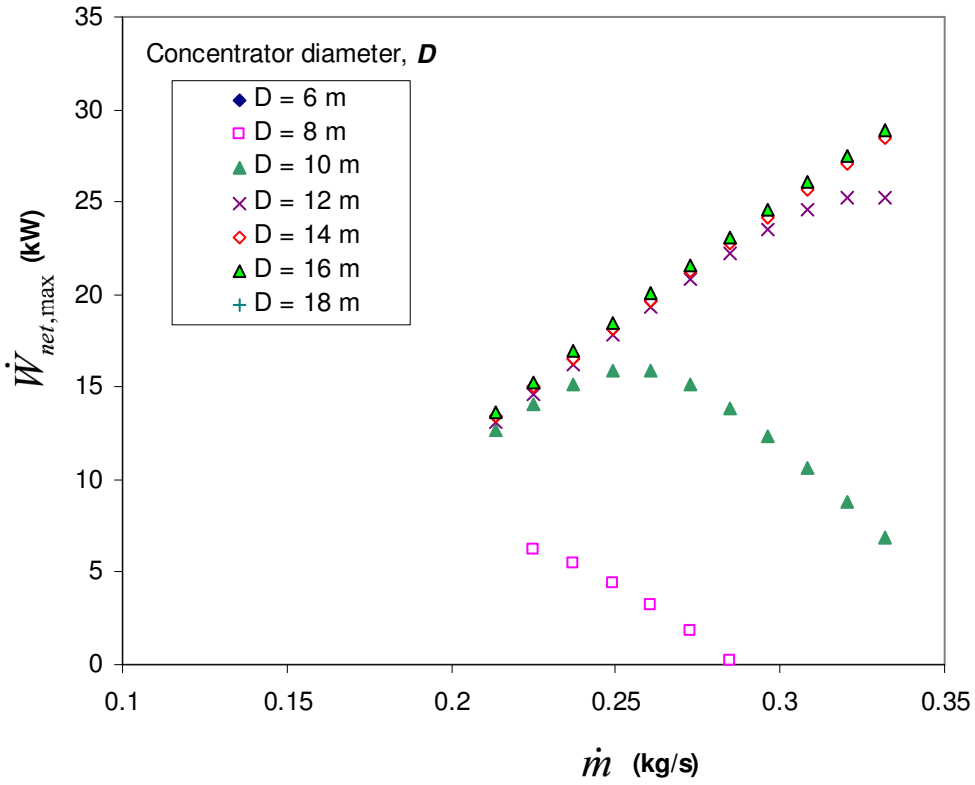

Figure 5.15 Roofline for the maximum net power output for micro-turbine number 27.

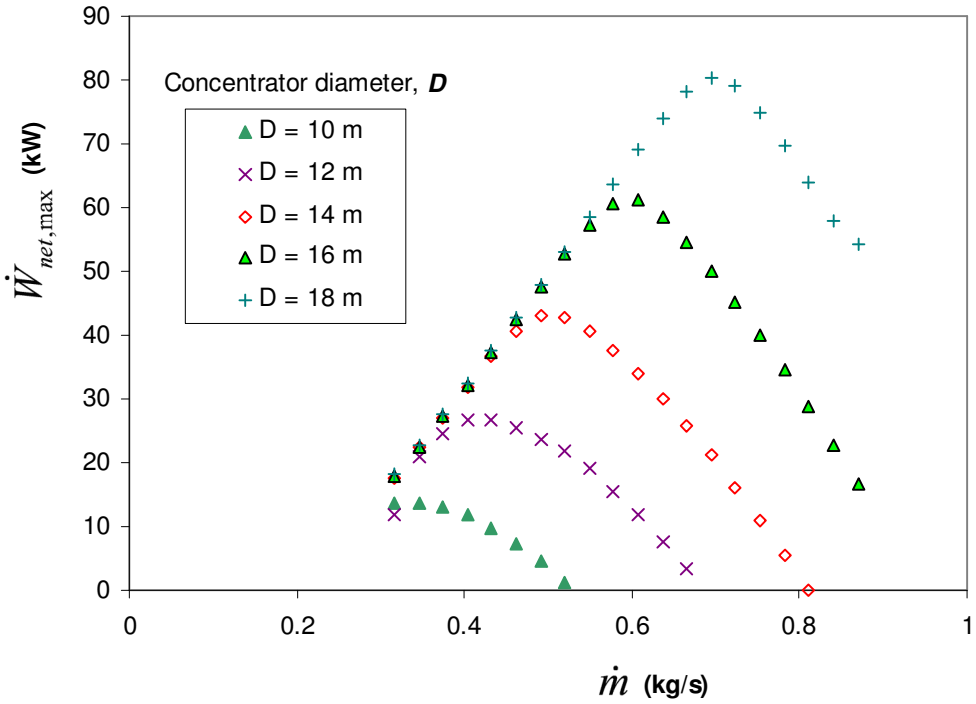

Figure 5.16 Roofline for the maximum net power output for micro-turbine number 41 with different concentrator diameters.

All the data points (where a plate cavity receiver construction method was used) which were geometrically optimised in this analysis, converged to one of two constraint limits. Results showed that a large cavity aperture or small aspect ratio but not necessarily both, is beneficial for the rectangular receiver channel. The two constraints were $CR \geq 100$ and $a/b_{rec} \geq 2.5$. When considering the circular tube receiver construction method, it is interesting to note that most of these optima also lie on an aperture size constraint of $CR = CR_{\min} = 100$. One can come to the conclusion that it is beneficial for the system's net power output, that the receiver aperture is relatively large in comparison with the concentrator. This can be expected since the effect of wind was neglected.

The optimum recuperator length, $L_{reg,opt}$, mostly converged on its constraint, as was set in Section 3.8. This is shown in Figure 5.17, where all the data points are shown, and in Figure 5.18, where the optimum recuperator length is shown for micro-turbine 41 at ***D*** = 16 m. The optimum recuperator length increased as the mass flow rate increased until the constraint was reached. It is therefore more beneficial for a system with small mass flow rate to have a short recuperator. Systems with short recuperator lengths (relative to the concentrator radius), however, usually do not have high maximum net power outputs.

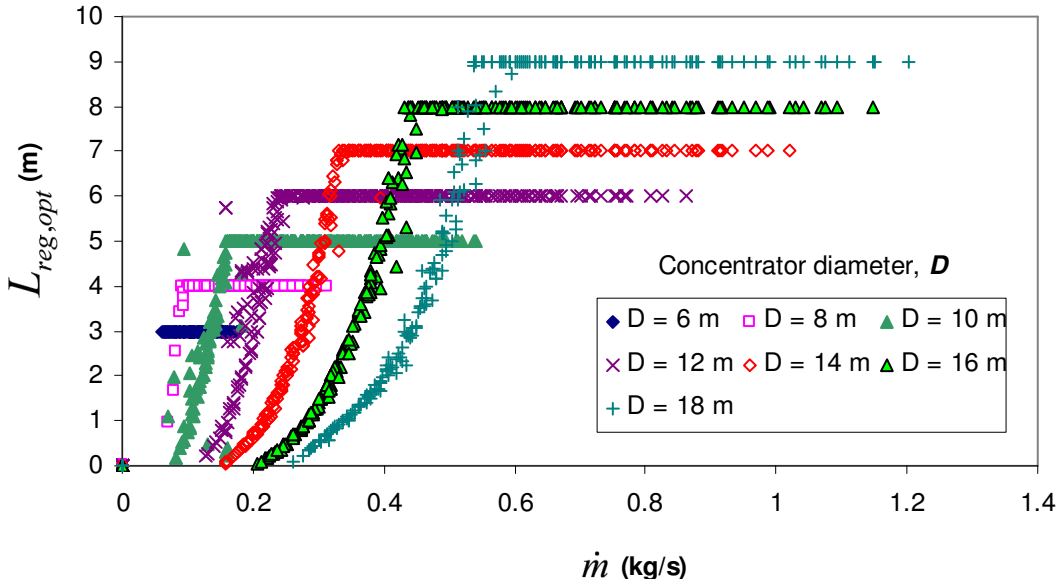

Figure 5.17 Convergence of the optimum recuperator length to its maximum constraint.

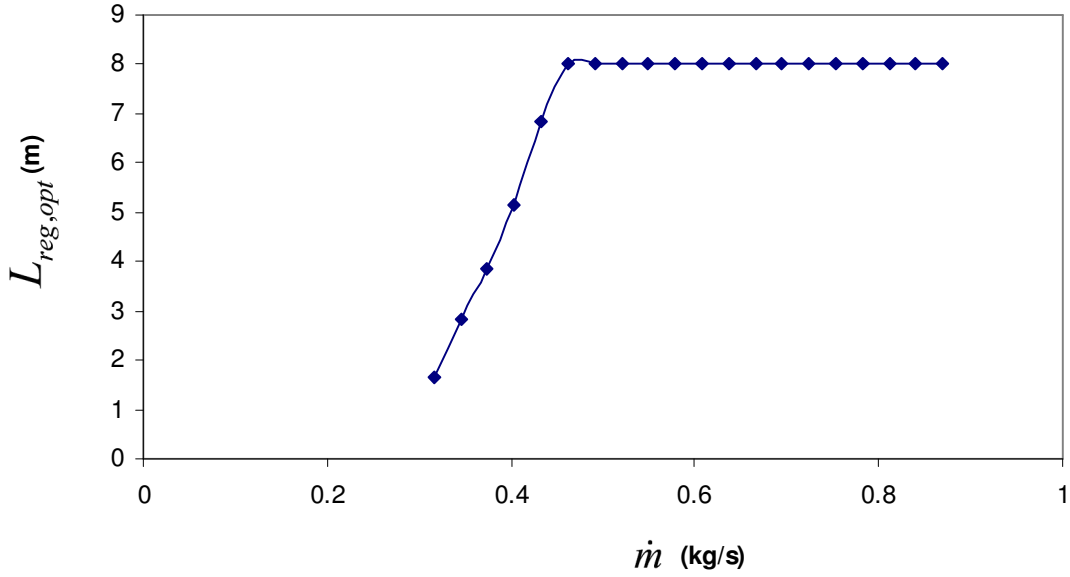

Figure 5.18 Convergence of the optimum recuperator length for *D* = 16 m with micro-turbine 41.

In Figure 5.19, the optimum hydraulic diameter of the recuperator channels is shown as a function of system mass flow rate. At small mass flow rates, the optimum hydraulic diameter increases as system mass flow rate increases, until the recuperator length constraint is reached. For increasing mass flow rate, the optimum hydraulic diameter decreases until a minimum diameter is reached where the maximum pressure drop exists. The optimum hydraulic diameter increases slightly as the mass flow rate increases.

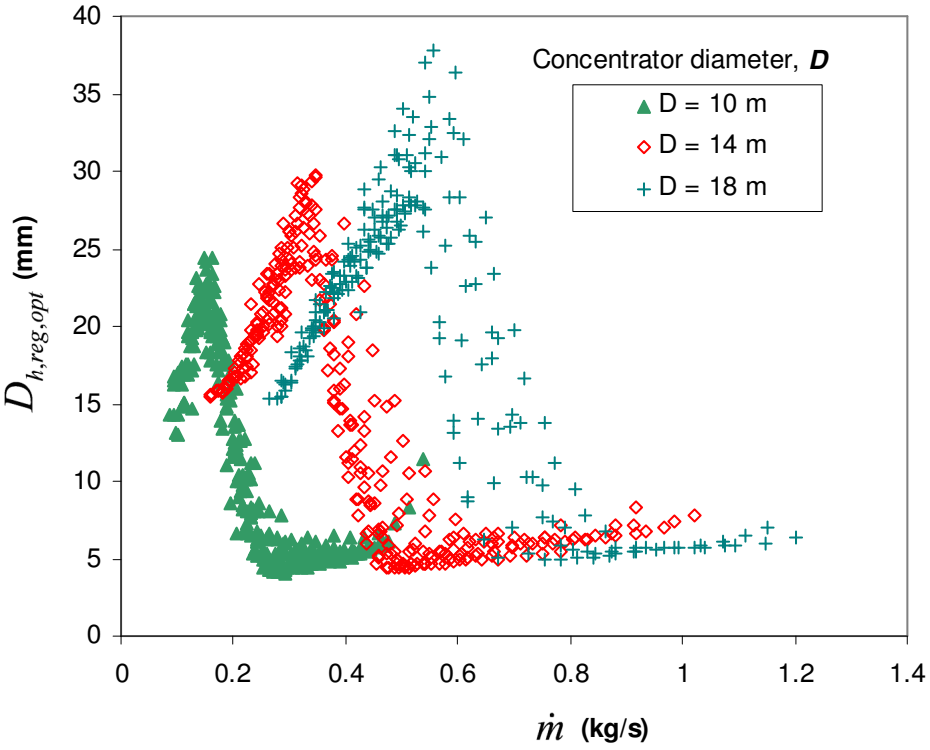

Figure 5.19 Optimum hydraulic diameter of recuperator channels as a function of system mass flow rate for *D* = 10, 14 and 18 m.

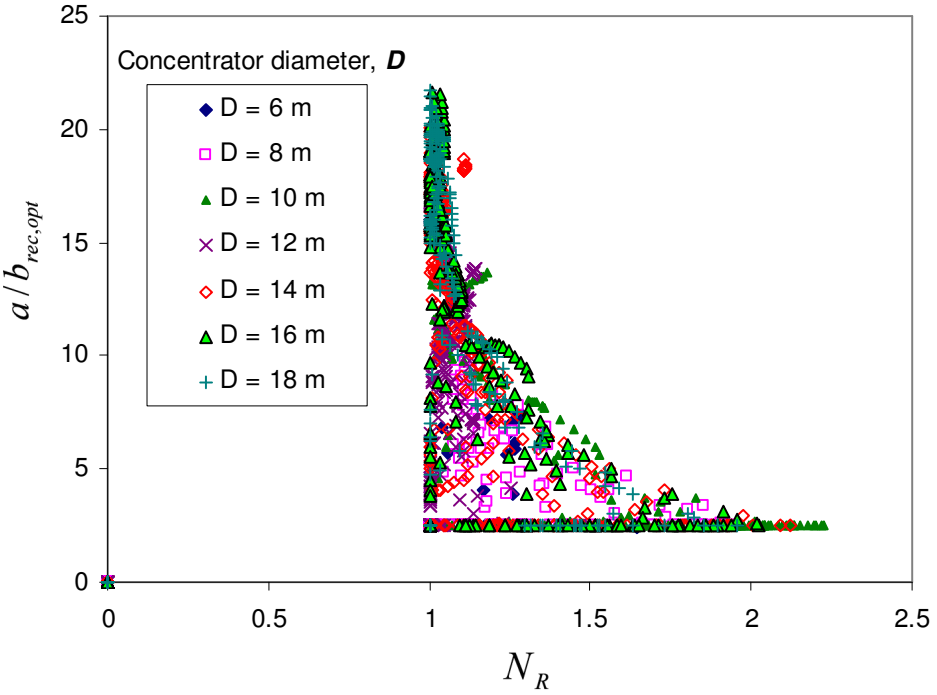

Figure 5.20 Optimum number of rectangular tubes between the receiver edge and the receiver aperture as a function of the optimum receiver channel aspect ratio.

It was also found that the receiver of the optimised system would not necessarily have the aperture diameter that intercepts the maximum solar heat input, as shown in Figure A.4. According to the results, a larger aperture diameter, which absorbs less solar heat (see Appendix A) can produce a larger net power output in some systems. From each of the optimised data points in the analysis, it was found that there exists an optimum number of tube diameters, N_D, or rectangular channels, N_R, which fit in between the receiver aperture edge and the receiver edge (in Figure 3.6, for example, N_D = 4). The definition of N_D is shown in equation 5.13.

$$N_D = \left(\left(\sqrt{3}-1\right)d\right)/\left(2D_{h,rec}\right) \tag{5.13}$$

For a specific concentrator diameter, N_D decreases as the mass flow rate increases until it reaches its constraint of two, except for systems using large concentrators with a plate-type receiver. The optimum receiver tube diameter was found to be relatively large compared with the receiver. It was found that, for all the data points in the analysis, $2 \le N_D \le 4$. This means that the optimum receiver tube diameter is mostly relatively large. For the rectangular channel receiver, $D_{h,rec}$ in equation 5.12 can be replaced with a – the longest side of the rectangular channel. For all the optimised plate-type receiver geometries in the analysis, it was found that $1 \le N_R \le 2.3$. For the rectangular channel receiver at large concentrators, N_R did not decrease as the mass flow rate increased, but for small concentrators, it behaved similarly to the circular tube receiver. Figure 5.20 shows that, for an optimum receiver channel geometry in all of the cases, a large aspect ratio is accompanied with a small N_R and a large N_R is accompanied with a small aspect ratio. Note that all the data points are shown in Figure 5.20.

Another interesting observation for the circular tube receiver is the relationship between the optimum receiver diameter, $D_{rec,opt}$ and the optimum receiver length, $L_{rec,opt}$. This is shown in Figure 5.21. It is optimum for a long receiver tube to have a small tube diameter and vice versa, except at very small receiver tube lengths where the tube diameter is also small. For the rectangular channel receiver, however, there is no established pattern between the hydraulic diameter and channel length. This can be expected because the hydraulic diameter of a rectangular channel is a function of the channel aspect ratio.

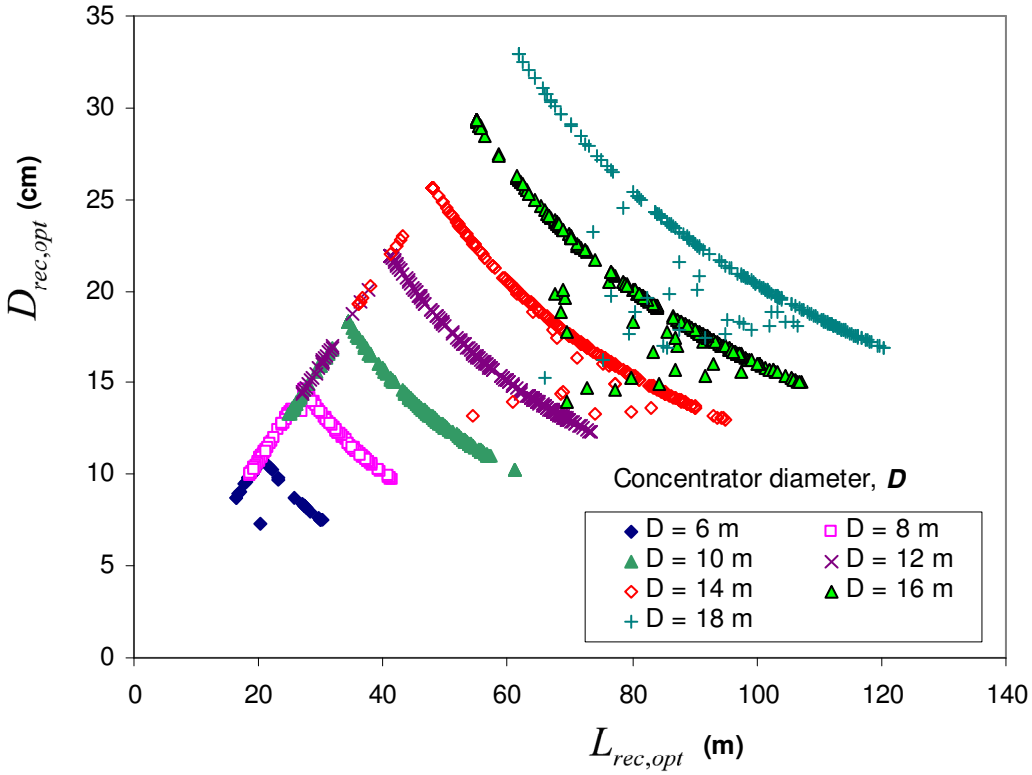

Figure 5.21 Relationship between the optimum tube diameter and the optimum length for the circular tube receiver.

This section showed the optimum recuperator and receiver geometries for a recuperative open and direct solar thermal Brayton system, which produces its maximum net power output, as calculated with the method of entropy generation minimisation.

5.3.3 Maximum net power output with optimum operating conditions and system properties

Consider again the constants given in Table 5.2. For all the optimised data points (all ***D***, and all operating points of all the micro-turbines), the optimum recuperator channel mass flow rate behaved in a specific way relative to the mass flow rate of the system. This is shown in Figure 5.22. The optimum NTU (see equation 3.31) also behaved in a very specific manner as a function of the system mass flow rate, as shown in Figure 5.23.

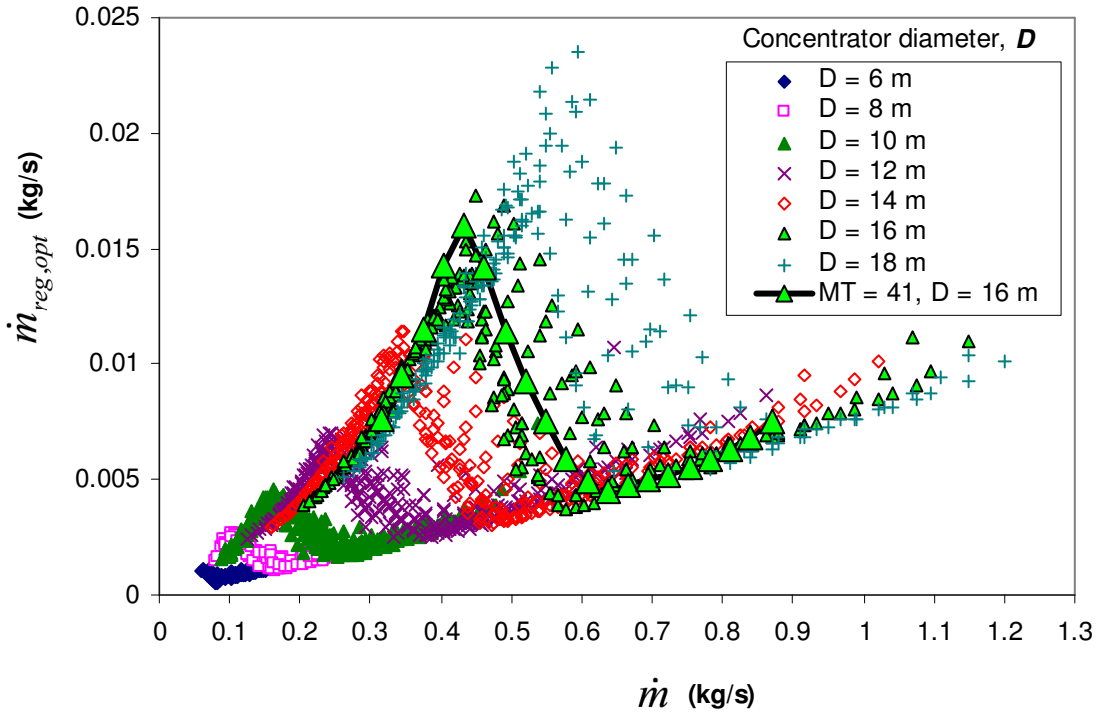

Figure 5.22 Optimum recuperator channel mass flow rate for all data points.

The behaviour of the optimum mass flow rate of the recuperator is shown more clearly in Figure 5.24 (showing only ***D*** = 8, 12 and 16 m). Note the similarity between Figures 5.24 and 5.19. Take note that each data point in Figure 5.24 has an optimum geometry and gives maximum net power output at its specific mass flow rate. When inspecting Figure 5.25 (again, ***D*** = 6, 10, 14 and 18 m are not shown, but behaved similarly), it can be concluded that, for all the data points, the optimum NTU increases as the system mass flow rate increases until it reaches its maximum. This means that it is most beneficial for a system with a small mass flow rate to have a small NTU. The following paragraph explains why.

Micro-turbine 41 is considered because it has a very large operating range at its maximum compressor efficiency. Understanding the behaviour of this micro-turbine is very helpful in understanding Figures 5.24 and 5.25. The optimum distribution of the minimum entropy generation is shown for ***D*** = 16 m with micro-turbine 41 in Figure 5.26. This distribution was found to be similar for all the combinations of concentrator diameters and micro-turbines optimised in this analysis. Note that for the optimised system, the entropy generation in the receiver is the largest (Figure 5.26a).

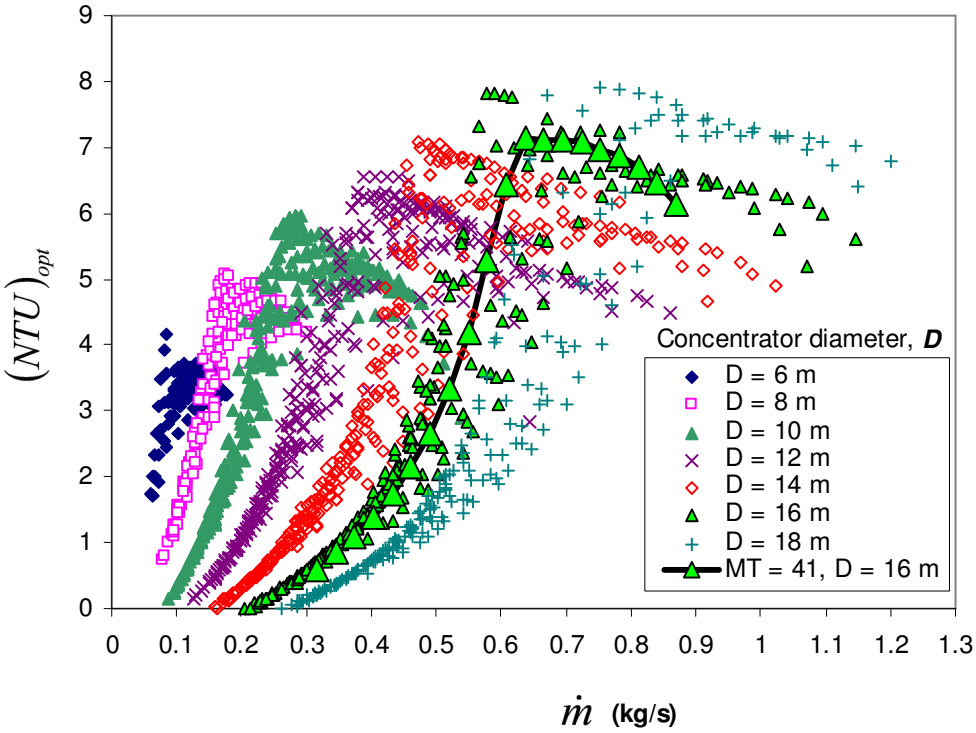

Figure 5.23 Optimum *NTU* for all data points.

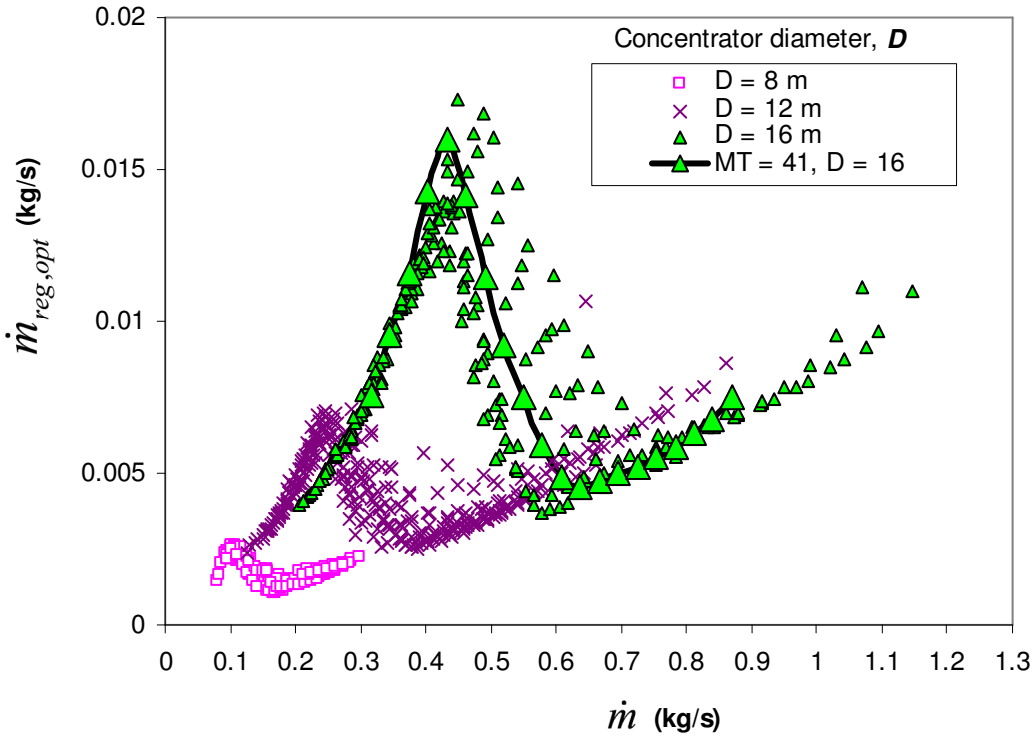

Figure 5.24 Optimum recuperator channel mass flow rate (*D* = 8, 12 and 16 m).

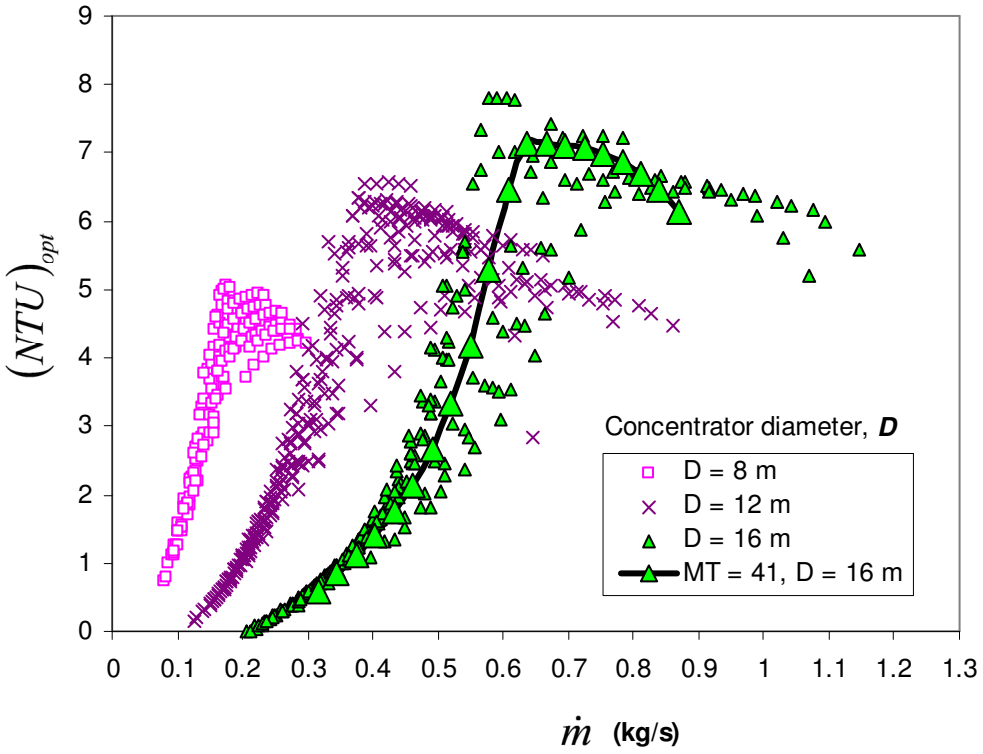

Figure 5.25 Optimum *NTU* for all data points (*D* = 8, 12 and 16 m).

Consider the point where the minimum external irreversibility rate, $\dot{I}_{ext,\min}$, is at its highest (Figure 5.26d). $\dot{I}_{ext,\min}$ seems to be at a maximum when the mass flow rate is small.

$$\dot{I}_{ext} = \dot{m}c_{p0}(T_1 - T_{11}) - \dot{m}T_0 c_{p0} \ln\left(\frac{T_1}{T_{11}}\right) \tag{5.14}$$

From equation 5.14 it follows that, for high external irreversibilities, T_{11} must be high, which means that η_{reg} should be small (see equation 3.57). This is why the optimum NTU is small at small mass flow rates, as shown in Figure 5.25. The optimum NTU increases as the mass flow rate increases. The optimised data shows that a small NTU is established with the use of a small surface area, large hydraulic diameter (Figure 5.19) and large recuperator channel mass flow rate, which increase respectively until the maximum recuperator length constraint is reached (around 0.45 kg/s in Figure 5.24). A large hydraulic diameter also keeps the pressure drop and minimum entropy generation rate due to fluid friction, $\dot{S}_{gen,\text{int},\min,\Delta P}$, low for the recuperator (Figure 5.26c). After the length constraint is reached (Figures 5.17 and 5.18), the recuperator mass flow rate and hydraulic diameter decrease (Figure 5.19) as the mass flow rate increases to

ensure an increase in NTU as the system mass flow rate increases. Note that $\dot{S}_{gen,\text{int},\min,\Delta P}$ grows quite big at these mass flow rates because the hydraulic diameter decreases. At these mass flow rates, the high pressure drops can be considered as most beneficial for the net power output of the system.

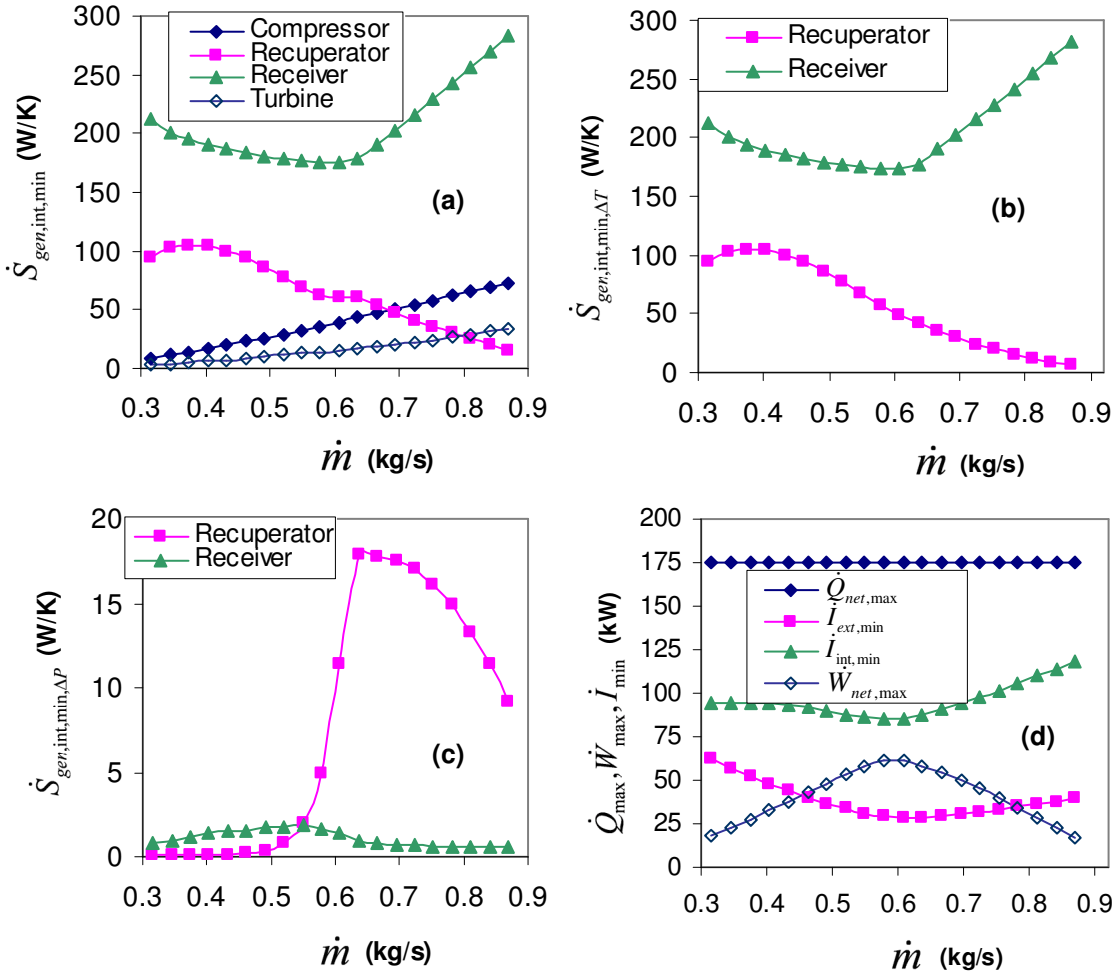

Figure 5.26 Geometry optimised system data points (*MT* = 41, *D* = 16 m) : (a) – Minimum total internal entropy generation rate; (b) – Contribution to total minimum internal $\dot{S}_{gen}$ due to temperature difference; (c) – Contribution to minimum internal $\dot{S}_{gen}$ due to frictional pressure drop; (d) – Minimum irreversibilities and maximum power.

In Figure 5.27 it is shown that the maximum receiver surface temperature of the optimised data stays constant as a function of mass flow rate at small mass flow rates. This is due to the temperature constraint of 1 200 K, as shown in Section 3.8. At higher mass flow rates, the maximum surface temperature of the optimised data decreases as a function of mass flow rate. The larger the concentrator diameter, the larger the mass flow rate at which the maximum surface

temperature would start decreasing. When comparing Figure 5.27 with Figures 2.13 – 2.17, it can be concluded that the operating temperature range of a solar thermal power cycle depends also on the mass flow rate through the receiver and the receiver melting temperature.

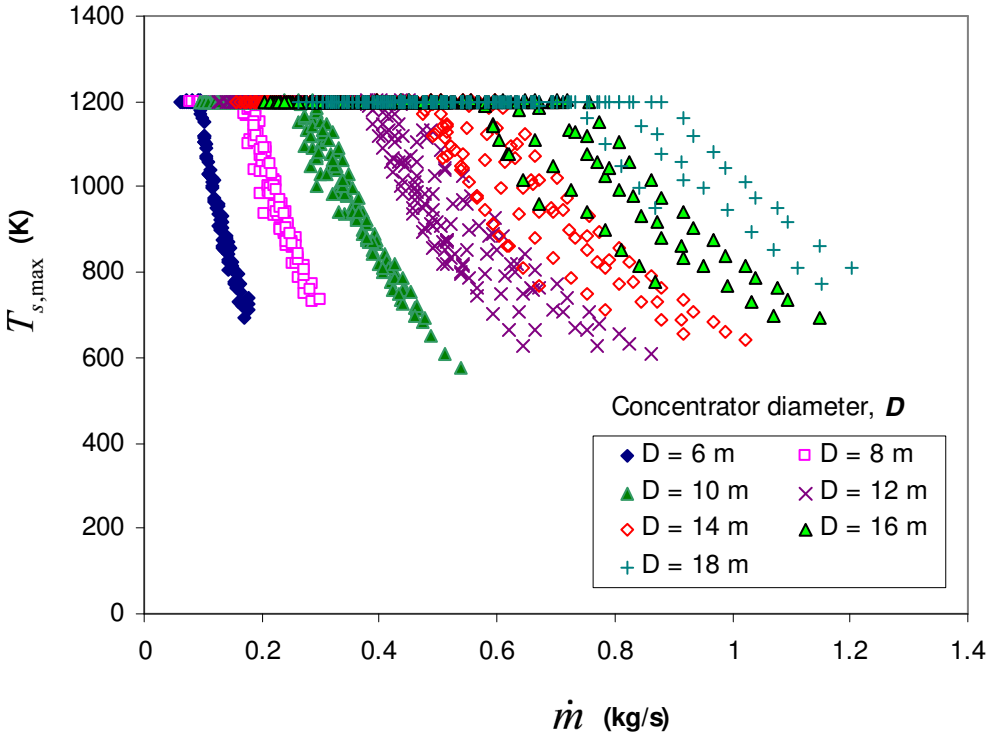

Figure 5.27 Maximum receiver surface temperature of all the optimised data points (all micro-turbines and each of its operating conditions).

When considering the minimum entropy generation rate in the solar receiver (Figure 5.26a - c), it follows that the receiver performs optimally when $\dot{S}_{gen,\text{int},\min,\Delta P}$ is as small as possible. The largest component of the minimum receiver entropy generation rate should be the temperature difference component, $\dot{m}c_p \ln(T_6/T_5)$. The downward minimum entropy generation slope for the receiver at small mass flow rates (Figure 5.26a) is due to an increase in the NTU, which increases T_5 (see equations 3.58 and 3.59). In the receiver, at small mass flow rates, the optimum $T_{s,\max}$ stays constant as a function of mass flow rate (Figure 5.27), which means that $\dot{S}_{gen,\text{int},\min,\Delta T}$, due to temperature difference (T_6/T_5), decreases as the mass flow rate increases (Figure 5.26b). Eventually, the optimum NTU reaches its maximum at a high mass flow rate (Figure 5.25). For increasing mass flow rate, $\dot{S}_{gen,\text{int},\min,\Delta T}$ increases as a function of mass flow rate (Figure 5.26b) and the maximum receiver surface temperature of the optimised data decreases (Figure 5.27).

Consider the point where $\dot{I}_{ext,\min}$ is at a minimum (Figure 5.26d). T_{11} will be at a minimum and the recuperator efficiency will be at a maximum. As $\dot{I}_{ext,\min}$ increases slightly with mass flow rate, the optimum NTU decreases slightly as shown in Figure 5.25. At the highest optimum NTU point, the recuperator channel mass flow rate is again utilised to be increased as the system mass flow rate increases in order to keep the optimum NTU at its maximum. In most of the cases (but not all cases), the highest maximum net power output in the operating range of the micro-turbine was found at a mass flow rate close to the point of highest optimum NTU or at higher mass flow rates. To keep the optimum NTU constant, the hydraulic diameter is also kept constant, but increases slightly (Figure 5.19) as the system mass flow rate increases to keep $\dot{S}_{gen,\text{int},\min,\Delta P}$ in the recuperator small. This, in turn, forces the recuperator mass flow rate to also increase slightly as the system mass flow rate increases, as shown in Figure 5.24.

It seems to be more beneficial for the system when $\dot{S}_{gen,\text{int},\min,\Delta T}$ in the receiver is higher at higher mass flow rates. For this reason, there is a decrease in the optimum NTU (and T_5) at high mass flow rates.

Consider Figure 5.26d in more detail and note how the maximum net power output increases as the minimum entropy generation decreases as a function of mass flow rate. The highest maximum net power output is at the point where the minimum entropy generation rate or minimum irreversibility rate ($\dot{I}_{ext,\min} + \dot{I}_{\text{int},\min}$) is the lowest.

Figure 5.28 shows the optimum performance of the system in terms of the optimum pressure drop in the receiver and recuperator, as a function of mass flow rate, for micro-turbine 41 with ***D*** = 16 m. It is interesting to note that, for optimum systems, the pressure drop of the receiver is larger than the pressure drop in the recuperator when the mass flow rate is small. This changes at a specific mass flow rate, whereafter it is optimal for the recuperator pressure drop to be larger than the receiver pressure drop. This change is due to a decreased hydraulic diameter, as was found from Figure 5.26. Note how Figure 5.28 relates to $\dot{S}_{gen,\text{int},\min,\Delta P}$ in Figure 5.26c. Exactly the same behaviour was found for the other micro-turbines with ***D*** = 16 m.

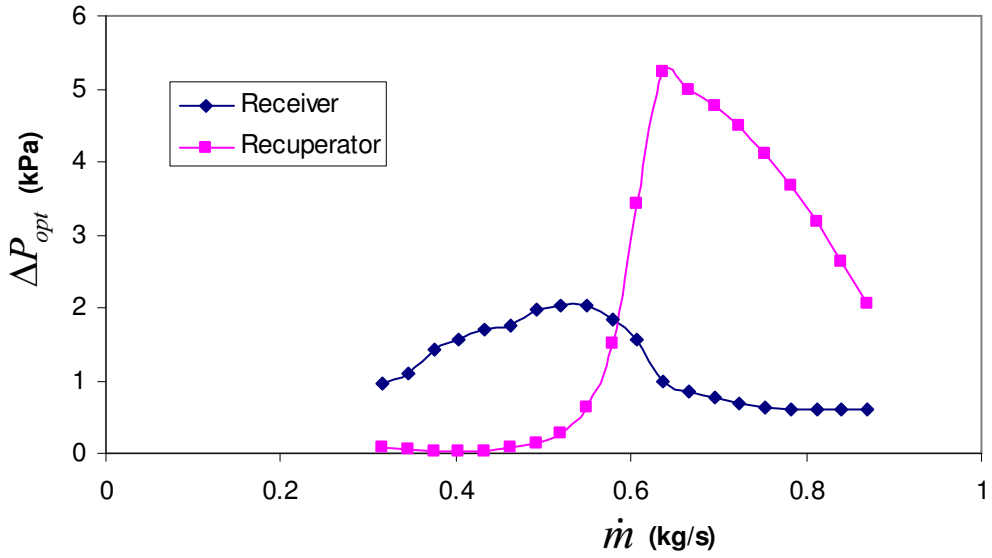

Figure 5.28 Optimum pressure drop in receiver and recuperator channel for micro-turbine 41 and *D* = 16 m.

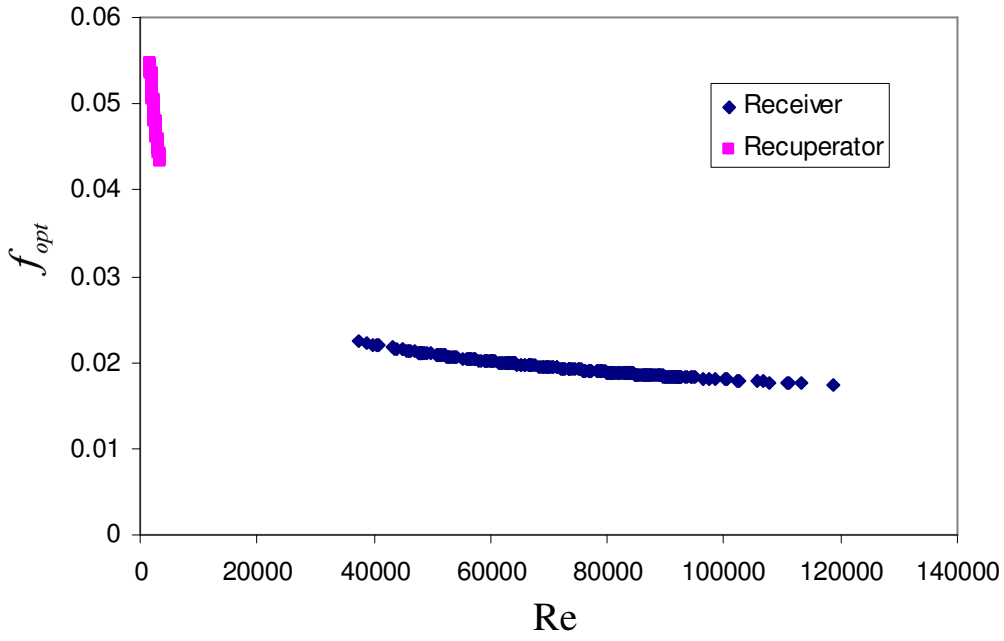

Figure 5.29 Optimum friction factor in receiver and recuperator for *D* = 16 m.

The optimum friction factor of the receiver and recuperator channels, as a function of Reynolds number, is shown in Figure 5.29 for systems with different micro-turbines and operating mass flow rates with ***D*** = 16 m. It is optimum for the recuperator to operate in the laminar flow regime while the receiver operates in the turbulent flow regime. From Figure 5.30, this can also be concluded for all systems analysed in this study. Figure 5.30 shows the optimum range of friction factors as a function of mass flow rate for all the data points. The optimum receiver friction factor decreases as a function of system mass flow rate or Reynolds number. For the large concentrator

diameters, the optimum recuperator friction factor increases with system mass flow rate until it reaches a maximum whereafter it slowly decreases with system mass flow rate. It is more beneficial for recuperators in systems with large concentrators to have a smaller friction factor when the system mass flow rate is small.

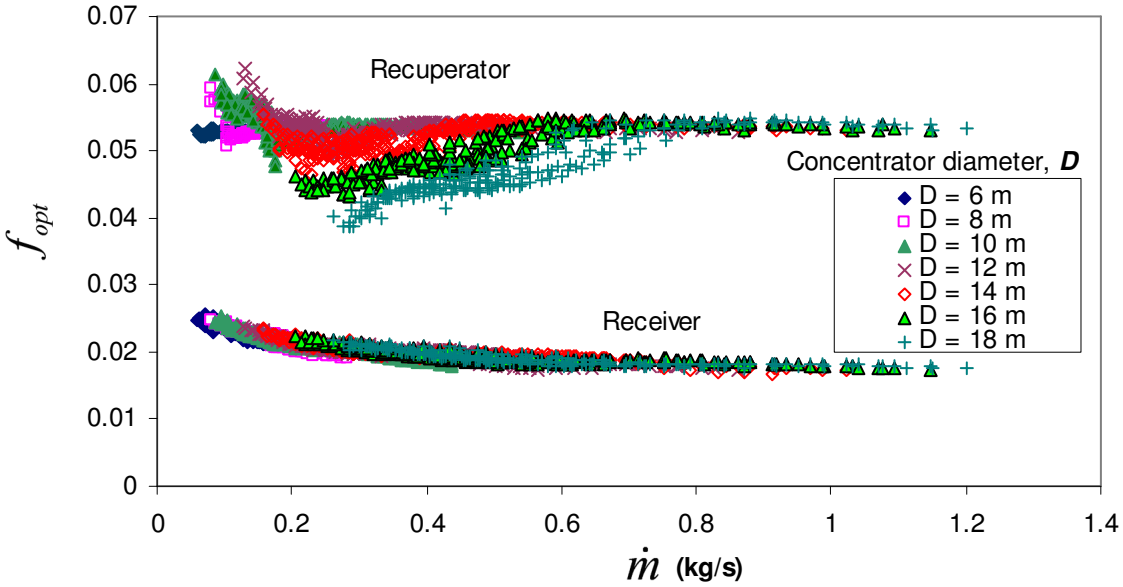

Figure 5.30 Optimum friction factor for all data points.

Figure 5.31 reveals that there exist linear relationships between the optimum recuperator efficiency and the optimum recuperator channel hydraulic diameter. Note that only the data points which gave the highest maximum net power output of a micro-turbine are shown. For small concentrator diameters, the optimum recuperator efficiency is smaller compared with the optimum recuperator efficiency required for larger concentrator diameters. When the optimum recuperator channel hydraulic diameter is large, it is more beneficial for the system that the recuperator efficiency is smaller. This can be compared with the results shown in Figures 5.25 and 5.26c where a high optimum NTU is accompanied with a large pressure drop or small hydraulic diameter.

Figure 5.32 shows that there exists an optimum ratio of system mass flow rate to recuperator channel mass flow rate. Again, only the data points with highest maximum net power output are shown. When comparing these results with the results from Figure 5.24, one finds that this line (Figure 5.32) falls on the third section of optimum system behaviour (or close to the mass flow rate with the highest NTU or at higher mass flow rates). This optimum linear ratio seems to have a slope close to 0.01. The result is shown in equation 5.15.

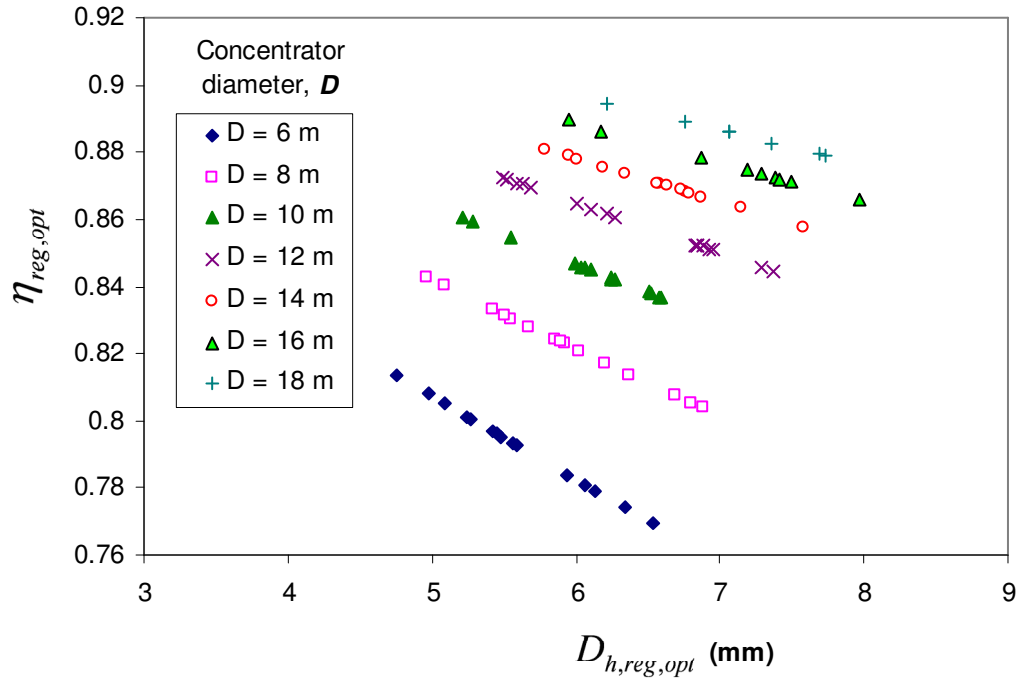

Figure 5.31 Linear relationship between optimum recuperator efficiency and channel hydraulic diameter.

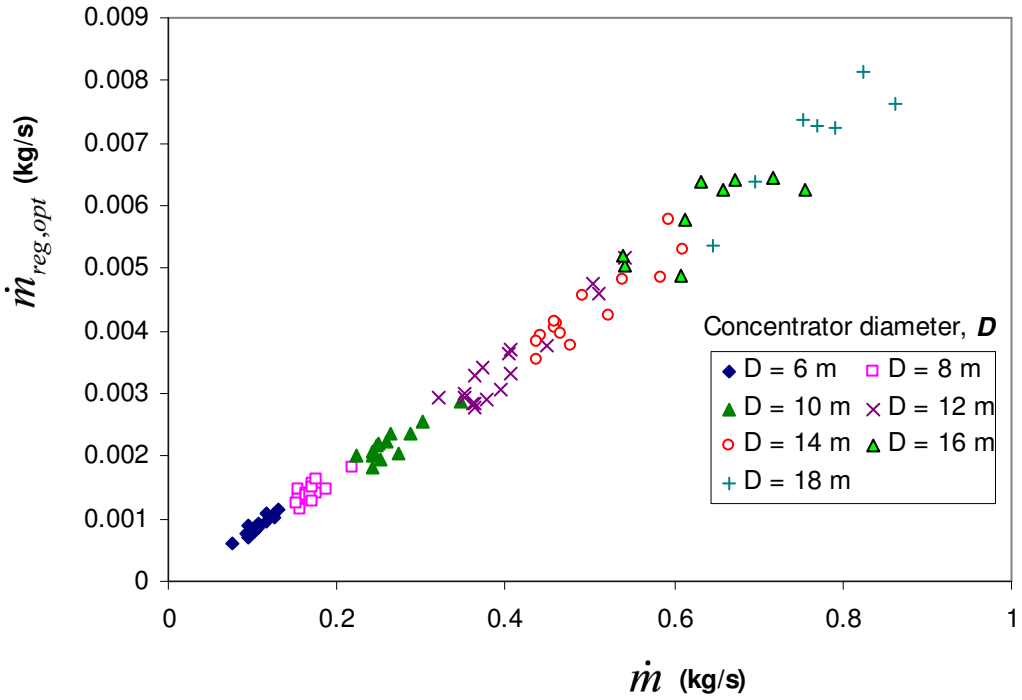

Figure 5.32 Linear relationship between optimum recuperator channel mass flow rate and optimum system mass flow rate.

$$\dot{m}_{opt} \approx 115\dot{m}_{reg,opt} \tag{5.15}$$

Figure 5.33 shows that there exists a relationship between the minimum internal and external irreversibilities of the system, when the data points with highest maximum net power output are considered.

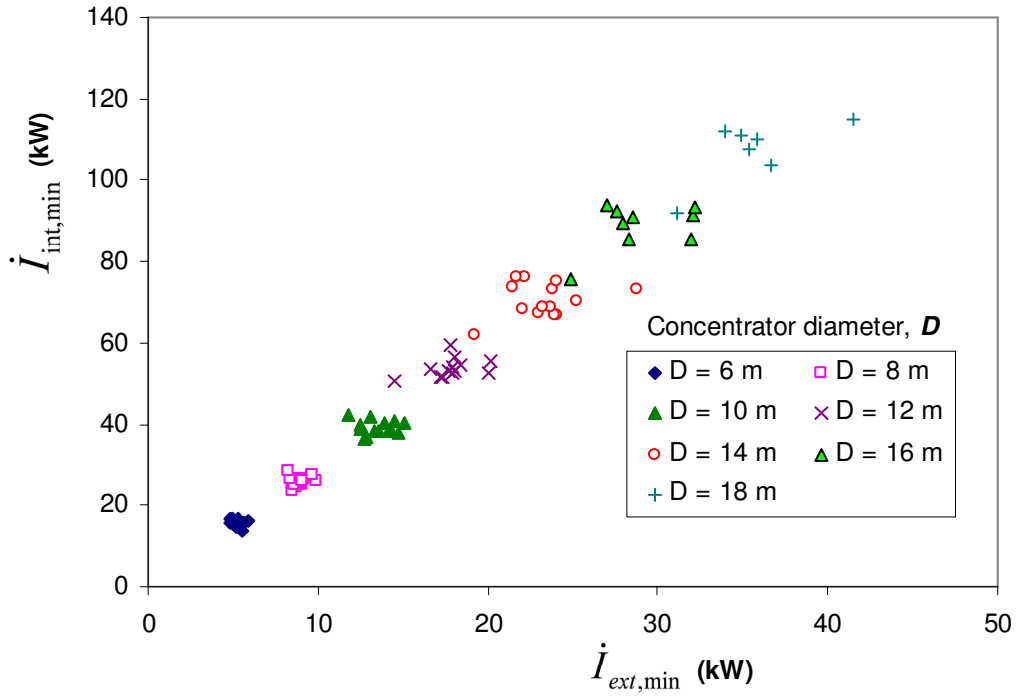

Figure 5.33 Minimum internal system irreversibility rate as a function of minimum external system irreversibility rate for maximum system net power output.

From Figure 5.33, it follows that the largest maximum net power output for a system (or optimum operating point) is at a point where the internal irreversibility rate is approximately three times larger than the external irreversibility rate. This result can be approximated with equation 5.16 for all optimisation results in this analysis (with different concentrators and micro-turbines) where an optimum operating condition was found:

$$-T_0\left[\dot{S}_{gen}\right]_{\text{int,min}} \approx C_W\left[\dot{m}c_{p0}(T_1 - T_{11}) - \dot{m}T_0 c_{p0}\ln(T_1/T_{11})\right]_{ext,\min} \tag{5.16}$$

where $C_W = \dot{I}_{\text{int,min}} / \dot{I}_{ext,\min} \approx 3$.

Figure 5.34 shows that C_W mostly increases as the system mass flow rate increases. The rate of increase decreases as the concentrator diameter increases. Figure 5.34 shows that 2.4 ≤ C_W ≤ 4, depending on the mass flow rate and concentrator diameter. Other data points which are not at an optimum operating point (or highest maximum net power output), or close to one, do not fall in this range.

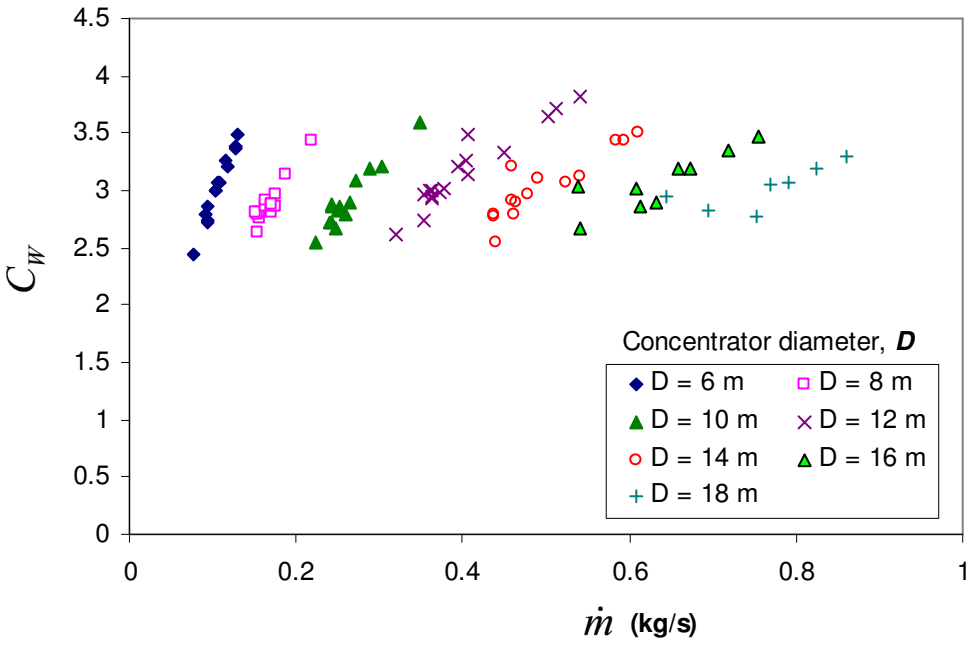

Figure 5.34 C_W as a function of the system mass flow rate.

The results shown in the previous two sections can be considered in the preliminary stages of the design of an open and direct solar thermal Brayton cycle.

5.3.4. Comparison of second and first law results

The net power output for the solar thermal Brayton cycle can also be calculated with the first law of thermodynamics together with the temperatures and pressures of the system, as described in Section 3.6. Equation 5.17 can be used to compare the net power output in terms of the first law with the net power output described in terms of the second law, i.e. in terms of the total entropy generation rate of the components in the system (equation 3.61 – the objective function).

$$\dot{W}_{net(FirstLaw)} = \dot{m}c_{p,7-8}(T_7 - T_8) - \dot{m}c_{p,1-2}(T_2 - T_1) \tag{5.17}$$

These maximum net power output curves are compared in Figure 5.35. The curves show the results for a system using a concentrator diameter of 8 m with micro-turbine 13 and a

concentrator with 12 m diameter using micro-turbine 32. The first and second law curves compare very well. This means that the second law net power output was accurately modelled in terms of the total entropy generation rate of the system. The small difference can be due to the entropy generation rate in the ducting of the system, which was not accurately modelled.

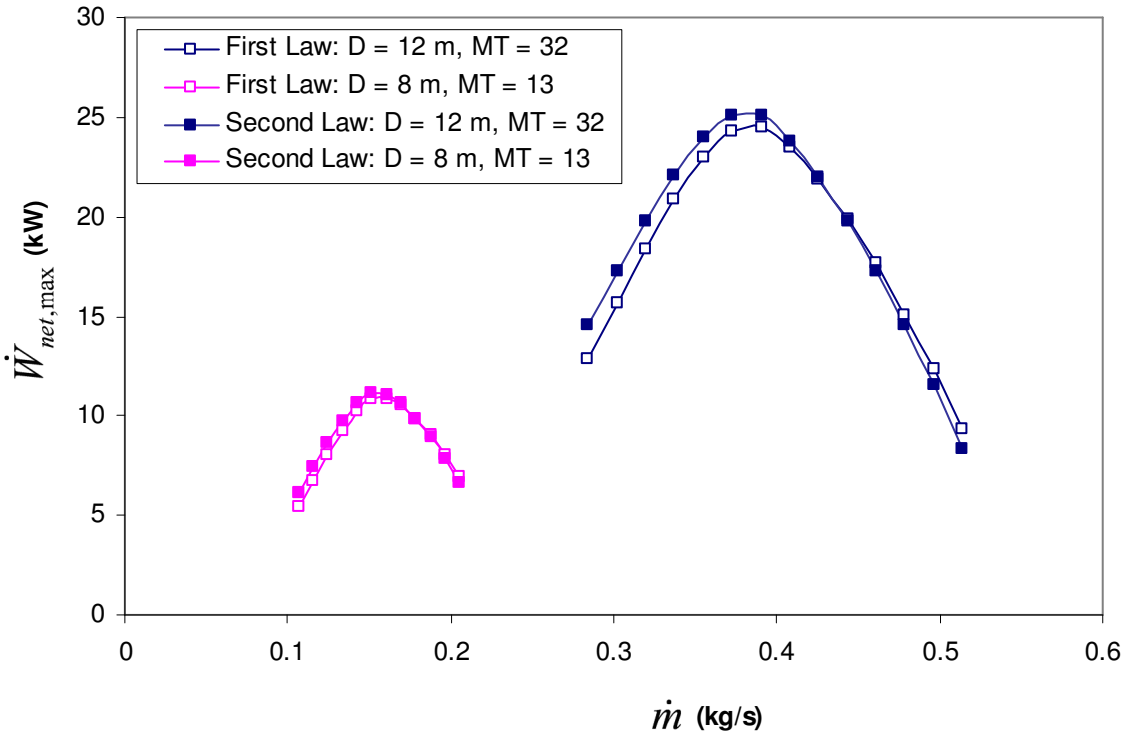

Figure 5.35 Comparison of net power output calculated for two optimised systems using the first and second laws of thermodynamics. The one system uses *MT* = 13 with *D* = 8 m and the other uses *MT* = 32 with *D* = 12 m.

5.3.5 The effect of the changing of a constant on the maximum net power output, optimum geometry and optimum operating conditions of the system

Consider again the constants from Table 5.2. In this section, these constants are considered as the default settings. The results shown in this section are for systems where one of these constants was changed. Table 5.5 shows the values that were changed one at a time for two specific micro-turbine and concentrator diameter combinations to see what effect it would have on the optimum geometry and operating conditions of the system.

Figures 5.36 and 5.37 show the maximum net power output for micro-turbine 13 with ***D*** = 8 m and micro-turbine 32 with ***D*** = 12 m, where the results using the default settings and changed constants are compared. It is concluded that a temperature decrease and pressure increase of the surroundings increase the maximum net power output. The decrease in maximum net power output due to wind, decreased specular reflectivity, concentrator error, recuperator material

conductivity and increased concentration ratio minimum are shown. A higher concentration ratio decreases the maximum net power output because the size of the receiver decreases as the concentration ratio increases. The results shown in Figures 5.36 and 5.37 are expected to be similar for all the other configurations of concentrator diameter and micro-turbine.

Table 5.5 Each constant is changed to a new value to see the effect of the changing of one constant.

	D = 8 m, *MT* = 13	***D*** = 12 m, *MT* = 32	Unit
T_0	308	288	K
P_1	100	100	kPa
I	1 200	800	W/m^2
w	10	10	-
φ_{rim}	60	30	degrees
β	30	60	degrees
e_p	0.035	0.035	mrad
$T_{s,\max}$	1 100	1 100	K
$refl$	0.98	0.8	-
k	237	237	W/mK
H	0.5	2	m
$L_{reg,\max}$	8	12	m
$CR_{\min}$	500	1 000	-

A decrease in rim angle and receiver inclination makes no difference to the maximum net power output. It does, however, make a big change in the optimum receiver geometry variables. For a higher maximum allowable receiver temperature, the maximum net power output is higher. The increase of recuperator length and irradiance results in an increase in maximum net power output. The change in recuperator height makes no difference to the maximum net power output, but it changed the optimum dimensions of the recuperator. Take note how the receiver and recuperator geometry variables are altered due to wind, the doubling of recuperator height and minimum concentration ratio, in Figures 5.38 and 5.39 (for ***D*** = 12 m and *MT* = 32). For heavy wind, high concentration ratio, changed inclination and rim angles, it is more beneficial for the system to have a smaller receiver tube diameter (Figure 5.38). In Figure 5.39, it is shown that a doubled recuperator height decreases the optimum recuperator channel aspect ratio tremendously.

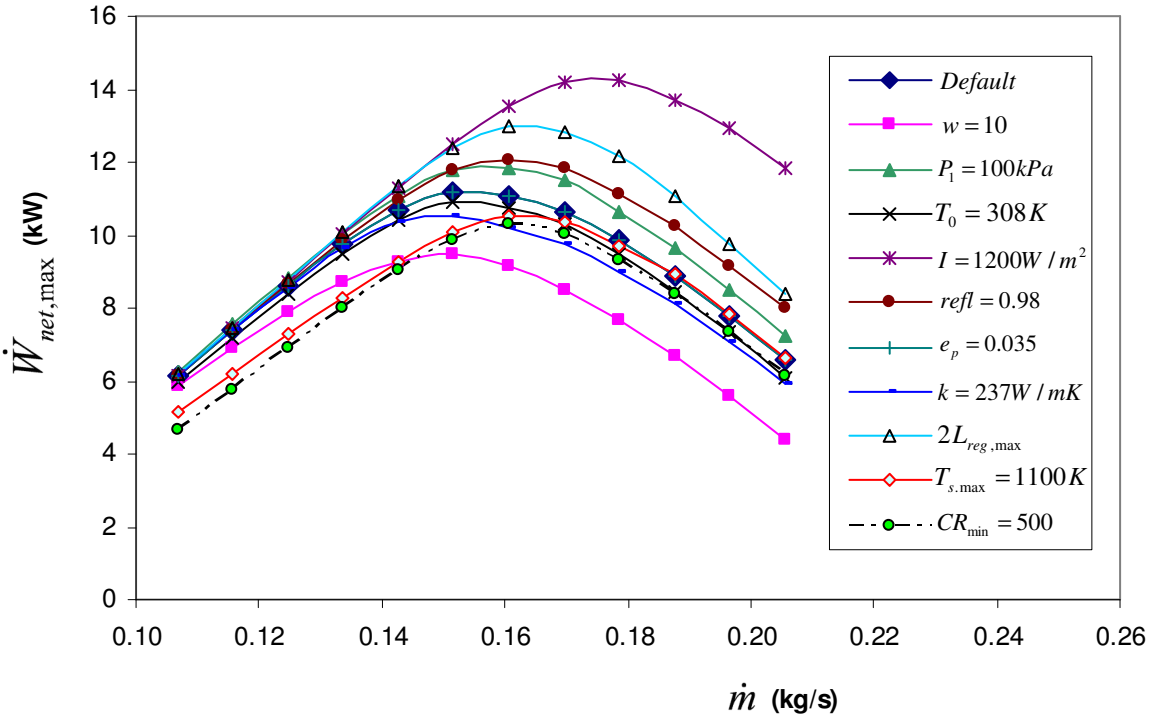

Figure 5.36 Change in maximum net power output for system using *MT* = 13 and *D* = 8 m.

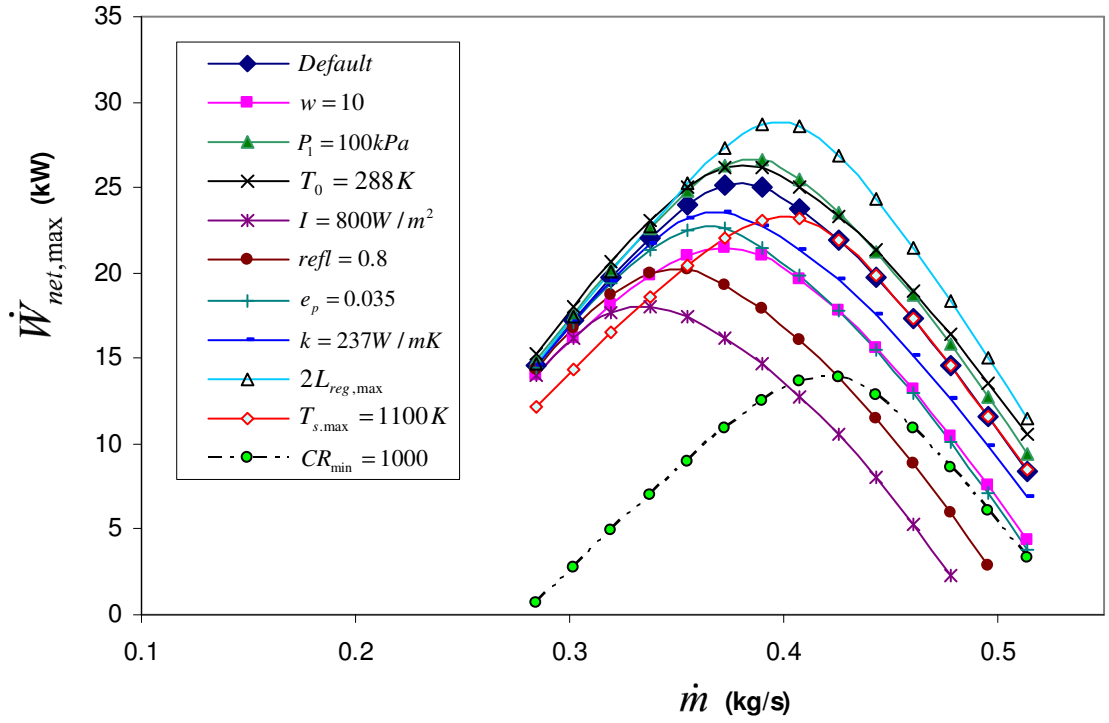

Figure 5.37 Change in maximum net power output for system using *MT* = 32 and *D* = 12 m.

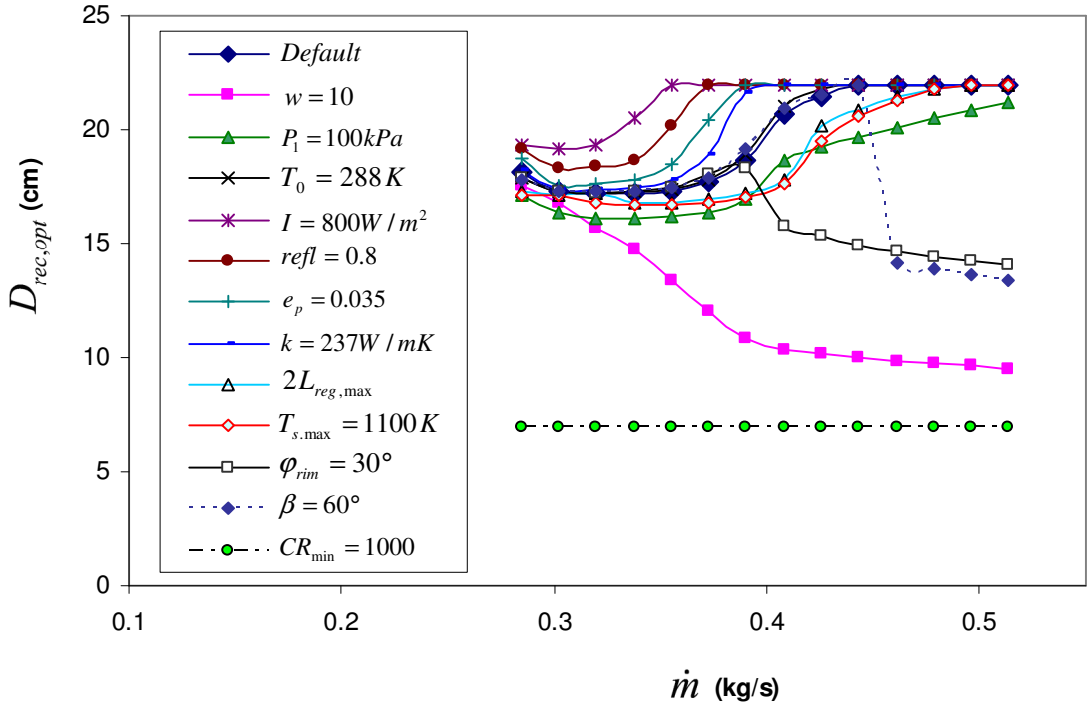

Figure 5.38 Change in optimum receiver tube diameter due to changes in constants for *D* = 12 m and *MT* = 32.

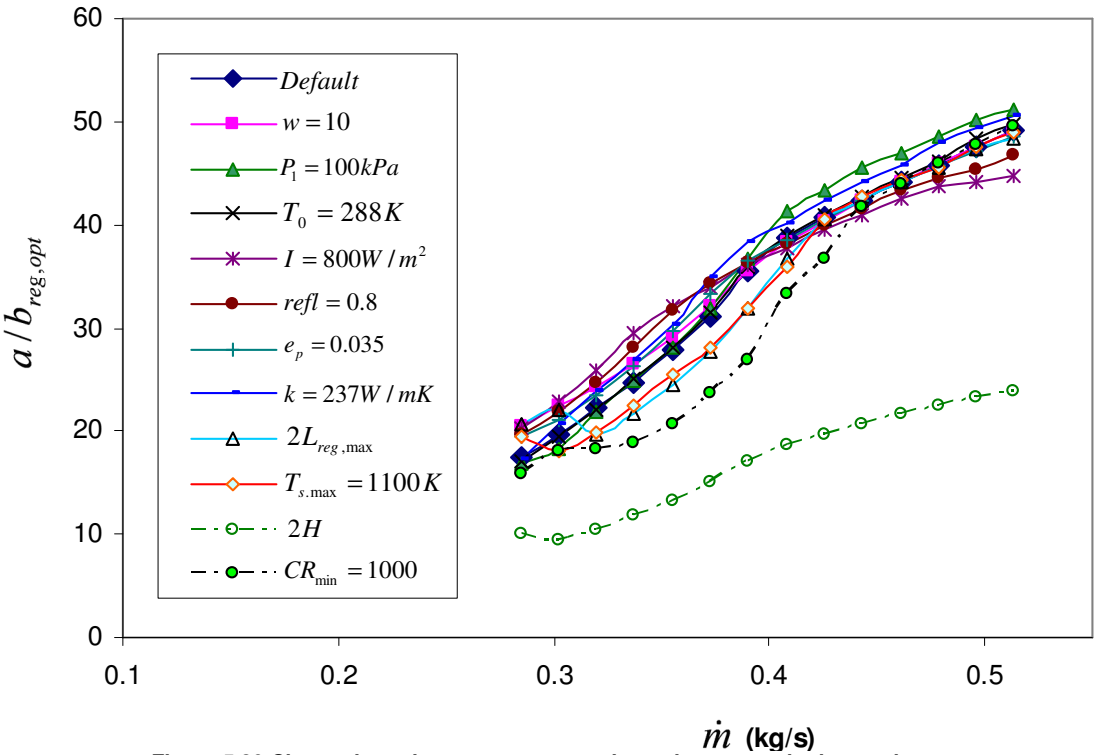

Figure 5.39 Change in optimum recuperator channel aspect ratio due to changes in constants for *D* = 12 m with *MT* = 32.

Consider Figures 5.40 and 5.41. The effect of a few selected constants on the mass flow rate of a recuperator channel is shown for both the configurations. A lowest optimum recuperator mass

flow rate exists. Also note how these figures compare with Figure 5.22. Note how this minimum is shifted due to the constants. It was found that the operating point at this minimum does not necessarily provide the highest maximum net power output. A doubled recuperator length, halved recuperator height, high minimum concentration ratio and higher irradiance shift the maximum recuperator mass flow rate to a higher value and a different system mass flow rate (compare with Section 5.3.3).

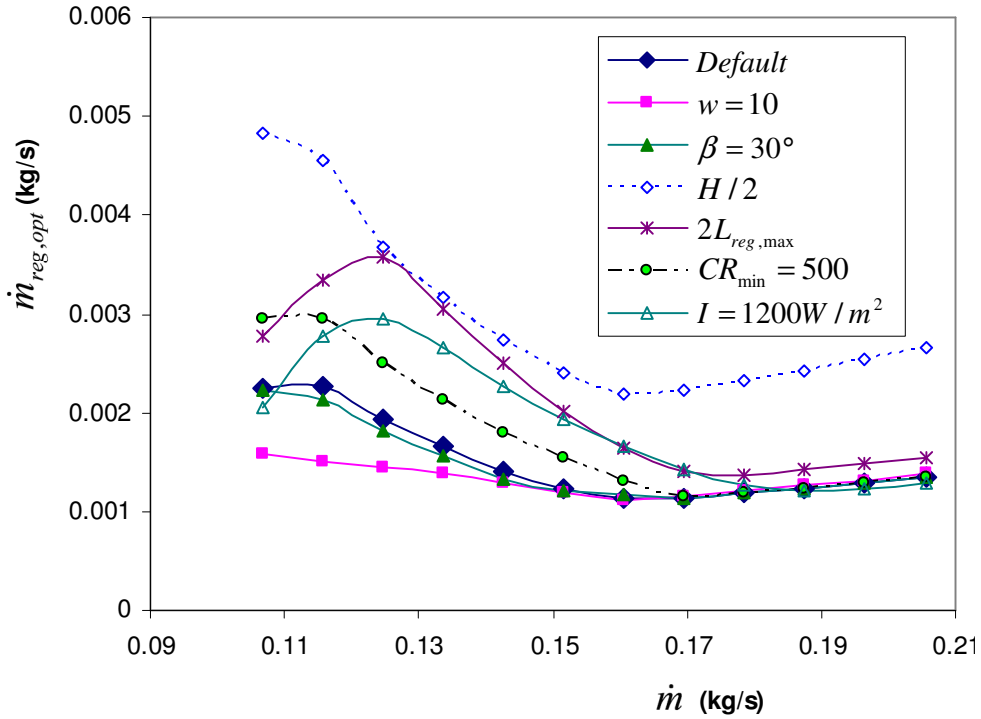

Figure 5.40 Optimum recuperator channel mass flow rate with changes in constants for *D* = 8 m with *MT* = 13.

Now consider Figures 5.42 and 5.43. Here the optimum recuperator NTU is shown for ***D*** = 8 m, using micro-turbine 13 and ***D*** = 12 m with micro-turbine 32. In both of these figures, the extended recuperator length increases the maximum of the optimum NTU. The effect of the wind was to increase the optimum NTU slightly at lower system mass flow rates. The effect of higher minimum concentration ratio was to decrease the optimum NTU at smaller mass flow rates. The effect of irradiance at lower mass flow rates was to increase or decrease the optimum NTU as the irradiance decreased and increased respectively. At higher mass flow rates, the effect was opposite. The other changes did not affect the optimum NTU much.

Note that the highest maximum net power output for the default settings in Figures 5.36 and 5.37 is at a mass flow rate of 0.15 and 0.375 respectively. When looking at the optimum operating conditions of these mass flow rates, the net power output is not necessarily a maximum when the

NTU is at its highest. This confirms that an optimum condition for an individual component in a system does not necessarily guarantee an optimum net power output, as was emphasised from the literature.

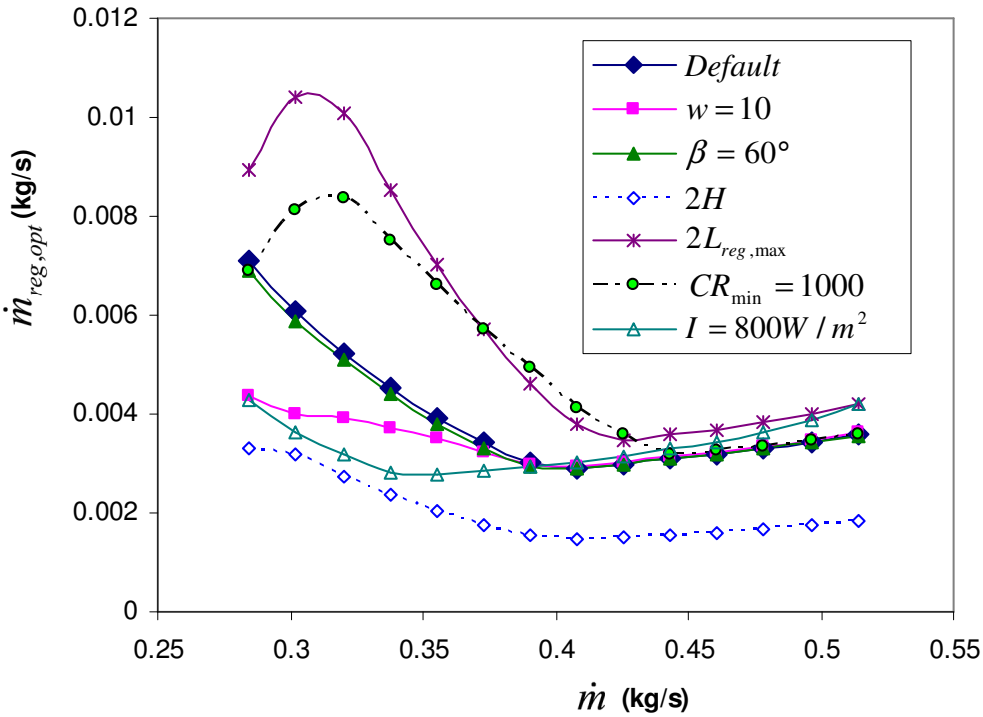

Figure 5.41 Optimum recuperator channel mass flow rate with changes in constants for *D* = 12 m with *MT* = 32.

It is interesting to note that, in some cases, the system property curves do not differ from the default curves and in other cases they differ a lot. A 60° inclination (Figure 5.43) does not do much to the shape of the optimum NTU but it does, however, change the shape of the optimum receiver tube diameter (Figure 5.38). When considering Figures 5.36 and 5.37 again, the effect due to receiver inclination and recuperator height is not shown. The system variables were altered so that the system can still provide the same maximum net power output for the system with inclined receiver or altered recuperator height. The devastating effect of wind on the system, however, is shown in these figures. The system variables were not able to 'save' the maximum net power output, even though the attempts made to do so are shown in all the figures. Note that if the curve for a changed constant is not shown in a figure, it means that it was found to be the same as the default. Some constants do not change the maximum net power output of the system, but the geometry of the recuperator or receiver. This change is due to the optimal spreading of irreversibilities in the different system components. The change of a constant or the change of surroundings can have positive or devastating effects.

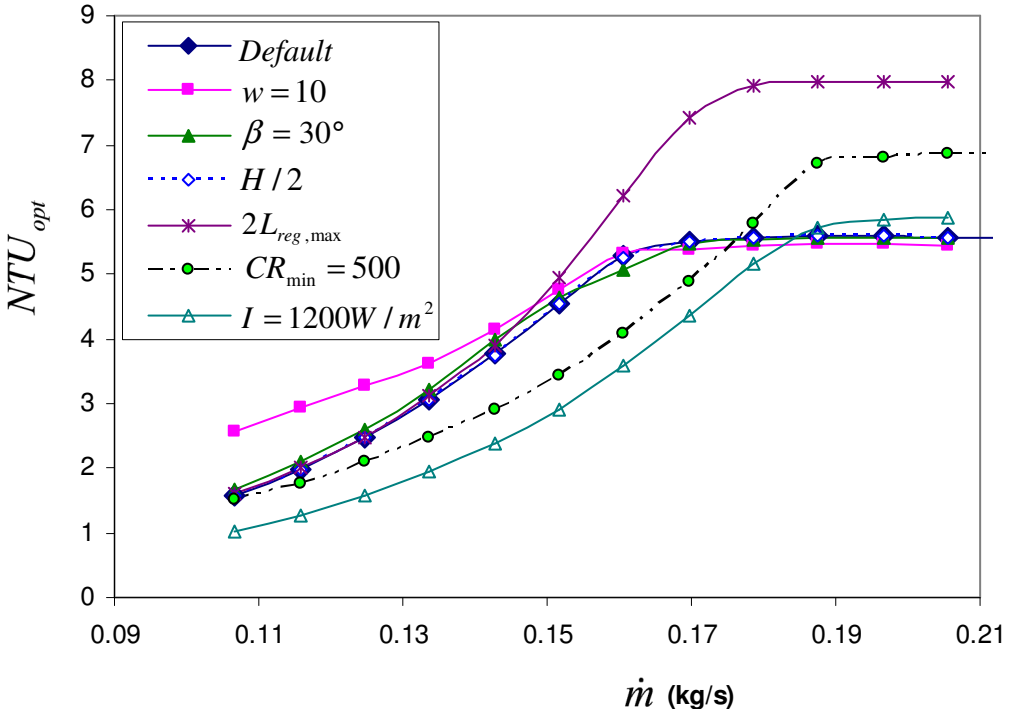

Figure 5.42 The optimum recuperator *NTU* with specific scenarios *D* = 8 m and micro-turbine 13 for changed constants.

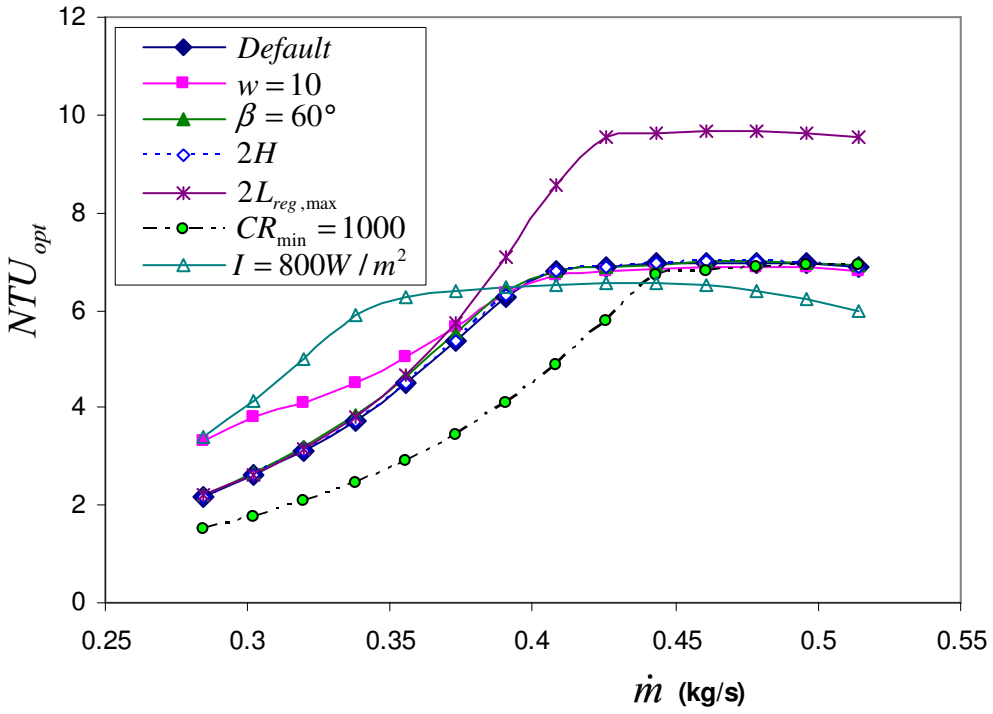

Figure 5.43 The optimum recuperator *NTU* with specific scenarios for *D* = 12 m and micro-turbine 32 for changed constants.

Figure 5.44 shows the effect of environmental conditions and changed constants on the optimum spreading of irreversibilities (*MT* = 41, ***D*** = 16 m). Figure 5.45 shows the maximum net power output and minimum irreversibility rates for the default settings. Note that, from above and left in the figures, the following data points are shown: maximum absorbed heat rate, minimum internal and external irreversibility rates and maximum net power output, as shown in Figure 5.26d. Most of the results in Figure 5.44 do not differ much from the results of the default. However, the optimum geometry was usually changed to accommodate for the change in environment or change of situation.

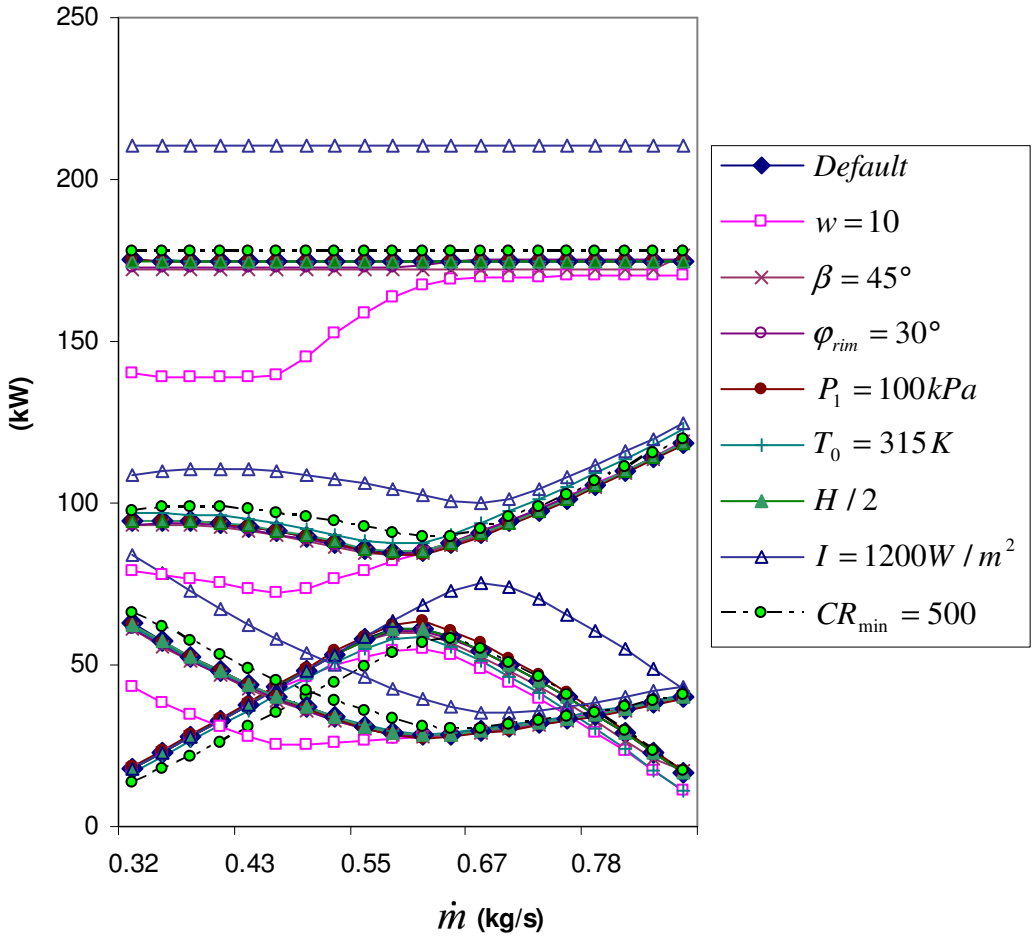

Figure 5.44 The effect of different conditions on the optimum performance of *MT* = 41 and *D* = 16 m.

Note that the highest maximum net power output is at the same mass flow rate as where the minimum internal and external irreversibility rates are lowest. This was not the case for extreme wind since the wind affects the absorbed heat rate at smaller system mass flow rates. The wind calls for a smaller aperture diameter, which constrains the rate of heat absorbed. Note that C_W

(see Section 5.3.3) is again approximately three, even for extreme conditions such as an irradiance of 1 200 W/m^2, extreme wind and large concentration ratio.

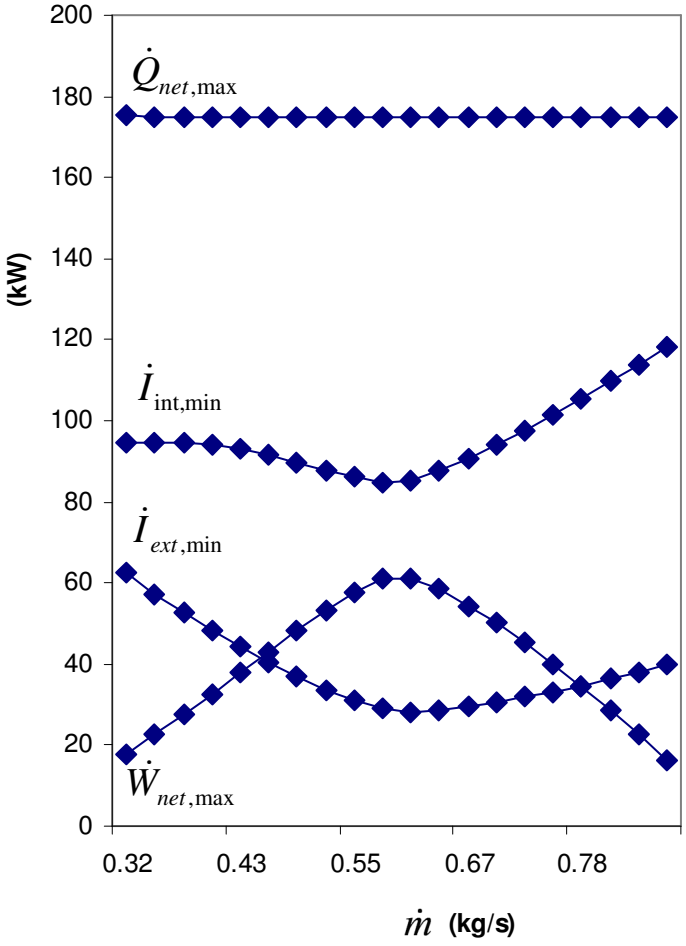

Figure 5.45 Maximum net power output and minimum irreversibility rates for *D* = 16 m with *MT* = 41.

In Figure 5.45, the data point where $\dot{m}$ = 0.607 kg/s (or r = 2.4) gives the maximum net power output of 61.2 kW with an optimum geometry of $D_{rec,opt}$ = 0.2 m, $L_{rec,opt}$ = 61 m, $a/b_{reg,opt}$ = 56, $D_{h,reg,opt}$ = 6 mm and $L_{reg,opt}$ = 8 m. This optimum geometry was found using the optimisation algorithm and objective function where r = 2.4 is a parameter. A validation is done by changing these variables, one at a time, from the optimum values as shown above. When one of the variables is changed, the other variables stayed constant at their optimum points. Figures 5.46 and 5.47 show the net power output as a function of changing receiver tube diameter and receiver tube length respectively. The total irreversibility rate ($T_0\dot{S}_{gen,(\text{int}+ext)}$) and the net rate of heat absorbed are also shown. In Figure 5.46, the constraints are D_{rec} ≤ 26.37 cm, D_{rec} ≤ 32.5

cm and 17 ≤ D_{rec} ≤ 21 cm, from Constraint 1, 3 and 4 respectively (see Section 3.8). In Figure 5.47 the constraints are L_{rec} ≤ 78 m, L_{rec} ≥ 39 m and L_{rec} ≥ 61 m, from Constraints 1, 3 and 4 respectively. These graphs show that the maximum net power output is at the point where the total irreversibility rate is a minimum. The maximum net power output in each of these graphs, however, depends on the constraints.

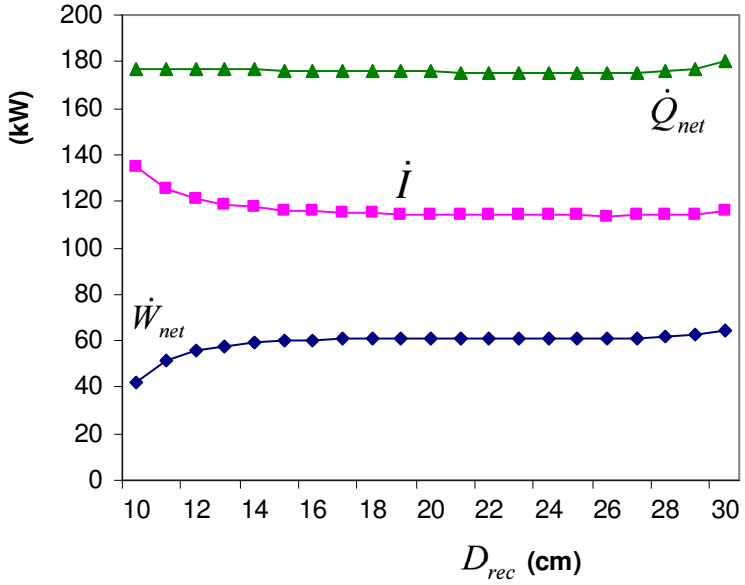

Figure 5.46 Validation of the optimum receiver tube diameter.

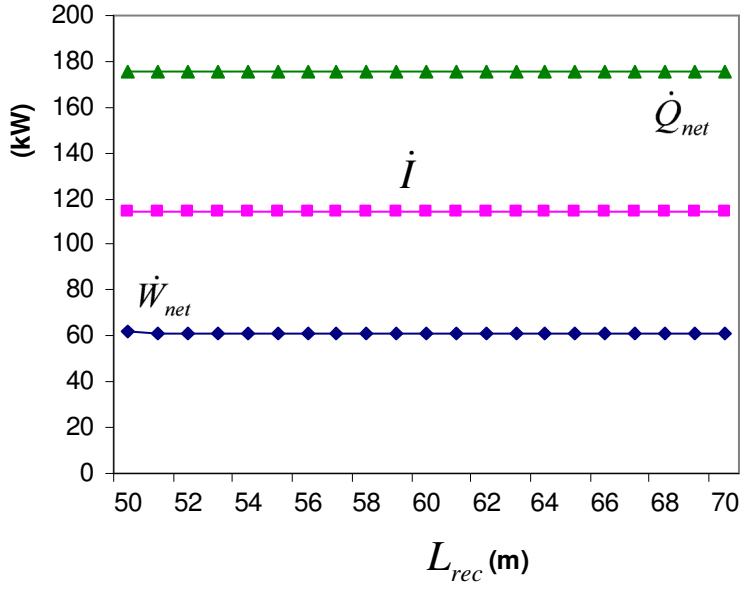

Figure 5.47 Validation of the optimum receiver tube length.

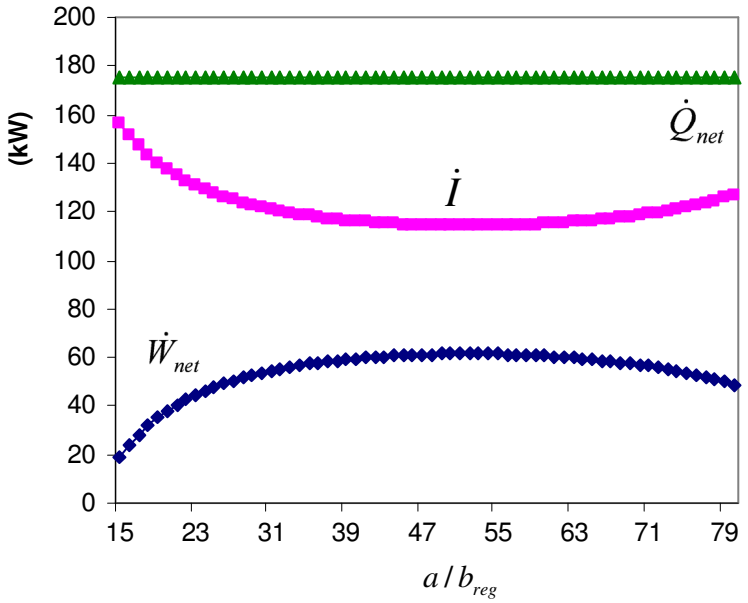

Figure 5.48 Validation of the optimum recuperator channel aspect ratio.

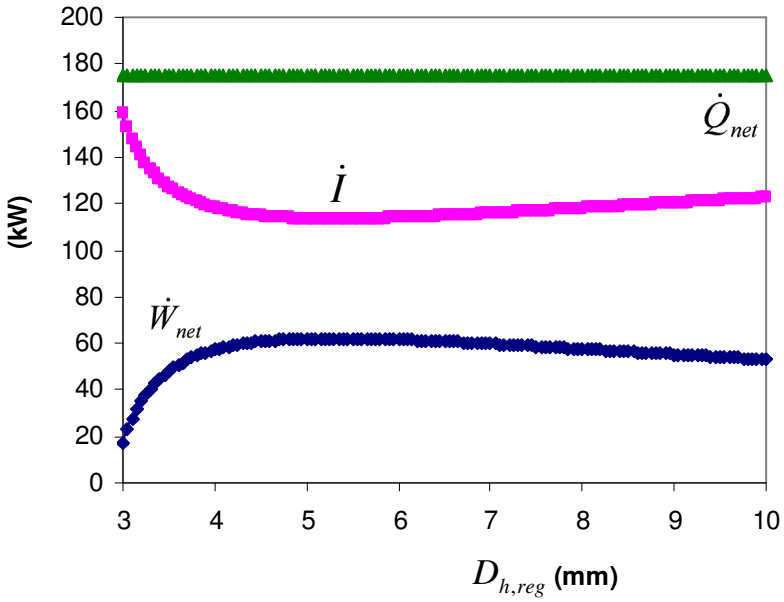

Figure 5.49 Validation of the optimum recuperator channel hydraulic diameter.

Figures 5.48, 5.49 and 5.50 show the net power output, total irreversibility rate and net absorbed power for changing recuperator geometry variables. Once again the net power output and total irreversibility rate mirror each other. In Figure 5.48, the constraint is a/b_{reg} ≥ 56 as was set from Constraint 4. In Figure 5.49, the constraint is $D_{h,reg}$ ≥ 6.2 mm from Constraint 4. Figure 5.50 has

the constraint of L_{reg} ≤ 8 m from Constraints 4 and 7. The optimum geometry for maximum net power output, in each of these graphs, also depends on the constraints.

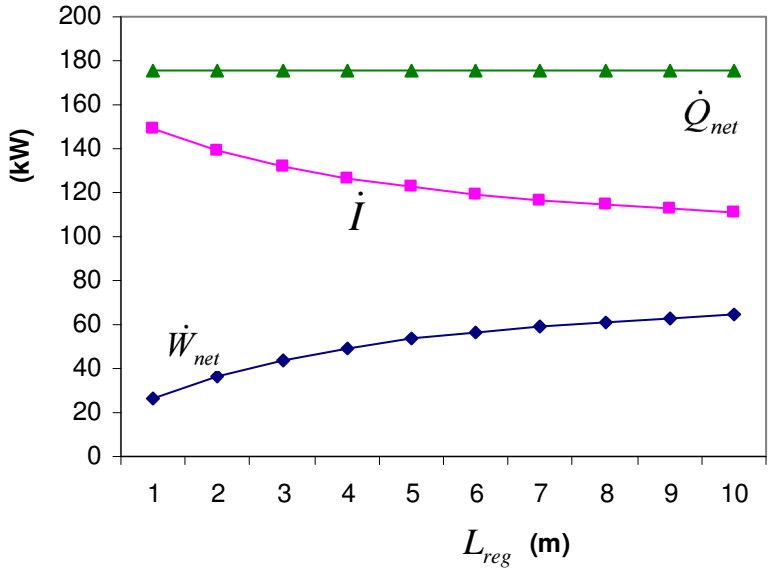

Figure 5.50 Validation of the optimum recuperator length.

These figures confirm that the optimum geometry variables found with the optimisation algorithm are indeed the optimum variables which give maximum net power output of the system. It is also confirmed that the net power output as a function of each of the geometry variables has a maximum at the same position as where the total irreversibility rate is a minimum.

5.3.6 Future work

There are many possibilities regarding future work. This work only focused on the open and direct solar thermal Brayton cycle. Similar work can be done on a closed and direct solar thermal Brayton cycle with different working fluids. Similarly, work can be done on indirect cycles. More heat exchangers can be included in the model (multistaging) and their geometries could also be optimised for maximum system net power output using the method of entropy generation minimisation.

Another interesting possibility would be to not only look at a steady-state process, but to include the transient, since the sun's irradiance changes throughout the day. An optimum geometry must exist for the components in the open and direct solar thermal Brayton cycle at a specific location, so that the yearly and daily average net power output of the system is a maximum.

In this work, the compressor and turbine efficiencies were chosen to be at their maximum by selecting a specific range of operating conditions. Since it was found that an individual component in a system should not necessarily operate at its optimum, other operating ranges, which give lower compressor and turbine efficiencies, should also be investigated.

In this study, only standard (off-the-shelf) micro-turbines were used. The geometries of the compressor and turbine can also be included for optimisation to produce maximum net power output of a system at a specific location.

The entropy generation rate in the ducts can be more accurately modelled by adding the duct diameters and lengths as variables in the objective function. One would expect to find that some ducts would be required to be larger or longer than others so that the net power output of the system can be a maximum.

Further constraints can be added to the optimisation algorithm, especially cost constraints. Further size constraints and different receiver and recuperator designs can be incorporated to establish an exceptionally compact solar thermal power system.

This work and the future work that might sprout from it, have the potential of a user-friendly software which asks the user for the properties of the specific location where a solar thermal power system is to be installed. The software would then calculate the optimum geometry of the components required for the system. The groundwork for such software was done in this study (Appendix C) without the user-friendliness.

The results found in this work (the analytical approach) should be compared with experimental work.

Chapter 6
Conclusion

Southern Africa has a lot of potential to generate large amounts of its power from small-scale and large-scale solar power. The small-scale open and direct solar thermal Brayton cycle with recuperator has several advantages, including lower cost, low operation and maintenance costs and high recommendation. The main disadvantages of this cycle are the pressure losses in the recuperator and receiver, turbomachine efficiencies and recuperator effectiveness, which limit the net power output of such a system. The method of entropy generation minimisation can be used to tackle these disadvantages to optimise the receiver and recuperator and to maximise the net power output of the system.

In this work, a modified cavity receiver and a counterflow plate-type recuperator were optimally sized so that the solar thermal power system can have maximum net power output at steady-state. Two construction methods were considered for this receiver: a circular tube and a rectangular channel. A sizing algorithm was used to establish the net absorbed heat rate of the cavity receiver as a function of the cavity aperture diameter for a specific concentrator diameter with fixed focal length and rim angle. As a result, a specific geometry of the cavity receiver would fix the amount of power absorbed.

Off-the-shelf micro-turbines, operating in their range of maximum compressor efficiency, were considered in the analysis. These micro-turbines and its technical data are freely available in South Africa. The operating point in the range of maximum compressor efficiency, specific micro-turbine and concentrator diameter were used as parameters in the analysis. Forty-five different micro-turbines and seven concentrator diameters between 6 and 18 metres were considered. For each set of parameters an objective function, the net power output, was maximised by optimising geometry variables of the modified cavity receiver and counterflow plate-type recuperator. This optimisation was done with limiting constraints. The dynamic trajectory optimisation method for constrained optimisation was used.

An exergy analysis of the solar thermal power system, identification of total entropy generation within the system and an iteration to determine the temperatures and pressures at each point in the system in terms of geometry variables, were used to establish the objective function. The net power output of the system was described in terms of the total entropy generation within the

system. The constraints on the objective function included constraints on maximum recuperator length and minimum concentration ratio between receiver aperture area and concentrator area. A maximum receiver surface temperature of 1 200 K was set. An average irradiance of 1 000 W/m^2 was assumed. Systems with a 45° concentrator rim angle and a receiver aperture in the horizontal plane, were analysed.

The optimum recuperator channel aspect ratio for the counterflow plate-type recuperator with a constant recuperator height was found to be a linear function of the system mass flow rate. Other studies have found that, for a rectangular channel, an aspect ratio of eight should be used for minimum entropy generation in the channel. In this work, however, results showed that an aspect ratio of eight is not necessarily the optimum aspect ratio for the receiver and recuperator channels in a system which should produce maximum net power output. This is the result of minimising total entropy generation for the whole system, instead of for components individually.

Results showed that the optimum recuperator length increased as a function of mass flow rate until the length constraint was reached. The same result was found for optimum NTU. It was concluded that for maximum system net power output at lower system mass flow rates, it is more beneficial to have a low recuperator efficiency (or a bypassed recuperator). This result validated that a high efficiency for an individual component in a system does not necessarily provide optimum results for the system as a whole. When maximum net power output is required, it is in some cases better for the system to have a component with low efficiency.

No major differences could be found in the maximum net power output between cavity receivers constructed with a rectangular channel and cavity receivers constructed with a circular tube respectively. It was found that a large solar cavity receiver aperture or a small rectangular channel aspect ratio, but not necessarily both, is most beneficial. It was also found that the receiver tube diameter should be relatively large. For the circular tube and rectangular channel receiver, the optimum number of tube diameters or rectangular channels that should fit in between the aperture edge and the receiver edge was found.

Optimum system operating conditions were established in the analysis. The results showed how the irreversibilities should be spread throughout the system optimally in order for the system to produce maximum net power output. The optimum recuperator channel mass flow rate, receiver hydraulic diameter and optimum NTU behaved very specifically with the system mass flow rate. It was found that it is best for the receiver to operate in the turbulent flow regime, and for the recuperator channels to operate in the laminar flow regime. Results showed that at higher mass flow rates, the maximum receiver surface temperature decreased as a function of mass flow rate.

It was noted that the minimum rate of internal irreversibility of the optimised systems was always more than the minimum rate of external irreversibility. It was found that the solar receiver is the main contributor to the total rate of internal entropy generation for the optimised systems with maximum net power output. Results showed that the irreversibilities were spread throughout the system in such a way that the minimum internal irreversibility rate was almost three times the minimum external irreversibility rate for all data points, which gave the highest maximum net power output of a micro-turbine. A constant was given for this optimum ratio of minimum internal irreversibility rate to minimum external irreversibility rate (C_W), where the maximum net power output in a micro-turbine's operating range is the largest (at optimum operating point of a micro-turbine). Results showed that C_W increases as the mass flow rate increases for a specific concentrator diameter. The highest maximum thermal efficiency of these optimised systems was found to be a function of the solar concentrator diameter and choice of micro-turbine.

The effect of various conditions such as wind, receiver inclination, concentrator rim angle and irradiance on the maximum net power output and optimum geometries of the system components was investigated. The maximum net power output was found to stay constant in certain cases while the optimum geometry was shifted around to accommodate for the change. This was observed in changes in recuperator height, receiver inclination and concentrator rim angle. In other cases, the maximum net power output could be changed by changing a constant such as the effect of wind, irradiance, minimum concentration ratio, recuperator length, surrounding pressure, recuperator material and maximum surface temperature. Results showed that, for a specific environment and parameters, an optimum receiver and recuperator geometry exists so that the system can produce maximum net power output.

It was found that the second law of thermodynamics is a valuable contribution to the optimisation of solar thermal power systems. The geometry of components in a solar thermal power system should be optimised by minimising the total rate of entropy generation in the system in such a way that the system produces maximum net power output. The results of this study give insight into the optimal behaviour and component geometries of the recuperative solar thermal Brayton cycle limited to challenging constraints. These results can be considered in the preliminary stages of design. The results found in this work (the analytical approach) should be compared with experimental work. The small-scale open and direct solar thermal Brayton cycle with optimised geometry for maximum net power output, using the method of entropy generation minimisation, can be regarded as a good local power generation method for the near future.

References

Agudelo, A., Cortés, C. 2010. Thermal radiation and the second law. *Energy*, 35 (2), p. 679 - 691.

Bejan, A., 1982. *Entropy generation through heat and fluid flow*. Colorado: John Wiley.

Bejan, A. 1996. Method of entropy generation minimization, or modelling and optimization based on combined heat transfer and thermodynamics. *Rev Gén Therm*, 35, p. 637 - 646.

Bejan, A., Tsatsaronis, G. and Moran, M. 1996. *Thermal design and optimization*. New York: John Wiley.

Bejan, A. 1997. *Advanced engineering thermodynamics.* 2nd ed. Durham: John Wiley.

Bertocchi, R., Karni, J. and Kribus, A. 2004. Experimental evaluation of a non-isothermal high temperature solar particle receiver. *Energy*, 29, p. 687 – 700.

Burden, R.L. and Faires, J.D. 2005. *Numerical analysis*. 8th ed. Youngston State University: Thomson Brooks/Cole.

Çengel, Y.A. 2006. *Heat and mass transfer*. 3rd ed. Nevada, Reno: McGraw-Hill.

Chen, L., Zhang, W. and Sun, F. 2007. Power, efficiency, entropy-generation rate and ecological optimization for a class of generalized irreversible universal heat-engine cycles. *Applied Energy,* 84, p. 512 - 525.

Cheremisinoff, P.N. and Regino, T.C. 1978. *Principles and applications of solar energy*. Michigan: Ann Arbor Science Publishers.

Copper Development Association. 2006. *The Copper Tube Handbook*. New York: Copper Development Association.

Cornelissen, R.L. and Hirs, G.G. 1997. Exergetic optimization of a heat exchanger. *Energy Conversion and Management*, 1 (15-17), p. 1567 - 1576.

DME, Department of Minerals and Energy, Republic of South Africa. 2010. *Solar Energy*. [online]. Available at: http://www.dme.gov.za/energy/renew_solar.stm [Accessed: 20 July 2010].

Dittus, F.W. and Boelter, L.M.K. 1930. *University of California Publications on Engineering*, *2*, p. 433.

Dixon, S.L. 2005. *Fluid mechanics and thermodynamics of turbomachinery*. 5th ed. Liverpool: Elsevier Butterworth-Heinemann.

Duffie, J.A. and Beckman, W.A. 1991. *Solar engineering of thermal processes.* New York: John Wiley.

Fluri, T.P. 2009. The potential of concentrating solar power in South Africa. *Energy Policy*, 37, p. 5075 – 5080.

Garrett. 2009. *Garrett by Honeywell: Turbochargers, Intercoolers, Upgrades, Wastegates, Blow-Off Valves, Turbo-Tutorials.* Available at: http://www.TurboByGarrett.com [Accessed: 26 April 2010].

Gnielinski, V. 1976. New equations for heat and mass transfer in turbulent pipe and channel flow. *International Chemical Engineering*, 16, p. 359 - 368.

Heller, P., Pfänder, M., Denk, T., Tellez, F., Valverde, A., Fernandez, J. and Ring, A. 2006. Test and evaluation of a solar powered gas turbine system. *Solar Energy*, 80, p. 1225 - 1230.

Hesselgreaves, J.E. 2000. Rationalisation of second law analysis of heat exchangers. *International Journal of Heat and Mass Transfer*, 43 (22), p. 4189 - 4204.

Howell, J.R., Bannerot, R.B. and Vliet, G.C. 1982. *Solar-thermal energy systems.* New York: McGraw-Hill.

Ishikawa, H. and Hobson, P.A. 1996. Optimisation of heat exchanger design in a thermoacoustic engine using a second law analysis. *International Communications in Heat and Mass Transfer*, 23 (3), p. 325 - 334.

Johnson, G. 2009. Plugging into the sun. *National Geographic*, 216(3), p. 28 - 53.

Joshi, A.S., Dincer, I. and Reddy, B.V. 2009. Development of new solar exergy maps. *International Journal of Energy Research*, 33, p. 709 – 718.

Jubeh, N.M. 2005. Exergy analysis and second law efficiency of a regenerative Brayton cycle with isothermal heat addition. *Entropy*, 7 (3), p. 172 - 187.

Kreith, F. and Kreider, J.F. 1978. *Principles of solar engineering*. Colorado: Hemisphere.

Lerou, P.P.P.M., Veenstra, T.T., Burger, J.F., Ter Brake, H.J.M. and Rogalla, H. 2005. Optimization of counterflow heat exchanger geometry through minimization of entropy generation. *Cryogenics*, 45, p. 659 - 669.

Mills, D. 2004. Advances in solar thermal electricity technology. *Solar Energy*, 76, p. 19 - 31.

Narendra, S., Kaushik, S.C. and Misra, R.D. 2000. Exergetic analysis of a solar thermal power system. *Renewable Energy*, 19, p. 135 - 143.

Oğulata, R.T., Doba, F. and Yilmaz, T. 2000. Irreversibility analysis of cross flow heat exchangers. *Energy Conversion and Management*, 41 (15), p. 1585 - 1599.

Ordóñez, J.C. and Bejan, A. 2000. Entropy generation minimization in parallel-plates counterflow heat exchangers. *International Journal of Energy Research*, 24, p. 843 - 864.

Petela, R. 2010. *Engineering thermodynamics of thermal radiation*. New York: McGraw Hill.

Petukhov, B.S. 1970. Heat transfer and friction in turbulent pipe flow with variable physical properties. *Advances in Heat Transfer*, 6.

Pitz-Paal, R. 2007. High temperature solar concentrators. *Solar Energy Conversion and Photoenergy Systems*, [Ed. Galvez, J.B. and Rodriguez, S.M.], in *Encyclopedia of Life Support Systems (EOLSS),* Developed under the Auspices of UNESCO, Eolss Publishers, Oxford [http://www.eolss.net].

Prakash, M., Kedare, S.B. and Nayak, J.K. 2009. Investigations on heat losses from a solar cavity receiver. *Solar Energy*, 83, p. 157 - 170.

Ratts, B.E. and Raut, A.G. 2004. Entropy generation minimization of fully developed internal flow with constant heat flux. *Journal of Heat Transfer*, 126 (4), p. 656 - 659.

Reddy, K.S. and Sendhil Kumar, N. 2008. Combined laminar natural convection and surface radiation heat transfer in a modified cavity receiver of solar parabolic dish. *International Journal of Thermal Sciences*, 47, p. 1647 – 1657.

Reddy, K.S. and Sendhil Kumar, N. 2009. An improved model for natural convection heat loss from modified cavity receiver of solar dish concentrator. *Solar Energy*, 83, p. 1884 – 1892.

Sama, D.A. 1995. The use of the second law of thermodynamics in process design. *Journal of Energy Resources Technology*, 117, p. 179 - 185.

Sarangi, S. and Chowdhury, K. 1982. On the generation of entropy in a counterflow heat exchanger. *Cryogenics*, 22 (2), p. 63 - 65.

Schwarzbözl, P., Buck, R., Sugarmen, C., Ring, A., Jesús Marcos Crespo, M., Altwegg, P. and Enrile, J. 2006. Solar gas turbine systems: design, cost and perspectives. *Solar Energy*, 80, p. 1231 - 1240.

Sendhil Kumar, N. and Reddy, K.S. 2007. Numerical investigation of natural convection heat loss in modified cavity receiver for fuzzy focal solar dish concentrator. *Solar Energy*, 81, p. 846 – 855.

Sendhil Kumar, N. and Reddy, K.S. 2008. Comparison of receivers for solar dish collector system. *Energy Conversion and Management*, 49, p. 812 - 819.

Shah, R.K. 2005. Compact heat exchangers for micro-turbines. In *Micro Gas Turbines* (p. 2-1 – 2-18). Educational Notes RTO-EN-AVT-131, Paper 2. Neuilly-sur-Seine, France: RTO. Available from: http://www.rto.nato.int/abstracts.asp.

Shiba, T. and Bejan, A. 2001. Thermodynamic optimization of geometric structure in the counterflow heat exchanger for an environmental control system. *Energy*, 26, p. 493 - 511.

Shuai, Y., Xia, X. and Tan, H. 2008. Radiation performance of dish solar concentrator/cavity receiver systems. *Solar Energy*, 82, p. 13 - 21.

Snyman, J.A. 2000. The LFOPC leap-frog algorithm for constrained optimization. *Computers and Mathematics with Applications*, 40, p. 1085 - 1096.

Snyman, J.A. 2009. *Practical mathematical optimization*. Pretoria: University of Pretoria.

Steinfeld, A. and Schubnell, M. 1993. Optimum aperture size and operating temperature of a solar cavity-receiver. *Solar Energy*, 50, p. 19 – 25.

Stewart, J. 2003. *Calculus, early transcendentals.* McMaster: Brooks/Cole.

Stine, B.S. and Harrigan, R.W. 1985. *Solar energy fundamentals and design*. New York: John Wiley.

Sonntag, R.E., Borgnakke, C. and Van Wylen, G.J. 2003. *Fundamentals of thermodynamics.* New York: John Wiley.

STG International. 2010. *Specifications* [Online].
Available at: http://www.stginternational.org/specs.html
[Accessed: 2 August 2010].

Tsai, L. 2004. *Design and performance of a gas-turbine engine from an automobile turbocharger*. Unpublished. BSc Eng Mech., Massachusetts Institute of Technology.

Weston, K.C. 2000. *Energy Conversion*. [e-book]. Tulsa: Brooks/Cole.
Available at: http://www.personal.utulsa.edu/~kenneth-weston/
[Accessed: 16 February 2010]

Wilson, J.I.B. 1979. *Solar energy*. London: Wykeham.

Yilmaz, M., Sara, O.N. and Karsli, S. 2001. Performance evaluation criteria for heat exchangers based on second law analysis. *Exergy, an International Journal*, 1 (4), p. 278 - 294.

Zimparov, V. 2001. Extended performance evaluation criteria for enhanced heat transfer surfaces: heat transfer through ducts with constant heat flux. *International Journal of Heat and Mass Transfer*, 44 (1), p. 169 -180.

Zimparov, V.D., Da Silva, A.K. and Bejan, A. 2006a. Thermodynamic optimization of tree-shaped flow geometries with constant channel wall temperature. *International Journal of Heat and Mass Transfer*, 49, p. 4839 - 4849.

Zimparov, V.D., Da Silva, A.K. and Bejan, A. 2006b. Constructal tree-shaped parallel flow heat exchangers. *International Journal of Heat and Mass Transfer*, 49, p. 4558 - 4566.

Zimparov, V.D., Da Silva, A.K. and Bejan, A. 2006c. Thermodynamic optimization of tree-shaped flow geometries. *International Journal of Heat and Mass Transfer*, 49, p. 1619 - 1630.

Appendix A

COLLECTOR

This section describes the methodology behind the MATLAB function: '*collector*' (see Appendix C). This function follows the receiver-sizing algorithm of Stine and Harrigan (1985) shown in Figure A.1. A better understanding of the concentrator and its geometry is also given.

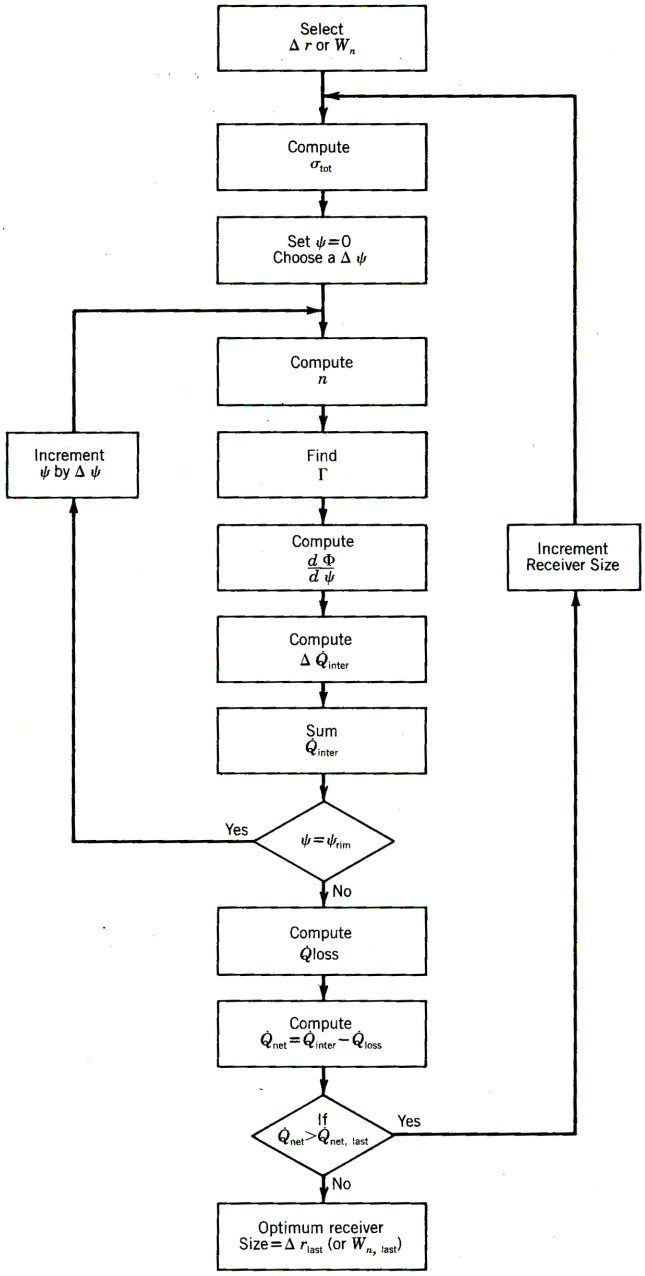

Figure A.1 Receiver-sizing algorithm (Stine and Harrigan, 1985).

The method of Figure A.1 is applied to establish the net absorbed heat rate of the cavity receiver as a function of the cavity receiver aperture, similar to Figure 2.27 in the literature. This is done in the function '*collector*' (Appendix C). The function starts of by asking the user to give the dish concentrator area and its rim angle. Figure A.2 shows the definition of the rim angle (Stine and Harrigan, 1985). The aperture area of a paraboloid (parabolic dish concentrator) is defined by

$$A_s = \pi R^2 \qquad \text{or} \qquad A_s = 4\pi f_c^{\,2} \frac{\sin^2 \psi_{rim}}{(1+\cos \psi_{rim})^2} \tag{A.1}$$

in terms of the focal length (f_c) and the rim angle, ψ_{rim} (Stine and Harrigan, 1985).

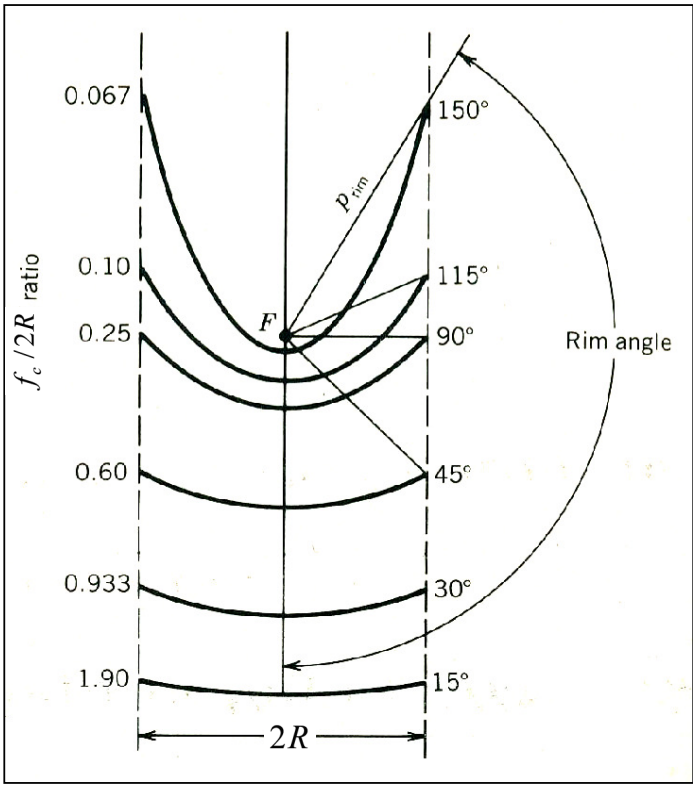

Figure A.2 Definition of the rim angle (Stine and Harrigan, 1985).

The focal length can be calculated when the rim angle and concentrator area are specified. Stine and Harrigan's algorithm requires one to compute the total parabolic concentrator error. According to Stine and Harrigan (1985), a typical parabolic concentrator error is 6.7 mrad. This error could be regarded as a user-specified constant since this error depends on the collector design, structure, tracking, alignment, mirror specular reflectance, etc. After these steps, the

function goes to a while loop, starting at a rim angle of 0° through to an angle of ψ_{rim} in increments of 1° and computes the amount of intercepted solar energy per segment of concentrator area. The projection of the image width onto the focal plane (see Figure A.3) can be written as

$$d = \frac{\Delta r}{\cos\psi} \tag{A.2}$$

where ψ is the specific rim angle at the segment of the concentrator.

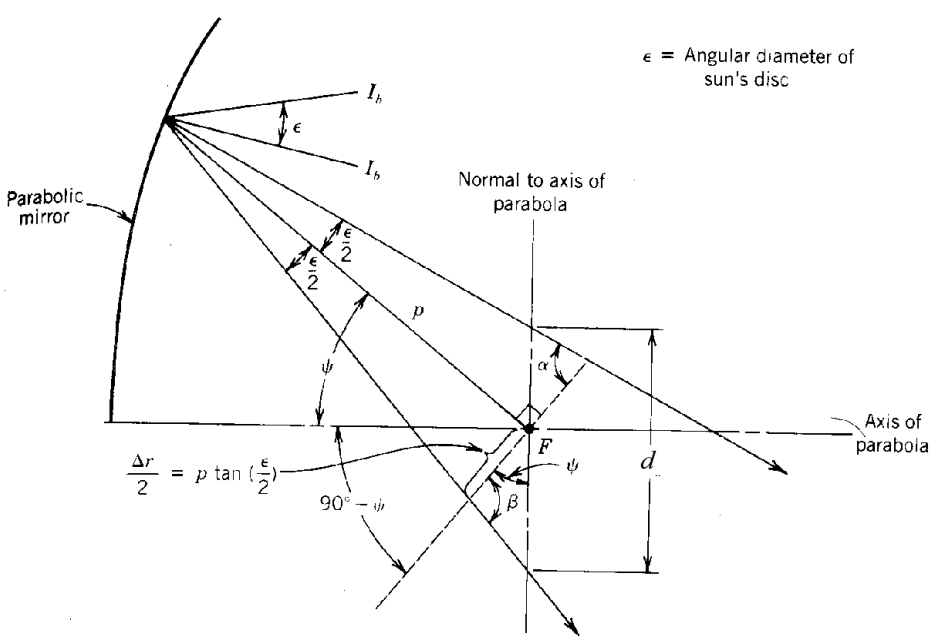

Figure A.3 Reflection of non-parallel rays from a parabolic mirror (Stine and Harrigan, 1985).

For a specific cavity receiver aperture diameter, d, Δr can be calculated. The parabolic radius at that segment can be calculated using equation A.3 (Stine and Harrigan, 1985).

$$p = \frac{2f_c}{1+\cos\psi} \tag{A.3}$$

The number of standard deviations, n, being considered can be calculated using equation A.4 (Stine and Harrigan, 1985),

$$\Delta r = 2p\tan\left(n\frac{\sigma_{tot}}{2}\right), \tag{A.4}$$

where σ_{tot} is the total parabolic concentrator error. According to Stine and Harrigan (1985), a typical parabolic concentrator error is 6.7 mrad. The next step is to find Γ. According to Stine and Harrigan (1985), the flux capture fraction is the ratio of the flux reflected from a parabolic surface in a shaft of light having width of n standard deviations of the total angular error. For the normally distributed reflected flux, the flux capture fraction is simply the area under the normal distribution function integrated from $-n/2$ to $+n/2$. A polynomial approximation to this normal integral, from Abramowitz and Stegun (1970, cited in Stine and Harrigan, 1985), can be written as:

$$\Gamma = 1 - 2*Q \tag{A.5}$$

where:

r = 0.2316419
b_1 = 0.319381530
b_2 = -0.356563782
b_3 = 1.781477937
b_4 = -1.821255978
b_5 = 1.330274429
y = $n/2$
f_1 = $\frac{1}{\sqrt{2\pi}}e^{\frac{y^2}{2}}$
t_1 = $1/(1+r\,y)$
Q = $f_1\,(b_1t_1 + b_2t_1^2 + b_3t_1^3 + b_4t_1^4 + b_5t_1^5)$

The next step in Stine and Harrigan's algorithm is to compute the slope: $\frac{d\Phi}{d\Psi}$ where, according to Stine and Harrigan (1985), for a parabolic dish:

$$d\Phi_{PD} = \frac{8\pi I_b f_c^{\,2}\sin\psi d\psi}{(1+\cos\psi)^2} \tag{A.6}$$

$d\Phi_{PD}$ is the total radiant flux reflected from the differential area (assuming no reflectance loss) to the point of focus. The following equation (Stine and Harrigan, 1985) is used to compute the rate of energy reflected from a strip (the parabolic mirror dish is divided into incremental rings) and intercepted by the receiver with aperture diameter, d .

$$\Delta\dot{Q}_i = \rho_s \alpha \Gamma \left(\frac{d\Phi}{d\psi} \right) \Delta\psi \tag{A.7}$$

All of these intercepted energy rates for all the rings are then added to give the total rate of intercepted energy, $\dot{Q}_i$, for the collector with d as receiver aperture diameter. The next step is to calculate $\dot{Q}_0$. According to Stine and Harrigan (1985), ideally, in a well-insulated cavity, the cavity temperature is reasonably uniform and heat loss occurs primarily by convection and radiation from the cavity aperture. The heat loss rate from the cavity is described in Section 3.5.1.1. Once the heat loss rate is available, $\dot{Q}_{net}$ can be calculated as:

$$\dot{Q}_{net} = \dot{Q}_i - \dot{Q}_0 \tag{A.8}$$

It is clear that the amount of absorbed heat rate, $\dot{Q}_{net}$, can be described in terms of the cavity aperture diameter, d . The function '*collector*' determines the net heat rate absorbed by the receiver for different cavity aperture sizes. The result is the curve shown in Figure A.4. This is for e_p = 0.0067 and ψ_{rim} = 45°, as suggested by Stine and Harrigan (1985). From these curves, one can see that there exists an aperture diameter that allows the maximum amount of solar power to be absorbed by the working fluid. Such a curve can be numerically approximated with the discrete least squares approximation method (Burden and Faires, 2005) or by using the function '*curvefit*' in MATLAB ($\dot{Q}_{net} = \sum_{i=0}^{10} x_i d^i$).

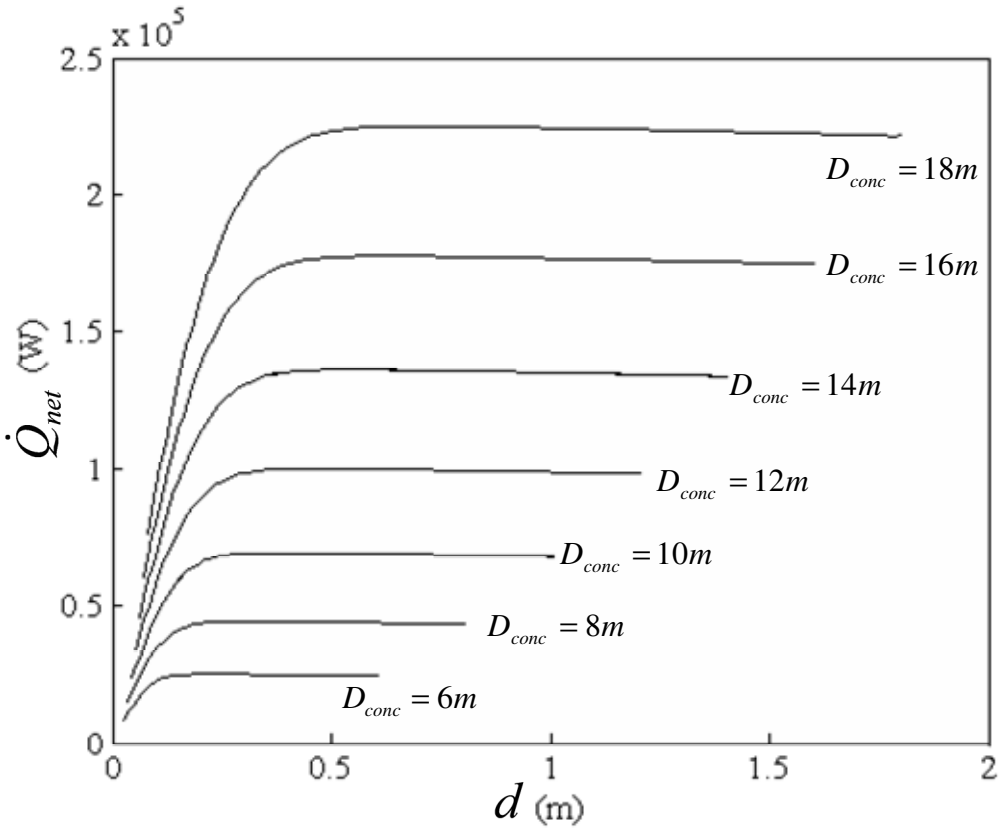

Figure A.4 Relation between net absorbed heat rate and the aperture diameter for a range of concentrator diameters according to the function '*collector*'.

The specific aperture diameter is coupled to the receiver's channel dimensions (its length, hydraulic diameter and aspect ratio – only for a plated receiver, see equation 3.20). The method of entropy generation minimisation can now be used to show whether or not it is better to have an aperture size at the optimum d, as suggested from the curve. The literature suggests that the optimum geometry for a component in a system is not necessarily the optimum geometry when considering the whole system. For this reason, d will not be chosen to be at its optimum, since this optimum is not necessarily the optimum for the whole system. Rather, the aperture diameter is written in terms of the geometry variables so that the net rate of heat absorbsion can be written as a function of the receiver geometry and can be included in the objective function (equation 3.61). The optimum aperture diameter can be found when the optimum geometry variables are found. In the function '*collector*', the shadow of the receiver and its insulation are also accounted for when calculating the available power at the receiver. Heat loss through conduction at the cavity receiver through the insulation is usually small and omitted. In the function '*collector*', however, it was assumed that the conduction heat loss rate is 10% of the sum of the radiation and convection heat loss rates.

References

Burden, R.L. and Faires, J.D. 2005. *Numerical analysis*. 8th ed. Youngston State University: Thomson Brooks/Cole.

Stine, B.S. and Harrigan, R.W. 1985. *Solar energy fundamentals and design*. New York: John Wiley.

Nomenclature

A	Area	m^2
d	Aperture diameter of cavity receiver (or W_n)	m
D	Diameter	m
e_p	Parabolic concentrator error	rad
f	Focal length	m
F	Focal point	-
I	Irradiance	W/m^2
n	Number of standard deviations in receiver-sizing algorithm	-
p	Parabolic radius	m
$\dot{Q}$	Heat transfer rate	W
Δr	Diameter of sun's disc at the focal point	m
R	Radius of parabolic dish concentrator	m
W_n	Aperture diameter of cavity receiver (or d)	m
x	Discrete least-squares approximation constant	-
α	Receiver absorptance	-
α	Defining angle at receiver aperture	rad
β	Defining angle at receiver aperture	rad
Γ	Flux capture fraction	-
$\Delta\psi$	Incremental parabola angle defining ring	-
ε	Angular diameter of sun's disc	-
ρ_s	Mirror surface specular reflectance	-
σ	Parabolic concentrator error	rad
Φ	Radiant flux	W

$d\Phi$	Total radiant flux reflected from differential concentrator area to focus point	-
ψ	Specific concentrator rim angle	-
ψ_{rim}	Concentrator rim angle	-

Subscripts:

0	Loss due to convection and radiation
b	Beam
c	Concentrator
$conc$	Concentrator
i	Intercepted total
inter	Intercepted
last	Last
loss	Loss
net , net	Net available for receiver fluid
PD	Parabolic dish
rim , rim	Rim / to the rim
s	Surface
tot	Total

Appendix B

ENTROPY GENERATION RATE TABLE

Table B.1 Entropy generation rate equations from the literature.

Eq.	Entropy generation research field		Entropy generation rate equation	Comments/ Symbols	References
1	**A. Internal flow**	Per unit tube length, constant heat flux, for all ducts (one-dimensional heat transfer duct)	$\dot{S}'_{gen} = \frac{d\dot{S}_{gen}}{dx} = \frac{q'\Delta T}{T^2(1+\tau)} + \frac{\dot{m}}{\rho T}\left(-\frac{dp}{dx}\right)$	$\tau = \Delta T / T$	Yilmaz et al. (2001); Bejan et al. (1996); Hesselgreaves (2000); Zimparov et al. (2006c); Bejan (1982)
2		Constant heat flux, per unit tube length, for all ducts	$\dot{S}'_{gen} = \frac{q'^2}{4T^2\dot{m}c_p}\frac{D_h}{St} + \frac{2\dot{m}^3}{\rho^2 T}\frac{f}{D_h A^2}$	T = bulk temperature of the stream	Bejan (1982); Bejan et al. (1996)
3		Constant heat flux, per unit tube length, for a circular tube, single-phase fluid	$\dot{S}'_{gen} = \frac{q'^2}{\pi k T^2 Nu_D} + \frac{32\dot{m}^3 f}{\pi^2 \rho^2 T D^5}$	T = bulk temperature of the stream	Bejan (1982); Bejan et al. (1996); Bejan (1996)

4		Constant heat flux, incompressible viscous fluid, laminar, fully developed	$\dot{S}_{gen} = \frac{q'}{\pi k Nu T_0^2} q' L_i + \frac{128\nu}{\rho \pi T_i} \dot{m}_i^2 \frac{L}{D_i^4}$	T_i = inlet temperature and assuming $\tau << 1$, where $T_i T_0 = T_i^2 = T_0^2$	Zimparov et al. (2006c)
5		Constant and uniform heat flux, per unit length of tube, for all tubes, single-phase, fully developed	$\dot{S}'_{gen} = \frac{\dot{q}'' P (T_w - T)}{T^2} + \frac{\dot{m}^3 f}{2\rho T D_h A^2}$	$T =$ bulk fluid temperature, $P =$ perimeter	Ratts and Raut (2004)
6		Constant and uniform heat flux, for all tubes with tube length L, fluid properties assumed to be constant, single-phase, fully developed	$\dot{S}_{gen} \cong \frac{(\dot{q}'')^2 P D_h L}{Nu T_1 T_2 k} + \frac{8\dot{m}^3 f L}{\rho^2 T_{ave} D_h^3 P^2}$	T_1 and T_2 are the inlet and outlet fluid temperatures, $P =$ perimeter	Ratts and Raut (2004)
7		Constant heat flux, including the fluid temperature variation along tube length of heat exchanger, for ideal gas or incompressible flow, circular	$\dot{S}_{gen} = \dot{m} c_p \Delta T \frac{4St(\Delta T / D)L}{T_i^2 \left[1 + 4St(\Delta T / T_i)(L/D)\right]} + \frac{\dot{m} u_m^2 f}{2St\Delta T} \ln\left(1 + 4St \frac{\Delta T L}{T_i D}\right)$	$u_m = 4\dot{m} / \rho / \pi / D^2$	Zimparov (2001)

8		Per unit tube length, constant channel wall temperature for all ducts (one-dimensional heat transfer duct)	$\dot{S}'_{gen} = \frac{d\dot{S}_{gen}}{dx} = \dot{m}c_p \frac{\Delta T dT}{T^2 dx} + \frac{\dot{m}}{\rho T}\left(-\frac{dp}{dx}\right)$	Assuming ideal gas or incompressible fluid and $\tau = \Delta T / T << 1$	Zimparov et al. (2006a)
9		Convective heat transfer in a duct with constant wall temperature, circular	$\dot{S}_{gen} = \dot{Q}_t \frac{\theta_o}{T_i T_o} + \frac{32\dot{m}^3 f}{\rho^2 \pi^2 D^5} \frac{L}{T_w}$	$\dot{Q}_t = \dot{m}c_p(T_o - T_i)$ $\theta_o = T_w - T_o$	Yilmaz et al. (2001)
10	**B. External flow**	Heat transfer and drag on an immersed body	$\dot{S}_{gen} = \frac{\dot{Q}_B (T_B - T_\infty)}{T_B T_\infty} + \frac{F_D U_\infty}{T_\infty}$		Bejan (1996)
11		Heat transfer and drag on an immersed body	$\dot{S}_{gen} = \frac{\dot{Q}(\overline{T}_w - T_\infty)}{T_\infty^2} + \frac{F_D U_\infty}{T_\infty}$		Bejan et al. (1996)
12	**C. Augmentation techniques**	For a single fin	$\dot{S}_{gen} = \frac{\dot{Q}_B \theta_B}{T_\infty^{\ 2}} + \frac{F_D U_\infty}{T_\infty}$	$\theta_B = T_B - T_\infty$, $\theta_B << T_\infty$	Bejan (1982)

13	**D. Local entropy generation**		$\dot{S}'''_{gen} = \frac{1}{T}\left(\frac{\partial q_x}{\partial x} + \frac{\partial q_y}{\partial y}\right) - \frac{1}{T^2}\left(q_x \frac{\partial T}{\partial x} + q_y \frac{\partial T}{\partial y}\right) + \rho\left(\frac{\partial s}{\partial t} + v_x \frac{\partial s}{\partial x} + v_y \frac{\partial s}{\partial y}\right) + s\left[\frac{\partial \rho}{\partial t} + v_x \frac{\partial \rho}{\partial x} + v_y \frac{\partial \rho}{\partial y} + \rho\left(\frac{\partial v_x}{\partial x} + \frac{\partial v_y}{\partial y}\right)\right]$		Bejan (1982)
14		The volumetric rate of entropy generation	$\dot{S}'''_{gen} = k\frac{(\nabla T)^2}{T^2} + \mu\frac{\phi}{T}$		Yilmaz et al. (2001); Bejan et al. (1996); Bejan (1982)
15	**E. Heat Exchangers**	For tubular, full size heat exchanger with constant heat flux, assume ideal gas or incompressible fluid	$\dot{S}_{gen} = \frac{\dot{Q}_t \Delta T}{T_i^2\left[1+\left(\frac{\Delta T_m}{T_i}\right)\right]} + \frac{32\dot{m}^3 fL}{\rho^2\pi^2 T_i D^5}\frac{\ln\left[1+\left(\frac{\Delta T_m}{T_i}\right)\right]}{\left(\frac{\Delta T_m}{T_i}\right)}$	$u_m = 4\dot{m}/\rho/\pi/D^2$ and $\dot{Q}_t = \dot{m}c_p(T_o - T_i)$	Zimparov (2001); Yilmaz et al. (2001)
16		Counterflow and cross-flow heat exchangers, where the working fluid is an ideal gas with constant specific heat, for all tubes	$\dot{S}_{gen} = (\dot{m}c_p)_1 \ln\frac{T_{1,out}}{T_{1,in}} + (\dot{m}c_p)_2 \ln\frac{T_{2,out}}{T_{2,in}} - (\dot{m}R)_1 \ln\frac{P_{1,out}}{P_{1,in}} - (\dot{m}R)_2 \ln\frac{P_{2,out}}{P_{2,in}}$	1 represents the cold stream and 2 represents the hot stream	Yilmaz et al. (2001); Hesselgreaves (2000); Bejan (1982); Bejan et al. (1996); Oğulata et al. (2000)

17		Gas-to-gas application	$\dot{S}_{gen} = X\left\{\omega\ln\left[1+\varepsilon\left(\tau^{-1}-1\right)\right]+\ln\left[1+\omega\varepsilon\left(\tau-1\right)\right]+Y\right\}$ where $Y = -\omega\frac{R_1}{c_{p1}}\ln\left(1-\frac{\Delta p_1}{p_1^{\ in}}\right)-\frac{R_2}{c_{p2}}\ln\left(1-\frac{\Delta p_2}{p_2^{\ in}}\right)$	1 represents the cold stream and 2 represents the hot stream and $X=\left(\dot{m}c_p\right)_2$, $\omega=\left(\dot{m}c_p\right)_1/\left(\dot{m}c_p\right)_2\le 1$ and $\tau=T_1/T_2$	Yilmaz et al. (2001)
18		Balanced counterflow heat exchanger, water, with perfect insulation	$\dot{S}_{gen}=\dot{I}/T_0$, where $\dot{I}=\dot{I}^{\Delta T}+\dot{I}^{\Delta P}$ and $\dot{I}^{\Delta T}=T_0\left[\dot{m}c_p\ln\frac{T_{1,out}}{T_{1,in}}+\dot{m}c_p\ln\frac{T_{2,out}}{T_{2,in}}\right]$ and $\dot{I}^{\Delta P}=\frac{\dot{m}}{\rho}\left(P_{1,in}-P_{1,out}\right)+\frac{\dot{m}}{\rho}\left(P_{2,in}-P_{2,out}\right)$	1 represents the cold stream and 2 represents the hot stream	Cornelissen and Hirs (1997)
19		Parallel plates counterflow, single-phase ideal gas fluids, fully developed, laminar or turbulent, adiabatic boundary	$\dot{S}_{gen}=(\dot{m}c_p)_a\left[\ln\frac{T_2}{T_1}-\left(\frac{R}{c_p}\right)_a\ln\frac{P_2}{P_1}\right]+(\dot{m}c_p)_e\left[\ln\frac{T_4}{T_3}-\left(\frac{R}{c_p}\right)_e\ln\frac{P_4}{P_3}\right]$	1 - cold stream in, 2 - cold stream out, 3 - hot stream in, 4 - hot stream out	Ordóñez and Bejan (2000)
20		Counterflow heat exchanger (with zero pressure drop)	$\dot{S}_{gen}=(\dot{m}c_p)_1\ln\frac{T_{1,out}}{T_{1,in}}+(\dot{m}c_p)_2\ln\frac{T_{2,out}}{T_{2,in}}$	1 represents the cold stream and 2 represents the hot stream	Bejan (1982); Hesselgreaves (2000)

21		Balanced counterflow with zero pressure drop	$\dot{S}_{gen} = \dot{m}c_p \ln\left[\frac{(1+T_1 NTU/T_2)(1+T_2 NTU/T_1)}{(1+NTU)^2}\right]$	1 represents the cold stream and 2 represents the hot stream and $\varepsilon = NTU/(NTU+1)$	Hesselgreaves (2000)
22		Balanced counterflow with finite pressure drop, constant heat flux, fully developed, perfect gas, 1 - cold stream	$\dot{S}_{gen} = -\dot{m}c_p\left[\frac{A}{2\Delta T}(T_1^2 - T_{1,out}{}^2) - \Delta T\left[\frac{1}{T_{1,out}} - \frac{1}{T_1}\right]\right]$	$A = \frac{fG^2R^2}{2Stp^2c_p}$	Hesselgreaves (2000)
23	**F. Solar Receiver**	Isothermal collector	$\dot{S}_{gen} = \frac{\dot{Q}_0}{T_0} + \frac{\dot{Q}}{T_c} - \frac{\dot{Q}^*}{T^*}$ $= \frac{1}{T_0}\left[\dot{Q}^*\left(1-\frac{T_0}{T^*}\right) - \dot{Q}\left(1-\frac{T_0}{T_c}\right)\right]$		Bejan (1982); Bejan (1997)
24		Non-isothermal collector receiver - where a stream of single-phase fluid circulated through receiver	$\dot{S}_{gen} = \dot{m}c_p \ln\frac{T_{out}}{T_{in}} - \frac{\dot{Q}^*}{T^*} + \frac{\dot{Q}_0}{T_0}$	Pressure drop was neglected	Bejan (1982)

25		Entropy generation due to transformation of monochromatic radiation into blackbody radiation	$S_{gen} = \frac{S\pi k T}{15^{0.25} hv} \left(\frac{\Delta v}{v}\right)^{-0.25} [\exp(hv/kT) - 1]^{0.25} - S$	$S =$ original entropy inventory of system where $S = 4U/3T$ and $\Delta v / v =$ slenderness ratio of frequency band	Bejan (1997)
26		Entropy generation due to scattering	$S_{gen} = \frac{4}{3} i_{vb} \left(\frac{1}{T_2} - \frac{1}{T_1}\right)$	T_1 and T_2 represent monochromatic radiation temperatures before and after scattering	Bejan (1997)
27	**G. Components for whole system analysis**	Compressor or turbine for ideal gas	$\dot{S}_{gen} = \dot{m} c_{p1-2} \ln(T_2/T_1) - \dot{m} R \ln(P_2/P_1)$	1 - in, 2 - out	Jubeh (2005)
28		Ideal gas regenerator	$\dot{S}_{gen} = \dot{m} c_{p2-6} \ln(T_6/T_2) - \dot{m} R \ln(P_6/P_2) + \dot{m} c_{p5-7} \ln(T_7/T_5) - \dot{m} R \ln(P_7/P_5)$	2 - 6: cold stream, 5 - 7: hot stream	Jubeh (2005)
29		Open cycle ideal gas regenerator	$\dot{S}_{gen} = \dot{m} c_{p0} \left[\ln \left[\frac{T_0 T_4}{T_1 T_3} \left(\frac{P_0 P_4}{P_1 P_3} \right)^{(1-k)/k} \right] + \frac{T_2 - T_0}{T_0} \right] + Y$	1 - 2:cold stream, 3 - 4:hot stream, 0: atmospheric and $Y = \frac{\dot{Q}_{loss}}{T_0}$	Ordóñez and Bejan (2000)

References

Bejan, A., 1982. *Entropy generation through heat and fluid flow*. Colorado: John Wiley.

Bejan, A. 1996. Method of entropy generation minimization, or modelling and optimization based on combined heat transfer and thermodynamics. *Rev Gén Therm*, 35, p. 637 - 646.

Bejan, A., Tsatsaronis, G. and Moran, M. 1996. *Thermal design and optimization*. New York: John Wiley.

Bejan, A. 1997. *Advanced engineering thermodynamics.* 2nd ed. Durham: John Wiley.

Cornelissen, R.L. and Hirs, G.G. 1997. Exergetic optimization of a heat exchanger. *Energy Conversion and Management*, 1 (15-17), p. 1567 - 1576.

Hesselgreaves, J.E. 2000. Rationalisation of second law analysis of heat exchangers. *International Journal of Heat and Mass Transfer*, 43 (22), p. 4189 - 4204.

Jubeh, N.M. 2005. Exergy analysis and second law efficiency of a regenerative Brayton cycle with isothermal heat addition. *Entropy*, 7 (3), p. 172 - 187.

Oğulata, R.T., Doba, F. and Yilmaz, T. 2000. Irreversibility analysis of cross flow heat exchangers. *Energy Conversion and Management*, 41 (15), p. 1585 - 1599.

Ordóñez, J.C. and Bejan, A. 2000. Entropy generation minimization in parallel-plates counterflow heat exchangers. *International Journal of Energy Research*, 24, p. 843 - 864.

Ratts, B.E. and Raut, A.G. 2004. Entropy generation minimization of fully developed internal flow with constant heat flux. *Journal of Heat Transfer*, 126 (4), p. 656 - 659.

Yilmaz, M., Sara, O.N. and Karsli, S. 2001. Performance evaluation criteria for heat exchangers based on second law analysis. *Exergy, an International Journal*, 1 (4), p. 278 - 294.

Zimparov, V. 2001. Extended performance evaluation criteria for enhanced heat transfer surfaces: heat transfer through ducts with constant heat flux. *International Journal of Heat and Mass Transfer*, 44 (1), p. 169 -180.

Zimparov, V.D., Da Silva, A.K. and Bejan, A. 2006a. Thermodynamic optimization of tree-shaped flow geometries with constant channel wall temperature. *International Journal of Heat and Mass Transfer*, 49, p. 4839 - 4849.

Zimparov, V.D., Da Silva, A.K. and Bejan, A. 2006c. Thermodynamic optimization of tree-shaped flow geometries. *International Journal of Heat and Mass Transfer*, 49, p. 1619 - 1630.

Nomenclature

A	Cross-sectional area	m^2
c	Specific heat	J/kgK
D	Diameter	m
f	Friction factor	-
F_D	External drag force	N
G	Mass velocity	kg/sm^2
h	Planck's constant (solar radiation)	-
k	Boltzmann's constant (solar radiation)	-
k	Gas constant (c_p / c_v)	-
k	Thermal conductivity of a fluid	W/mK
i_{vb}	Number of watts arriving per unit area	W
$\dot{I}$	Irreversibility rate	W
L	Length	m
$\dot{m}$	Mass flow rate	kg/s
NTU	Number of transfer units	-
Nu	Nusselt number	-
P	Perimeter	m
P, p	Pressure	Pa
q	Heat transfer rate	W
$\dot{q}''$	Heat transfer flux	W/m^2
$\dot{Q}$	Heat transfer rate	W
R	Gas constant	J/kgK
s	Specific entropy	J/kgK
S	Entropy	J/K
$\dot{S}$	Entropy rate	W/K

$\dot{S}'''_{gen}$	Entropy generation rate per unit volume	W/m^{3}K
St	Stanton number	-
T	Temperature	K
T_0	Fluid flow temperature or environment temperature	K
T^*	Apparent temperature of the sun as an exergy source	K
U	Total energy inventory of the blackbody radiation	J
U_∞	Free-stream velocity	m/s
v	Frequency (solar radiation)	Hz
v	Kinematic viscosity	m^2/s
v	Velocity	m/s
x	Distance in x-direction	m
y	Distance in y-direction	m
ε	Heat transfer effectiveness	-
μ	Dynamic viscosity	kg/ms
ρ	Density	kg/m^3
ϕ	Dimensionless viscous dissipation	-

Subscripts:

0	Surrounding/Loss
0	Zero pressure (ideal gas) for c_p
a	Cold stream
ave	Average
B	Base
c	Collector
D	Based on diameter
e	Hot stream
gen	Generation
h	Hydraulic
i	Channel rank
i	Inlet
in	Inlet
$loss$	Loss

m	Mean
o	Out
out	Outlet
p	For constant pressure
v	For constant volume
w	Wall
x	In x-direction
y	In y-direction
∞	Surrounding area

Superscripts:

*	Solar
‘	Per unit length
.	Time rate of change
_	Average
in	Inlet
ΔP	Due to pressure difference
ΔT	Due to temperature difference

Appendix C

MATLAB CODE

M-File - *collector*

```
clc;
format long;

global Gyes
global a0
global a1
global a2
global a3
global a4
global a5
global a6
global a7
global a8
global a9
global a10
global tel
global Wn
global As
global r
global choice
global change
global T0g
global Ig
global wg
global P1g
global hightg
global lengthg
global eg
global Tsg
global specreflg
global kg
global tg
global ksolidg
global betag
global alphag

%assumptions:
Ts          = 1050;


Tsurr       = 300;
if change ==1 & T0g>0
    Tsurr = T0g;
end


%Nu          = 14;
%air at 750K
k           = 0.05;


specrefl    = 0.93;
%Duffie & Beckman, 1991, p212
if change ==1 & specreflg>0
    specrefl = specreflg;
end


alpha       = 0.98;
if change ==1 & alphag>0
    alpha = alphag;
end
```

```
beta        = 90;
if change ==1 & betag>0
    beta = betag;
end


%average irradiance:
I           = 1000;
if change ==1 & Ig>0
    I = Ig;
end


%concentrator error:
e           = 0.0067;
if change==1 & eg~=[]
    e = eg;
end


%wind factor: 1-10 times natural
w           = 1;
if change==1 & wg>0
    w = wg;
end


t = 1;

disp('THE RELATIONSHIP BETWEEN THE INTERCEPTED ENERGY AND CAVITY APERTURE DIAMETER,')
disp('WILL NOW BE CALCULATED FOR THE CAVITY RECEIVER')
disp(' ')
As = input('Collector area (m^2): ')
%might want to include a optical efficiency here?


rim = input('Rim angle of collector (in degrees): ')

f = sqrt(As/(4*pi*(sind(rim))^2/(1+cosd(rim))^2))


%This is only a starting guess - a small guess such that it increases
Wn(t) = sqrt(4*(As/50000)/pi);

%According to Reddy & Senhil Kumar (2008 & 2009) for Aw/A1 = 8

WnAs(t) = 8*pi*Wn(t)^2/4;

rsphere(t) = sqrt((WnAs(t) + pi*Wn(t)^2/4)/3/pi);



Qnetfirst = 0.001;

increment = 0.01;

%first calculation


%assume total error



angle = 0;

dangle = 1;

sum = 0;
```

```
while angle < rim

    dr = Wn(t)*cosd(angle)
    p = 2*f/(1+cosd(angle))
    n = 2*atan(dr/2/p)/e

    %from appendix G
    r = 0.2316419;
    b1 = 0.319381530;
    b2 = -0.356563782;
    b3 = 1.781477937;
    b4 = -1.821255978;
    b5 = 1.330274429;

    x = n/2;
    f1 = 1/sqrt(2*pi)*exp(-(x^2)/2);
    t1 = 1/(1+r*x);
    Q = f1*(b1*t1 + b2*t1^2 + b3*t1^3 + b4*t1^4 + b5*t1^5);
    F = 1 - 2*Q;



    slope = 8*pi*I*f^2*sind(angle)/(1+cosd(angle))^2;

    %Global Pressure ratio should be global variable

    %insulation thickness
    Gr = 9.81*(Wn(t)*sqrt(3))^3/(4.765*10^-5/0.8)^2
    Nu = 0.698*Gr^0.209*(1+cosd(beta))^0.968*(3.5)^-0.317*(1/sqrt(3))^0.425

    h = w*Nu*k/2/rsphere(t);
    Qloss(t) = 2*h*pi/4*Wn(t)^2*(Ts-Tsurr);
    kins = 0.05;

    thick(t) = kins*4*pi*rsphere(t)^2*(Ts-Tsurr)/Qloss(t)*10;


    dQinter = specrefl*alpha*F*slope*pi/180*dangle;



    if pi*(rsphere(t)+thick(t))^2 < 4*pi*f^2*(sind(rim))^2/(1+cosd(rim))^2
    sum = sum + dQinter;
    end

    angle = angle + dangle;

end




%aperture used to determine h
Gr = 9.81*(Wn(t)*sqrt(3))^3/(4.765*10^-5/0.8)^2
    Nu = 0.698*Gr^0.209*(1+cosd(beta))^0.968*(3.5)^-0.317*(1/sqrt(3))^0.425
h = w*Nu*k/2/rsphere(t)



Qloss(t) = 2*h*pi/4*Wn(t)^2*(Ts-Tsurr);
%include conduction heat loss
Qloss(t) = Qloss(t) + Qloss(t)/10;



Qnet(t) = sum - Qloss(t)
```

```
iteration = 0;

while pi/4*Wn(t)^2 < As/100
    %this is to make sure the concentration ratio ratio is larger than 100
    %according to Solar (Robert Pitz-Paal)

    iteration = iteration +1;
    t = t+1;

Wn(t) = Wn(t-1) + increment



%According to Reddy & Senhil Kumar (2008 & 2009) for Aw/A1 = 8

WnAs(t) = 8*pi*Wn(t)^2/4;

rsphere(t) = sqrt((WnAs(t) + pi*Wn(t)^2/4)/3/pi);



angle = 0;

dangle = 1;

sum = 0;

while angle < rim

    dr = Wn(t)*cosd(angle);
    p = 2*f/(1+cosd(angle));
    n = 2*atan(dr/2/p)/e

    %from appendix G
    r = 0.2316419;
    b1 = 0.319381530;
    b2 = -0.356563782;
    b3 = 1.781477937;
    b4 = -1.821255978;
    b5 = 1.330274429;

    x = n/2;
    f1 = 1/sqrt(2*pi)*exp(-(x^2)/2);
    t1 = 1/(1+r*x);
    Q = f1*(b1*t1 + b2*t1^2 + b3*t1^3 + b4*t1^4 + b5*t1^5);
    F = 1 - 2*Q;



    slope = 8*pi*I*f^2*sind(angle)/(1+cosd(angle))^2;

    %insulation thickness
    Gr = 9.81*(Wn(t)*sqrt(3))^3/(4.765*10^-5/0.8)^2
    Nu = 0.698*Gr^0.209*(1+cosd(beta))^0.968*(3.5)^-0.317*(1/sqrt(3))^0.425
    h = w*Nu*k/2/rsphere(t);
    Qloss(t) = 2*h*pi/4*Wn(t)^2*(Ts-Tsurr);
    kins = 0.05;

    thick(t) = kins*4*pi*rsphere(t)^2*(Ts-Tsurr)/Qloss(t)*10;

    dQinter = specrefl*alpha*F*slope*pi/180*dangle;



    if pi*(rsphere(t)+thick(t))^2 < 4*pi*f^2*(sind(rim))^2/(1+cosd(rim))^2
```

```
    sum = sum + dQinter;
    end

    angle = angle + dangle;

end




Gr = 9.81*(Wn(t)*sqrt(3))^3/(4.765*10^-5/0.8)^2
    Nu = 0.698*Gr^0.209*(1+cosd(beta))^0.968*(3.5)^-0.317*(1/sqrt(3))^0.425

h = w*Nu*k/2/rsphere(t)


Qloss(t) = 2*h*pi/4*Wn(t)^2*(Ts-Tsurr);
%include conduction heat loss
Qloss(t) = Qloss(t) + Qloss(t)/10;



Qnet(t) = sum - Qloss(t);

end

plot(Wn,Qnet)


p = polyfit(Wn,Qnet,10)

for z = 1:length(Wn)

        PQnet(z) = p(11) + p(10)*Wn(z) + p(9)*Wn(z)^2 + p(8)*Wn(z)^3 + p(7)*Wn(z)^4 +
p(6)*Wn(z)^5 + p(5)*Wn(z)^6 + p(4)*Wn(z)^7 + p(3)*Wn(z)^8 + p(2)*Wn(z)^9 + p(1)*Wn(z)^10;

end

 fid = fopen('gauss.txt','w');

        fprintf(fid,'%6.10f    ',c);
        fclose(fid);

        %it seems that the ALG061 is very sensitive for digits, therefor
        %'%6.10f: meaning 10 digits.

        ALG061

        a0 = p(11);
        a1 = p(10);
        a2 = p(9);
        a3 = p(8);
        a4 = p(7);
        a5 = p(6);
        a6 = p(5);
        a7 = p(4);
        a8 = p(3);
        a9 = p(2);
        a10 = p(1);



        for z = 1:length(Wn)

        FQnet(z) = X(1) + X(2)*Wn(z) + X(3)*Wn(z)^2 + X(4)*Wn(z)^3 + X(5)*Wn(z)^4;

        end

        Figure(1)
```

```
        plot(Wn,FQnet)
        hold on
        plot(Wn,PQnet)
        hold off

        Figure(2)
        plot(Wn,PQnet)
        xlabel('Wn: Aperture diameter (m)');
        ylabel('Qnet intercepted (W)');

        clear X
        clear r
        clear k

%so now, FQnet is a function of Wn, which is a function of D and L of the
%receiver

% thus, if Wn = Dap = sqrt(D*L/2/pi)

%Q* - Qloss = a0 + a1*sqrt(D*L/2/pi) + a2*(D*L/2/pi) + a3*(sqrt(D*L/2/pi))^3 +
a4*(sqrt(D*L/2/pi))^4;
%also, accompanying this equation, are two constraints for the smallest and
%largest diameter
```

```
function [F]=fun(X);

% fun
%
% Function evaluation for optimisation. This function should yield
% the objective function value.
%
%   synopsis:
%
%     [F] = fun(X)
%
%   where:
%
%       F = objective function value
%       X = variable vector
%
global Gyes
global a0
global a1
global a2
global a3
global a4
global a5
global a6
global a7
global a8
global a9
global a10
global tel
global Wn
global As
global r
global choice
global change
global T0g
global Ig
global wg
global P1g
global hightg
global lengthg
global eg
global Tsg
global specreflg
global kg
global tg
global ksolidg
global betag
global alphag


%parameters:
ec = Gyes(tel,2)/100;
et = Gyes(tel,5)/100;



rlow = Gyes(tel,3);
rhigh = Gyes(tel,4);
mlow = Gyes(tel,8);
mhigh = Gyes(tel,9);

%for r = rlow:0.05:rhigh


m = (mhigh - mlow)/(rhigh-rlow)*(r-rlow)+mlow;



%Recuperator:
hight = 1;
```

```
%if hightg>0
 %   hight=hightg;
%end


t = 0.001;
%if tg>0
 %  t = tg;
%end

ksolid = 401;
%if ksolidg>0
 %   ksolid=ksolidg;
%end


P1 = 80000;
%if P1g>0
 %   P1=P1g;
%end

T1 = 300;
%if T0g>0
 %   T1=T0g;
%end

T0=T1;


%X(4) = X4/1000 for scaling

%Cold side point3-4:
%assume mu,cold and Pr,c at +-350C
muc = 3.101*10^-5;
Prc = 0.6937;
kc = 0.04721;
cpc = 1056;
rhoc = 0.5664*(r*P1)/100000;

mplate = 2*m/hight*(t+X(4)/1000/X(3)/2*(X(3)+1));


Rec = 4*X(3)*mplate/muc/X(4)*1000/(X(3)+1)^2;

fc = (0.79*log(Rec)-1.64)^-2;

Nuc = fc/8*Prc*(Rec-1000)/(1+12.7*(fc/8)^0.5*(Prc^(2/3)-1));

hc = kc/X(4)*1000*Nuc;


%Hot side point9-10:
%assume mu,hot and Pr,h at +-450C
muh = 3.415*10^-5;
Prh = 0.6965;
kh = 0.05298;
cph = 1081;
rhoh = 0.488*(r*P1)/100000;


Reh = 4*X(3)*mplate/muh/X(4)*1000/(X(3)+1)^2;

fh = (0.79*log(Reh)-1.64)^-2;

Nuh = fh/8*Prh*(Reh-1000)/(1+12.7*(fh/8)^0.5*(Prh^(2/3)-1));

hh = kh/X(4)*1000*Nuh;


Rf = 0.0004;
Asplate = X(5)*X(4)/1000*(X(3)+1)*(1+1/X(3));
```

```
U = (1/hc + 2*Rf + X(5)/ksolid + 1/hh)^-1;

NTU = U*Asplate/mplate/cpc;

c = cpc/cph;

er = (1-exp(-NTU*(1-c)))/(1-c*exp(-NTU*(1-c)));


%constants


R = 287;
cp = 1004;
dT23 = 2;
dT45 = 2;
dT67 = 2;
dT89 = 2;



dP23 = 0.001;



dP34 = (fc*X(5)/(X(4)/1000)^5*8*mplate^2*X(3)^2/(X(3)+1)^4/rhoc)/(P1*r*(1-dP23))


%the pipes going up to the receiver should be smaller in diameter to
%maximize solar availability (according to Shah the pipe losses are 1%)
dP45 = 0.004;
dP56 = 0.04;
dP67 = 0.004;
dP89 = 0.001;



dP910 = (fh*X(5)/(X(4)/1000)^5*8*mplate^2*X(3)^2/(X(3)+1)^4/rhoh)/P1



Qloss23 = 2;
Qloss45 = 2;
Qloss67 = 2;
Qloss89 = 2;
Qlossr = 2;


k = 1.4;

clear i
clear D
clear E


%phase1:


    T2 = (T1*(1+(r^((k-1)/k)-1)/ec));
    T3 = (T2 - dT23);

%phase2:

    %initial guess

    T5 = 800;

     %choice 2 = pipe
    if choice == 2
```

```
        X(6)=1;
    end

    %round/plate - X(6) =1
    Q = a0 + a1*sqrt((X(1)/100)*X(2)/4/pi*(X(6)+1)) + a2*((X(1)/100)*X(2)/4/pi*(X(6)+1))
+ a3*((X(1)/100)*X(2)/4/pi*(X(6)+1))^(3/2) + a4*((X(1)/100)*X(2)/4/pi*(X(6)+1))^2 +
a5*((X(1)/100)*X(2)/4/pi*(X(6)+1))^(5/2) + a6*((X(1)/100)*X(2)/4/pi*(X(6)+1))^3 +
a7*((X(1)/100)*X(2)/4/pi*(X(6)+1))^(7/2) + a8*((X(1)/100)*X(2)/4/pi*(X(6)+1))^4 +
a9*((X(1)/100)*X(2)/4/pi*(X(6)+1))^(9/2) + a10*((X(1)/100)*X(2)/4/pi*(X(6)+1))^5;


    T6 = Q/m/1145 + T5;
    T7 = T6 - dT67;

%phase3:


    P2 = P1*r;
    P3 = P2*(1-dP23);


    P4 = P3*(1-dP34);
    P5 = P4*(1-dP45)

    mu = 4.2*10^-5;
    rho = 0.34*(r*P1)/100000;
    %round/plate:
    if choice==1
        P6 = P5 - ((0.79*log(4*m*X(6)/mu/(X(6)+1)^2/(X(1)/100))-1.64)^-
2)*(X(2)/(X(1)/100)^5)*(8*m^2*X(6)^2/rho/(X(6)+1)^4)
    end

    if choice == 2
        P6 = P5 - ((0.79*log(4*m/mu/pi/(X(1)/100))-1.64)^-
2)*(X(2)/(X(1)/100)^5)*(8*m^2/rho/pi^2);
    end

    P7 = P6*(1-dP67);
    P10 = P1;


    P9 = P10*(1+dP910);
    P8 = P9*(1+dP89);

%phase4:

    T8 = T7*(1-et*(1-1/((P7/P8)^((k-1)/k))));
    T9 = T8 - dT89;
    T10 = T9 - er*(T9-T2);

%phase5:

    T4 = er*(T9-T3)+T3;
    T5 = T4 - dT45;

 D(1) = 800;
 D(2) = T5;



 %_____________________________________________________________________
    %repeat:

  i=2;
 while (abs(D(i)-D(i-1))  > 0.001) & (i < 100)
 i = i+1;

 %phase2:

    %initial guess
```

```
    %choice 2 = pipe
    if choice == 2
        X(6)=1;
    end

    %round/plate - X(6) =1
        Q = a0 + a1*sqrt((X(1)/100)*X(2)/4/pi*(X(6)+1)) +
a2*((X(1)/100)*X(2)/4/pi*(X(6)+1)) + a3*((X(1)/100)*X(2)/4/pi*(X(6)+1))^(3/2) +
a4*((X(1)/100)*X(2)/4/pi*(X(6)+1))^2 +  a5*((X(1)/100)*X(2)/4/pi*(X(6)+1))^(5/2) +
a6*((X(1)/100)*X(2)/4/pi*(X(6)+1))^3 + a7*((X(1)/100)*X(2)/4/pi*(X(6)+1))^(7/2) +
a8*((X(1)/100)*X(2)/4/pi*(X(6)+1))^4 + a9*((X(1)/100)*X(2)/4/pi*(X(6)+1))^(9/2) +
a10*((X(1)/100)*X(2)/4/pi*(X(6)+1))^5;


    T6 = Q/m/1145 + T5;
    T7 = T6 - dT67;

%phase3:


    P2 = P1*r;
    P3 = P2*(1-dP23);


    P4 = P3*(1-dP34);
    P5 = P4*(1-dP45);

    mu = 4.2*10^-5;
    rho = 0.34*(r*P1)/100000;
    if choice==1
        P6 = P5 - ((0.79*log(4*m*X(6)/mu/(X(6)+1)^2/(X(1)/100))-1.64)^-
2)*(X(2)/(X(1)/100)^5)*(8*m^2*X(6)^2/rho/(X(6)+1)^4);
    end

    if choice == 2
        P6 = P5 - ((0.79*log(4*m/mu/pi/(X(1)/100))-1.64)^-
2)*(X(2)/(X(1)/100)^5)*(8*m^2/rho/pi^2);
    end

    P7 = P6*(1-dP67);
    P10 = P1;


    P9 = P10*(1+dP910);
    P8 = P9*(1+dP89);

%phase4:

    T8 = T7*(1-et*(1-1/((P7/P8)^((k-1)/k))));
    T9 = T8 - dT89;
    T10 = T9 - er*(T9-T2);

%phase5:

  T4 = er*(T9-T3)+T3;
  T5 = T4 - dT45;

  D(i) = T5;

 end



Sgen1 = m*1007*log(T2/T1) - m*R*log(P2/P1)
Sgen2 = m*1007*log(T3/T2) - m*R*log(P3/P2) + Qloss23/T0
Sgen3 = m*1145*log(T5/T4) - m*R*log(P5/P4) + Qloss45/T0
Sgen4 = m*1070*(log((T4*T10/T3/T9)*(P4*P1/P3/P9)^((1-k)/k)) + (T10-T1)/T0) + Qlossr/T0
Sgen4a = m*1070*(log((T4*T10/T3/T9))+(T10-T1)/T0)-m*R*log((P4*P1/P3/P9))+Qlossr/T0
Sgen5 = m*1145*log(T6/T5) - m*R*log(P6/P5)
Sgen6 = m*1145*log(T7/T6) - m*R*log(P7/P6) + Qloss67/T0
Sgen7 = m*1070*log(T9/T8) - m*R*log(P9/P8) + Qloss89/T0
```

```
Sgen8 = m*1145*log(T8/T7) - m*R*log(P8/P7)

Sgen = Sgen1+Sgen2+Sgen3+Sgen4+Sgen5+Sgen6+Sgen7+Sgen8

%syms Wnet

-Q;
-T0*Sgen;
%objective function

%Wnet = -T0*Sgen + Q + m*1007*(T1-T10) - m*T1*1007*log(T1/T10);
Wnet = -T0*Sgen + Q - m*T1*1007*log(T1/T10);
%Note: The term m*1070*(T10-T1)/T0) at the recuperator entropy generation
% Sgen4, should actually be added here, but as it is it is fine

F1 = m*1145*(T7-T8)-m*1007*(T2-T1);
%T1
%T2
%T3
%T4
%T5
%T6
%T7
%T8
%T9
%T10
%m

%m*1007*(T1-T10)-m*T1*1007*log(T1/T10)

F=-Wnet
F1
```

```
function [GF]=gradf(X);
% gradf
%
% Gradient evaluation for optimisation. This function should yield
% the gradient vector of the objective function.
%
%   synopsis:
%
%    [GF] = gradf(X)
%
%   where:
%
%      GF = gradient vector of the objective function
%       X = variable vector
%

h = 0.00000001;

clear Xgradientp
clear Xgradientn

Xgradientp = X + [h 0 0 0 0 0];
Xgradientn = X - [h 0 0 0 0 0];

GF(1) = (fun(Xgradientp) - fun(Xgradientn))/(h*2);

clear Xgradientp
clear Xgradientn

Xgradientp = X + [0 h 0 0 0 0];
Xgradientn = X - [0 h 0 0 0 0];

GF(2) = (fun(Xgradientp) - fun(Xgradientn))/(h*2);

clear Xgradientp
clear Xgradientn

Xgradientp = X + [0 0 h 0 0 0];
Xgradientn = X - [0 0 h 0 0 0];

GF(3) = (fun(Xgradientp) - fun(Xgradientn))/(h*2);

clear Xgradientp
clear Xgradientn

Xgradientp = X + [0 0 0 h 0 0];
Xgradientn = X - [0 0 0 h 0 0];

GF(4) = (fun(Xgradientp) - fun(Xgradientn))/(h*2);

clear Xgradientp
clear Xgradientn

Xgradientp = X + [0 0 0 0 h 0];
Xgradientn = X - [0 0 0 0 h 0];

GF(5) = (fun(Xgradientp) - fun(Xgradientn))/(h*2);

clear Xgradientp
clear Xgradientn

Xgradientp = X + [0 0 0 0 0 h];
Xgradientn = X - [0 0 0 0 0 h];

GF(6) = (fun(Xgradientp) - fun(Xgradientn))/(h*2);
```

```
function [C]=conin(X);
% conin
%
% Inequality constraint function evaluation for optimisation. This
% function should yield the inequality constraint function values.
%
%   synopsis:
%     [C] = conin(X)
%
%   where:
%
%       C = inequality constraint function values
%       X = variable vector
global Gyes
global a0
global a1
global a2
global a3
global a4
global a5
global a6
global a7
global a8
global a9
global a10
global tel
global Wn
global As
global r
global choice
global change
global T0g
global Ig
global wg
global P1g
global hightg
global lengthg
global eg
global Tsg
global specreflg
global kg
global tg
global ksolidg
global betag
global alphag

  if choice == 2
    X(6)=1;
end

C(1) = (X(1)/100)*X(2)*(X(6)+1)/16-As/100;
C(2) = Wn(2) -sqrt((X(1)/100)*X(2)*(X(6)+1)/4/pi);

%pipe/plate
if choice==1
    C3 = X(1)/100/2*(X(6)+1)-(sqrt(3)-1)/2*sqrt(X(1)/100*X(2)/4/pi*(X(6)+1));
end
if choice == 2
    C3 = 2*X(1)/100 - (sqrt(3)-1)/2*sqrt(X(1)/100*X(2)/2/pi);
end

C(3) = C3;
C(4) = Tsfunc(X) - 1200;
C(5) = -(X(1)/100);
C(6) = -X(2);
C7 = sqrt(As/pi)
C(7) = X(5) - C7;

if choice==1
C(8) = 2.5-X(6);
end
```

```
function [GC]=gradc(X);
% gradc
%
% Gradient evaluation for optimisation. This function should yield
% the gradient vectors of the inequality constraint functions.
%
%   synopsis:
%
%    [GC] = gradc(X)
%
%   where:
%
%      GC = gradient vectors for inequality constraints
%       X = variable vector
%
global Gyes
global a0
global a1
global a2
global a3
global a4
global a5
global a6
global a7
global a8
global a9
global a10
global tel
global Wn
global As
global r
global choice
global change
global T0g
global Ig
global wg
global P1g
global hightg
global lengthg
global eg
global Tsg
global specreflg
global kg
global tg
global ksolidg
global betag
global alphag


GC(1,1) = X(2)/100*(X(6)+1)/16;
GC(1,2) = (X(1)/100)*(X(6)+1)/16;
GC(1,3) = 0;
GC(1,4) = 0;
GC(1,5) = 0;
if choice==1
    GC(1,6) = (X(1)/100)*X(2)/16;
end

if choice==2
    GC(1,6) = 0;
end


GC(2,1) = -X(2)/100*(X(6)+1)/4/pi*0.5*((X(1)/100)*X(2)*(X(6)+1)/4/pi)^-0.5;
GC(2,2) = -(X(1)/100)*(X(6)+1)/4/pi*0.5*((X(1)/100)*X(2)*(X(6)+1)/4/pi)^-0.5;
GC(2,3) = 0;
GC(2,4) = 0;
GC(2,5) = 0;
if choice==1
     GC(2,6) = -(X(1)/100)*X(2)/4/pi*0.5*((X(1)/100)*X(2)*(X(6)+1)/4/pi)^-0.5;
end
```

```
if choice ==2
   GC(2,6)=0;
end



if choice ==1
    GC(3,1) = 1/200*X(6)+1/200-
1648431872091733/180143985094819840/(X(1)*X(2)/pi*(X(6)+1))^(1/2)*X(2)/pi*(X(6)+1);
    GC(3,2) = -
1648431872091733/180143985094819840/(X(1)*X(2)/pi*(X(6)+1))^(1/2)*X(1)/pi*(X(6)+1);
    GC(3,3) = 0;
    GC(3,4) = 0;
    GC(3,5) = 0;
    GC(3,6) = 1/200*X(1)-
1648431872091733/180143985094819840/(X(1)*X(2)/pi*(X(6)+1))^(1/2)*X(1)*X(2)/pi;
end

if choice == 2
    GC(3,1) = 1/50-
1648431872091733/180143985094819840*2^(1/2)/(X(1)*X(2)/pi)^(1/2)*X(2)/pi;
    GC(3,2) = -1648431872091733/180143985094819840*2^(1/2)/(X(1)*X(2)/pi)^(1/2)*X(1)/pi;
    GC(3,3) = 0;
    GC(3,4) = 0;
    GC(3,5) = 0;
    GC(3,6) = 0;
end



h = 0.00001;
GC(4,1) = (Tsfunc(X+[h 0 0 0 0 0])-Tsfunc(X-[h 0 0 0 0 0]))/(2*h);
GC(4,2) = (Tsfunc(X+[0 h 0 0 0 0])-Tsfunc(X-[0 h 0 0 0 0]))/(2*h);
GC(4,3) = (Tsfunc(X+[0 0 h 0 0 0])-Tsfunc(X-[0 0 h 0 0 0]))/(2*h);
GC(4,4) = (Tsfunc(X+[0 0 0 h 0 0])-Tsfunc(X-[0 0 0 h 0 0]))/(2*h);
GC(4,5) = (Tsfunc(X+[0 0 0 0 h 0])-Tsfunc(X-[0 0 0 0 h 0]))/(2*h);
GC(4,6) = (Tsfunc(X+[0 0 0 0 0 h])-Tsfunc(X-[0 0 0 0 0 h]))/(2*h);

GC(5,1) = -1/100;
GC(5,2) = 0;
GC(5,3) = 0;
GC(5,4) = 0;
GC(5,5) = 0;
GC(5,6) = 0;

GC(6,1) = 0;
GC(6,2) = -1;
GC(6,3) = 0;
GC(6,4) = 0;
GC(6,5) = 0;
GC(6,6) = 0;

GC(7,1) = 0;
GC(7,2) = 0;
GC(7,3) = 0;
GC(7,4) = 0;
GC(7,5) = 1;
GC(7,6) = 0;

if choice==1
    GC(8,1) = 0;
    GC(8,2) = 0;
    GC(8,3) = 0;
    GC(8,4) = 0;
    GC(8,5) = 0;

    GC(8,6) = -1;
end
```

```
function [Tsout]=Tsfunc(X);

global Gyes
global a0
global a1
global a2
global a3
global a4
global a5
global a6
global a7
global a8
global a9
global a10
global tel
global Wn
global As
global r
global choice
global change
global T0g
global Ig
global wg
global P1g
global hightg
global lengthg
global eg
global Tsg
global specreflg
global kg
global tg
global ksolidg
global betag
global alphag

%parameters:
ec = Gyes(tel,2)/100;
et = Gyes(tel,5)/100;


 rlow = Gyes(tel,3);
rhigh = Gyes(tel,4);
mlow = Gyes(tel,8);
mhigh = Gyes(tel,9);

%for r = rlow:0.05:rhigh


m = (mhigh - mlow)/(rhigh-rlow)*(r-rlow)+mlow;



%Recuperator:
hight = 1;
%if hightg>0
 %   hight=hightg;
%end


t = 0.001;
%if tg>0
 %  t = tg;
%end

ksolid = 401;
%if ksolidg>0
 %   ksolid=ksolidg;
%end


P1 = 80000;
```

```
%if P1g>0
 %   P1=P1g;
%end

T1 = 300;
%if T0g>0
 %   T1=T0g;
%end

T0=T1;


%X(4) = X4/1000 for scaling

%Cold side:
%assume mu,cold and Pr,c at +-350C
muc = 3.101*10^-5;
Prc = 0.6937;
kc = 0.04721;
cpc = 1056;
rhoc = 0.5664*(r*P1)/100000;

mplate = 2*m/hight*(t+X(4)/1000/X(3)/2*(X(3)+1));


Rec = 4*X(3)*mplate/muc/X(4)*1000/(X(3)+1)^2;

fc = (0.79*log(Rec)-1.64)^-2;

Nuc = fc/8*Prc*(Rec-1000)/(1+12.7*(fc/8)^0.5*(Prc^(2/3)-1));

hc = kc/X(4)*1000*Nuc;


%Hot side:
%assume mu,hot and Pr,h at +-450C
muh = 3.415*10^-5;
Prh = 0.6965;
kh = 0.05298;
cph = 1081;
rhoh = 0.488*(r*P1)/100000;


Reh = 4*X(3)*mplate/muh/X(4)*1000/(X(3)+1)^2;

fh = (0.79*log(Reh)-1.64)^-2;

Nuh = fh/8*Prh*(Reh-1000)/(1+12.7*(fh/8)^0.5*(Prh^(2/3)-1));

hh = kh/X(4)*1000*Nuh;


Rf = 0.0004;
Asplate = X(5)*X(4)/1000*(X(3)+1)*(1+1/X(3));

U = (1/hc + 2*Rf + X(5)/ksolid + 1/hh)^-1;

NTU = U*Asplate/mplate/cpc;

c = cpc/cph;

er = (1-exp(-NTU*(1-c)))/(1-c*exp(-NTU*(1-c)));



%constants


R = 287;
cp = 1004;
dT23 = 2;
```

```
dT45 = 2;
dT67 = 2;
dT89 = 2;

dP23 = 0.001;


 dP34 = (fc*X(5)/(X(4)/1000)^5*8*mplate^2*X(3)^2/(X(3)+1)^4/rhoc)/(P1*r*(1-dP23));



dP45 = 0.004;
dP56 = 0.04;
dP67 = 0.004;
dP89 = 0.001;



dP910 = (fh*X(5)/(X(4)/1000)^5*8*mplate^2*X(3)^2/(X(3)+1)^4/rhoh)/P1;


Qloss23 = 2;
Qloss45 = 2;
Qloss67 = 2;
Qloss89 = 2;
Qlossr = 2;


k = 1.4;

clear i
clear D
clear E


%phase1:


    T2 = (T1*(1+(r^((k-1)/k)-1)/ec));
    T3 = (T2 - dT23);

%phase2:

    %initial guess

    T5 = 800;

    if choice == 2
        X(6)=1;
    end
    %round/plate - X(6) =1

    Q = a0 + a1*sqrt((X(1)/100)*X(2)/4/pi*(X(6)+1)) + a2*((X(1)/100)*X(2)/4/pi*(X(6)+1))
+ a3*((X(1)/100)*X(2)/4/pi*(X(6)+1))^(3/2) + a4*((X(1)/100)*X(2)/4/pi*(X(6)+1))^2 +
a5*((X(1)/100)*X(2)/4/pi*(X(6)+1))^(5/2) + a6*((X(1)/100)*X(2)/4/pi*(X(6)+1))^3 +
a7*((X(1)/100)*X(2)/4/pi*(X(6)+1))^(7/2) + a8*((X(1)/100)*X(2)/4/pi*(X(6)+1))^4 +
a9*((X(1)/100)*X(2)/4/pi*(X(6)+1))^(9/2) + a10*((X(1)/100)*X(2)/4/pi*(X(6)+1))^5;


    T6 = Q/m/1145 + T5;
    T7 = T6 - dT67;

%phase3:

    P2 = P1*r;
    P3 = P2*(1-dP23);


    P4 = P3*(1-dP34);
    P5 = P4*(1-dP45);
```

```
    mu = 4.2*10^-5;
    rho = 0.34*(r*P1)/100000;
    if choice==1
        P6 = P5 - ((0.79*log(4*m*X(6)/mu/(X(6)+1)^2/(X(1)/100))-1.64)^-
2)*(X(2)/(X(1)/100)^5)*(8*m^2*X(6)^2/rho/(X(6)+1)^4);
    end

    if choice == 2
        P6 = P5 - ((0.79*log(4*m/mu/pi/(X(1)/100))-1.64)^-
2)*(X(2)/(X(1)/100)^5)*(8*m^2/rho/pi^2);
    end

    P7 = P6*(1-dP67);
    P10 = P1;


    P9 = P10*(1+dP910);
    P8 = P9*(1+dP89);

%phase4:

    T8 = T7*(1-et*(1-1/((P7/P8)^((k-1)/k))));
    T9 = T8 - dT89;
    T10 = T9 - er*(T9-T2);

%phase5:

    T4 = er*(T9-T3)+T3;
    T5 = T4 - dT45;

 D(1) = 800;
 D(2) = T5;



 %_____________________________________________________________
    %repeat:

  i=2;
 while (abs(D(i)-D(i-1))  > 0.001) & (i < 100)
 i = i+1;

 %phase2:

    %initial guess


    %round/plate - X(6) =1

    if choice == 2
        X(6)=1;
    end
    Q = a0 + a1*sqrt((X(1)/100)*X(2)/4/pi*(X(6)+1)) + a2*((X(1)/100)*X(2)/4/pi*(X(6)+1))
+ a3*((X(1)/100)*X(2)/4/pi*(X(6)+1))^(3/2) + a4*((X(1)/100)*X(2)/4/pi*(X(6)+1))^2 +
a5*((X(1)/100)*X(2)/4/pi*(X(6)+1))^(5/2) + a6*((X(1)/100)*X(2)/4/pi*(X(6)+1))^3 +
a7*((X(1)/100)*X(2)/4/pi*(X(6)+1))^(7/2) + a8*((X(1)/100)*X(2)/4/pi*(X(6)+1))^4 +
a9*((X(1)/100)*X(2)/4/pi*(X(6)+1))^(9/2) + a10*((X(1)/100)*X(2)/4/pi*(X(6)+1))^5;


    T6 = Q/m/1145 + T5;
    T7 = T6 - dT67;

%phase3:


    P2 = P1*r;
    P3 = P2*(1-dP23);


    P4 = P3*(1-dP34);
    P5 = P4*(1-dP45);
```

```
    mu = 4.2*10^-5;
    rho = 0.34*(r*P1)/100000;
    if choice==1
        P6 = P5 - ((0.79*log(4*m*X(6)/mu/(X(6)+1)^2/(X(1)/100))-1.64)^-
2)*(X(2)/(X(1)/100)^5)*(8*m^2*X(6)^2/rho/(X(6)+1)^4);
    end

   if choice == 2
        P6 = P5 - ((0.79*log(4*m/mu/pi/(X(1)/100))-1.64)^-
2)*(X(2)/(X(1)/100)^5)*(8*m^2/rho/pi^2);
    end

    P7 = P6*(1-dP67);
    P10 = P1;


    P9 = P10*(1+dP910);
    P8 = P9*(1+dP89);

%phase4:

    T8 = T7*(1-et*(1-1/((P7/P8)^((k-1)/k))));
    T9 = T8 - dT89;
    T10 = T9 - er*(T9-T2);

%phase5:

  T4 = er*(T9-T3)+T3;
  T5 = T4 - dT45;

  D(i) = T5;

 end

mu = 4.2*10^-5;



  if choice==1
      Tsout =
T6+Q/(X(1)/100)/X(2)/(X(6)+1)/(1+1/X(6))/(0.068/(X(1)/100))/0.023/0.71^0.4/(4*m*X(6)/mu/(
X(1)/100)/(X(6)+1)^2)^0.8;
  end

if choice == 2
    Tsout =
T6+(Q/(X(1)/100)/X(2)/pi)/(0.068/(X(1)/100)*0.023*0.71^0.4*(4*m/mu/pi/(X(1)/100))^0.8);
end
```

M-File - *getdata*

```
%uses 'Garrett.txt'

global Gyes
global a0
global a1
global a2
global a3
global a4
global tel
global choice

G = textread('Garrett.txt')


tel =0;

for i = 1:45

 %   if (G(i,10) < Qlow & G(i,11) > Qlow)|(G(i,10) < Qhigh & G(i,11) > Qhigh)|(G(i,10) <
Qmid & G(i,11) > Qmid)
        tel = tel+1;
        for j = 1:11
           Gyes(tel,j) = G(i,j);
       end
   end
%end


Gyes'


%number of turbochargers to be considered
tel

maxQ = max(Qnet)

%get the horsepower range

Qhigh = (maxQ + 0.3*maxQ)/750/0.3*0.4;
Qlow = (maxQ - 0.3*maxQ)/750/0.3*0.4;
Qmid = maxQ/750/0.3*0.4;

tel =0;

for i = 1:45

    if (G(i,10) < Qlow & G(i,11) > Qlow)|(G(i,10) < Qhigh & G(i,11) > Qhigh)|(G(i,10) <
Qmid & G(i,11) > Qmid)
        tel = tel+1;
        for j = 1:11
           Gyes2(tel,j) = G(i,j);
       end
   end
end

if tel>0
    Gyes2'
end
```

M-File - *once*

```
clear all;
clc;

disp('DEFAULT SETTINGS ');
disp(' ')
disp(' ')

disp('Surroundings:')
disp('I          =   1000')
disp('w          =   1')
disp('P1         =   80000')
disp('Tsurr      =   300')
disp(' ')

disp('Available space for recuperator:')
disp('height     =   1;')
disp('length     =   Diameter of dish')
disp(' ')

disp('Collector:')
disp('Ts         =   1050')
disp('e          =   0.0067')
disp('k          =   0.05')
disp('specrefl   =   0.93')
disp('alpha      =   0.98')
disp('beta       =   90')
disp(' ')

disp('Recuperator: ')
disp('t          =   0.001')
disp('ksolid     =   401')
disp(' ')


ask = input('Change default? Y/N ','s');

global change
global T0g
global Ig
global wg
global P1g
global hightg
global lengthg
global eg
global Tsg
global specreflg
global kg
global tg
global ksolidg
global betag
global alphag

if ask == 'Y' | ask == 'y'

    change = 1


    ask2 = input('Change default settings for surroundings? Y/N ','s');
    if ask2 == 'Y' | ask2 == 'y'
            T0g = input('Surrounding temperature (K): ');
            Ig = input('Average irradiance (W/m^2): ');
            wg = input('Wind factor (1-10): ');
            P1g = input('Atmospheric pressure (Pa): ');
    end

    ask2 = input('Change default settings for available space for recuperator? Y/N
','s');
    if ask2 == 'Y' | ask2 == 'y'
            hightg = input('Height of recuperator (m): ');
```

```
            lengthg = input('Maximum length of recuperator (m): ');

    end

    ask2 = input('Change default settings for the collector? Y/N ','s');
    if ask2 == 'Y' | ask2 == 'y'
            eg = input('Concentrator error (rad): ');
  %             Tsg = input('Maximum material surface temperature of receiver (K): (Note
that if this changes, the properties of air should be revised)' );
            specreflg =input('Reflectivity of the collector (<1): ');
  %         kg = input('Material conductivity of receiver: ');
            betag = input('Inclination of receiver in degrees (90degrees for system at
noon/horisontal receiver) ');
            alphag = input('Absorbtivity of receiver: ')

    end

       ask2 = input('Change default settings for the recuperator? Y/N ','s');
    if ask2 == 'Y' | ask2 == 'y'
            tg = input('Recuperator heat exchanger wall thickness between hot and cold
streams (m): ');
            ksolidg = input('Recuperator material conductivity: ');

    end

    end

collector;
ask = input('Run for all (type 52) or just 1 (type 1) ?','s')

    if ask=='1'
        getdata;


       tel=input('Choose number: (0 to stop)')
        while tel~=0


        rlow = Gyes(tel,3)
        rhigh = Gyes(tel,4)

        global r




        while r~=1
             r = input('Choose pressure ratio: ')
            choice = input('Should the receiver use plate or pipe: 1=plate, 2=pipe? ')
        %1=plate
        %2=pipe

            if tel>4 & tel<20
            lfopc([7 8 7 8 7 8],1,1e-7)
            end
            if tel<5
              lfopc([5 5 5 5 5 5],1,1e-7)
            end
            if tel>19
                lfopc([20 20 20 20 20 20],1,1e-7)
            end
              r=input('Select r (type 1 to end): ')


        end
         tel=input('Choose number: (0 to stop)')
        end
    end

    if ask =='52'
```

```
    ask2=input('What is the range of micro-turbines to be looked at? First type the
lowest number: ')
    ask3 = input('Now type the highest number: ')
     choice = input('Should the receiver use plate or pipe: 1=plate, 2=pipe? ')

    global r
    getdata

    clear Willem
    clear Willem2
    qqq=1


            if tel>4 & tel<20
            start = [7 8 7 8 7 8]
            end
            if tel<5
              start = [5 5 5 5 5 5]
            end
            if tel>19
                start = [20 20 20 20 20 20]
            end


        for tel=ask2:1:ask3

            if tel>4 & tel<20
            start = [7 8 7 8 7 8]
            end
            if tel<5
              start = [10 10 10 10 10 10]
            end
            if tel>19
                start = [20 20 20 20 20 20]
            end


            rlow = Gyes(tel,3)+0.001;
            rhigh = Gyes(tel,4)+0.001;

        for r = rlow:0.1:rhigh
            Willem(qqq,1)=r;
            lfopc(start,1,1e-7)
            result = ans;
            for www = 2:1:7
                Willem(qqq,www) = result(www-1);
                start(www-1) =result(www-1)
            end
        Willem2(qqq) = fun(result);
        qqq=qqq+1;
        end

            qqq=qqq+1;
            for www = 1:1:6
                Willem(qqq,www) = 0;
            end
            Willem2(qqq) = 0;

        end


    end
```

Appendix D

GARRETT MICRO-TURBINES

Table D.1 Data for the Garrett micro-turbines (Garrett, 2009).

		Compressor							Turbine
Micro-turbine description	**Micro-turbine model number (*MT*)**	Maximum compressor efficiency	Pressure ratio range for maximum compressor efficiency		Mass flow rate range for maximum compressor efficiency (lb/min)		Mass flow rate range for maximum compressor efficiency (kg/s)		Maximum turbine efficiency
GT1241	1	76	2	2.7	7.7	10.5	0.06087	0.08300	65
GT1544	2	75	1.7	2.25	8	11	0.06324	0.08696	62
GT1548	3	72	1.6	1.8	11	13	0.08696	0.1028	62
GT2052a	4	77	1.4	2.2	10.5	17	0.08300	0.1344	70
GT2052b	5	75	1.6	2	10	14	0.07905	0.1107	70
GT2052c	6	74	1.4	1.7	9	13	0.07115	0.1028	70
GT2056	7	78	1.65	2.5	16	22.5	0.1265	0.1779	65
GT2252	8	78	1.5	2.5	12.5	23	0.09881	0.1818	68
GT2259	9	76	1.65	2.1	13	18	0.1028	0.1423	70
GT2554R	10	71	1.4	2	12	21	0.0949	0.1660	65
GT2560R	11	78	1.3	2	13	26	0.1028	0.2055	65
GT2854R	12	71	1.4	2	12	21	0.0949	0.1660	76
GT2859R	13	75	1.5	2.6	13.5	26	0.1067	0.2055	75
GT2860Ra	14	71	1.5	2.1	12	18	0.0949	0.1423	75
GT2860Rb	15	77	1.5	2.4	16	30	0.1265	0.2372	68
GT2860Rc	16	76	1.5	2.3	16.5	28	0.1304	0.2213	72
GT2871R	17	76	1.6	2.6	20	36	0.1581	0.2846	60
	18	75	1.6	2.5	19	30	0.1502	0.2372	66
	19	75	1.6	2.6	20	35	0.1581	0.2767	66
GT2876R	20	75	1.5	2.25	20	36	0.1581	0.2846	62
GT3071R	21	77	1.7	2.8	23	37	0.1818	0.2925	72
	22	77	1.7	2.8	23	37	0.1818	0.2925	64
GT3076R	23	77	1.5	2.5	20	38	0.1581	0.3004	72
GT3271	24	77	1.9	2.75	20.5	30	0.1621	0.2372	64
GT3582R	25	79	1.5	2.5	26	43	0.2055	0.3399	70
GT3776	26	77	1.9	2.6	28	37	0.2213	0.2925	68
GT3782	27	76	1.75	2.75	27	42	0.2134	0.3320	68
GT3788R	28	78	1.8	2.4	35	48	0.2767	0.3795	71
GT4088	29	74	1.7	3	29	58	0.2292	0.4585	66
GT4088R	30	78	1.8	2.4	35	48	0.2767	0.3795	70
GT4094Ra	31	78	1.7	2.4	37	52	0.2925	0.4111	70
GT4094Rb	32	77	1.5	2.8	30	63	0.2846	0.5138	70
GT4294	33	78	1.8	3	36	65	0.2846	0.5138	74
GT4294R	34	78	1.8	3.1	36	64	0.2846	0.5059	74
GTX4294R	35	80	1.6	2.9	42	68	0.3320	0.5376	74
GT4202	36	77	1.5	2.75	30	70	0.2371	0.5534	74
GTX4202R	37	78	2	3.5	54	78	0.4269	0.6166	74
GT4508R	38	79	1.7	2.8	48	85	0.3794	0.6719	92
GT4708	49	79	1.5	2.7	40	85	0.3162	0.6719	69
GT4718	40	78	1.6	2.8	53	99	0.4190	0.7826	69
GT5533	41	77	1.4	3.3	40	110	0.3162	0.8696	80
	42	77	1.5	2.7	60	116	0.4743	0.9170	80
GT5541R	43	75	1.75	3.2	75	148	0.5929	1.170	80
GT6041a	44	80	1.3	2.5	55	136	0.4348	1.075	78
GT6041b	45	79	1.3	2.8	50	152	0.3953	1.202	78
					lb/min		kg/s		

Reference

Garrett. 2009. *Garrett by Honeywell: Turbochargers, Intercoolers, Upgrades, Wastegates, Blow-Off Valves, Turbo-Tutorials.* Available at: http://www.TurboByGarrett.com [Accessed: 26 April 2010].